Geochronological and Structural Evolution of the Western and Central Kaoko Belt in NW Namibia

Dissertation

zur Erlangung des Grades

„Doktor der Naturwissenschaft“

am Fachbereich Chemie, Pharmazie und Geowissenschaften

der Johannes Gutenberg-Universität in Mainz

Stephan Ulrich Georg Kröner,

geboren in Geislingen an der Steige

Mainz, Mai 2005

Erklärung

Ich versichere hiermit, die vorliegende Arbeit selbständig und nur unter Verwendung der angegeben Quellen und Hilfsmittel verfasst zu haben.

All views and results presented in this thesis are those of the author, Stephan Kröner, unless stated otherwise

Mainz, Mai 2005

Tag der mündlichen Prüfung: 15.07.2005

Table of Contents

Abstract

This thesis focusses on the tectonic evolution and geochronology of part of the Kaoko orogen, which is part of a network of Pan-African orogenic belts in NW Namibia. By combining geochemical, isotopic and structural analysis, the aim was to gain more information about how and when the Kaoko Belt formed.

The first chapter gives a general overview of the studied area and the second one describes the basis of the Electron Probe Microanalysis dating method. The reworking of Palaeo- to Mesoproterozoic basement during the Pan-African orogeny as part of the assembly of West Gondwana is discussed in Chapter 3. Field observations and mapping in Kaokoland was accompanied by selective sampling for age dating. In the study area, high-grade rocks occupy a large area, and the belt is marked by several large-scale structural discontinuities. The two major discontinuities, the Sesfontein Thrust (ST) and the Puros Shear Zone (PSZ), subdivide the orogen into three tectonic units: the Eastern Kaoko Zone (EKZ), the Central Kaoko Zone (CKZ) and the Western Kaoko Zone (WKZ). An important lineament, the Village Mylonite Zone (VMZ), has been identified in the WKZ. Since plutonic rocks play an important role in understanding the evolution of a mountain belt, zircons from granitoid gneisses were dated by conventional U-Pb, SHRIMP and Pb-Pb techniques to identify different age provinces. Four different age provinces were recognized within the Central and Western part of the belt, which occur in different structural positions. The VMZ seems to mark the limit between Pan-African (intrusive events at ~650 and 580-550 Ma) granitic rocks east of the lineament and Palaeo- to Mesoproterozoic basement to the west.

In Chapter 4 the tectonic processes are discussed that led to the Neoproterozoic architecture of the orogen. The results of fieldwork during three field seasons (2001, 2002 and 2003) are summarised in this part. The main field observations were made in 2002 together with Jiří Konopásek, who is the main author of this chapter. Data from more than two months of mapping, structural measurements and selective sampling suggest that the Kaoko Belt experienced three main phases of deformation, D_1-D_3, during the Pan-African orogeny. Early structures in the central part of the study area indicate that the initial stage of collision was governed by underthrusting of the medium-grade Central Kaoko zone below the high-grade Western Kaoko zone, resulting in the development of an inverted metamorphic gradient. The early structures were overprinted by a second phase D_2, which was associated with the development of the PSZ and extensive partial melting and intrusion of ~550 Ma granitic bodies in the high-grade WKZ. Transcurrent deformation continued during cooling of the entire belt, giving rise to the localized low-temperature Village Mylonite Zone that separates a segment of elevated Mesoproterozoic basement from the rest of the Western zone in which only Pan-African ages

have so far been observed. The data suggest that the boundary between the Western and Central Kaoko zones represents a modified thrust zone, controlling the tectonic evolution of the Kaoko belt.

The geodynamic evolution and the processes that generated this belt system are discussed in Chapter 5. Geochemical and isotopic studies (U-Pb, Sm-Nd, Rb-Sr) were carried out at the Max-Planck-Institut für Chemie at Mainz. Neodymium mean crustal residence ages of granitoid rocks permit subdivision of the belt into four provinces. Province I is characterised by mean crustal residence ages <1.7 Ga and is restricted to the Neoproterozoic granitoids. A wide range of initial Sr isotopic values ($^{87}Sr/^{86}Sr_{initial}$ = 0.7075 to 0.7225) suggests heterogeneous sources for these granitoids. The second province consists of Mesoproterozoic (1516-1448 Ma) and late Palaeo-proterozoic (1776-1701 Ma) rocks and is probably related to the Eburnian cycle with Nd model ages of 1.8-2.2 Ga. The $\varepsilon_{Nd(initial)}$ values of these granitoids are around zero and suggest a pre-dominantly juvenile source. Late Archaean and middle Palaeoproterozoic rocks with model ages of 2.5 to 2.8 Ga make up Province III in the central part of the belt and are distinct from two early Proterozoic samples taken near the Puros Shear Zone which show even older T_{DM} ages of ~3.3 Ga (Province IV). There is no clear geological evidence for the involvement of oceanic lithosphere in the formation of the Kaoko-Dom Feliciano orogen.

Chapter 6 presents the results of isotopic analyses of garnet porphyroblasts from high-grade meta-igneous and metasedimentary rocks of the sillimanite-K-feldspar zone. Minimum P-T conditions for peak metamorphism were calculated at 731±10 °C at 6.7±1.2 kbar, substantially lower than those previously reported. A well-defined Sm-Nd garnet-whole rock errorchron obtained on a single meta-igneous rock yielded an unexpectedly old age of 692±13 Ma, which is interpreted as an inherited metamorphic age reflecting an early Pan-African granulite-facies event. The dated garnets survived a younger high-grade metamorphism that occurred between ca. 570 and 520 Ma and apparently maintained their old Sm-Nd isotopic systematics, implying that the closure temperature for garnet in this sample was higher than 730 °C. The metamorphic peak of the younger event was dated by Electron Probe Microanalysis (EPMA) on monazite at 567±5 Ma. These results imply fast heating and cooling rates at different times during the Pan-African orogeny, thus preventing isotopic homogenisation at the sample scale. Moreover, it would appear from this study that trace element diffusion is considerably shorter than major element diffusion. From a regional viewpoint, it is possible that these specific granulites of igneous origin may be unrelated to the early Pan-African metamorphic evolution of the Kaoko Belt and may represent a previously unrecognised exotic terrane.

Kurzfassung

Die vorliegende Arbeit beschäftigt sich mit der tektonischen und geochronologischen Entwicklung des westlichen und zentralen Teils des Kaoko-Gebirges in Namibia, das zu einem weit verzweigten Pan-Afrikanischen Gebirgssystem gehört. Ziel der Arbeit war es, durch eine Kombination von Geochemie-, Isotopen- und Strukturanalysen mehr Informationen über die Entstehungsgeschichte des Kaoko-Orogens zu bekommen.

Das erste Kapitel gibt einen allgemeinen Überblick zu dem untersuchten Gebiet, der zweite Teil beschreibt die Grundlagen der Mikrosondendatierung von Monaziten (*EPMA dating*). Die Monazitdatierung wurde benutzt, um das Temperaturmaximum der Pan-Afrikanischen Metamorphose zu bestimmen. Darüber hinaus wurde die Anwendbarkeit dieser Methode auf die untersuchten Gesteine getestet.

Die Überprägung von palaeo- und mesoproterozoischem Grundgebirge während der Pan-Afrikanischen Orogenese im Kontext der Bildung von West Gondwana wird in Kapitel 3 erläutert. Die Region wird durch zwei bedeutende Störungen – die Sesfontein Überschiebung (ST) und die Puros Scherzone (PSZ) – in drei Zonen aufgeteilt: die östliche Kaoko Zone, die zentrale Kaoko Zone und die westliche Kaoko Zone (EKZ, CKZ und WKZ). Außerdem konnte eine weitere wichtige Störung, die Village Mylonitzone (VMZ), in der WKZ kartiert werden. Um die Evolution der Gebirgskette besser verstehen zu können, wurden Zirkone aus granitischen Gneisen mit der U-Pb, SHRIMP und Pb-Pb Methode datiert. Vier verschiedene Altersprovinzen konnten im zentralen und westlichen Teil des Orogens identifiziert werden. Zusätzlich ergab sich aus den Datierungen, dass die VMZ eine Grenze von Pan-Afrikanischen Gesteinen mit palaeo– und mesoproterozoischen Gesteinen markiert.

Das vierte Kapitel handelt von den tektonischen Prozessen, die zur Architektur des Orogens beigetragen haben. In diesem Teil sind die Ergebnisse von drei Geländesaisons eingearbeitet (2001, 2002 und 2003). Der größte Teil der Geländearbeit wurde 2002 mit Jiří Konopásek durchgeführt. Basierend auf einer mehr als zwei Monate dauernden Kartierung wurden drei Hauptdeformation $D_{1\text{-}3}$ erkannt, welche die Pan-Afrikanische Tektonik des Kaoko Orogens prägen. Frühe Strukturen im zentralen Teil zeigen, dass die beginnende Kontinentkollision durch die Überschiebung der hochgradigen westlichen Kaokozone über die mittelgradig metamorphisierte zentrale Kaokozone geprägt ist, die zu einer Inversion der Metamorphosegraden führte. Diese frühen Strukturen wurden durch die zweite Deformationsphase überprägt, die im Zusammenhang mit der Bildung der PSZ steht und mit partieller Schmelzbildung und granitischen Instrusionen um ~550 Ma in der hochgradigen WKZ einhergeht. Der gesamte Gebirgsgürtel wurde auch während der Abkühlung von einer Transpressionsphase geprägt, die zur Entwicklung der Niedrigtemperatur Village Mylonitzone führte.

Die geodynamische Entwicklung und die Prozesse, die dieses Gebirgssystem gebildet haben, werden in Kapitel 5 diskutiert. Geochemische und Isotopenanalysen (U-Pb, Sm-Nd und Rb-Sr) wurden am Max-Planck Institut für Chemie in Mainz durchgeführt. Neodym Modellalter von krustalen Gesteinen ermöglichen eine Unterteilung des Arbeitsgebietes in vier Teile (Provinz I-IV). Die Provinz I ist durch eine mittlere Krustenverweildauer <1.7 Ga gekennzeichnet und auf die neoproterozoischen Granitoide beschränkt. Die stark streuenden Sr Isotopenwerte ($^{87}Sr/^{86}Sr_{initial}$ = 0.7075 to 0.7225) deuten auf eine heterogene Quelle der Granitoide. Außerdem konnten weder Hinweise auf eine Beteiligung von ozeanischer Lithosphäre bei der Genese der Neoproterozoischen Magmen im Kaoko, noch im Dom Feliciano Gebirge gefunden werden. Die zweite Provinz besteht aus mesoproterozoischen (1516-1448 Ma) und spät-palaeoproterozoischen (1776-1701 Ma) Gesteinen. Diese sind durch Nd-Modellalter von 1.8-2.2 Ga charakterisiert und werden im Zusammenhang mit dem Eburnischen Gebirgszyklus gesehen. Die $\varepsilon_{Nd(initial)}$ Werte dieser Gesteine streuen um Null und weisen auf eine vorwiegend juvenile Quelle hin. Die vierte Provinz besteht aus spätarchaischen und mittel-palaeoproterozoischen Gesteinen, die ein Modellalter von 2.5-2.8 Ga aufweisen. Diese unterscheiden sich deutlich von zwei Proben die in der Nähe der Puros Scherzone entnommen wurden und T_{DM}-Alter von ~3.3 Ga aufweisen (Provinz IV, Intrusionsalter: ~2.4 Ga).

In Kapitel 6 werden die Ergebnisse der Sm-Nd Datierung von Granaten und die P-T Berechnungen von metamagmatischen und metasedimentären Gesteinen aus der Sillimanit-K-Feldspat Zone vorgestellt. Minimum P-T Bedingungen von 731±10 °C bei einem Druck von 6.7±1.2 kbar wurden mit *Thermocalc 3.21* berechnet. Eine gut definierte sieben Punkt Granat-„errorchron“ in einem metamagmatischen Gestein ergab ein unerwartet hohes Alter von 692±13 Ma. Dies wird als ererbtes metamorphes Alter interpretiert, das ein früheres granulitfazielles Pan-Afrikanisches Ereignis wiederspiegelt. Es konnte gezeigt werden, dass die datierten Granate ein jüngeres hochgradiges Ereignis überstanden haben, das zwischen ca. 570 Ma und 520 Ma auftrat, ohne dass die Sm-Nd Isotopie gestört wurde. Dies bedeutet, dass die Schließungstemperatur von Granat in dieser Probe mehr als 730 °C betragen hat. Das Temperaturmaximum der jüngeren Metamorphose wurde mit Hilfe der Mikrosondendatierung von Monaziten (*EPMA dating*) auf 567±5 Ma bestimmt. Diese Ergebnisse implizieren, dass eine Homogenisierung der Isotopensystematik im Probenmaßstab verhindert wurde. Außerdem kann daraus gefolgert werden, dass die Diffusion von Spurenelementen beträchtlich langsamer als die der Hauptelemente ist. Regionalgeologisch bedeutet dies, dass diese speziellen Granulite möglicherweise nichts mit der Pan-Afrikanischen metamorphen Evolution des Kaoko Orogens zu tun haben, sondern von einem bisher unentdeckten exotischen Terrane herkommen.

Zusammenfassung für Fachfremde

Die vorliegende Arbeit beschäftigt sich mit der Entstehungsgeschichte des Kaoko-Gebirges in NW Namibia. Dieses bildete sich höchstwahrscheinlich aufgrund der Kollision zweier kontinentaler Platten vor ca. 550 Millionen Jahren. Teile des heutigen südamerikanischen Kontinents (*Rio de la Plata Kraton*) wurden dabei vermutlich unter einen alten krustalen Block im südlichen Afrika (*Kongo Kraton*) geschoben (*subduziert*). Zwischen diesen kontinentalen Schilden existierte ein Vorläufer des heutigen Atlantischen Ozean (*Proto-Atlantik* oder *Adamastor Ozean*), der aufgrund der Kollision geschlossen wurde. Das Pendant zum Kaoko-Gebirges ist das Dom-Feliciano Gebirge, welches sich ungefähr zwischen Porto Alegre (Brasilien) und Montevideo (Uruguay) befindet. Mit dieser Forschungsarbeit soll dazu beigetragen werden den Zeitpunkt der Gebirgsbildung zu bestimmen sowie die einhergehenden Prozesse zu beschreiben und auszuwerten. Eine geologische Karte wurde erstellt sowie Messungen an den Gesteinen (wie ist die räumliche Orientierung?) wurden durchgeführt, um Rückschlüsse auf die Situation vor und während der Gebirgsbildung zu ziehen. Außerdem wurden Gesteinsproben entnommen, die dann in Mainz untersucht wurden.

Die Dissertation gliedert sich in vier Haupteile (Kapitel 3-6), die alle in Fachzeitschriften entweder veröffentlicht sind oder zur Veröffentlichung eingereicht wurden. Das erste Kapitel gibt einen allgemeinen Überblick zu dem untersuchten Gebiet, der zweite Teil beschreibt die Grundlagen einer relativ neuen Datierungsmethode.

Das dritte Kapitel beschäftigt sich mit der Datierung granitoider Gneise (ehemalige Granite). Im westlichen Teil des Gebirges (*Orogen*) wurden diese Gesteine unter hohen Temperaturen (bis zu 730 °C) und Drücken von ~6.5-7 kbar (~25 km Tiefe) deformiert und kristallisierten dabei teilweise um (*Metamorphose*). Das uranreiche Mineral Zirkon wurde aus diesen Gesteinen extrahiert, im Labor mit verschiedenen Säuren aufgelöst (HF, HNO_3, HCl) und die Uranisotope (*Mutterisotope*) von den durch radioaktiven Zerfall entstandenen Bleiisotopen (*Tochterisotope*) getrennt. An einem Massenspektrometer wurden diese Isotope dann gemessen und am Verhältnis Mutter/Tochterisotop das Alter des Minerals bestimmt. Dieses entspricht der Schließungstemperatur des Minerals (keine Diffusion in benachbarte Minerale, oder in die Schmelze), die bei Zirkonen über 900 °C beträgt, und deswegen meistens auch als das Alter der granitischen Intrusion angesehen wird. Für das Kaoko-Orogen konnten vier Altersprovinzen identifiziert werden, wobei eine deutliche geographische Trennung von „jungen" Gesteinen (730-540 Millionen Jahre) und älteren Gesteinen (2000-1500 Millionen Jahre) durch eine Störungszone entdeckt wurde.

Im vierten Kapitel wird auf die Strukturen eingegangen, die durch die Gebirgsbildung entstanden sind. Durch die Kollision der beiden kontinentalen Platten kam es zu starker

Deformation der Gesteine, was zur Einregelung von Mineralen, Vergneisung und Faltung der Gesteine führte. Indem man diese Parameter im Gelände einmisst, kann man Rückschlüsse z. B. auf die relative Bewegungsrichtung der beiden Platten ziehen. Hier ergab sich, dass das Gebirge durch drei Hauptdeformationen geprägt wurde, die sich durch die Subduktion des südamerikanischen kontinentalen Teils von NW nach SE – aus heutiger geographischer Sicht – unter den Kongo Kraton bildeten.

Woher stammen diese Gesteine? Recycelte Kruste, oberer Erdmantel oder eine Mischung aus beiden? Handelte es sich damals um einen großen Ozean, der diese kontinentalen Blöcke trennte? Auf diese Fragen wird im fünften Kapitel anhand der Analyse der Isotopenmutter/-tochterpaare Samarium-Neodym und Rubidium-Strontium, sowie der Analyse von Spurenelementen und Seltenen Erdelementen eingegangen. Bei dem „Verschwinden" eines großen Ozeans durch die Kollision zweier tektonischer Platten bleiben meistens kleine Überreste des Ozeans (*Ophiolite*) im sich auffaltenden Gebirge übrig, da diese oft nicht vollständig subduziert werden können. Außerdem wird durch die Subduktion neue kontinentale Kruste (juveniles Material) gebildet. Im untersuchten Gebiet konnten aber keine offensichtlichen Hinweise auf einen alten Ozean, also z.B. Ophiolite, gefunden werden. Desweiteren stellte sich heraus, dass die granitoiden Schmelzen, die während der Gebirgsbildung vor 580-550 Millionen Jahren intrudierten, ihrerseits recyceltes Material älterer kontinentaler Kruste beinhalten. Die sich daraus ergebenden Schlussfolgerungen wurden auf ihre Konsistenz mit schon publizierten Arbeiten verglichen, die ebenfalls Gebiete im Kaoko-Gebirge, aber auch Regionen im südamerikanischen Teil untersuchten. Daraus ergab sich, dass es sich vermutlich nicht um einen großen Ozean (wie z. B. der heutige Pazifik) gehandelt haben kann, sondern eher um einen kleineren (z.B. wie das heutige Mittelmeer).

Im sechsten Kapitel wird die Datierung von Granat in ehemaligen magmatischen Gesteinen mit der Samarium-Neodym Methode beschrieben. Granat ist ein aluminiumreiches, recht komplexes Insel-Silikat, welches aus mehreren Mischkristallen zusammengesetzt ist. Oft bildet sich dieses Mineral während oder kurz nachdem die subduzierten Gesteine ihre maximale Temperatur (Metamorphose-Höhepunkt) erreicht haben. Da die Kollision der Platten vor ~580-550 Millionen Jahren stattfand, würde man ein Granatalter in diesem Zeitraum erwarten. Überraschenderweise ergab jedoch die Datierung mehrerer Granatfraktionen ein Alter von ca. 692 Millionen Jahren. Dies bedeutet, dass ein älteres hochmetamorphes Ereignis von dem zweiten Ereignis, welches zur Gebirgsbildung führte, nicht beeinflusst wurde. Die Schließungstemperatur der Samarium und Neodymisotope muss in diesem konkreten Fall also über der oben beschriebenen Temperatur von ca. 730 °C gelegen haben. Aus paläogeographischer Sicht ergibt sich darausfolgend, dass im westlichen Teil des Kaoko-Gebirges mindestens ein zusätzliches krustales Fragment (*Terrane*) angelagert wurde, welches dieses ungewöhnliche Alter konservierte.

Published parts

Parts of this thesis were prepared for publication in international journals and are either published, in press or under review. These parts are included as specific manuscripts except for the layout and numbering of tables and figures.

Chapter 3 – **Kröner, S.,** Konopásek, J., Kröner, A., Poller, U., Wingate, M.W.D., Passchier, C.W. and Hofmann, K.-H. (2004). U-Pb and Pb-Pb zircon ages for metamorphic rocks in the Kaoko Belt of NW Namibia: A Palaeo- to Mesoproterozoic basement reworked during the Pan-African orogeny. *South African Journal of Geology*, **107**, 455-476.

Chapter 4 – Konopásek, J., **Kröner, S.,** Kitt, S.L., Passchier, C.W. and Kröner, A. (2005). Oblique collision and evolution of large-scale transcurrent shear zones in the Kaoko belt, NW Namibia. *Precambrian Research*, **136**, 139-157.

Chapter 5 – **Kröner, S.,** Jung, S. and Kröner, A. (submitted). An unusually old Sm-Nd garnet-whole rock age from the granulite-facies Western Kaoko Zone (Namibia): Evidence for a Neoproterozoic cryptic high-grade polymetamorphic event?. *Lithos*.

Chapter 6 – **Kröner, S.,** Kröner, A. and Jung, S. (submitted). Delineation of crustal provinces in the Pan-African Kaoko Belt (Namibia): constraints from U-Pb and Pb-Pb zircon ages and Nd isotopes. *Gondwana Research*.

Chapter 1

Introduction

1.1 General introduction: The Kaoko Belt within the framework of West Gondwana assembly

1.1.1 The African and South American cratonic blocks and the Kaoko-Dom Feliciano-Ribeira Belt system

The African and South American continents are composed of Archaean to Mesoproterozoic nuclei surrounded by Neoproterozoic and younger mobile belts (Fig. 1.1). The largest cratons in Africa and South America are the Congo-São Francisco Craton, the Kalahari Craton, the West African Craton, the Borborema–Trans-Sahara Craton and the Amazonian Craton (Fig. 1.1). The surrounding Neoproterozoic orogenic belts were generated during the Pan-African-Brasiliano orogenic cycle. The Kaoko Belt on the African side and the Dom Feliciano and Ribeira Belts on the South American side, are part of this widely distributed belt system (Fig. 1.1). Between ~900 and 550 Ma ago a proto-South Atlantic ocean (Adamastor ocean of Hartnady) may have existed between these mobile belts. The term 'Pan-African-Brasiliano Cycle' has been introduced by Porada (1979) to describe the successive opening and closure of the proto-South Atlantic. Closure of the Adamastor Ocean with collision of the Kalahari and Congo Cratons in Africa and the Sao Francisco and Rio de la Plata Craton in South America resulted in the structurally complex Kaoko-Dom Feliciano-Ribeira Belt system (Fig. 1.1).

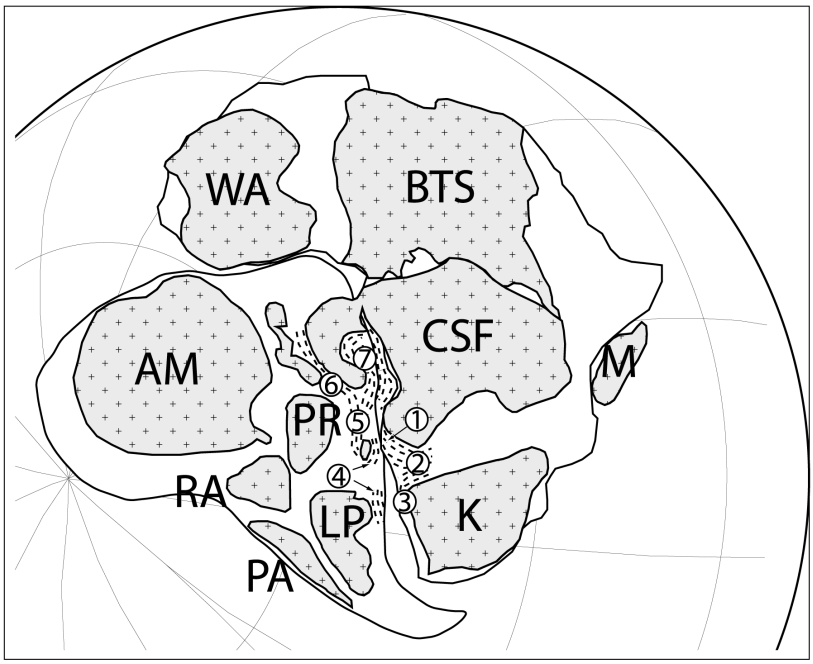

Fig. 1.1. Modified reconstruction of the African and South American Cratons at ~600 Ma after Cordani et al. (2003) and Trompette (1997). AM, Amazonia; BTS, Borborema–Trans-Sahara; CSF, Congo – São Francisco; K, Kalahari; LA, Luis Alves; LP, Rio de la Plata; PA, Pampia; PR, Paraná; RA, Rio Apa; WA, West Africa. Pan-African-Brasiliano belts:

1-Kaoko 5-Ribeira
2-Damara 6-Brasília
3-Gariep 7-Araçuaí
4-Dom Feliciano

1.1.2 Tectono-metamorphic evolution of the Kaoko-Damara Belt system

The tectonic evolution and timing of the metamorphic history of the Kaoko Belt with respect to the adjacent Damara orogen is described in detail in the published parts (Chapters 3-6). Here, I briefly summarise the geological setting of the Kaoko Belt in the study area.

The Kaoko Belt was interpreted by Coward (1983) as the 'northern arm' of the Damara Orogen and probably resulted from collision of the Rio de la Plata, the Congo–São Francisco and the Kalahari Cratons during the assembly of Western Gondwanaland (Fig. 1.1). Both the Kaoko and Damara Orogens can be subdivided on the basis of tectono-stratigraphic and metamorphic domains into three units. The Damara Belt is subdivided into a Southern, Central and Northern Zone, which are bordered by the Kalahari Craton in the South and the Congo Craton in the North. The Kaoko Belt is subdivided into a Western, Central and an Eastern zone.

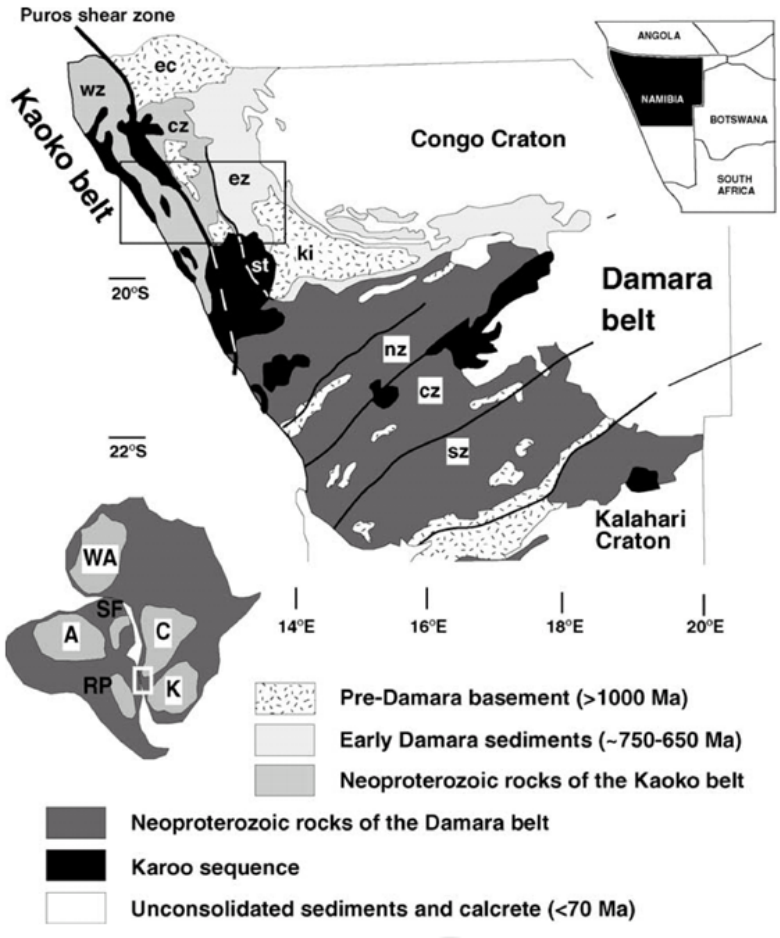

Fig. 1.2. Schematic geological map of northwestern Namibia showing position of the Pan-African Kaoko and Damara belts and of the Congo and Kalahari Cratons. Tectonic units of the Kaoko Belt (wz: Western zone; cz: Central zone; ez: Eastern zone; ki: Kamanjab Inlier; ec: Epupa Complex; st: Sesfontein thrust) and of the Damara Belt (nz: Northern zone; cz: Central zone; sz: Southern zone) after Miller (1983). Cratons indicated in inset: A: Amazon; C: Congo; K: Kalahari; RP: Rio de la Plata; SF: São Francisco; WA: West African. The Dom Feliciano Belt is located east of the Rio de la Plata Craton.

The belt developed along the southwestern margin of the Congo Craton, and the Atlantic Ocean borders its western extension (Fig. 1.2). The southern extension represents the connection with the Damara Belt but is hidden by the Etendeka Plateau Basalts (Karoo) and the Kamanjab Inlier (Fig. 1.2). The Karoo basalts originated ~130-120 Ma ago due the break-up of Gondwana, whereas the Kamanjab Inlier is a large basement window of the Congo Craton composed of Palaeoproterozoic ortho- and paragneisses (Siendner and Mitchell, 1976; Renne et al., 1992; Ernesto et al., 1999; Burger and Coertze, 1973; Burger et al., 1976; Tegtmeyer and Kröner, 1985). The different tectonic units of the Kaoko Belt exhibit different metamorphic and structural histories and are separated by two major discontinuities: the Puros Shear Zone and the Sesfontein Thrust (Figs. 1.2, 1.4). These main units can easily be identified on satellite images (Fig. 1.4).

1.2 Purpose and aims of present investigation

In contrast to many young orogenic belts the Neoproterozoic Kaoko Belt provides a good opportunity to study the deeply eroded parts of an orogen. Another advantage is the absence of cover vegetation as a result of the dry climate, leading to almost continuous exposure from the core of the orogen to its foreland. On the other hand, due to the opening of the Atlantic Ocean, a considerable part of the original Kaoko Belt is missing.

Until recently, the Kaoko Belt was largely unmapped and no structural or isotopic data were available due to the inaccessibility of this part of NW Namibia. Since Guj (1970) undertook systematic mapping and stratigraphic and structural analysis in the Central Kaoko Zone other authors presented detailed tectono-stratigraphic data for parts of the Kaoko Belt or the entire orogen (Miller, 1983; Dingeldey et al., 1994; Dürr and Dingeldey, 1996; Dingeldey, 1997; Goscombe et al., 2003b, 2005). The metamorphic evolution has been discussed by Franz et al. (1999), Gruner (2000) and Goscombe et al. (2003a), and first systematic geochronological results were presented by Seth et al. (1998). The results of these studies contributed to a better understanding of the evolution of the Kaoko Belt, but many problems remained:

a) The tectono-stratigraphic subdivision of part of the belt by Dingeldey et al. (1994) only partly corresponds to that proposed by Miller (1983).
b) There is no convincing explanation for the observed inverted metamorphic isograds within the orogen.
c) The evolution of the belt prior to amalgamation of West Gondwana is still unknown.
d) It is not known whether the Kaoko Belt experienced a diachronous metamorphic evolution as proposed by Franz et al. (1999) or whether it originated from accretion of several so far unknown terranes (Fig. 1.3).

Structural analyses as well as geochemical and isotopic surveys were carried out on granitoid gneisses in parts of the Central and Western Kaoko Zones (CKZ and WKZ) in order to clarify the complex history of the Kaoko Belt. Mapping of part of the WKZ near the village of Puros was accompanied by selective sampling for radiometric age determinations. U-Pb and Pb-Pb dating of zircons was carried out to identify different magmatic and thermal events, whereas Sm-Nd isotopic work on garnets and Electron Probe Microanalysis (EPMA) on monazites was undertaken to date metamorphic event(s). Petrographical investigations on garnet, plagioclase, K-feldspar and biotite supplied P-T estimates for near peak metamorphic conditions. Furthermore, the aim of the study was to provide information on the sources and processes that generated these granitoids by means of Sm-Nd, Rb-Sr and Rare Earth Element analyses on whole-rock samples.

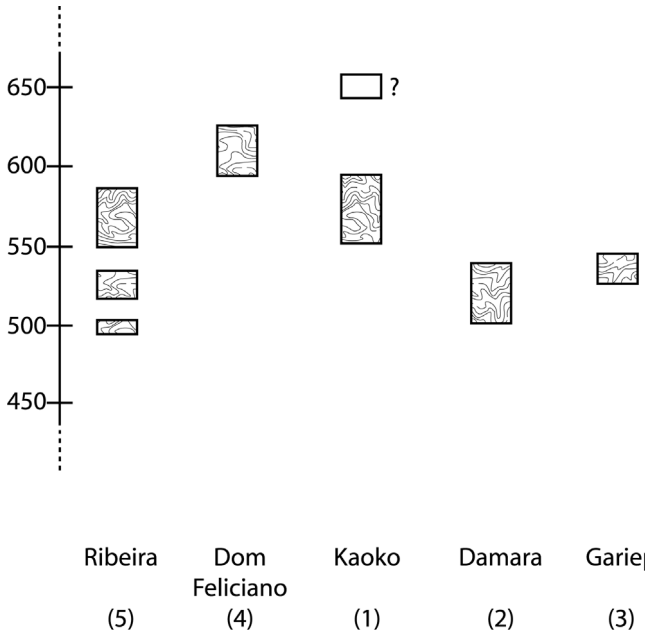

Fig. 1.3. Main and post-metamorphic events (in Ma) in the Neoproterozoic mobile belts of southern Africa and South America. Labels (1)-(5) correspond to Fig. 1. U-Pb zircon and monazite ages in the Kaoko Belt are either metamorphic or igneous ages (Seth et al., 1998; Franz et al., 1999). Data from: Reid et al., 1991; Machado et al., 1996; Seth et al., 1998; Franz et al., 1999; Jung and Mezger, 2001; Jung and Mezger, 2003a; Jung and Mezger, 2003b; Heilbron et al., 2003.

Fig. 1.4. Six ASTER satellite images have been rectified, geo-referenced and stuck together (visible light bands). The Gomatum, Khumib, Hoarusib and Hoanib valleys as well as the Sesfontein Thrust (ST) and the Puros Shear Zone (PSZ) are indicated. East-West extension of the image is ~150 km.

1.3 References

Burger, A.J. and Coertze, F.J. (1973). Radiometric age measurements on rocks from southern Africa to the end of 1971. *Annals of the Geological Survey of South Africa,* **82**, 185-204.

Burger, A.J., Clifford, T.N. and Miller, R.Mc.G. (1976). Zircon U-Pb ages of the Fransfontein granitic suite, northern South West Africa. *Precambrian Research*, **3**, 405-431.

Cordani, U. G., D'Agrella-Filho, M. S., Brito-Neves, B. B. and Trindade, R. I. F (2003). Tearing up Rodinia: the Neoproterozoic palaeogeography of South American cratonic fragments. *Terra Nova*, **15**, 350-359.

Coward, M.P. (1983). The tectonic history of the Damara belt. In: Miller, R.Mc.G. (Ed.), The Damara orogen. *Geological Society of South Africa Special Publication*, **11**, 431–515.

Dingeldey, D.P., Dürr, S.B., Charlesworth, E.G., Franz, L., Okrusch, M. and Stanistreet, I.G. (1994). A geotraverse through the northern coastal branch of the Damaran Orogen west of Sesfontein, Namibia. *Journal of African Earth Sciences*, **19**, 315–329.

Dingeldey, D.P. (1997). Tectono-metamorphic evolution of the Pan-African Kaoko belt, NW-Namibia. Unpublished Doctoral dissertation, University of Würzburg, Germany, 247 p.

Dürr, S.B. and Dingeldey, D.P. (1996). The Kaoko belt (Namibia): part of a late Neoproterozoic continental-scale strike-slip system. *Geology*, **24**, 503–506.

Ernesto, M., Raposo, M.I.B, Marques, L.S., Renne, P.R., Diogo, L.A. and de Min, A. (1999). Paleomagnetism, geochemistry and $^{40}Ar/^{39}Ar$ dating of the north-eastern Paraná Magmatic Province: tectonic implications. *Journal of Geodynamics*, **28**, 32–340.

Franz, L., Romer, R.L. and Dingeldey, D.P. (1999). Diachronous Pan-African granulite-facies metamorphism (650 Ma and 550 Ma) in the Kaoko belt, NW Namibia. *European Journal of Mineralogy*, **11**, 167-180.

Goscombe, B., Hand, M., Gray, D. and Mawby, J. (2003a). The metamorphic architecture of a transpressional orogen: the Kaoko belt, Namibia. *Journal of Petrology*, **44**, 679-711.

Goscombe, B., Hand, M. and Gray, D. (2003b). Structure of the Kaoko belt, Namibia: progressive evolution of a classic transpressional orogen. *Journal of Structural Geology*, **25**, 1049–1081.

Goscombe, B., Gray, D. and Hand, M. (2005). Extrusional tectonics in the core of a transpressional orogen; the Kaoko Belt, Namibia. *Journal of Petrology*, Advance Access published.

Guj, P. (1970). The Damara mobile belt in the south-western Kaokoveld, South West Africa. *Precambrian Research Unit, University of Cape Town, South Africa, Bulletin,* **10**, 168pp.

Gruner, B. (2000). Metamorphoseentwicklung im Kaokogürtel, NW-Namibia: Phasen-petrologische und geothermobarometrische Untersuchungen panafrikanischer Metapelite. Unpublished Doctoral dissertation, University of Würzburg, Germany, 248pp.

Heilbron, M. and Machado, N. (2003). Timing of terrane accretion in the Neoproterozoic–Eopaleozoic Ribeira orogen (se Brazil). *Precambrian Research*, **125**, 87-112.

Jung, S. and Mezger, K. (2001). Geochronology in migmatites - a Sm-Nd, U-Pb and Rb-Sr study from the Proterozoic Damara belt (Namibia): implications for polyphase development of migmatites in high-grade terranes. *Journal of Metamorphic Geology*, **19**, 77-97.

Jung, S. and Mezger, K. (2003a). Petrology of basement-dominated terranes: I. Regional metamorphic T-t path from U-Pb monazite and Sm-Nd garnet geochronology (Central Damara orogen, Namibia). *Chemical Geology*, **198**, 223-247.

Jung, S. and Mezger, K. (2003b). U-Pb garnet chronometry in high-grade rocks – Case studies from the central Damara orogen (Namibia) and implications for the interpretation of Sm-Nd garnet ages and the role of high U-Th inclusions. *Contributions to Mineralogy and Petrology*, **146**, 382-396.

Machado, N., Valladares, C., Heilbron, M. and Valeriano, C. (1996). U-Pb geochronolohy of the central Ribeira belt (Brazil) and implications for the evolution of the Brazilian orogeny. *Precambrian Research*, **79**, 347-361.

Miller, R.Mc.G. (1983). The Pan-African Damara Orogen of South West Africa/ Namibia. In: Miller, R.Mc.G. (Ed.), The Damara Orogen. *Geological Society of South Africa Special Publication,* **11**, 431–515.

Porada, H. (1979). The Damara-Ribeira orogen of the Pan-African-Brasiliano cycle in Namibia (South West Africa) and Brazil as interpreted in terms of continental collision. *Tectonophysics*, **57**, 237-265.

Reid, D.L., Ransome, I.G.D., Onstott, T.C. and Adams, C.J. (1991). Time of emplacement and metamorphism of Late Precambrian mafic dykes associated with the Pan-African Gariep orogeny, Southern Africa: implications for the age of the Nama Group. *Journal of African Earth Science,* **13**, 531-541.

Renne, P.R., Ernesto, M., Pacca, I.G., Coe, R.S., Glen, J.M., Prévot, M. and Perrin, M. (1992). The age of Paraná flood volcanism, rifting of Gondwanaland, and the Jurassic–Cretaceous boundary. *Science*, **258**, 975–979.

Seth, B., Kröner, A., Mezger, K., Nemchin, A.A., Pidgeon, R.T. and Okrusch, M. (1998). Archaean to Neoproterozoic magmatic events in the Kaoko belt of NW Namibia and their geodynamic significance. *Precambrian Research*, **92**, 341–363.

Siendner, G. and Mitchell, J.G. (1976). Episodic Mesozoic volcanism in Namibia and Brazil: a K–Ar isochron study bearing on the opening of the south Atlantic. *Earth Planetary Science Letters*, **30**, 292–302.

Tegtmeyer, A. and Kröner, A. (1985). U–Pb zircon ages for granitoid gneisses in northern Namibia and their significance for Proterozoic crustal evolution of southwestern Africa. *Precambrian Research*, **28**, 311–326.

Trompette, R. (1997). Neoproterozoic (~600Ma) aggregation of Western Gondwana: a tentative scenario. *Precambrian Research*., **82**, 101–112.

Chapter 2

Electron Probe Microanalysis (EPMA) dating

2.1 Theoretical basis and age calculation procedure for EPMA dating of monazite

2.1.1 General backround

Several different geochronological tools exist to detect and quantify age relations due to magmatic or metamorphic events. The most reliable information for geochronology is probably U-Pb dating of single zircon grains, because i) two isotopically coupled chronometers ($^{235}U/^{207}Pb$ and $^{238}U/^{206}Pb$) are used and, therefore, assumptions on the geological significance of the ages obtained are rather well constrained; ii) zircons are able to record several thermal events (Kröner et al. 1994) because they are robust against resetting at high temperatures (Gulson and Krogh, 1973; Mezger and Krogstad, 1997; Möller et al., 2002) and, consequently, have a good potential to unravel complex magmatic and metamorphic events.

Although zircon has been the preferential mineral for dating thermal events, U-Pb chronology on monazite grains is a powerful tool to obtain supplementary information of the metamorphic (or magmatic) history of complex belts with multiple thermal events. Monazite is a La-Ce phosphate ($[Ce,La,Th]PO_4$) that frequently occurs in meta- to peraluminous granitoid rocks and in metapelitic rocks of upper amphibolite and granulite metamorphic grade (Overstreet 1967; Parrish 1990). Dodson (1973) has shown that, in high-grade metamorphic terrains, U-Pb mineral ages are based on the concept of diffusion of U and Pb. In metamorphic complexes mineral ages therefore reflect a cooling age through the blocking temperature during uplift, if the closure temperature for the corresponding mineral was exceeded. The closure temperature for the U-Pb system in monazite is regarded to be in the range of 725-750 °C (Copeland et al. 1988; Parrish 1990; DeWolf et al. 1993; Suzuki et al 1994). It probably varies depending on several parameters, particularly heating/cooling rate and grain size. Another important factor controlling the closing temperature is probably the presence of fluids during metamorphic reactions (nondiffusive process) leading to recrystallisation (Bingen and Breemen 1998; Cherniak et al., 2004). Cherniak et al. (2004), for example, calculated a cooling rate of 10 °C/Ma and a blocking temperature in excess of 900 °C for a 10μm size monazite grain. Several studies have shown that, like in zircon grains, inheritance does occur in monazite (Copeland et al. 1988; Parrish 1990; Zhu et al. 1997; Cherniak et al. 2004). Therefore, conventional U-Pb analyses on monazite grains have the same advantages as zircon dating. On the other hand, while dissolving one single monazite grain or

monazite grain fractions from a high-grade metamorphic terrane, mixing ages with no geological significance may be calculated. A still under-utilised geochronological tool to overcome this problem is Electron Probe Microanalyser (EPMA) dating of monazite grains. Several studies have shown that this method provides reliable though generally imprecise ages (Suzuki et al. 1994; Montel et al. 1996; Braun et al. 1998; Finger et al. 1998; Cocherie and Albarède 2001), and compared to other in-situ analyses such as Laser Ablation ICP-MS it is a fast and cheap alternative. The limitations of the chemical U-Th-Pb_{total} age are controlled by the detection limit and precision of the EPMA.

Compared to other minerals such as zircon, monazite is generally rich in Th and U and, consequently, a considerable amount of radiogenic Pb (Pb^*) accumulates in old monazites. Additionally, the amount of non-radiogenic Pb is normally negligible (<1 ppm, Parrish 1990) compared to Pb^*, and thus EPMA-dating of monazite grains is a suitable method. One disadvantage of EPMA-dating compared to conventional dating is that no isotopic ratios can be measured and, therefore, no assessment of concordance can be made. Because the amount of excess ^{206}Pb (due to incorporation of excess ^{230}Th) of Pb^*_{total} is <2 % the EPMA monazite age is regarded to be reliable (Suzuki et al. 1994). For age calculation only Th, U and Pb have to be measured and no correction has to be done. Other elements (Si, Ca, Nd, Er, Al, P, Ce, Dy, U, Y, La, Gd, Eu, Sm, Pr) have also been analysed for completion and REE interpretations.

2.2 Age calculation

The age per spot was calculated using the basic equation after Montel et al. (1996):

$$Pb_{calc} = \frac{Th}{232}\left[\exp(\lambda_{232} \times t) - 1\right] \times 208 + \frac{U}{238.04} \times 0.9928 \times \left[\exp(\lambda_{238} \times t) - 1\right] \times 206 + \frac{U}{235} \times 0.0072 \times \left[\exp(\lambda_{235} \times t) - 1\right] \times 207 \quad (1)$$

where Pb, Th and U are in ppm, λ_{232}, λ_{235} and λ_{238}, are the radioactive decay constants of ^{232}Th, ^{235}U and ^{238}U respectively. The following decay constants have been used (Holmes, 1946; Houtermans, 1946).

λ_{232}= 4.9475•10^{-11}; λ_{235}= 9.8485•10^{-10}; λ_{238}= 1.55125•10^{-10}. By iteration the equation can be solved by varying t (age) until $Pb_{calculated} = Pb_{measured}$.

$$S = \left[\left(\frac{a_{206}}{a_{238}} \times 0.9928 \times \left(e^{\lambda_{232}t} - 1\right)\right)\right] + \left[\left(\frac{a_{207}}{a_{235}} \times 0.0072 \times \left(e^{\lambda_{235}t} - 1\right)\right)\right] \div \left[\left(\frac{a_{208}}{a_{232}} \times \left(e^{\lambda_{232}t} - 1\right)\right)\right] \quad (2)$$

where a_{207}, a_{207}, a_{208}, a_{232}, a_{235} and a_{238} are the atomic masses of ^{206}Pb, ^{207}Pb, ^{208}Pb, ^{232}Th, ^{235}U and ^{238}U.

2.2.1 Error calculation

For error assessment several different methods are common. Suzuki et al. (1994) calculated a ThO_2^* versus PbO isochron age (CHIME). UO_2 is converted by a simple calculation into a theoretical amount of ThO_2 and is added to the measured ThO_2 (sum = ThO_2^*). A regression line after York (1966) can be fitted to the data, where the slope corresponds to the age and the uncertainty of the line provides the error. Consequently, the higher the variation in ThO_2^* content the lower the error. Montel et al. (1996) assumed that errors are randomly generated and only due to counting statistics of the EPMA. Therefore, the error is calculated using the least-square method for a normal Gaussian probability distribution.

However, these methods do not consider the correlation between the U, Th and Pb errors. Considering this error correlation, a recently developed method by Cocherie and Albarède (2001) was applied. Since the errors of U/Pb and Th/Pb are correlated, a correlation factor R can be

calculated and the analyses can be represented as ellipses. The correlation factor R is calculated as follows Cocherie and Albarède, 2001):

$$R = \frac{E_{Pb}^2}{\sqrt{\left(E_U^2 + E_{Pb}^2\right) \times \left(E_{Th}^2 + E_{Pb}^2\right)}} \tag{3}$$

where E_{Pb}, E_U and E_{Th} are the errors in Pb, U and Th in per cent.

The ISOPLOT program version 2.01 for Microsoft Excel (Ludwig, 1999) was used to calculate best-fit lines and the X-Y-[Z]-plot for representing the ellipses in a U/Pb versus Th/Pb diagram. The U/Pb and Th/Pb errors are only due to counting statistics, and a worst-case scenario for error propagation was calculated using the derivation of the U/Pb and Th/Pb ratios:

$$\Delta\left(\frac{U}{Pb}\right) = \frac{\Delta U}{Pb} + \frac{U}{Pb^2} \times \Delta Pb \tag{4}$$

$$\Delta\left(\frac{Th}{Pb}\right) = \frac{\Delta Th}{Pb} + \frac{Th}{Pb^2} \times \Delta Pb \tag{5}$$

where ΔPb, ΔU and ΔTh are the absolute errors in Pb, U, and Th. An error hyperbola can be plotted for one age population of monazite grains, using the ISOPLOT program of Ludwig (1999). The intercept of a perpendicular line through a focal point (Xbar-Ybar) provides minimum and maximum ages for the population, thus the error.

Between 1 and 12 analytical spots were measured per monazite grain with EPMA, and a total of 277 points on 147 grains from four different metapelite samples have been obtained (see Chapter 6). Concentrations of Th, U and Pb are given in Table 6.1 (chapter 6), together with the individual spot-ages. The calculated Th*, U/Pb, Th/Pb and R are also presented. The expected error in the concentration of each element is directly correlated with the absolute amount for each element (Figs 2.1a-c).

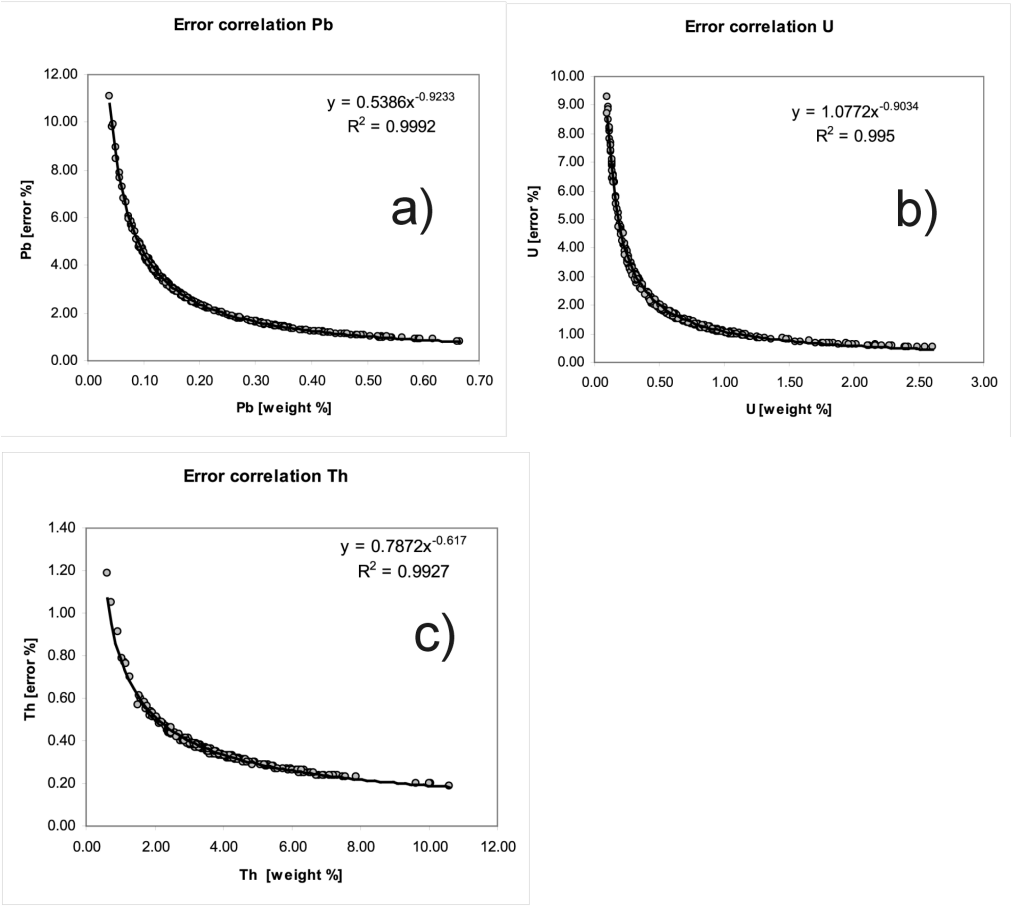

Fig. 2.1. Correlation of measured Pb, U and Th with error of each element. Data from chapter 6, table 6.1.

2.3 References

Bingen, B. and Breemen, O. (1998). U-Pb monazite ages in amphibolite- to granulite-facies orthogneiss reflect hydrous mineral breakdown reactions. Sveconorwegian Provine of SW Norway. *Contributions to Mineralogy and Petrology*, **132**, 336-353.

Braun, I., Montel, J.-M. and Nicollet, C. (1998). Electron microprobe dating of monazites from high-grade gneisses and pegmatites of the Kerala Khondalite Belt, southern India. *Chemical Geology*, **146**, 65-85.

Cherniak, D.J., Watson, E. B., Grove, M. and Harrison, T.M. (2004). Pb diffusion in monazite: A combined RBS/SIMS study. *Geochimica et Cosmochimica Acta*, **68**, 829-840.

Cocherie, A. and Albarède, F. (2001). An improved U-Th-Pb age evaluation for electron micro-probe dating of monazite. *Geochimica et Cosmochimica Acta*, **65 (24)**, 4509-4522.

Copeland, P., Parrish, R.R. and Harrison, T.M. (1988). Identification of inherited radiogenic Pb in monazite and implications for U-Pb systematics. *Nature*, **333**, 760-763.

DeWolf, C.P., Belshaw, N.S. and O'Nions, R.K. (1993). A metamorphic history from micron-scale chronometry of monazite. *Earth and Planetary Science Letters*, **120**, 207-220.

Dodson, M.H. (1973). Closure temperature in cooling geochronological and petrological systemns. *Contributions to Mineralogy and Petrology*, **40**, 259-274.

Finger F., Broska I., Roberts M. P. and Schermaier A. (1998). Replacement of primary monazite by apatite-allanite-epidote coronas in amphibolite facies granite gneiss from the eastern Alps. *American Mineralogist*, **83**, 248–258.

Gulson, B. L. and Krogh, T.T. (1973). Old lead components in the young Bergell Massif, southeast Swiss Alps. *Contributions to Mineralogy and Petrology*, **40**, 239-252.

Holmes, A. (1946). An estimate of the age of the Earth. *Nature*, **157**, 680–684

Houtermans, F.G. (1946). Die Isotopen-Häufigkeiten im natürlichen Blei und das Alter des Urans. *Naturwissenschaften*, **33**, 185–187

Kröner, A., Jaeckel, P. and Williams, I.S. (1994). Pb-loss patterns in zircons from a high-grade metamorphic terrain as revealed by different dating methods; U-Pb and Pb-Pb ages of igneous and metamorphic zircons from northern Sri Lanka. *Precambrian Research*, **66**, 151-181.

Ludwig, K.R. (1999). Using Isoplot/Ex, Version 2.01: a geochronological toolkit for Microsoft Excel. *Berkeley Geochronology Center, Special Publication*, **No. 1a**, 47

Mezger, K. and Krogstad, E.J. (1997). Interpretation of discordant U-Pb zircon ages: an evaluation. *Journal of Metamorphic Geology*, **15**, 127-140.

Möller, A., O'Brien, P.J., Kennedy, A. and Kröner, A. (2002). Polyphase zircon in ultrahigh-temperature granulites (Rogaland, SW Norway): constraints for Pb diffusion in zircon. *Journal of Metamorphic Geology*, **20**, 727-740.

Montel, J-M., Foret, S., Veschambre, M., Nicollet, C., and Provost, A (1996). Electron microprobe dating of monazite. *Chemical Geology*, **131**, 37-53.

Overstreet, W. C., 1967. The geological occurrence of monazite. *United States Geological Survey, Professional Paper*, 530.

Parrish, R.R. (1990). U-Pb dating of monazite and its application to geological problems. *Canadian Journal of Earth Sciences*, **27**, 1431-1450.

Suzuki, K., Adachi, M., and Kajizuka, I. (1994). Electron microprobe observations of Pb diffusion in metamorphosed detrital monazites. *Earth and Planetary Science Letters*, **128**, 391-405.

York D. (1966). Least-square fitting of a straight line. *Canadian Journal of Physics*, **44**, 1079-1088.

Zhu, X. K., O'Nions, R. K., Belshaw, N.S. and Gibb, A.J. (1997). Significance of in situ SIMS chronometry of zoned monazite from the Lewisian granulites, northwest Scotland. *Chemical Geology*, **135**, 35-53.

Chapter 3

U-Pb and Pb-Pb zircon ages for metamorphic rocks in the Kaoko Belt of NW Namibia: A Palaeo- to Mesoproterozoic basement reworked during the Pan-African orogeny

(published in South African Journal of Geology, 107, 455-476, 2004)

U-Pb and Pb-Pb zircon ages for metamorphic rocks in the Kaoko Belt of NW Namibia: A Palaeo- to Mesoproterozoic basement reworked during the Pan-African orogeny

S. Kröner[1], J. Konopásek[1], A. Kröner[1], U. Poller[2], M.T.D. Wingate[3], C.W. Passchier[1] and K.-H. Hofmann[4]

[1]*Institut für Geowissenschaften, Universität Mainz, 55099 Mainz, Germany*

[2]*Max-Planck-Institut für Chemie, Abteilung Geochemie, 55020 Mainz, Germany*

[3]*Tectonics Special Research Centre, University of Western Australia, Nedlands, WA 6907, Australia*

[4]*Geological Survey of Namibia, P.O. Box 2168, Windhoek, Namibia*

3.1 Abstract

The Kaoko Belt belongs to the Neoproterozoic mobile belt system of western Gondwana, whose geodynamic evolution is assumed to have resulted from collision between the Congo Craton (present Africa) and the Rio de la Plata Craton (present South America). Several magmatic intrusion periods can be distinguished in the coastal area of this belt, based on conventional U-Pb, SHRIMP and Pb-Pb evaporation analyses on zircons. The prevailing igneous rock types are of granitic to tonalitic composition. A Palaeoproterozoic terrain with U-Pb magmatic emplacement ages between 2028 and 1961 Ma may be correlated with the Eburnian event (~1.8-2.0 Ga), which is widespread in Africa. Additionally, two distinct magmatic events appear to be significant in the southwestern Congo Craton in late Palaeoproterozoic and Mesoproterozoic times, indicated by magmatic ages around 1770 Ma and between 1516 and 1448 Ma. These two events have so far not been reported from the Dom Feliciano Belt (southeastern Brazil), which is considered to represent the South American counterpart of the Kaoko Belt. Therefore, a possible link of these two belts prior to the Pan-African orogeny (~750-450 Ma) can neither be confirmed nor rejected on the basis of our data.

Emplacement ages for several Pan-African granitoids, obtained by U-Pb and SHRIMP analyses, range from 730 to 655 Ma. The youngest granitoids, representing the last major magmatic activity in that area, were emplaced at ~550 Ma during a transpressional regime at peak Pan-African temperatures.

Keywords: Kaoko Belt, Namibia, Pan-African, Proterozoic basement, transpressional orogeny, zircon geochronology

3.2 Introduction

Conflicting interpretations of geochronological results from high-grade metamorphic terrains are often due to different closure temperatures of the relevant isotopic systems. The mean closure temperature for the U-Pb system in zircon, calculated from Pb-diffusion parameters, is well in excess of 900 °C (Lee et al., 1997; Cherniak et al., 1997; Cherniak and Watson, 2000), and ages obtained on non-metamict igneous zircons, even from high-grade metamorphic rocks, therefore reflect protolith crystallization or inherited xenocrystic material that makes zircon geochronology suitable for dating of meta-igneous rocks that have experienced multiple deformation and repeated metamorphism.

The Kaoko Belt of northwestern Namibia is composed of meta-igneous and metasedimentary rocks of the Neoproterozoic Damara Supergroup and a poorly defined Mesoproterozoic to Archaean basement (Guj, 1970; Miller, 1983; Seth et al., 1998; Franz et al., 1999). Due to high-grade metamorphism and strong ductile deformation during the late Neoproterozoic to early Palaeozoic Pan-African orogeny the distinction between Neoproterozoic rocks and older basement is often difficult, if not impossible, in the field. Moreover, much of the belt is only known from reconnaissance studies, and controversies on lithostratigraphic subdivisions and correlations make field interpretations difficult so that published data from one part of the belt cannot simply be extrapolated to other parts. Several papers have emphasized the role of transpressional deformation in the present-day structure of the Kaoko Belt (Dürr and Dingeldey, 1996; Goscombe et al., 2003a,b; Konopásek et al., 2005) but controversies regarding the succession of major structural events still persist. Moreover, little is known about the early evolution of the Kaoko Belt, and conclusions drawn by several authors about the broad tectonic setting are still controversial (Porada, 1989; Dürr and Dingeldey, 1996; Passchier et al., 2002; Konopásek et al., 2005).

In order to clarify the relationship between structural and metamorphic zonation of the belt and timing of igneous activity and deformation, we applied the U-Pb and Pb-Pb zircon geochronometers in the analysis of medium- to high-grade meta-igneous rocks in the west-central part of the belt. There are few reliable and precise zircon ages from the deeply eroded central and western parts of this orogen (Seth et al., 1998; Franz et al., 1999), and the purpose of our study was to provide reliable age constraints on the timing of igneous and metamorphic events in tectonically well defined deep crustal domains that are separated from each other by major shear zones. Selection of samples followed a detailed structural study (Konopásek et al., in press) in a previously unmapped area in the west-central part of the belt, around the settlement of Puros (Fig. 3.2), and our new zircon ages are discussed in terms of the structural evolution and tectonic setting of this region.

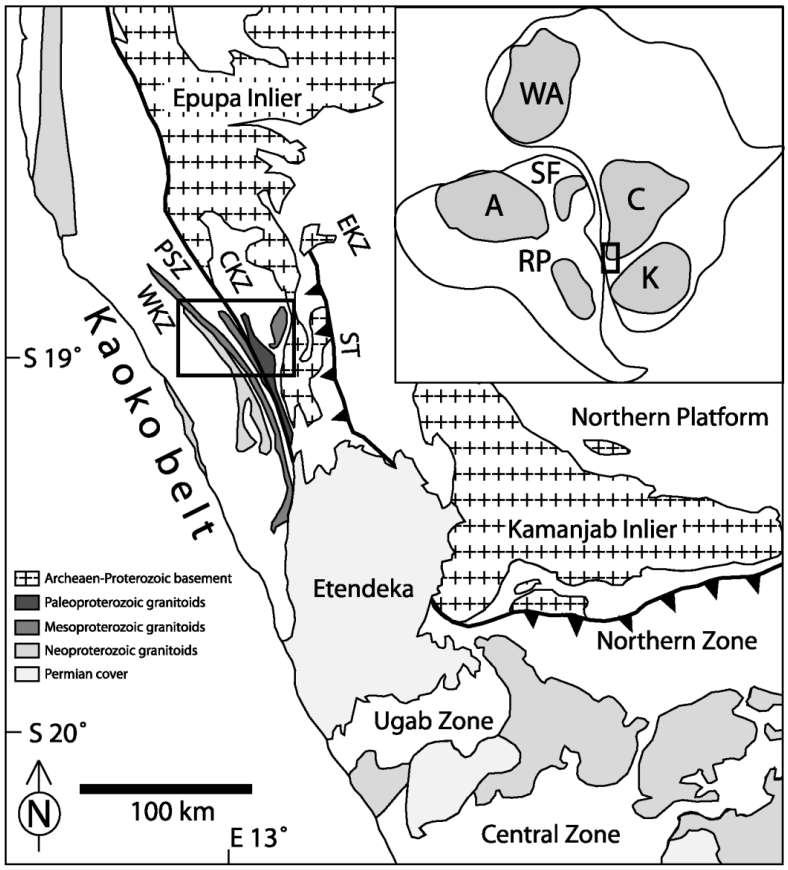

Fig 3.1. Schematic location map of the Kaoko and Damara belts modified after Miller (1983) and Goscombe et al. (2003a,b); the investigated area is marked by a box (Fig 3.2). Cratons indicated in inset: A: Amazon; C: Congo; K: Kalahari; RP: Rio de la Plata; SF: São Francisco; WA: West African. The Dom Feliciano Belt lies east of the Rio de la Plata Craton. ST-Sesfontein Thrust, PSZ-Puros Shear Zone, EKZ-Eastern Kaoko Zone, CKZ-Central Kaoko Zone, WKZ-Western Kaoko Zone.

3.3 Geological setting

The Kaoko and Damara belts of northern and central Namibia are part of a Neoproterozoic (Pan-African) system of orogenic belts (Fig. 3.1). The Damara Belt is the broad ENE-WSW trending main branch of the orogen, linking up with the Lufilian arc in south-central Africa, whereas the Kaoko Belt is the NNW-trending coastal part of the orogen exposed in Kaokoland and neighbouring Angola. The Damara-Kaoko Belt system has been interpreted in terms of collision of cratonic blocks in Africa and South America (Porada, 1989; Dürr and Dingeldey, 1996; Passchier et al., 2002). Two large-scale major structural discontinuities, the Puros Shear Zone (PSZ) and the Sesfontein Thrust (ST), subdivide the Kaoko Belt into three tectono-stratigraphic units (Miller, 1983). The ST (Guj, 1970) is a west dipping, low-angle thrust separating a folded sequence of low-grade autochthonous Damara Supergroup metasediments of the Eastern Kaoko Zone from a fold-and-thrust belt of the Central Kaoko Zone. The Puros Shear Zone is located on the western flank of the Central Kaoko Zone and defines the boundary with the westerly exposed Western Kaoko Zone. Autochthonous Damara metasediments cover the southwestern margin of the Congo Craton, the basement of which is exposed in large tectonic windows of the Kamanjab and Epupa inliers (Fig. 3.1).

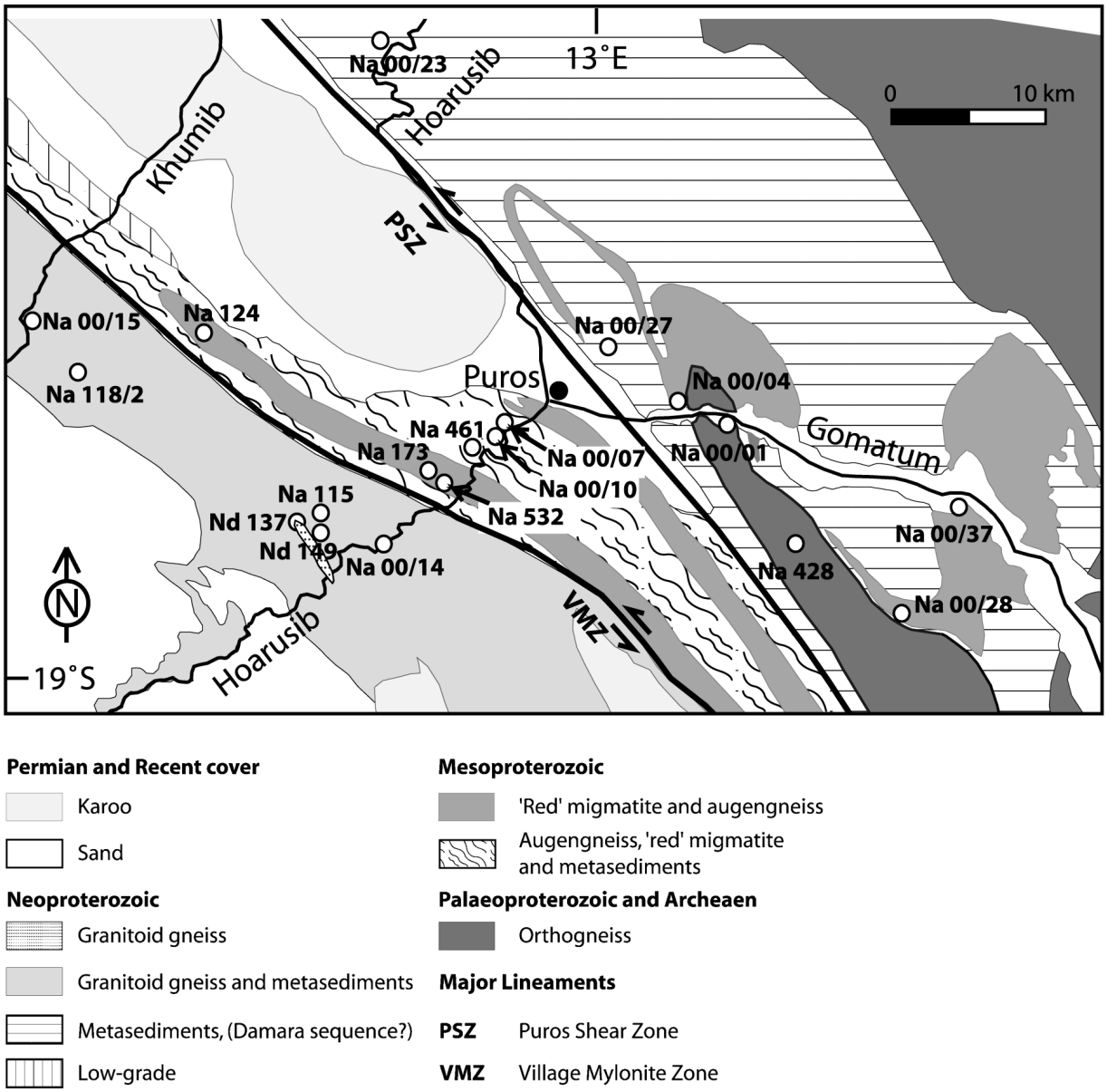

Fig. 3.2. Schematic and simplified geological map showing major rock units of the study area and sample location. Base map modified after Guj (1970), Goscombe et al. (2003a,b). PSZ-Puros Shear Zone, VMZ-Village Mylonite Zone.

The Epupa inlier extends into southern Angola and is composed of largely migmatitic ortho- and paragneisses, granites, a prominent gabbro-anorthosite body known as the Kunene Anorthosite Complex, and a newly discovered granulite terrain (Brandt et al., 2003; Seth et al., 2003). The general geological relationships are poorly constrained since no detailed mapping is available. Rb-Sr whole-rock isochron ages for rocks of the Epupa inlier in southern Angola range between 1654 Ma and 1100 Ma (Carvalho et al., 1987; Carvalho and Alves, 1993), whereas Tegtmeyer and Kröner (1985) dated zircon grains of the Ruacana gneiss at the Kunene River at 1795 $^{+33}/_{-29}$ Ma. Seth et al. (2003) dated metamorphic zircon grains from a small granulite-facies terrain south of the Kunene Anorthosite Complex at between 1520 and 1510 Ma (SHRIMP II). Zircon xenocryst

ages between 1635 and 1810 Ma from these granulites indicate derivation from Palaeoproterozoic protoliths. U-Pb zircon ages for granitoids in the Kamanjab inlier range between 1987 Ma and 1519 Ma (Burger et al., 1976; Burger and Coertze, 1973; Tegtmeyer and Kröner, 1985) and the deposition of the Neoproterozoic Damara sequence on its southwestern margin began with clastic sediments and interlayered felsic volcanic rocks dated at 756±2 Ma (U-Pb, Hoffman et al., 1996).

In the study area the crustal-scale sinistral Puros Shear Zone (PSZ) separates two units exhibiting different metamorphic and structural histories (Miller, 1983; Gruner, 2000; Goscombe et al., 2003a, b), namely the Western Kaoko Zone (WKZ) west of the PSZ and the Central Kaoko Zone (CKZ) east of the PSZ (Miller, 1983).

3.4 Rock types, metamorphic conditions and previous geochronology

The Eastern Kaoko Zone (EKZ) is situated east of the ST (Fig. 3.1) and is characterized by a Damara shelf sequence, whereas the basement rocks of the CKZ are partly covered by feldspathic and quartz-rich meta-arenites, metapelites and marbles, which were also correlated with the Damara sequence (Dürr and Dingeldey, 1996). The metasediments in the WKZ are more monotonous and consist of metapelites and marbles.

The metamorphic history was established from mineral assemblages in metapelites and shows a progressive increase, from east to west, from greenschist-facies at the ST to typical inverted Barrovian-type metamorphism reaching amphibolite-facies conditions at the PSZ (Guj, 1970). The WKZ rocks underwent high temperature/low pressure Buchan-type metamorphism accompanied by extensive partial melting (Dingeldey et al., 1994; Gruner, 2000; Goscombe et al., 2003a). Gruner (2000) calculated peak metamorphic conditions of 650±20 °C and 9±1.5 kbar for mica schists from the kyanite-sillimanite-muscovite zone in the westernmost part of the CKZ (conventional thermobarometrie, petrographic grids and calculation of pseudosections using the Gibbs method), whereas Goscombe et al. (2003a) provided PT estimates of 690±50 °C and 8.5±1.3 kbar for the same region (calculation from prograde garnet rims and matrix mineral cores, using Thermocalc v3.0). Garnet-cordierite migmatites of the WKZ were generated during peak metamorphic conditions at 700-830 °C and 6-6.3 kbar as calculated by Goscombe et al. (2003a) for garnet core compositions.

Seth et al. (1998) and Franz et al. (1999) dated zircon grains along a traverse following the Hoanib River valley to the Atlantic coast. That study yielded the oldest rocks so far known in Namibia with SHRIMP and Pb-Pb evaporation ages between 2584 and 2645 Ma (Seth et al., 1998) as well as Palaeoproterozoic ages of 1961 to 1985 Ma. The above authors also postulated

two Pan-African high-grade metamorphic events. A U-Pb zircon age of 656±8 Ma for an augengneiss of monzogranitic composition (Seth et al., 1998), and a U-Pb zircon age for a garnet gneiss of 645±4 Ma (Franz et al., 1999) were interpreted to represent a first high-grade event in the WKZ. A second event was dated at 564±13 Ma on zircon grains from an anatectic granite (Seth et al., 1998) and is in good agreement with recent Sm-Nd isotopic studies on garnets, dating peak metamorphism in the Puros area at 576±15 Ma (Goscombe et al., 2003a).

3.5 Structural evolution

A detailed structural analysis of the study area was undertaken by Konopásek et al. (2005), who recognized three phases of deformation. The first and second phases developed under ductile conditions during amphibolite- to granulite-facies metamorphism, whereas the third phase occurred during brittle-ductile conditions. The first phase (D_1) gave rise to a flat penetrative foliation (S_1), boudinage of amphibolitic layers (possibly mafic dykes) and isoclinal folds. The metamorphic foliation is probably related to southeastward thrusting of the WKZ over the CKZ. The second phase (D_2) folded the S_1 foliation and the boudins, and the associated S_2 foliation is either subvertical or dips steeply to the NE. D_2 developed kilometer-scale folds in both the WKZ and CKZ. Both phases of deformation created mineral lineations (L_1-L_2) generally plunging 10-20° NW. The vertical S_2 foliation and the shallow lineations suggest a transpressional tectonic regime during D_2, in which the PSZ was generated (Dürr and Dingeldey, 1996; Konopásek et al., 2005). Low-temperature retrogression and the development of kink folds were associated with the development of the sinistral Village Mylonite Zone (VMZ; Goscombe et al., 2003b) west of the PSZ (Fig. 3.2) during D_3. This shear zone is regarded as a younger branch of the PSZ and marks the contact between a porphyritic granite (Amspoort granite) to the west and paragneisses and augengneisses to the east. The last phase of deformation, D_3, reworked a migmatitic subvertical foliation S_2 under low-temperature brittle-ductile conditions (Konopásek et al., 2005).

3.6 Sample preparation, geochemistry and dating procedures

Fresh rock samples weighing about 5-6 kg were crushed and zircon grains were extracted by standard procedures using a jaw crusher, steel roller mill, magnetic separator and heavy liquids. Representative zircon grains with variable morphology, colour and size were handpicked, cast into a low-luminescent resin and sectioned into half. After polishing and carbon coating, the zircon grains were examined under cathodoluminescence (CL) on a JEOL microprobe at the University of Mainz. Operation conditions were 20 kV and 20 nA. Magmatic growth phases,

metamictization and metamorphic overgrowth can be revealed by CL images (Hanchar and Rudnick, 1995). Three different dating techniques using thermal ion mass spectrometry (TIMS) were employed, namely Pb-Pb evaporation, conventional U-Pb analysis following zircon dissolution after HF-vapour transfer, and conventional analysis after separation of U and Pb in ion exchange columns.

To classify the dated rocks, major element oxides were determined by XRF on fused glass discs at the University of Mainz, and the data are presented in Table 3.1. Rock names were derived using the triangular diagram of O'Connor (1965) after calculating the CIPW normative values for the feldspar components. Sample localities are shown in Fig. 3.2 and in Table 3.5.

Conventional U-Pb zircon dating: Single zircon grains or small fractions of 2-4 grains were analysed to minimize the effects of mixed populations and post-crystallization alteration using the HF-vapour transfer technique, developed by Krogh (1978) and Parrish (1987) and modified by Wendt and Todt (1991). In this method, morphologically identical grains are placed in separate holes at the bottom of a multisample teflon vessel. A detailed description of the technique including excellent agreement between the results obtained from conventional analyses and those obtained after vapour transfer is given in Wendt (1993). The advantage of the vapour transfer technique is fast processing because chemical separation of U and Pb is not required. Furthermore, procedural Pb blanks are reduced to a total blank value of ~3 pg Pb per zircon sample. The following Pb ratios were used for common Pb correction: $^{206}Pb/^{204}Pb$ = 18.15; $^{207}Pb/^{204}Pb$ = 15.63; $^{208}Pb/^{204}Pb$ = 38.14. Since the zircon grains were not weighted prior to decomposition, individual U and Pb concentrations could not be determined, but the use of a mixed $^{205}Pb/^{233}U$ spike solution allowed the U/Pb ratio to be calculated that is required to obtain U-Pb ages. In cases where the zircon grains contained high amounts of iron, U and Pb were separated using 20 µl columns with cation exchange resin. For these zircon grains additional Pb-blanks were measured and resulted in total blank values of less then 10 pg.

Isotopic measurements were carried out on a Finnigan-MAT 261 mass spectrometer, using a Secondary Electron Multiplier (SEM) and operated in peak-jumping mode The isotopic ratios reported in Table 3.2 were corrected for blank, spike, common Pb and instrumental mass fractionation of 3 ‰ per atomic mass unit as established by multiple analysis of NBS-981 and 982 standards during the course of this study. Age calculations are based on the decay constants proposed by Steiger and Jäger (1977). All errors are 2-σ (95 % confidence). The ISOPLOT program version 2.01 for Microsoft Excel of Ludwig (1999) was used to calculate best-fit lines and concordia intercept ages for the U-Pb isotopic data

Pb-Pb evaporation: This method, developed by Kober (1986, 1987), involves repeated evaporation and deposition of Pb from chemically untreated single zircon grains or small grain fractions in a double-filament arrangement. Our laboratory procedures as well as comparisons with conventional and ion-microprobe zircon dating are described in Kröner et al. (1991) and Kröner and Hegner (1998). Isotopic measurements were carried out on a Finnigan-MAT 261 mass spectrometer at the Max-Planck-Institut für Chemie in Mainz, using a Secondary Electron Multiplier (SEM) and operated in peak-jumping mode. The calculated ages and uncertainties are based on the means of all ratios evaluated and their 2-σ (mean) errors. Mean ages and errors for several zircon grains from the same sample are presented as weighted means of the entire population. Based on repeated analysis of an internal zircon standard, an error of about 0.2% is considered the best estimate for the reproducibility of our evaporation data. In the case of combined data sets, the 2-σ (mean) error may become very low, and whenever this error was less than the reproducibility of the internal standard, we have used the latter value.

The analytical data are presented in Table 3.3, and the $^{207}Pb/^{206}Pb$ values are shown in histograms (Figs. 3.6a-d). The evaporation technique provides only Pb isotopic ratios, and there is no *a priori* way to determine whether a measured $^{207}Pb/^{206}Pb$ ratio reflects a concordant age. However, comparative studies by evaporation, conventional U–Pb dating, and ion-microprobe analyses have shown reasonable agreement, even for zircon grains from complex metamorphic terrains (Kröner et al., 1991, 2001; Cocherie et al., 1992; Jaeckel et al., 1997; Karabinos, 1997).

SHRIMP II analyses: Single zircon grains of samples Na 00/04, 00/15 and 00/37 were handpicked and mounted in epoxy resin, together with chips of the Perth Consortium zircon standard CZ3. The handling procedure is described in Kröner *et al.* (1999). Isotopic analyses were performed on the Perth Consortium SHRIMP II ion microprobe. The analytical procedures are described in Compston et al. (1992), Claoue-Long et al. (1995), and Nelson (1997), and the analytical data are presented in Table 3.4. Errors for single analyses are 1-σ (63 % confidence), whereas pooled ages are reported at the 2-σ level. Regression line calculation was after Ludwig (1999).

Table 3.1. Chemical composition of samples dated in this study. Major elements in weight percent

Sample	Na 00/01	Na 00/04	Na 00/07	Na 00/10	Na 00/14	Na 00/15	Na 00/23	Na 00/28	Na 00/27	Na 00/37
SiO_2	65.02	66.77	65.66	61.81	71.83	70.16	70.45	75.99	67.62	76.40
Al_2O_3	17.09	14.63	15.52	16.30	13.91	14.09	13.38	12.22	14.53	10.99
Fe_2O_3	3.99	5.25	4.90	5.67	2.13	3.81	3.89	1.61	5.27	1.13
MnO	0.05	0.09	0.05	0.06	0.03	0.06	0.08	0.03	0.22	0.05
MgO	1.58	1.58	1.43	1.87	0.57	1.63	0.87	0.25	2.60	0.22
CaO	4.15	2.72	2.69	3.91	1.48	1.66	1.58	0.70	2.83	1.64
Na_2O	4.52	3.22	3.65	3.82	2.88	2.65	3.24	2.78	2.12	3.02
K_2O	2.00	3.34	4.01	3.94	5.36	4.32	4.33	5.62	2.53	4.51
TiO_2	0.48	0.72	0.74	0.84	0.33	0.60	0.64	0.33	0.93	0.23
P_2O_5	0.20	0.17	0.29	0.34	0.12	0.17	0.17	0.04	0.12	0.03
LOI	0.64	0.89	0.64	0.77	0.55	0.36	0.50	0.44	0.88	1.32
Total	99.72	99.38	99.58	99.33	99.19	99.51	99.13	100.01	99.65	99.54
An	19.28	12.38	11.45	15.81	6.56	7.13	6.73	3.21	13.26	3.19
Ab	38.25	27.25	30.89	32.32	24.37	22.42	27.42	23.52	17.94	25.55
Or	11.82	19.74	23.70	23.28	31.67	25.53	25.59	33.21	14.95	26.65
Rock type *	Tonalite	Grano-diorite	Granite	Grano-diorite	Granite	Granite	Granite	Granite	Grano-diorite	Granite

Sample	Na 115	Na 118/2	Na 124	Na 173	Na 428	Na 461	Na 532	Nd 137	Nd 149
SiO_2	74.44	66.20	72.62	74.18	75.82	69.39	61.17	77.22	70.88
Al_2O_3	14.66	16.37	13.68	13.78	13.12	13.70	15.14	12.39	14.89
Fe_2O_3	0.81	4.23	2.78	1.31	1.16	6.14	10.21	0.99	2.59
MnO	0.02	0.07	0.02	0.02	0.02	0.07	0.18	0.04	0.04
MgO	0.13	1.42	0.76	0.30	0.08	1.24	3.44	0.09	0.86
CaO	1.00	3.18	0.54	1.82	0.59	2.80	5.66	0.79	2.34
Na_2O	3.24	3.09	3.58	3.51	2.52	3.03	1.56	3.54	3.82
K_2O	4.85	4.32	4.97	4.12	6.09	2.06	2.89	4.44	2.99
TiO_2	0.09	0.61	0.39	0.15	0.29	0.84	1.39	0.10	0.47
P_2O_5	0.07	0.27	0.10	0.08	0.03	0.15	0.16	0.01	0.10
LOI	0.54	0.58	0.35	0.32	0.04	0.37	0.84	0.24	0.59
Total	99.85	100.34	99.79	99.59	99.76	99.79	102.64	99.86	99.56
An	4.50	14.01	2.03	8.51	2.73	12.91	25.88	3.85	10.96
Ab	27.42	26.15	30.29	29.70	21.32	25.64	13.20	29.95	32.32
Or	28.66	25.53	29.37	24.35	35.99	12.17	17.08	26.24	17.67
Rock type *	Granite	Granite	Granite	Granite	Granite	Grano-diorite	Grano-diorite	Granite	Grano-diorite

* The normative minerals Ab, An and Or, calculated from the CIPW norm, were plotted in the triangular diagram of O'Conner (1965) to obtain the rock type.

3.7 Zircon geochronology

The analysed rocks underwent amphibolite- (CKZ and WKZ, close to the PSZ) to granulite-facies metamorphism (westernmost part of the WKZ) at 575±15 Ma (Gruner, 2000; Goscombe et al., 2003a). However, only a few zircon grains seem to have been affected by this event, and conventional U-Pb dating has shown that most zircon grains record only one magmatic event, interpreted as the time of emplacement of the host protolith. Fig. 3.3 shows typical cathodo-

luminescence (CL) photographs of the dated samples. Figs. 3.3f-h show oscillatory zoning of typical zircon grains analysed in this study and confirming the above assumption. Only samples Na 00/27, Na 428, Na 532 and Na 00/23 seem to record two (or more) thermal events. CL-photographs of these zircon grains show a dark-coloured, inherited component (Figs. 3.3a-e, central part), and dark areas in CL are known to be enriched in U and Hf (e.g. Hanchar and Miller, 1993; Hanchar and Rudnick, 1995; Rubatto and Gebauer, 2000). The zircon grains of sample Na 00/01 are heavily fractured (Fig. 3.3a), and the bright CL at the margin of the grain shown in Fig. 3.3a is probably due to metamorphic overgrowth.

Several studies have shown that zircon grains are robust against resetting at high temperatures (Gulson and Krogh, 1973; Mezger and Krogstad, 1997; Möller et al., 2002) and thus keep at least a partial record of different thermal events (Kröner et al., 1994). On the other hand, zircon grains are known to lose Pb during major thermal events but also for no obvious geological reason (e.g. documented by recent Pb loss, Mezger and Krogstad, 1997). As a consequence, zircon grains with crystal damage, frequently caused by high U-contents, have a tendency to yield discordant U-Pb ages. All our U-Pb analyses define discordant data points and corresponding *minimum* ages. Most zircon grains experienced variable Pb-loss in recent times, and the $^{207}Pb/^{206}Pb$ ages therefore approximate the time of protolith emplacement.

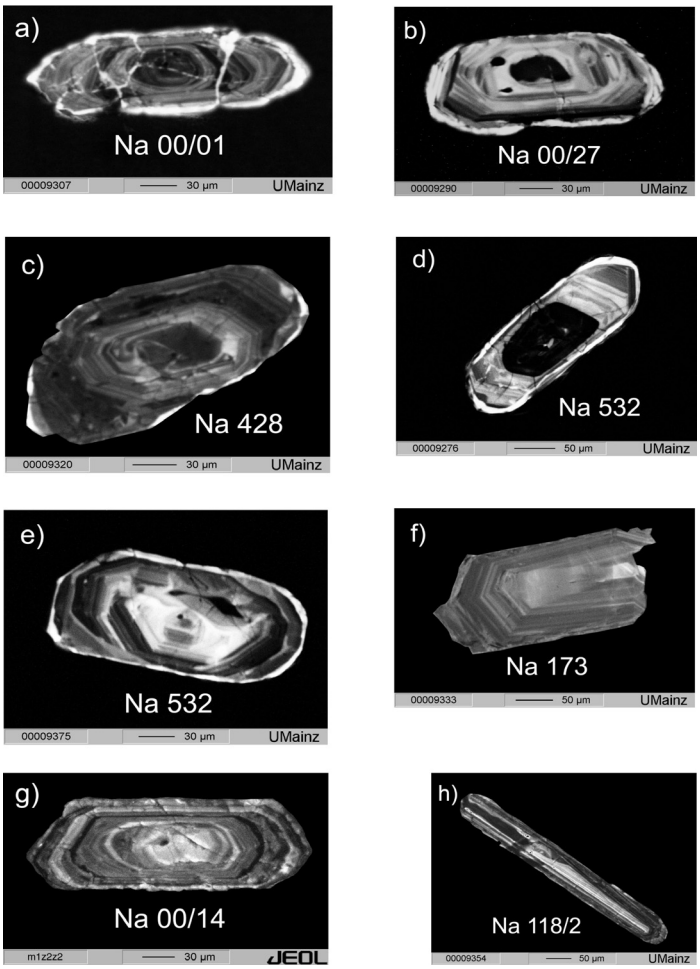

Figs. 3.3 a-h. Cathodoluminescence photographs from typical grains analysed in this study. Discussion chapter 3.8.

Table 3.2. Pb and U analytical data for conventional zircon analysis in granitic gneisses in Kaokoland, Namibia.

Central Kaoko Zone

No.	Sample	Isotopic ratios a)						Age [Ma], 2σ error		
		Utot Pb*	measured 206 Pb 204 Pb	207 Pb* 235 U	206Pb* 238 U	207 Pb* 206 Pb*	cor.	206 Pb* 238 U	207 Pb* 235 U	207 Pb* 206 Pb*
1	Na 00 01 L1	2.53	2691	6.4308±86	0.3322±25	0.1404±8	0.794	1849±12	2036±12	2232±10
2	Na 00 01 L5	2.78	2841	5.6202±36	0.3038±15	0.1342±2	0.957	1710±7	1919±5	2153±2
3	Na 00 01 L6	3.00	3079	5.3259±53	0.2803±26	0.1378±1	0.996	1593±13	1873±8	2199±1
4	Na 00 01 L2	5.14	8456	2.1513±13	0.1569±80	0.0994±7	0.992	939±4	1165±4	1613±1
5	Na 00 01 L3	2.80	1857	6.2088±49	0.2936±20	0.1534±22	0.977	1659±10	2005±7	2384±2
6	Na 00 01 L4	2.69	1533	6.2857±45	0.3031±19	0.1504±1	0.989	1707±9	2016±6	2350±2
7	Na 428 L3	3.53	712	3.4779±57	0.2235±31	0.1128±4	0.974	1301±16	1522±13	1845±6
8	Na 428 L5	2.58	1774	4.6471±362	0.2850±217	0.1182±2	1.000	1617±108	1758±65	1930±4
9	Na 428 L6	2.74	1042	4.4964±26	0.2749±11	0.1186±3	0.879	1566±6	1730±5	1935±4
10	Na 00 27 L1	3.14	2245	3.3485±63	0.2354±40	0.1032±2	0.994	1363±21	1492±15	1682±3
11	Na 00 27 L2	4.75	2051	2.2870±23	0.1862±14	0.0890±2	0.940	1101±7	1208±7	1405±5
12	Na 00 27 L4	4.10	3069	2.3721±21	0.1899±88	0.0906±4	0.739	1121±5	1234±6	1438±8
13	Na 00 27 L6 b)	4.28	728	2.8752±84	0.2041±46	0.1022±14	0.843	1197±24	1375±22	1664±26
14	Na 00 28 L2	9.83	846	1.1131±13	0.0860±78	0.0938±3	0.929	532±5	760±6	1505±7
15	Na 00 28 L4	3.24	739	3.2344±41	0.2566±20	0.0914±6	0.775	1472±10	1465±10	1455±11
16	Na 00 28 L5	5.61	682	1.9470±70	0.1474±45	0.0958±7	0.972	886±25	1097±24	1544±14
17	Na 00 28 L6	4.00	492	2.6992±36	0.2046±23	0.0957±4	0.943	1200±12	1328±10	1541±7
18	Na 00 23 L1	7.10	1237	1.4118±13	0.1222±7	0.0838±3	0.836	743±4	894±5	1287±8
19	Na 00 23 L2	5.28	431	1.9056±27	0.1580±11	0.0874±9	0.523	946±6	1083±10	1370±20
20	Na 00 23 L3	6.81	176	1.4868±20	0.1253±12	0.0860±15	0.465	761±7	925±8	1339±32
21	Na 00 23 L4	5.47	1698	1.9278±13	0.1566±7	0.0893±2	0.857	938±4	1091±5	1410±5
22	Na 00 23 L5	6.20	177	1.6535±43	0.1396±25	0.0859±29	0.427	843±14	991±17	1335±65
23	Na 00 23 L6	9.38	340	1.0374±9	0.0925±46	0.0813±5	0.577	571±3	723±5	1228±12

Western Kaoko Zone

No.	Sample	isotopic ratios a)						Age [Ma], 2σ error		
		Utot Pb*	measured 206 Pb 204 Pb	207 Pb* 235 U	206Pb* 238 U	207 Pb* 206 Pb*	cor.	206 Pb* 238 U	207 Pb* 235 U	207 Pb* 206 Pb*
24	NA 00 10 -1- L1	3.68	1523	2.7855±25	0.2155±15	0.0938±2	0.936	1258±8	1352±7	1503±5
25	NA 00 10 -1- L5	4.14	178	2.4345±54	0.1911±18	0.0924±23	0.315	1127±10	1253±16	1475±46
26	Na 00 10 -2- L1	4.40	1522	2.4676±21	0.1910±13	0.0937±2	0.942	1127±7	1263±6	1502±4
27	Na 00 10 -2- L3	4.38	1375	2.4915±71	0.1920±26	0.0941±16	0.591	1133±14	1270±20	1510±32
28	Na 00 10 -2- L5	4.28	1111	2.5516±19	0.1975±12	0.0937±2	0.938	1162±7	1287±5	1501±4
29	Na 00 10 -2- L6	3.65	861	2.8077±97	0.2174±47	0.0937±18	0.731	1268±25	1358±26	1501±36
30	Na 532 -1- L1	4.67	3019	2.2242±35	0.1816±20	0.0888±4	0.921	1076±11	1189±11	1400±9
31	Na 532 -1- L2	4.60	6840	2.2713±17	0.1841±12	0.0894±1	0.985	1090±6	1203±5	1414±2
32	Na 532 -1- L3	4.46	2398	2.3118±25	0.1852±136	0.0905±3	0.885	1096±7	1216±8	1436±7
33	Na 532 -1- L6	4.55	4697	2.2839±32	0.1847±19	0.0896±4	0.933	1093±10	1207±10	1418±8
34	Na 532 -2- L1	4.66	1917	2.1856±21	0.1796±12	0.0882±2	0.922	1065±7	1176±7	1388±5
35	Na 532 -2- L2	4.18	1965	2.5110±38	0.1944±14	0.0936±7	0.655	1146±8	1275±11	1501±15
36	Na 532 -2- L4	4.27	2074	2.3874±24	0.1898±13	0.0912±3	0.906	1121±7	1238±7	1450±6
37	Na 532 -2- L5	3.73	2218	3.0531±20	0.2197±11	0.1007±2	0.946	1281±6	1421±5	1637±3
38	Na 532 -1- L4 c)	13.11	1840	0.5845±30	0.0721±26	0.0588±1	0.886	449±2	467±2	559±4
39	Na 124 -1- L 1	7.76	154	1.4981±28	0.1076±8	0.1009±16	0.395	659±5	930±11	1641±29
40	Na 124 -1- L 2	7.61	1721	1.5301±61	0.1125±12	0.0986±29	0.312	687±7	942±24	1598±54
41	Na 124 -1- L 3	4.31	2995	2.7761±50	0.1953±16	0.1031±1	0.611	1150±8	1349±13	1680±18
42	Na 124 -1- L 4	6.40	3575	1.8321±53	0.1308±11	0.1016±20	0.368	792±6	1057±19	1653±36
43	Na 124 -1- L 6	6.00	4438	1.9704±28	0.1402±13	0.1019±5	0.892	846±7	1105±9	1660±9
44	Na 461 -1- L 1	12.4	2698	0.9683±12	0.0696±4	0.1010±7	0.658	433±3	688±6	1642±13
45	Na 461 -1- L 2	5.73	940	2.0467±105	0.1470±24	0.1009±38	0.376	884±14	1131±35	1641±69
46	Na 461 -1- L 4	3.79	3198	3.1074±28	0.2183±14	0.1032±3	0.918	1273±7	1435±7	1683±5
47	Na 461 -1- L 5	4.08	3298	2.9175±29	0.2070±10	0.1022±5	0.665	1213±5	1386±8	1665±10
48	Na 461 -1- L 3 b)	1.09	1283	11.1615±133	0.7778±45	0.1041±7	0.619	3709±16	2537±11	1698±13
49	ND 137 L1	16.7	94	0.4083±10	0.0489±4	0.0605±19	0.22	308±3	348±7	621±67
50	ND 137 L2	16	102	0.4526±74	0.0526±3	0.0623±15	0.23	331±2	379±5	685±51
51	ND 137 L3	18.8	96	0.3765±11	0.0447±4	0.0610±23	0.18	282±2	324±8	639±80
52	ND 137 L5	17.7	77	0.3681±9	0.0440±4	0.0607±18	0.23	278±2	318±7	627±64
53	ND 137 L6	13	119	0.5472±13	0.0632±1	0.0627±18	0.23	396±3	443±9	698±59
54	ND 149 -1- L2	14.63	456	0.5077±3	0.0580±2	0.0635±3	0.621	364±1	417±2	724±10
55	ND 149 -1- L3	22.52	249	0.3415±2	0.0385±1	0.0642±4	0.454	244±1	298±2	748±15

56	ND 149 -1- L4	27.83	178	0.2695±3	0.0312±1	0.0626±9	0.288	198±1	242±2	695±30
57	ND 149 -1- L5	14.44	122	0.5287±10	0.0598±7	0.0640±12	0.498	375±4	431±7	743±38
58	ND 149 -1- L6	26.24	87	0.2876±45	0.0332±2	0.0628±12	0.338	211±2	257±2	700±41
59	ND 149 -2- L2	18.11	82	0.4300±30	0.0489±14	0.0638±122	0.107	308±9	363±21	734±360
60	ND 149 -2- L3	19.44	80	0.3847±8	0.0432±4	0.0645±23	0.196	273±2	331±6	758±73
61	ND 149 -2- L4	15.15	183	0.5245±8	0.0597±3	0.0637±12	0.264	374±2	428±6	733±40
62	ND 149 -2- L5	22.70	129	0.3428±13	0.0398±7	0.0625±23	0.390	252±4	299±10	690±75
63	ND 149 -2- L6	11.11	131	0.6922±17	0.0767±9	0.0654±15	0.400	477±5	534±10	788±48
64	Na 115 L1	38.12	185	0.1933±101	0.0238±3	0.0588±35	0.200	152±2	179±9	561±125
65	Na 115 L2	39.61	143	0.1861±2	0.0230±1	0.0588±7	0.394	146±1	171±2	560±26
66	Na 115 L3	49.06	118	0.1518±2	0.0186±19	0.0592±13	0.379	119±1	144±3	575±48
67	Na 115 L4	42.20	146	0.1756±3	0.0213±1	0.0598±13	0.262	136±1	164±3	597±45
68	Na 115 L5	45.22	161	0.1641±2	0.0200±2	0.0595±11	0.409	128±1	154±2	587±40
69	Na 115 L6	41.07	127	0.1760±9	0.0216±3	0.0592±38	0.155	138±2	165±8	574±133
70	Na 115 -2- L5	23.10	217	0.3155±4	0.0377±1	0.0606±5	0.677	239±2	278±3	626±20
71	Na 115 -2- L6	34.91	108	0.1973±3	0.0250±1	0.0573±12	0.171	159±1	183±2	503±46
72	Na 173 -1- L 2	10.4	1997	0.6243±336	0.0778±36	0.0582±9	0.943	483±22	493±21	536±35
73	Na 173 -1- L 4	13.3	1037	0.5082±6	0.0632±5	0.058359	0.809	395±3	417±4	543±12
74	Na 173 -1- L 6	15.1	468	0.4843±8	0.0603±4	0.0583±8	0.425	377±2	401±6	541±30
75	Na 173 -2- L3	14.5	1491	0.4837±3	0.0603±2	0.0582±1	0.862	377±2	401±2	538±5

Phalaborwa Standard d)

87	Pal L3	1.63	11949	5.8196±81	0.3328±44	0.1268±1	0.997	1852±21	1949±12	2055±2
88	Pal L4	1.59	5168	5.6230±219	0.3215±121	0.1268±2	0.999	1797±59	1919±33	2055±3
89	Pal L5	2.51	3339	5.8738±120	0.3340±63	0.1276±4	0.990	1857±30	1957±17	2065±5

a) corrected for fractionation, blank, spike and common Pb

b) not considered for age calculation

c) metamorphic zircon

d) Phalaborwa. Mean age 2055.6±8.9 Ma. Precise age 2060.6±0.5 Ma [U-Pb, 2s-mean error]. T. Reischmann, S.Afr.J.Geol.,1995,98(1),1-4

* radiogenic lead

2σ errors refer to 2s standard deviation of the last 2-3 digits

3.7.1 Granitoids of the Central Kaoko Zone

3.7.1.1 Gomatum Valley

Strongly foliated gneiss sample Na 00/37 was collected in the Gomatum valley (Fig. 3.2), is of granitic composition (Table 3.1) and is composed of quartz, K-feldspar, plagioclase, and white mica. The zircon grains are clear to light brown, long-prismatic and have slightly rounded terminations. Five grain spots were analysed on SHRIMP II of which one is almost concordant

whereas the remaining four are variably discordant (Table 3.4) but define a discordia line (MSWD = 0.09) suggesting Pb-loss in recent times. The mean $^{207}Pb/^{206}Pb$ age of all five grains is 1776±2 Ma, and the upper concordia intercept age is identical, but less precise, at 1776±19 Ma (Fig. 3.4a). We interpret the age of 1776±2 Ma to most closely reflect the time of emplacement of the gneiss protolith.

Strongly foliated tonalitic gneiss sample Na 00/01 (Table 3.1, Fig. 3.2) has been collected in abroad antiform in Gomatum Valley and is composed of quartz, plagioclase and K-feldspar. The brownish zircon grains are long-prismatic with rounded terminations (Fig. 3.3a), and five single grains were analysed after U-Pb separation, yielding discordant $^{207}Pb/^{206}Pb$ ages between 2153 and 2384 Ma. One grain provided a $^{207}Pb/^{206}Pb$ age of 1613±1 Ma (Table 3.2, No. 4). No alignment of these analyses in the concordia diagram is obvious, and this may be due to a combination of Pb-loss and zircon growth at variable times. Alternatively, the older grains are xenocrysts or have xenocrystic cores, as can be seen in CL images, and the protolith emplacement age is 1613 Ma. No definite intrusion age for the gneiss protolith could therefore be determined.

A sample of reddish, migmatitic granodioritic gneiss (Na 00/04) was collected at the westernmost termination of Gomatum Valley (Table 3.1, Fig. 3.2). The rock-forming minerals are quartz, K-feldspar, plagioclase and biotite. The zircon grains are light brown, long-prismatic and have slightly rounded terminations. Four zircon grains were dated on SHRIMP II of which two are concordant and two slightly discordant (Table 3.4), yielding a combined mean $^{207}Pb/^{206}Pb$ age of 1752±3 Ma. The data can be fitted to a discordia line through the origin (MSWD = 0.02) with an upper concordia intercept at 1750±23 Ma (Fig. 3.4b). The zircon grains show no effect of younger overprint and obviously crystallized during emplacement of the gneiss protolith. The age is in the same range as for sample Na 00/37, in fact, the two concordia intercept ages overlap within their errors. It is therefore likely that these two gneisses were derived from the same granitoid pluton.

Another fine-grained grey gneiss (sample Na 00/27), exposed east of the Puros Shear Zone (Fig. 3.2) is of granodioritic composition (Table 3.1) and consists of quartz, K-feldspar, plagioclase and biotite. The zircon grains are clear to light yellow, long-prismatic with rounded terminations. Three grains were analysed after separation of U and Pb and yielded discordant results whose alignment (MSWD = 0.60) resulted in concordia intercept ages of 1979±38 and 849±19 Ma (Table 3.2, Fig. 3.5a). The upper intercept is interpreted to approximate the time of protolith emplacement, whereas the lower intercept does not seem to be due to major thermal event and may be fortuitous.

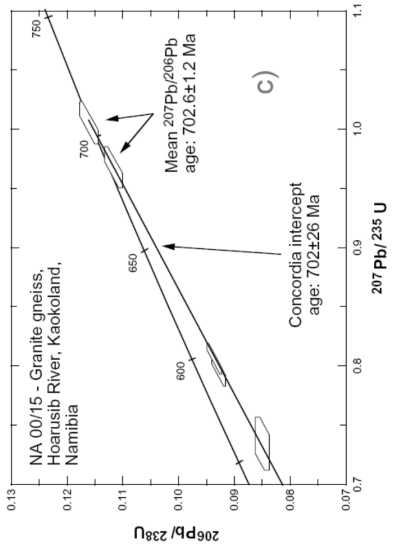

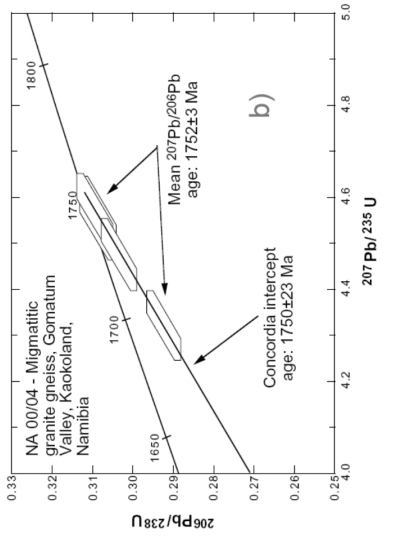

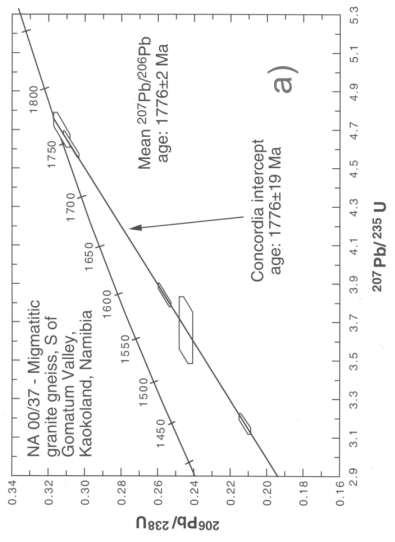

Figs. 3.4a-c. Concordia diagrams showing U-Pb zircon ages derived from SHRIMP analyses.

3.7.1.2 Hoarusib Valley

Granitic gneiss sample Na 00/23 was collected on the northern side of Gomatum Valley in the Hoarusib Valley (Fig. 3.2) and consists of quartz, K-feldspar, plagioclase and biotite. The zircon grains are clear to light yellow, long-prismatic and have slightly rounded terminations. Regression of four variably discordant analyses (Table 3.2) yielded concordia intercept ages of 1448±31 and 193±25 Ma (MSWD = 1.09, Fig. 3.5b). The upper intercept provides a minimum estimate for the emplacement of the original granite, whereas the lower intercept probably resulted from Pb-loss at variable times and has no geological significance.

3.7.1.3 Area between Gomatum and Hoanib Valleys

Migmatitic granite-gneiss sample Na 00/28 (Table 3.1) was collected in a synformal structure (Fig. 3.2) and, on the basis of field interpretation, belongs to the same rock unit as samples Na 00/04 and Na 00/37 (Goscombe et al., 2003a; Konopásek et al., 2005). The zircon grains are yellow-brown, long-prismatic having slightly rounded terminations. U-Pb analysis of three zircon grains each after U and Pb separation produced discordant results that can be fitted to a regression line (MSWD = 1.90) with concordia intercepts at 1550±10 Ma and 35±11 Ma. A further grain from this sample has an almost concordant $^{207}Pb/^{206}Pb$ age of

1468±10 Ma (Fig. 3.5c, Table 3.2, No 15). All four analyses together plot on a discordia line with an imprecise upper intercept at 1516±54 Ma. The older upper intercept may be a result of small inherited components (xenocrystic cores) in the analyzed discordant zircon grains. Since sample Na 00/28, though lithologically similar to Na 00/04 and 00/37, reveals a significantly different magmatic age for its granitic protolith it cannot be derived from the same pluton as the other two samples. Nevertheless, structural observations suggest that this igneous rock belongs to the same tectonic unit.

Sample Na 428 was collected in a large antiform east of the Puros Shear Zone (Fig. 3.2) and represents a well-foliated granitic gneiss (Table 3.1) consisting of quartz, K-feldspar, plagioclase, biotite and minor sphene. The zircon grains are yellow-brownish, long-prismatic and have rounded terminations, a typical feature generally found in medium to high grade rocks. Three zircon grains were analysed and produced variably discordant and poorly aligned isotopic ratios (Table 3.2) whose regression (MSWD=2.00) yielded concordia intercept ages of 2028±15 Ma and 492±38 Ma (Fig. 3.5d). The upper intercept probably approximates the time of protolith emplacement, whereas the lower intercept is probably the combined result of Pb-loss and new zircon growth during a pervasive late Pan-African metamorphic event and will be further discussed below.

3.7.2 Granitoids from the Western Kaoko Zone

3.7.2.1 Hoarusib Valley

Sample Na 00/07 is an augengneiss plotting in the granite field in the triangular diagram of O'Connor (1965) and is composed of quartz, rotated K-feldspar, plagioclase, biotite and minor hornblende. Zircon grains are yellow-brown, long-prismatic, and the terminations are slightly rounded. Evaporation of four single grains produced a combined mean $^{207}Pb/^{206}Pb$ age of 1513±1 Ma (Table 3.3, Fig. 3.6b), which is interpreted to reflect the time of protolith emplacement.

A large body of granodioritic augengneiss occurs west of the Puros Shear Zone and is represented by sample Na 00/10 (Table 3.1) collected in the Hoarusib River (Fig. 3.2). Xenoliths of this gneiss usually occur in 'red' migmatites, suggesting that the original extent of the augengneiss was considerable, and gneissification apparently predated migmatization. The rock contains quartz, plagioclase, K-feldspar and hornblende. The zircon grains are yellow-brown, long-prismatic and have slightly rounded terminations. Isotopic analysis, after separation of U and Pb, of six zircon grains yielded near-concordant results and an upper concordia intercept age of 1502±3 Ma (MSWD=0.41, Table 3.2, Fig. 3.5e) that we interpret to approximate the time of granodiorite

intrusion. In addition, this rock has been dated by the Pb-Pb evaporation method whereby four grains yielded a slightly younger combined mean $^{207}Pb/^{206}Pb$ age of 1489±1 Ma (Fig 3.4b). This age difference may be the result of a small amount of metamorphic overgrowth on some zircon grains which can bee seen in CL images.

Minor grey granodioritic migmatite (Table 3.1) is represented by sample Na 461 (Fig. 3.2). The rock is composed of quartz, plagioclase, K-feldspar and biotite, and the zircon grains are yellow-brown, long-prismatic and have rounded terminations. Four grains were analyzed after U-Pb separation and produced discordant data points (Table 3.2) regression of which (MSWD = 2.50) yielded concordia intercept ages of 1684±8 and 24±12 Ma respectively (Fig. 3.5f). As in previous samples, we consider the upper intercept age to approximate the time of protolith emplacement, whereas the lower intercept reflects recent Pb-loss. Analysis L3 of sample Na 461 (Table 3.2, No. 48) plots well above the concordia curve, but on the regression line defined by the other analyses, thus confirming the significance of the upper intercept ($^{207}Pb/^{206}Pb$ age = 1698±13 Ma). Inclusion of this sample in the regression calculation reduces the MSWD to 1.8 and the intercept ages become 1685±7 Ma and 26±11 Ma. This zircon was probably not completely dissolved in the teflon vessel, resulting in a relatively high U/Pb ratio of 11.2 and apparent U-gain.

Fine-grained grey migmatitic granodiorite-gneiss sample Na 532 (Table 3.1) was collected west of the PSZ (Fig. 3.2) and is composed of quartz, K-feldspar, plagioclase, biotite and minor garnet. The zircon grains are yellowish, long-prismatic and the terminations are rounded. Eight variably discordant but well aligned zircon grains (Table 3.2) define a discordia line (MSWD = 1.9) with concordia intercept ages of 2008±19 Ma and 835±10 Ma (Fig. 3.5g), virtually identical to those calculated for sample Na 00/27. The lower intercept ages of 835 Ma and 849 Ma for sample Na 00/27 and Na 532 (Figs. 3.5a, f) are difficult to interpret since no thermal event of this age is so far known from the Kaoko Belt. It is possible that the discordance patterns observed in these samples is either due to variable Pb-loss at unspecified times, or is due to a mixture of various age components (old core, young rim, Figs. 3.3d, e), or both, and in this case the lower intercept has uncertain geological significance. The upper intercept age for zircon grains from sample Na 532 is interpreted to approximate the time of protolith emplacement. One discordant grain showing the same morphology as the others has a minimum $^{207}Pb/^{206}Pb$ age of 559±4 Ma, and its relatively high U/Pb ratio of 13.1 suggests late magmatic growth in a U-rich environment, probably during migmatite formation (Table 3.2, No. 38).

Leucocratic pegmatitic melt patches consisting of quartz, K-feldspar and muscovite, fill the necks of D_2-boudins and are abundant in migmatites of sedimentary and magmatic origin between the Hoarusib and Khumib valleys. This rock is represented by sample Na 173 (Table 3.1), collected close the VMZ (Fig. 3.2). The zircon grains are yellowish, euhedral and long-prismatic,

and four single zircon grains were analysed after separation of U and Pb and yielded discordant results (Table 3.2) that define a regression line (MSWD = 0.12) with an upper concordia intercept age of 539±6 Ma (Fig. 3.5h). We interpret this to reflect a phase of decompression melting after the peak of regional high-grade metamorphism (Konopásek et al., 2005).

An inhomogeneously foliated pluton, represented by porphyritic monzogranite, is widespread in the WKZ and is known as Amspoort granite after an occurrence in the Hoanib River. It was previously dated by Pb-Pb evaporation at 551.9±1.5 Ma (Seth et al., 1998). Our sample Na 00/14 comes from an occurrence in the Hoarusib Valley (Fig. 3.2), whereas sample Na 118/2 was collected farther north, between the Hoarusib and Khumib Valleys (Fig. 3.2). At locality Na 118/2 this granite is undeformed, whereas at most localities in the area studied this rock-type was strongly foliated during late D_2-D_3. The matrix consists of plagioclase, quartz and biotite. The zircon grains in both samples are yellow-brown, euhedral and long-prismatic. Three homogeneous fractions of three to four zircon grains each from sample Na 00/14 were evaporated individually and produced identical $^{207}Pb/^{206}Pb$ ratios with a mean age of 550±1 Ma, whereas three similar grain fractions from sample 118/2 yielded a mean $^{207}Pb/^{206}Pb$ age of 549±4 Ma (Table 3.3, Figs. 3.6c, d). These two results are identical within error and confirm the age obtained by Seth et al. (1998).

The oldest dated Neoproterozoic plutonic rock of granodioritic composition in the WKZ occurs in the lower Hoarusib River and is represented by sample Nd 149 (Table 3.1, Fig. 3.2). The rock is composed of quartz, plagioclase, K-feldspar and biotite and the zircon grains are yellow-brown, long-prismatic with slightly rounded terminations. Analysis of ten grains resulted in variably discordant and poorly aligned data points (Table 3.2, Fig. 3.5i) which can be fitted to a regression line (MSWD = 3.20) suggesting recent Pb-loss and an upper concordia intercept age of 730±15 Ma. We consider this to approximate the time of early Pan-African granodiorite emplacement.

Granitic sample Nd 137 was collected about 500 m southeast of sample Nd 149 (Fig. 3.2). The rock is composed of quartz, K-feldspar, plagioclase and biotite and the zircon grains are yellowish, long-prismatic with slightly rounded terminations. Five grains analysed after dissolution and separation of U and Pb define a poorly aligned discordia (MSWD=2.1) with an upper concordia intercept at 661±21 Ma, and again this age is interpreted to approximate the time of the emplacement of the granite.

Reddish, strongly foliated granitic gneiss sample Na 115 (Table 3.1) was collected about 500 m west of Nd 137 (Fig. 3.2) and contains quartz, plagioclase, K-feldspar and biotite. The zircon grains are yellow-brown, long-prismatic with slightly rounded terminations. Seven grains were analyzed after U-Pb separation and produced discordant data points (Table 3.2) regression of

which (MSWD=1.50) yielded concordia intercept ages of 655±39 and 24±12 Ma respectively (Fig. 3.5k). Here again the older age most likely reflects the time of emplacement of the granitic protolith whereas the near-zero age may be the result of combined Pb-loss in recent times and at unspecified times in the past.

Table 3.3. Isotopic data from single grain zircon evaporation.

Sample no.	Zircon colour and morphology	Grain no.	Mass scansa)	Mean 207 Pb/ 206 Pb ratio and 2-σm error b)	^{207}Pb/ ^{206}Pb age and 2-σm error
Na 00/07	yellow-brown, long-prismatic, ends slightly rounded		154	0.094058±52	1509±1
			178	0.094441±25	1517±1
			155	0.094007±22	1508±1
			193	0.094361±29	1515±1
mean of 4		1-4	680	**0.094232±21**	**1513±1**
Na 00/10	yellow-brown, long-prismatic, ends slightly rounded		191	0.092720±39	1482±1
			126	0.093274±86	1482±1
			169	0.093292±62	1494±1
			99	0.093083±50	1490±1
mean of 4		1-4	585	**0.093066±35**	**1489±1**
Na 00/14	brownish, long-prismatic, ends rounded		177	0.058488±47	548±2
			99	0.058688±35	549±1
			111	0.058511±24	555±2
mean of 3		1-3	387	**0.058546±25**	**550±1**
Na 118/2	brownish, long-prismatic		112	0.058423±161	546±6
			82	0.058540±122	550±5
			112	0.058553±122	551±5
mean of 3		1-3	306	**0.058502±103**	**549±4**

a) Number of 207 Pb / 207 Pb ratios evaluated for age assesssment

b) Observed mean ratio corrected for nonradiogenic Pb where necessary. Errors based on uncertainties in counting statistics

3.7.2.2 Khumib River Valley

Coarse-grained, migmatized, reddish granititic gneiss sample Na 124 (Table 3.1) was collected close to the VMZ (Fig. 3.2) and is composed of equigranular-polygonal quartz, K-feldspar and biotite. The zircon grains are yellow-brown, long-prismatic with slightly rounded terminations. Five grains were analysed after vapour dissolution and yielded variably discordant but well aligned isotopic ratios defining a regression line (MSWD=0.53) with concordia intercepts at 1701±38 and 66±52 Ma respectively (Table 3.2, Fig. 3.5l). As in the previous cases, we interpret the upper intercept to approximate the time of protolith intrusion, whereas the near-zero lower intercept may be the result of combined Pb-loss in recent times and at unspecified times in the past.

Finally, a ductilely deformed granitic gneiss was sampled in the Khumib River Valley (Fig. 3.2), and our sample Na 00/15 (Table 3.1) consists of strongly aligned quartz, K-feldspar, plagioclase, biotite and minor garnet. SHRIMP-analysis of five grains yielded one concordant and one near-concordant point (mean $^{207}Pb/^{206}Pb$ age = 702.6±1.2 Ma), whereas the other three data points are between 30 and 40 % discordant (Table 3.4) but are aligned along a regression line (MSWD = 0.09), suggesting recent Pb-loss and with all five data points defining an upper concordia intercept age of 702±26 Ma (Fig. 3.4c). We consider the concordant age of 703±1 Ma to most closely approximate the time of intrusion of the gneiss protolith.

3.8 Proposed tectonostratigraphic subdivision of the Kaoko Belt

Combining the above results, the data of Seth et al. (1998) and the ages of Franz et al. (1999) with our structural observations in the Gomatum-Hoarusib area, six age groups can be identified in three major tectonic units in the central Kaoko Belt:

a) A late Archaean to Palaeoproterozoic unit (ages of 2616-2545 Ma and 2028-1961 Ma) constitutes the meta-igneous basement and occurs mostly in the Central Kaoko Zone.
b) A Palaeo- to Mesoproterozoic unit (ages of 1776-1684 Ma and 1516-1448 Ma) makes up a migmatitic basement at the eastern margin of the Western Kaoko Zone and constitutes a large, folded body in the central part of the Central Kaoko Zone.
c) A Neoproterozoic unit (ages of 730-550 Ma) occupies the rest of the Western Kaoko Zone. A crustal melt derived from the older migmatites of the eastern part of the Western Kaoko Zone provided an age of 539 Ma.

Two models for the subdivision of the Kaoko Belt have been discussed in the literature:

a) Miller (1983) proposed subdivision of the belt into three tectonostratigraphic units (EKZ, CKZ and WKZ), bordered by two major structural discontinuities: the Puros Lineament and the Sesfontein Thrust (Fig. 3.1).
b) Dingeldey et al. (1994) suggested subdivision of the region west of the Sesfontein Thrust into three tectono-metamorphic domains namely the Eastern, Central and Western Zones.

Our fieldwork and age data do not confirm the subdivision established by Dingeldey et al. (1994), and we consider the PSZ to mark an important structural and metamorphic boundary. A second important lineament, the Village Mylonite Zone, is defined by field observations and satellite imagery. This discontinuity is also recorded in our age data (Fig. 3.7), since there is a distinct boundary between Neoproterozoic rocks west and Mesoproterozoic rocks east of it (see below). This corresponds to the boundary between the Western and Central Zones as proposed by Dingeldey et al. (1994).

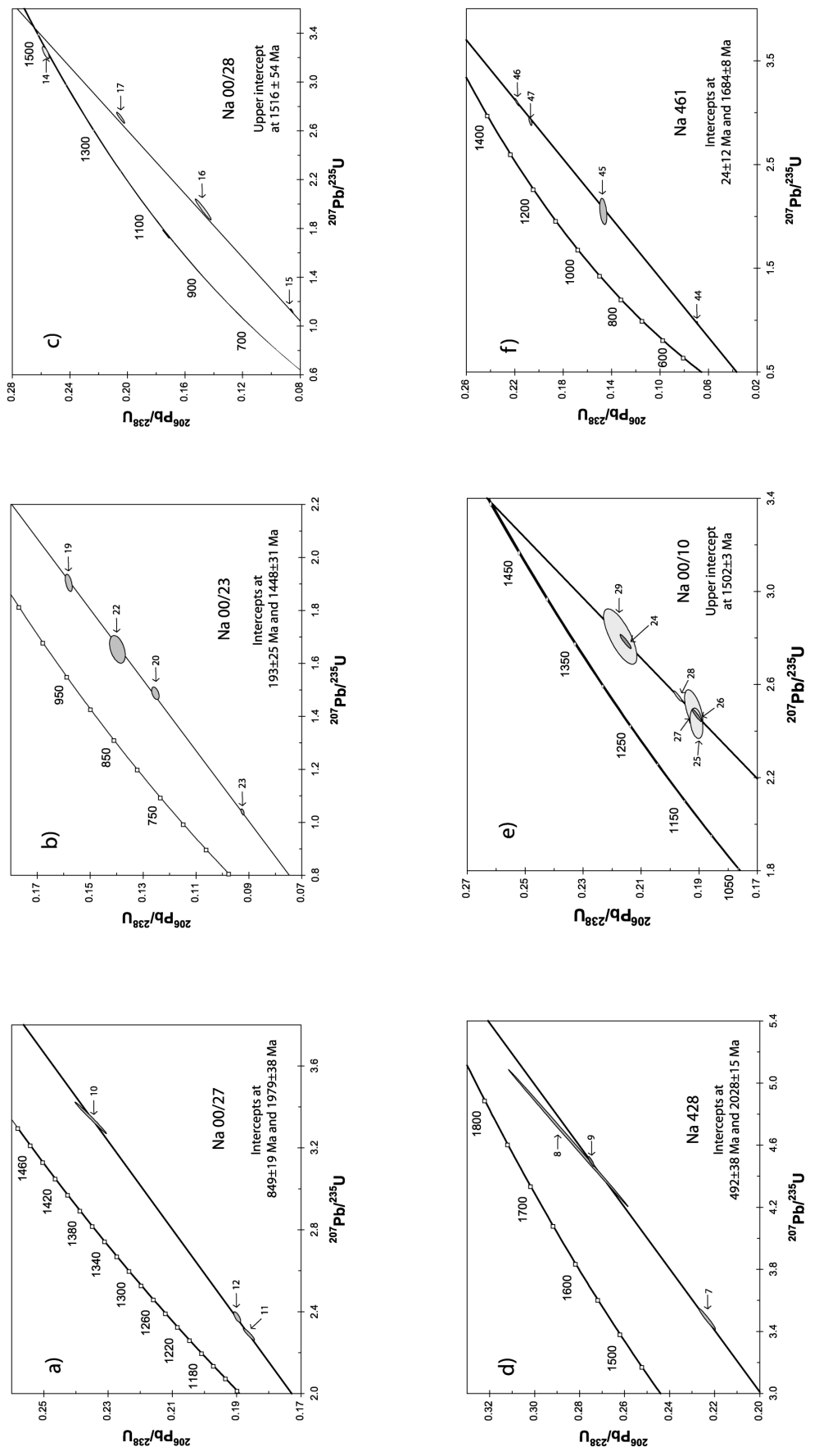
a)
Na 00/27
Intercepts at
849±19 Ma and 1979±38 Ma
b)
Na 00/23
Intercepts at
193±25 Ma and 1448±31 Ma
c)
Na 00/28
Upper intercept
at 1516 ± 54 Ma
d)
Na 428
Intercepts at
492±38 Ma and 2028±15 Ma
e)
Na 00/10
Upper intercept
at 1502±3 Ma
f)
Na 461
Intercepts at
24±12 Ma and 1684±8 Ma
$^{206}Pb/^{238}U$
$^{207}Pb/^{235}U$

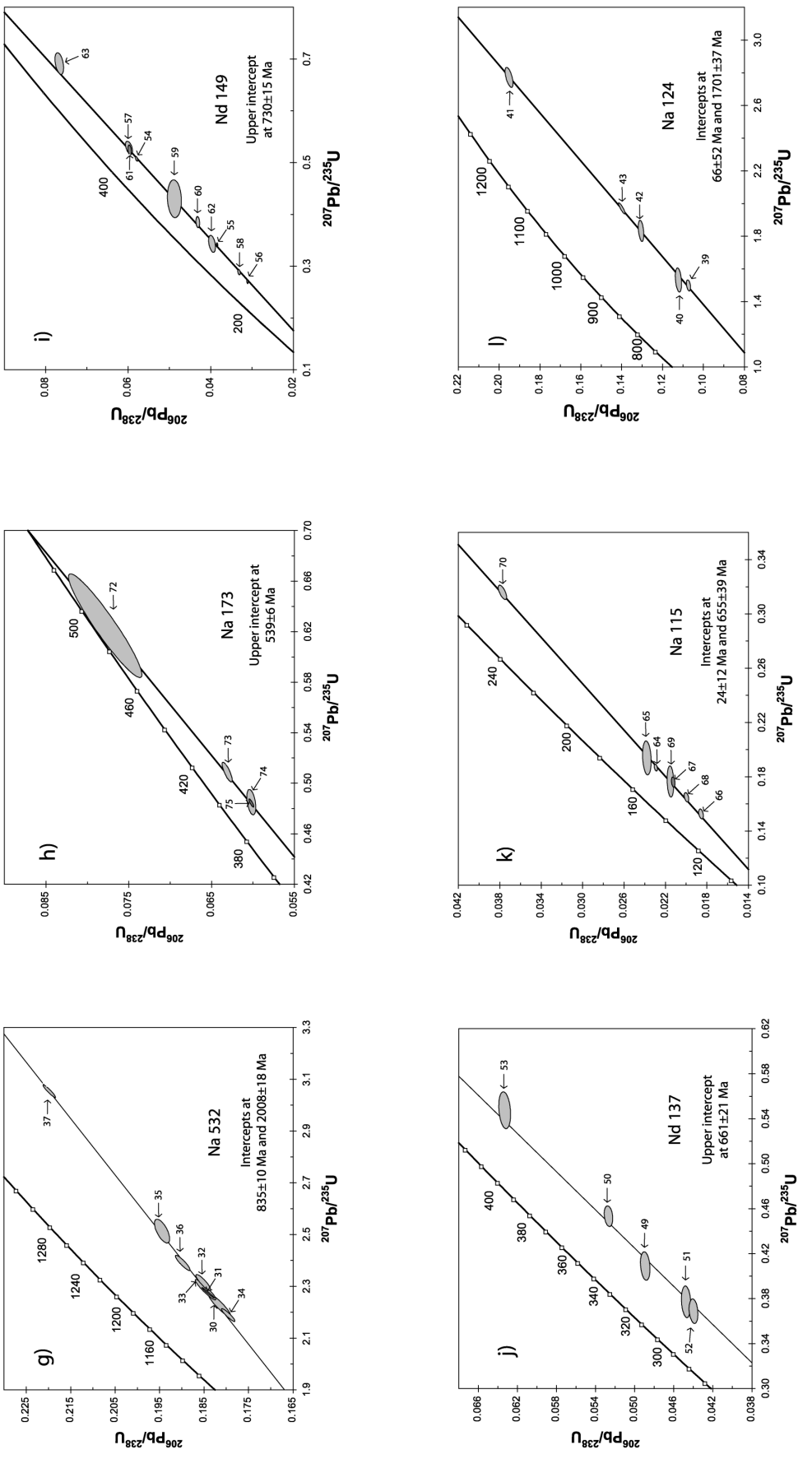

Fig. 3.5. Concordia diagrams a) - l) showing U-Pb isotopic ratios and ages for the granitoid gneisses. Error ellipses are based on 2s errors.

Table 3.4. SHRIMP II analytical data for spot analyses of single zircons from granitoid gneisses in Kaokoland, Namibia*.

Samle No.	U ppm	Th ppm	206Pb / 204Pb	208Pb / 206Pb	207Pb / 206Pb	206Pb / 238U	207Pb / 235U	206/238 age ± 1σ	207/235 age ± 1σ	207/206 age ± 1σ
Na 00/04.1	197	196	18044	0.2864± 24	0.1073± 9	0.2921±42	4.321± 76	1652±21	1697±14	1754±15
Na 00/04.2	192	157	53926	0.2362± 21	0.1070± 8	0.3032±44	4.475± 78	1707±22	1726±14	1750±14
Na 00/04.3	149	125	26410	0.2551± 31	0.1071±13	0.3085±45	4.555± 91	1733±22	1741±16	1751±21
Na 00/04.4	164	140	47943	0.2473± 23	0.1072± 9	0.3092±45	4.570± 81	1737±22	1744±15	1752±15
Na 00/15.1	633	129	11548	0.0659± 11	0.0624± 5	0.0928±13	0.797± 14	572± 8	595± 8	686±18
Na 00/15.2	805	170	389	0.0732± 36	0.0627±15	0.0850±12	0.735± 22	526± 7	559±13	699±52
Na 00/15.3	471	240	18211	0.1517± 13	0.0628± 5	0.1161±17	1.005± 18	708±10	706± 9	702±18
Na 00/15.4	780	88	850340	0.0414± 4	0.0625± 3	0.0936±13	0.806± 13	577± 8	600± 7	692±11
Na 00/15.5	467	205	17329	0.1315± 14	0.0629± 6	0.1116±16	0.968± 17	682± 9	687± 9	704±19
Na 00/37.1	548	211	14071	0.1402± 12	0.1085± 6	0.2561±36	3.831± 61	1470±19	1599±13	1775±10
Na 00/37.2	127	123	22669	0.2779± 29	0.1085±11	0.3125±46	4.677± 89	1753±23	1763±16	1775±19
Na 00/37.3	588	388	2331002	0.1912± 9	0.1087± 4	0.3074±44	4.606± 70	1728±22	1750±13	1778± 7
Na 00/37.4	261	92	7229	0.1455± 17	0.1086± 9	0.2118±30	3.171± 55	1238±16	1450±13	1776±14
Na 00/37.5	26.4	33.6	10593	0.5637±136	0.1084±45	0.2442±40	3.650±170	1409±21	1561±37	1773±76

* 04.1 is spot on grain 1, 04.2 is spot on grain 2, etc.

3.8.1 Late Archaean to Palaeoproterozoic basement of the Central Kaoko Zone

The unit consists of interlayered late Archaean to Palaeoproterozoic granitoid gneisses and forms the structurally lowermost basement in Gomatum Valley, similar to the Hoanib section farther south (Seth et al., 1998; Franz et al., 1999). This basement is exposed in the core of a large anti-form east of the PSZ as well as in the eastern part of Gomatum Valley (Figs. 3.7, 3.8) where it was dated by Seth (1999) at 1965±1 Ma. A large body of younger granitoid gneiss is exposed in the synform between these two structures (Fig. 3.8), and its position is discussed in the next section.

3.8.2 Palaeo- to Mesoproterozoic basement in the eastern part of the Western Kaoko Zone and in the Central Kaoko Zone

A large body of deformed Meso- to Palaeoproterozoic granitoid gneisses exposed in the central part of the CKZ witnessed early thrusting during the Pan-African evolution of the Kaoko Belt. This body structurally overlies the older Archaean to Palaeoproterozoic basement, and the two units are separated from each other by a sequence of metasediments (Guj, 1970; Goscombe, 2003; Konopásek et al., 2005). We interpret these Palaeo- to Mesoproterozoic gneisses as an allochthonous slab, which was derived from a basement originally occurring farther to the NW and thrust over the CKZ during an early phase of Pan-African thrusting (Konopásek et al., 2005).

Table 3.5. Summary of obtained ages, dating method and sample locations

	Sample	E	S	Method	Age in [Ma]
Palaeo-Proterozoic	Na 00/01	13.0738	18.7904	U-Pb	mind. 2200
	NA 428	13.1102	18.8962	U-Pb	2028±15
	NA 532	12.8764	18.8515	U-Pb	2008±18
	Na 00/27	12.9850	18.7260	U-Pb	1979±38
	Na 00/37	13.2338	18.8504	SHRIMP	1776±2
	Na 00/04	12.9852	18.7248	SHRIMP	1752±3
	NA 124	12.7170	18.7340	U-Pb	1701±37
	NA 461	12.8993	18.8207	U-Pb	1684±8
Meso-Proterozoic	Na 00/28	13.1848	18.9356	U-Pb	1516±54
	Na 00/07	12.9158	18.8043	Pb-Pb	1513±1
	Na 00/10	12.9161	18.8093	U-Pb,Pb-Pb	1502±3
	Na 00/23	12.8586	18.4869	U-Pb	1448±31
Neo-Proterozoic	ND149	12.7762	18.8884	U-Pb	730±15
	Na 00/15	12.6066	18.7202	SHRIMP	694±9
	ND137	12.7644	18.8825	U-Pb	661±21
	NA115	12.7857	18.8721	U-Pb	655±39
	Na 00/14	12.8256	18.8909	Pb-Pb	550±1
	NA 118/2	12.6666	18.7552	Pb-Pb	549±4
	NA 173	12.8645	18.8413	U-Pb	539±6

The easternmost part of the WKZ is composed mostly of Mesoproterozoic migmatites and Palaeoproterozoic granitoid gneisses, which are tectonically interlayered with subordinate migmatitized metasediments of unknown age (Figs. 3.2, 3.7). When compared to adjacent blocks, the relatively low proportion of metasediments suggests that the Mesoproterozoic segment represents a zone of higher elevation of the basement, which is bordered to the northeast by the PSZ and to the southwest by the VMZ (Fig. 3.7). Konopásek et al. (2005) and Dürr and Dingeldey (1996) interpreted this elevation as a result of early oblique thrusting of the WKZ over the CKZ and a subsequent change of the tectonic regime to sinistral transpression. Seth et al. (1998) determined a zircon age of 1507±16 Ma for a granitic gneiss in the Hoanib valley but hesitated to associate this rock with a major igneous event since only one sample in their study area yielded this age. However, our new 1516-1448 Ma ages from the WKZ and CKZ reported above suggest that two major magmatic events, one at around 1770 Ma and another one at around 1500-1620 Ma may have been significant in the southwestern Congo Craton, the more so since Seth et al. (2003) recently recognized high-grade Mesoproterozoic rocks farther north in the Epupa Complex near the Kunene River.

A clear distinction of these "young" ages in the Puros area from those of the structurally lowermost CKZ basement provides further evidence for the conclusion, that at least the easternmost flank of the WKZ represents an allochthonous slab exposed over a minimum length of ~80 km between the Khumib and Hoanib River valleys. Consistent sinistral kinematics in this area suggests that the migmatites occupying the eastern flank of the WKZ may, in fact, represent part of the Epupa Complex, brought to its present-day position as a result of large displacements

along the PSZ during Pan-African transpression. This idea is supported by two groups of protolith ages (1519 Ma and ages between 1660 and 1800 Ma, Seth et al. 2003) obtained from the above-described tectonic slab are similar to those of the elevated basement at the eastern flank of the WKZ, and we thus speculate that both these units were derived from the same Palaeo- to Mesoproterozoic segment of the western margin of the Congo Craton.

3.8.3 Neoproterozoic granitoids

The Mesoproterozoic basement in the Hoarusib-Khumib area is bordered to the SW by the medium- to low-temperature transcurrent Village Mylonite Zone, beyond which only Neoproterozoic (Pan-African) granitoids were observed. Limited mapping has shown that these granitoids are associated with metasedimentary rocks, suggesting that the entire segment represents the middle to upper crustal part of the Kaoko orogen. The original structural relationships between the Mesoproterozoic and Neoproterozoic segments of the WKZ remain unresolved due to strong overprinting during brittle-ductile transcurrent movements on the VMZ (Konopásek et al., 2005).

Samples Na 00/15 and Nd 149 represent the oldest Neoproterozoic granitoids so far dated in the WKZ, and their ages approach the age of magmatic rocks in the Damara Belt at the SW margin of the Congo Craton (756±2 Ma, Hoffman et al., 1996), which were interpreted to reflect the onset of rifting and deposition of the Damaran supracrustal assemblage. In our case, no contact with pre-Neoproterozoic basement has been observed, and we can therefore only speculate on the origin of these granitoids.

Samples Nd 137 and Na 115 were generated during a period of magmatism and metamorphism at around 650 Ma, which was also recognized in the Hoanib River valley (Seth et al., (1998; Franz et al., 1999). The latter authors proposed that anatexis and metamorphism of this age was either the result of continuous extension in the lower crust or the granitoids are not related to the evolution of the Kaoko Belt and were juxtaposed as an exotic terrain during the Damara orogeny. Our samples now document a much larger spatial extent of the ~650 Ma event as recognized by Franz et al. (1999) and thus cast doubt on the idea of an exotic origin for these granitoids. On the other hand, if this event was regionally extensive it is surprising that neither our SHRIMP data nor the Pb-loss patterns in zircon grains from U-Pb analyses reveal this event.

Granite samples Na 118/2, Na 00/14 and Na 173 reflect a period of crustal melting during the temperature peak of the Damaran orogeny in the Kaoko Belt. The large pluton of the porphyric Amspoort monzogranite within the WKZ reflects a major period of magmatic activity at ~550 Ma along the contact between Mesoproterozoic basement and mid- to upper-crustal meta-

sediments intruded by older granitoids. Moreover, our structural observations have shown that this magma intruded into a ductile, subvertical migmatitic fabric developed during transpressional deformation (D_2 of Konopásek et al., 2005). This implies that intrusion of the Amspoort granite was coeval with the thermal peak during the development of the vertical fabric and thus dates the transpressional phase at ~550 Ma. The formation of pegmatitic melts at ~540 Ma in neck-zones of amphibolite boudins within the subvertical fabric probably reflects the latest stages of magmatic activity during the transpressional phase and may thus approximate the beginning of cooling in this part of the Kaoko Belt.

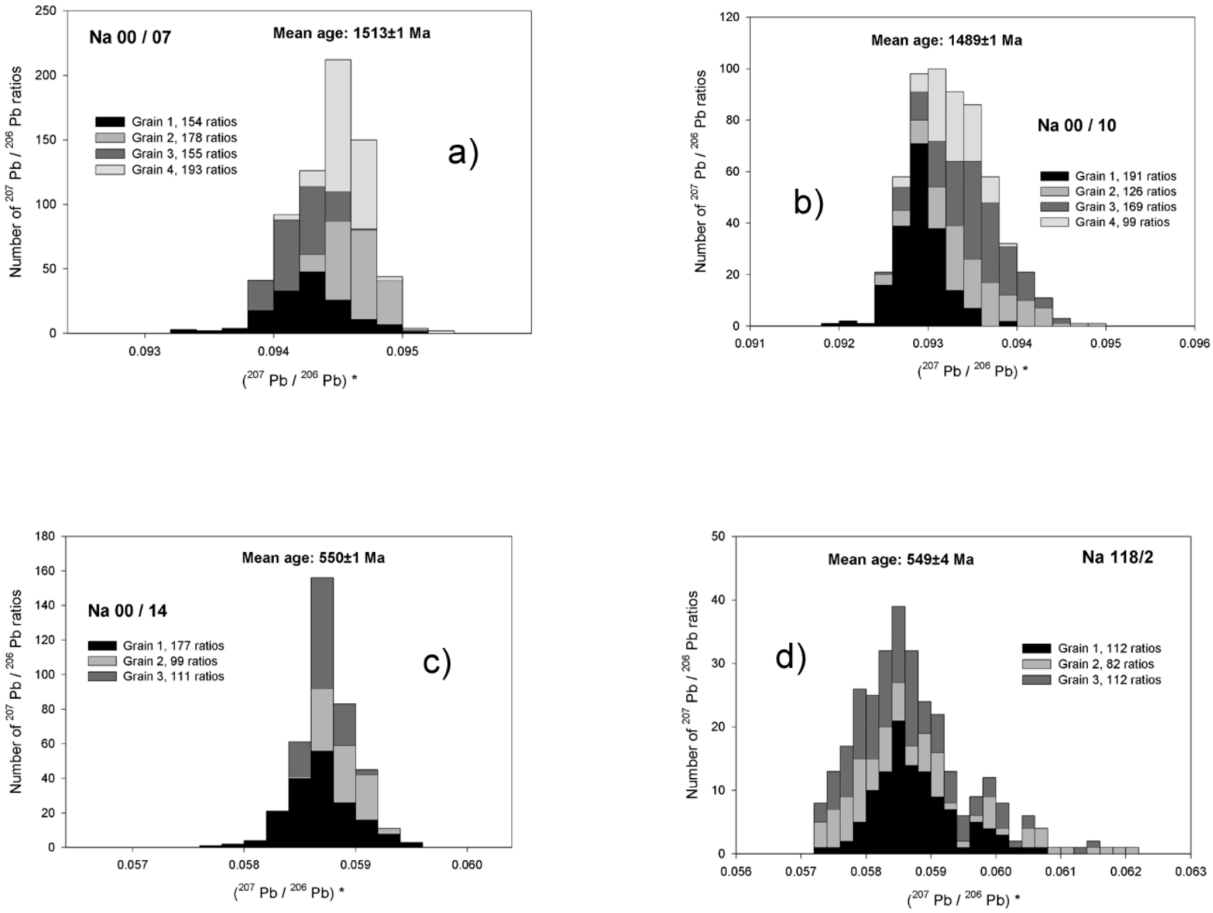

Fig. 3.6. Histograms showing distribution of radiogenic lead isotope ratios derived from evaporation of single zircons from granitoid gneisses. a)+b) augengneisses in the Hoarusib Valley interpreted to reflect age of protolith emplacement. Note b) Na 00/10 was dated with U-Pb at 1502±3 Ma (Fig. 3.5e). c)+d) are porhyritic granitoid gneisses in the Hoarusib and Khumib Valley. Both ages are interpreted to reflect age of protholith emplacement

3.8.4 Comparison with the Dom Feliciano Belt in Brazil and the Damara and Gariep belts of central and south-western Namibia

Formation of the Kaoko Belt in Namibia in virtually all published tectonic models is seen as the result of collision between the Congo and Rio de la Plata cratons (Porada, 1989; Dürr and Dingeldey, 1996; Passchier et al., 2002) although there are no palaeomagnetic data supporting this speculation. In this scenario, the counterpart of the Kaoko Belt in South America is the Dom Feliciano Belt in southeastern Brazil (Porada, 1989; Basei et al, 2000).

Comparison of our age data with previous zircon dating (Seth et al., 1998; Franz et al., 1999) shows two well-defined pre-Neoproterozoic terrains in the Central and Western Kaoko Zones. Leite et al. (2000) recorded 2.08 Ga basement gneisses in the Dom Feliciano Belt, but no intrusive rocks with ages between 2 and 0.9 Ga have so far been reported, and a stable Atlantica Supercontinent (of which the Rio de la Plata Craton was part) has been proposed during the Mesoproterozoic and part of the Neoproterozoic (Rogers, 1996; Hartmann et al., 2000).

There is no record of magmatic activity in the Kaoko Belt during the period ~1450 to 730 Ma. The oldest Neoproterozoic granitoids in our study area may reflect a magmatic event possibly related to the onset of rifting in the Damara Belt farther SE (Hoffman et al., 1996). Da Silva et al. (1999) and Hartmann et al. (2002) reported zircon ages of 762±8 and ~780 Ma for granitoids in the Dom Feliciano Belt, close to the age of 756±8 Ma reported by Hoffman et al. (1996). However, the Dom Feliciano Belt granitoids were never interpreted as being related to continental rifting. The ~650 Ma period of magmatism in the Kaoko Belt was interpreted by Franz et al. (1999) as a possible result of crustal melting during ongoing crustal extension whereas, in the Dom Feliciano Belt, ages of ~630-595 Ma for magmatic rocks are already related to the syn-collisional peak of regional metamorphism (Babinski et al., 1997; da Silva et al., 1999; Hartmann et al. 2000).

In the northern Damara Belt the Oas syenite was emplaced at 840±13 Ma (Rb-Sr whole-rock, Kröner, 1982). A U-Pb multigrain zircon age from an upper Nosib quartz porphyry dated by Miller and Burger (1983) at 728±40 Ma is interpreted by Miller (1983) to mark the end of rifting in the Damara Belt. The entire time span from 840 to 728 Ma is interpreted by Miller (1983) as a period of magmatic activity, characterizing the end of initial intracontinental rifting. In the central part of the belt, syntectonic granitoids intruded at 650-620 Ma (Rb-Sr whole-rock, Kröner 1982). Several phases of granitic intrusions with age peaks at ~580-550 Ma and ~500 Ma have been identified (Kröner, 1982; Miller, 1983; Jung, 2003).

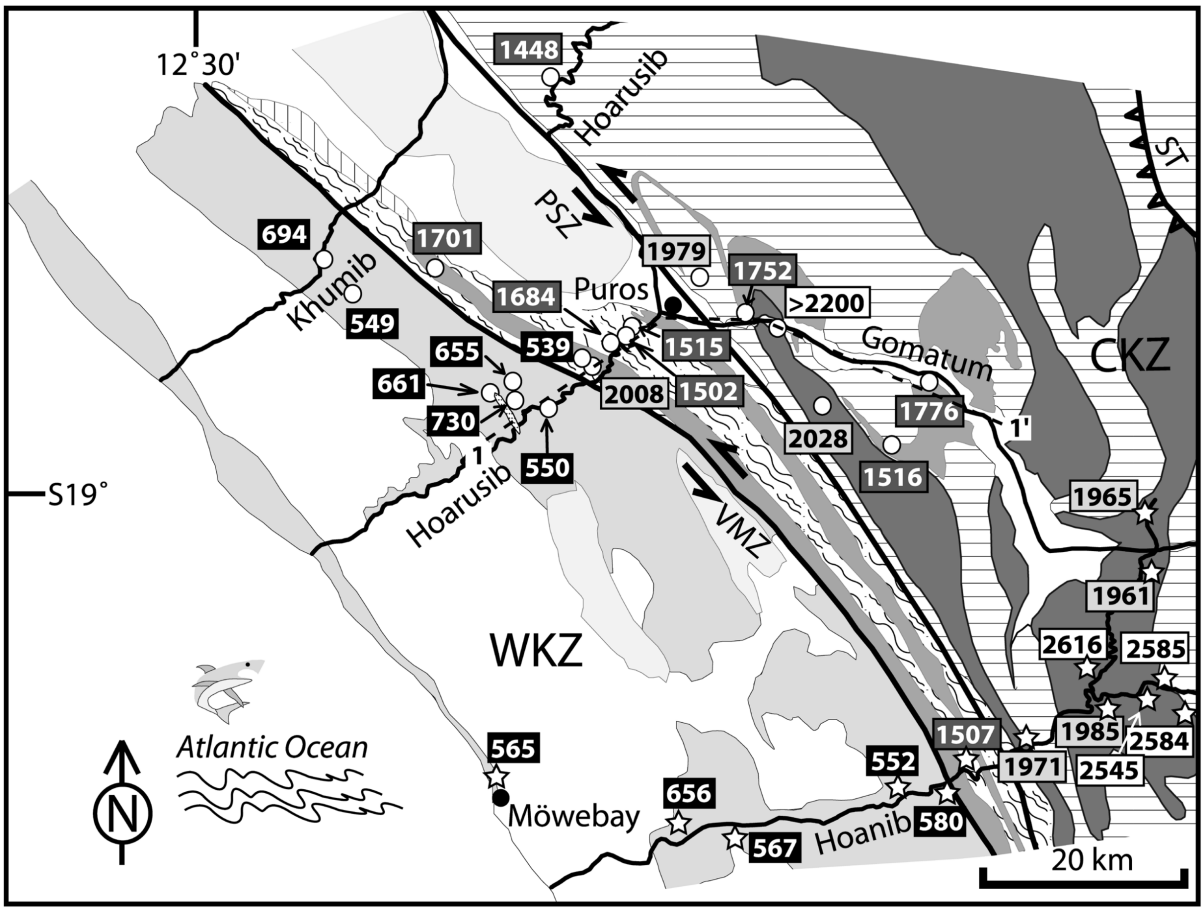

Fig. 3.7. Summary of obtained ages and comparison with previous work (Seth et al. 1998). Geological base map modified after Guj (1970), Dingeldey et al. (1994), Goscombe et al. (2003a,b). 1---1' trace of schematic cross-section indicated (Fig. 3.8).

In the Kaoko Belt, field relations show that emplacement of the Amspoort-type granite at ~550 Ma in the WKZ was related to a thermal peak during the transition from oblique thrusting to transcurrent faulting during the Kaoko orogeny (Konopásek et al., 2005). The main transpressional deformation occurred between 580 and 550 Ma (Goscombe et al., 2003a). In order to fully understand the evolution of the Kaoko Belt, detailed structural, geochemical and geochronological studies are required in the western (coastal) part of the WKZ to establish the geodynamic significance of pre-550 Ma igneous activity, metamorphism and deformation.

In the Central Damara orogen the peak of metamorphism probably occurred between 540 and 504 Ma (with thermal pulses at 540-530 Ma and 525-504 Ma) indicated by several U-Pb monazite and Sm-Nd garnet-whole rock ages obtained from migmatites, metapelites and granites (Jung and Mezger 2003; Jung et al. 2000). The main deformation probably occurred during that time span. These data are supported by recent work in the Ugab area, where two intrusions of the Voetspoor granite at 530±3 Ma (Seth et al. 2000) and 513±1 Ma are interpreted to have been emplaced during the main deformation (C.W. Passchier, unpublished data).

The Kaoko Belt is regarded to have its southern continuation in the Gariep Belt, separated by the Damara orogen. These two coastal branches are interpreted to mark the suture between the South American cratons and the cratons of southern Africa (Frimmel et al., 1996a). Single zircon dating of rhyolites from the Gariep Belt yielded an age of 741±6 Ma (Pb-Pb evaporation technique) and represent the initial stage of rifting (Frimmel et al., 1996b). This is coeval with the incipient rifting at the northern margin of the Damara Belt, dated by Hoffman (1996) at 756±2 Ma. Metamorphic amphibolite dykes emplaced during transpressional tectonics yielded a $^{40}Ar/^{39}Ar$ age of 545±2 Ma which is interpreted as reflecting the age of peak of metamorphism in the Gariep Belt (Reid et al., 1991). This age indicates continent-continent collision and is very similar to the syntectonic intruding Amspoort granite (~550 Ma) in the Kaoko Belt.

3.9 Conclusions

Based on our zircon ages and those of Seth et al. (1998) we distinguish four different age provinces in the CKZ and WKZ of the Kaoko Belt, which appear in different structural positions (Fig. 3.8):

a) A late Archaean terrain is located in the Hoanib River area of the Central Kaoko Zone, east of the Puros Shear Zone, and is characterized by zircon ages between 2645 and 2585 Ma (Seth et al., 1998).

b) A Palaeoproterozoic terrain of granitoid gneisses with U-Pb ages between 2028 and 1961 Ma (Seth et al., 1998; this paper) is also situated east of the Puros Shear Zone (Fig. 3.7). From a structural point of view, this represents the lowermost basement in the Central Kaoko Zone. The protoliths of these rocks probably formed during the Eburnian event which was widespread in Africa and occurred between ~1.8 and 2.0 Ga (Cahen et al., 1984). This event is also documented in the southwestern Congo Craton, particularly in southern Angola (Carvalho and Alves, 1993) and was also largely responsible for the formation of the Epupa and Kamanjab basement inliers in NW Namibia.

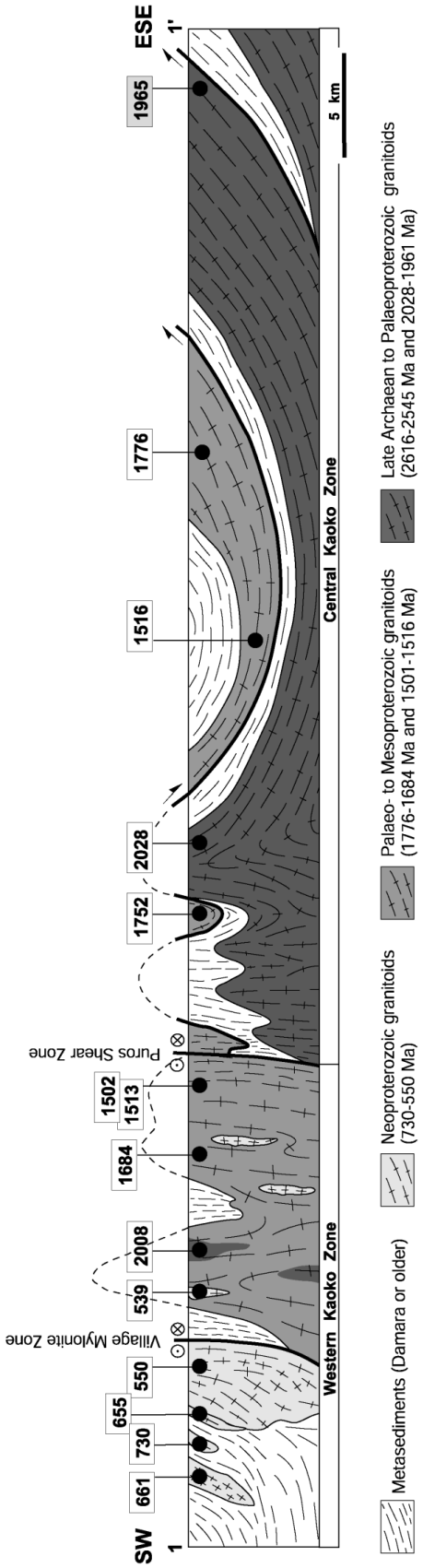

Fig. 3.8. Schematic interpretative profile across the area studied (see Fig. 3.7 for the position of the profile). The ages are discussed in the text, the age in the grey square is from Seth (1999).

c) A Palaeo- to Mesoproterozoic terrain is situated west of the PSZ (Fig. 3.5). East of the PSZ, metagranitoids of this age form an allochthonous body tectonically overlying older Palaeoproterozoic gneisses. Zircon protolith ages in this terrain fall into intervals between 1776-1684 Ma and 1516-1448 Ma; one sample recorded an older age of 2008 Ma.

d) A Neoproterozoic terrain is exposed in the westernmost part of the area, between the Hoanib and Khumib Rivers (Fig. 3.7). Zircon emplacement ages for several pre- to syntectonic granitoids range from 730 to 655 Ma. Still younger crustal-melt granites intruded into the metasedimentary gneisses and migmatites late tectonically at ~550 Ma during the transition from thrusting to transcurrent faulting and at peak temperature conditions of the Kaoko orogeny.

3.10 References

Babinski, M., Chemale, F., van Schmus, W.R., Hartmann, L.A. and da Silva, L.C. (1997). U-Pb and Sm-Nd geochronology of the Neoproterozoic granitic-gneissic Dom Feliciano Belt, Southern Brazil. *Journal of South American Earth Science*, **10**, 263-274.

Basei, M.A.S., Siga Jr., O., Masquelin, H., Harara, O.M., Reis Neto, J.M. and Preciozzi, P. (2000). The Dom Feliciano Belt of Brazil and Uruguay and its foreland domain, the Rio de la Plata Craton, framework, tectonic evolution and correlation with similar provinces of southwest Africa. In: Cordani, U.G., Milani, E.J., Thomaz Filho, A. Campos, D.A. (Eds.), Tectonic Evolution of South America, *31th International Geological Congress, Rio de Janeiro*, pp. 311-334.

Brandt, S., Klemd, R. and Okrusch, M (2003). Ultrahigh temperature metamorphism and multi-stage evolution of garnet-orthopyroxene granulites from the Proterozoic Epupa Complex, NW Namibia. *Journal of Petrology*, **44**, 1121-1144.

Burger, A.J. and Coertze, F.J. (1973). Radiometric age measurements on rocks from southern Africa to the end of 1971. *Annals of the Geological Survey of South Africa,* **82**, 185-204.

Burger, A.J., Clifford, T.N., Miller and R.Mc.G. (1976). Zircon U-Pb ages of the Fransfontein granitic suite, northern South West Africa. *Precambrian Research*, **3**, 405-431.

Cahen, L., Snelling, N.J., Delhal, J. and Vail, J.R. (1984). The geochronology and evolution of Africa. Clarendon Press, Oxford, 512 p.

Cherniak, D.J. and Watson, E.B. (2000). Pb diffusion in zircon. *Chemical Geology*, **172**, 5–24.

Cherniak, D.J., Hanchar, J.M. and Watson, E.B., 1997. Diffusion of tetravalent cations in zircon. *Contributions to Mineralogy and Petrology*, **127**, 383-390.

de Carvalho, H., Crasto, J-P, Silva, Z-C-G and Vialette, Y. (1987). The Kibaran Cycle in Angola; a discussion. *Geological Journal*, **22**, 85-102.

de Carvalho, H. and Alves, P. (1993). The Precambrian of SW Angola and NW Namibia. *Comunicações, Instituto de* Investigação *Cientifica Tropical, Série de Ciências da Terra*, **4**, Lisbon, pp.1-66.

Claoué-Long, J.C., Compston, W., Roberts,J. and Fanning, C.M. (1995). Two Carboniferous ages: a comparison of SHRIMP zircon dating with conventional zircon ages and $^{40}Ar/^{39}Ar$ analyses. *Society of Sedimentary Geology, Special Publication*, **54**, 3-21.

Cocherie, A., Guerrot, C. and Rossi, P. (1992). Single-zircon dating by step-wise Pb evaporation: comparison with other geochronological techniques applied to the Hercynian granites of Corsic, France. *Chemical Geology*, **101**, 131-141.

Compston, W., Williams, I.S., Kirschvink, J.L. and Zhang-Zichao, M.-G. (1992). Zircon U-Pb ages for the Early Cambrian time-scale. *Journal of the Geological Society of London*, **149**, 171-184.

da Silva, L.C., Hartmann, L.A., McNaughton, N.J. and Fletcher, I.R. (1999). SHRIMP U-Pb dating of Neoproterozoic granitic magmatism and collision in the Pelotas Batolith, southernmost Brazil. *International Geological Review*, **41**, 531-551.

Dingeldey, D.P., Dürr, S.B., Charlesworth, E.G., Franz, L., Okrusch, M. and Stanistreet, I.G. (1994). A geotraverse through the northern coastal branch of the Damaran Orogen west of Sesfontein, Namibia. *Journal of African Earth Science*, **19**, 315–329.

Dürr, S.B. and Dingeldey, D.P. (1996). The Kaoko belt (Namibia): part of a late Neoproterozoic continental-scale strike-slip system. *Geology*, **24**, 503–506.

Franz, L., Romer, R.L. and Dingeldey, D.P. (1999). Diachronous Pan-African granulite-facies metamorphism (650 Ma and 550 Ma) in the Kaoko belt, NW Namibia. *European Journal of Mineralogy*, **11**, 167-180.

Frimmel, H.E., Hartnady, C.J.H., and Koller, F. (1996a). Geochemistry and tectonic setting of magmatic units in the Pan-African Gariep Belt, Namibia. *Chemical Geology*, **130**, 101-121.

Frimmel, H.E., Klötzli, U.S., and Siegfried, P.R. (1996b). New Pb–Pb single zircon age constraints on the timing of neoproterozoic glaciation and continental break-up in Namibia. *The Journal of Geology*, **104**, 459–469.

Goscombe, B., Hand, M., Gray, D., and Mawby, J. (2003a). The metamorphic architecture of a transpressional orogen: the Kaoko belt, Namibia. *Journal of Petrology*, **44**, 679-711.

Goscombe, B., Hand, M. and Gray, D. (2003b). Structure of the Kaoko belt, Namibia: progressive evolution of a classic transpressional orogen. *Journal of Structural Geology*, **25**, 1049–1081.

Gruner, B. (2000). Metamorphoseentwicklung im Kaokogürtel, NW-Namibia: Phasenpetrologische und geothermobarometrische Untersuchungen panafrikanischer Metapelite. *Unpublished PhD Dissertation*, *University of Würzburg*, Germany, 248pp.

Gulson, B. L. and Krogh, T.T. (1973). Old lead components in the young Bergell Massif, southeast Swiss Alps. *Contributions to Mineralogy and Petrology*, **40**, 239-252.

Guj, P. (1970). The Damara mobile belt in the south-western Kaokoveld, South West Africa. *Precambrian Research Unit, University of Cape Town, South Africa, Bulletin,* **10**, 168pp.

Hanchar, J. M. and Miller, C. F. (1993). Zircon zonation patterns as revealed by cathodoluminescence and backscattered electron images: implications for interpretation of complex crustal histories. *Chemical Geology*, **110**, 1–13.

Hanchar, J.M. and Rudnick, R.L. (1995). Revealing hidden structures: The application of cathodoluminescence and back-scattered electron imaging to dating zircons from lower crustal xenoliths. *Lithos*, **36**, 289-303.

Hardtnady, C.J.H., Joubert, P. and Stowe, C. (1985). Proterozoic crustal evolution in south-western *Africa Episodes*, **8**, 236-244.

Hartmann, L.A., Santos, J.O.S., Bossi, J., Campal, N., Schipilov, A. and McNaughton, N.J. (2002). Zircon and titanite U-Pb SHRIMP geochronology of Neoproterozoic felsic magmatism on the eastern border of the Rio de la Plata Craton, Uruguay. *Journal of South American Earth Science*, **15**, 229-236.

Hartmann, L.A., Leite, J.A.D., Da Silva, L.C., Remus, M.V.D., Mcnaughton, N.J., Groves, D.I., Fletcher, I.R., Santos, J.O.S. and Vasconcellos, M.A.Z. (2000). Advances in SHRIMP geochronology and their impact on understanding the tectonic and metallogenic evolution of southern Brazil. *Australian Journal of Earth Sciences,* **47**, 829–844.

Hoffman, P.F., Hawkins, D.P., Isachsen, C.E. and Bowring, S.A. (1996). Precise U–Pb zircon ages for early Damaran magmatism in the Summas Mountains and Welwitschia Inlier, northern Damara belt, Namibia. *Communications of the Geological Survey of Namibia*, **11**, 47–52.

Jaeckel, P., Kröner, A., Kamo, S.L., Brandl, G. and Wendt, J.I. (1997). Late Archaean to early Proterozoic granitoid magmatism and high-grade metamorphism in the central Limpopo belt, South Africa. *Journal of the Geological Society of London*, **154**, 25-44.

Jung, S., Hoernes, S. and Mezger, K. (2000). Geochronology and petrology of migmatites from the Proterozoic Damara Belt—importance of episodic fluid-present disequilibrium melting and consequences for granite petrology. *Lithos*, **51**, 153–179.

Jung, S. and Mezger, K. (2003). Petrology of basement-dominated terranes: I. Regional metamorphic T-t path from U-Pb and Sm-Nd garnet geochronology (Central Damara orogen, Namibia). *Chemical Geology*, **198**, 223-247.

Karabinos, P. (1997). An evaluation of the single-grain zircon evaporation method in highly discordant samples. *Geochimica et Cosmochimica Acta*, **61**, 2467-2474.

Kober, B. (1986). Whole-grain evaporation for $^{207}Pb/^{206}Pb$ investigation on single zircons using a double-filament thermal ion source. *Contributions to Mineralogy and Petrology*, **93**, 482-490.

Kober, B. (1987). Single-zircon evaporation combined with Pb^{+} emitter-bedding for $^{207}Pb/^{206}Pb$-age investigation using thermal ion mass spectrometry, and implications to zirconchronology. *Contributions to Mineralogy and Petrology*, **96**, 63-71.

Konopásek, J., Kröner, S., Kitt, S.L., Passchier, C.W. and Kröner, A. (2005). Oblique collision and evolution of large-scale transcurrent shear zones in the Kaoko belt, NW Namibia. *Precambrian Research*, **136**, 139-157.

Kröner, A.(1982). Rb-Sr geochronology and tectonic evolution of the Pan-African Damara belt of Namibia, Southwestern Africa. *American Journal of Science*, **282**, 1471-1507.

Kröner, A., Byerly, G.R. and Lowe, D.R. (1991). Chronology of early Archaean granite-greenstone evolution in the Barberton Mountain Land, South Africa, based on precise dating by single zircon evaporation. *Earth and Planetary Science Letters*, **103**, 41-54.

Kröner, A. and Hegner, E. (1998). Geochemistry, single zircon ages and Sm-Nd systematics of granitoid rocks from the Góry Sowie (Owl Mts.), Polish West Sudetes: evidence for early Palaeozoic arc-related plutonism. *Journal of the Geological Society of London*, **155**, 711-724.

Kröner, A., Jaeckel, P. and Williams, I.S. (1994). Pb-loss patterns in zircons from a high-grade metamorphic terrain as revealed by differnent dating methods; U-Pb and Pb-Pb ages of igneous and metamorphic zircons from northern Sri Lanka. *Precambrian Research*, **66**, 151-181.

Kröner, A., Jaeckel, P., Brandl, G., Nemchin, A.A. and Pidgeon, R.T. (1999). Single zircon ages for granitoid gneisses in the Central Zone of the Limpopo belt, southern Africa, and geodynamic significance. *Precambrian Research*, **93**, 299-337.

Krogh, T.E. (1978). Vapour transfer for the dissolution of zircons in a multi-sample capsule, at high pressure. In: R.E. Zartman (ed.) 4th International Conference of Geochronology, Cosmochronology, Isotope Geology, 1978. *U.S. Geological Survey, Open-File Report.*, **78-701**, 233-234.

Lee, J.K.W., Williams, I.S. and Ellis, D.J. (1997). Pb, U and Th diffusion in natural zircon. *Nature*, **390**, 159-161.

Leite, J.A.D., Hartmann, L.A., Fernandes, L.A.D., McNaughton, N.J., Soliani, E., Koester, E., Santos, J.O.S. and Vasconcellos, M.A.Z. (2000). Zircon U-Pb SHRIMP dating of gneissic basement of the Dom Feliciano Belt, southernmost Brazil. *Journal of South American Earth Science*, **13**, 739-750.

Ludwig, K.R. (1999). Using Isoplot/Ex, Version 2.01: a geochronological toolkit for Microsoft Excel. *Berkeley Geochronology Center, Special Publication*, No. **1a**, 47

Mezger, K. and Krogstad, E.J. (1997). Interpretation of discordant U-Pb zircon ages: an evaluation. *Journal* of *Metamorphic Geology*, **15**, 127-140.

Miller, R.Mc.G. (1983). The Pan-African Damara Orogen of South West Africa/Namibia. In: Miller, R.Mc.G. (Ed.), The Damara Orogen. *Geological Society of South Africa Special Publication*, **11**, 431–515.

Möller, A., O'Brien, P.J., Kennedy, A. and Kröner, A. (2002). Polyphase zircon in ultrahigh-temperature granulites (Rogaland, SW Norway): constraints for Pb diffusion in zircon. *Journal of Metamorphic Geology*, **20**, 727-740.

Nelson, D.R. (1997). Compilation of SHRIMP U-Pb zircon geochronology data, 1996. *Geological Survey of Western Australia*, Record 1997/2, 189pp.

O'Connor, J.T. (1965). A classification for quartz-rich igneous rocks based on feldspar ratios. *US Geological Survey Professional Paper*, **B525**, 79-84.

Parrish, R.R. (1987). An improved microcapsule for zircon dissolution in U-Pb geochronology. *Isotope Geoscience*, **66**, 99-102.

Porada, H. (1989). Pan-African rifting and orogenesis in southern to equatorial Africa and Eastern Brazil. *Precambrian Research*, **44**, 103–136.

Passchier, C.W., Trouw, R.A.J., Ribeiro, A. and Paciullo, F.V. P. (2002). Tectonic evolution of the southern Kaoko belt, Namibia. *Journal of African Earth Science*, **35**, 61-75.

Reid, D.L., Ransome, I.G.D., Onstott, T.C. and Adams, C.J. (1991). Time of emplacement and metamorphism of Late Precambrian mafic dykes associated with the Pan-African Gariep orogeny, Southern Africa: implications for the age of the Nama Group. *Journal of African Earth Science,* **13**, 531-541.

Reischmann, T. (1995). Precise U/Pb age determination with baddeleyite (ZrO_2), a case study from the Phalabora Igneous Complex, South Africa. *South African Journal of Geology*, **98**, 1-4.

Rogers, J.J.W. (1996). A history of continents in the past three billion years. *The Journal of Geology*, **104**, 91-107.

Rubatto, D. and Gebauer, D. (2000). Use of cathodoluminescence for U-Pb zircon dating by ion microprobe; some examples from the Western Alps. *Cathodoluminescence in Geosciences Springer. Berlin*, 314pp.

Seth, B. (1999). Crustal evolution of the Kaoko belt, NW Namibia. Geochemical and geochronological study of Archaean to Mesoproterozoic basement gneisses and Pan-African migmatites and granitoids. *Unpublished PhD Dissertation*, *University of Würzburg*, Germany, 120pp.

Seth, B., Kröner, A., Mezger, K., Nemchin, A.A., Pidgeon, R.T. and Okrusch, M. (1998). Archaean to Neoproterozoic magmatic events in the Kaoko belt of NW Namibia and their geodynamic significance. *Precambrian Research*, **92**, 341–363.

Seth, B., Okrusch, M.,Wilde, M. and Hoffmann, K.H (2000). The Voetspoor intrusion, southern Kaoko Zone, Namibia: mineralogical, geochemical and isotopic constraints for the origin of a syenitic magma. Henno Martin Memorial Volume of the Geological Survey of Namibia. *Communications of the Geological Survey of Namibia*, **12**, 125-137.

Seth, B., Armstrong, R.A. Brandt, S., Villa, I.M. and Kramers, J.D. (2003). Mesoproterozoic U-Pb and Pb-Pb ages of granulites in NW Namibia: reconstructing a complete orogenic cycle. *Precambrian Research*, **126**, 1-2, 147-168.

Steiger, E.H. and Jäger, E. (1977). Subcommission on geochronology, convention of the use of decay constants in geo- and cosmochronology. *Earth and Planetary Science Letters*, **19**, 321-329.

Tegtmeyer, A. and Kröner, A. (1985). U–Pb zircon ages for granitoid gneisses in northern Namibia and their significance for Proterozoic crustal evolution of southwestern Africa. *Precambrian Research*, **28**, 311–326.

Wendt, J.I. (1993). Early Archaean crustal evolution in Swaziland, southern Africa, as revealed by combined use of zircon geochronology, Pb-Pb and Sm-Nd systematics. *Unpublished PhD Dissertation. University of Mainz*, Germany, 123 p.

Wendt, J.I. and Todt, W. (1991). A vapour digestion method for dating single zircons by direct measurement of U and Pb without chemical separation. *Terra Abstracts*, **3**, 507-508.

Chapter 4

Oblique collision and evolution of large-scale transcurrent shear zones in the Kaoko Belt, NW Namibia

(published in Precambrian Research, 136, 139-157, 2005)

Oblique collision and evolution of large-scale transcurrent shear zones in the Kaoko Belt, NW Namibia

J. Konopásek [1], S. Kröner [1], S. L. Kitt [2], C. W. Passchier [1], A. Kröner [1]

[1] *Institut für Geowissenschaften – Tektonophysik, Universität Mainz, 55099 Mainz, Germany*

[2] *Geological Survey of Namibia, P.O. Box 2168, Windhoek, Namibia*

4.1 Abstract

Early structures in the central part of the Kaoko orogenic belt of NW Namibia suggest that the initial stage of collision was governed by underthrusting of the medium-grade Central Kaoko zone below the high-grade Western Kaoko zone, resulting in the development of an inverted metamorphic gradient. In the Western zone, early structures were overprinted by a second phase of deformation, which is associated with localization of the transcurrent Puros Shear Zone along the contact between the Western and Central zones. During this second phase, extensive partial melting and intrusion of ~550 Ma granitic bodies occurred in the high-grade Western zone. In the Central zone, the second phase of deformation led to complete overprinting of the early foliation in the zone adjacent to the Puros Shear Zone, and to the development of kilometre-scale folds in the more distal parts. Strain partitioning into transcurrent deformation along the Puros Shear Zone and NE–SW oriented shortening in the Central zone is consistent with a sinistral transpressional regime during the second phase of deformation. Transcurrent deformation continued during cooling of the entire belt, giving rise to the localized low-temperature Village Mylonite Zone that separates a segment of elevated Mesoproterozoic basement from the rest of the Western zone in which only Pan-African ages have so far been observed. The data suggest that the boundary between the Western and Central Kaoko zones represents a modified thrust zone controlling the tectonic evolution of the Pan-African Kaoko Belt.

Keywords: Kaoko Belt, Namibia, Oblique collision, Pan-African, Puros Shear Zone, Transpression

4.2 Introduction

Crustal-scale transcurrent shear zones occur in several tectonic settings around the world. Several major shear zones such as the Alpine Fault in New Zealand and the San Andreas Fault in California accommodate subduction-related plate motion at their tips (e.g., Lamarche and Lebrun, 2000; Lebrun et al., 2000; Hole et al., 2000; McCrory, 2000). Other transcurrent shear zones accommodate continental collision, such as the North Anatolian and Tibetan fault systems (e.g., Bozkurt, 2001; Matte et al., 1996). A less spectacular but equally important type of transcurrent faulting occurs in the upper plate of oblique subduction systems parallel to the subduction zone and apparently accommodating the strike-slip component of subduction (e.g., Scheuber and Gonzalez, 1999). Nearly all these crustalscale shear zones are only exposed in their upper parts, mainly because the structures are relatively young and lack a dip-slip component so that deeper (mylonitic) equivalents are not exposed. For this reason, the geometry of these shear zones at depth and the way they interact with the external parts and thrust belts alongside have largely been ignored.

Several Neoproterozoic mobile belts, such as the Mozambique Belt of East Africa and the Ribeira and Dom Feliciano belts of Brazil contain orogen-parallel crustal-scale strike-slip fault systems (e.g., Ring et al., 2002; Egydio-Silva et al., 2002; Frantz and Botelho, 2000). Because of the age of these belts, much deeper levels of the crust are exposed than in modern orogens, providing an opportunity to study the deep structure of such belts and the relation with tectonics and metamorphism in adjacent blocks. The Neoproterozoic Kaoko Belt in NW Namibia contains a particularly well-exposed example of a crustal-scale transcurrent shear zone, known as the Puros Shear Zone (Goscombe et al., 2003a).

The Puros Shear Zone represents a ca. 400 km long crustal-scale structure that developed during the Pan- African tectono-metamorphic event in the Kaoko Belt (Fig. 4.1). In the central part of the belt, this shear zone is developed at the contact of two units, which were described by Miller (1983) as the Central and Western zones of the Kaoko Belt. Dingeldey et al. (1995), Dürr and Dingeldey (1996), Stanistreet and Charlesworth (2001) and Goscombe et al. (2003a) discussed the structural evolution of the central Kaoko Belt in which a shallow, westward dipping metamorphic foliation and associated west–northwestward plunging lineation in the eastern part of the Central zone contrast with the steep westward inclined foliation and the north–northwest inclined, gently plunging lineation developed in the area around the Puros Shear Zone. Dürr and Dingeldey (1996) suggested contemporaneous development of these structures and ascribed this phenomenon to a transpressional regime as a combination of pure- and simple-shear deformation. Goscombe et al. (2003a) attributed the fabric development in both the Western and Central

Kaoko zones to an early wrench- dominated transpressional phase, which created the geometry of the belt by progressive sinistral shearing, and interpreted a gradual change in the orientation of lineations towards the foreland and folding of metamorphic fabrics in the Central zone as a result of a progressive change from wrench-dominated to more convergence-dominated collision. In any case, there is a general agreement that the sub-vertical fabric along the Puros Shear Zone represents a first deformation event which is recognized in the central Kaoko Belt, and thus that the development of this shear zone controlled the structural and metamorphic architecture of the entire Kaoko Belt (Dürr and Dingeldey, 1996; Goscombe et al., 2003a,b).

We studied the development and localization of the Puros and adjacent shear zones and present a detailed analysis of the succession of deformation structures developed in the central part of the Kaoko Belt. In contrast to previous models, we argue that the tectonic evolution of the area is the result of a progressive deformation involving a distinct early period of SSE-directed thrusting preceding the development of the Puros Shear Zone. Combining our structural data with descriptions of metamorphic conditions and Pan-African intrusive, metamorphic and cooling ages, we discuss possible tectonic mechanisms leading to the present-day pattern of this part of the Neoproterozoic orogenic belt system of Namibia.

4.3 Geological setting

The Kaoko and Damara belts of Namibia represent two perpendicular branches of the Damara orogenic belt system, which developed as a result of Neoproterozoic (Pan-African) collision between the Congo and Kalahari Cratons in Africa, and the Rio de la Plata Craton in South America (Fig. 4.1; Porada, 1989). The Kaoko Belt developed on the southwestern margin of the Congo Craton and is today exposed along the Atlantic coast of northwestern Namibia and southwestern Angola.

Ortho- and paragneisses of the Congo Craton are exposed in the Kamanjab Inlier and in the Epupa Complex (Fig. 4.1), but most of the craton in Namibia is hidden below sedimentary cover (the northern platform of Miller, 1983). Emplacement ages of granitoids in the Kamanjab Inlier and granitoid gneisses of the Epupa Complex fall into the interval between 1662 and 1860 Ma (Burger and Coerze, 1973; Burger et al., 1976; Tegtmeyer and Kröner, 1985), suggesting a complex magmatic history in this part of the craton. Deposition of the Damara sedimentary sequence at the southwestern margin of the Congo craton began at about 756 Ma (Hoffman et al., 1996). Miller (1983) subdivided the Kaoko Belt into three structurally contrasting tectonic units resulting from Pan-African deformation and metamorphism (Fig. 4.2). From east to west these are: (a) The Eastern Kaoko zone, representing a low-grade, folded, autochthonous sedimentary cover of the

Kamanjab Inlier (Dingeldey et al., 1995; Goscombe et al., 2003a). To the west, the Eastern Kaoko zone is bounded by the low-angle Sesfontein thrust. (b) The Central Kaoko zone is exposed to the west of the Sesfontein thrust and is interpreted as a fold-and-thrust belt with basement-cored, kilometer- scale steep to recumbent anticlines and thrust sheets (Guj, 1970; Stanistreet and Charlesworth, 2001; Seth et al., 1998; Goscombe et al., 2003a).

Franz et al. (1999), Gruner (2000) and Goscombe et al. (2003b) described Barrovian-type metamorphism in Damaran metasediments of this zone with the metamorphic grade increasing towards the west. The western boundary of the Central Kaoko zone is the Puros Shear Zone. The Western Kaoko zone extends from the Puros Shear Zone to the Atlantic coast and experienced high-temperature/low- pressure metamorphism (Franz et al., 1999; Gruner, 2000; Goscombe et al., 2003b) and sinistral strike-slip deformation refolding an earlier metamorphic fabric (Miller, 1983; Dürr and Dingeldey, 1996; Goscombe et al., 2003a). Dingeldey et al. (1994) suggested a structural and lithological subdivision of the Kaoko Belt which only partially corresponds to that of Miller (1983). However, the zones of Miller (1983) better highlight differences in thermal and structural evolution of the Kaoko Belt and are therefore used in this paper.

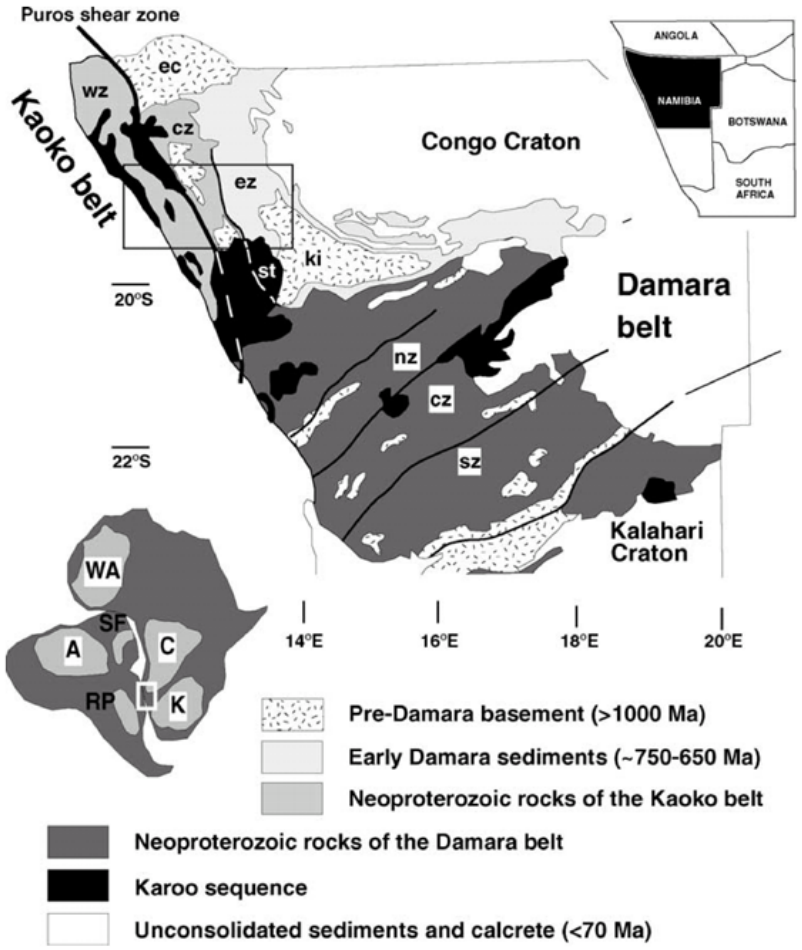

Fig. 4.1. Schematic geological map of the northern part of Namibia showing position of the Pan-African Kaoko and Damara belts and of the Congo and Kalahari Cratons. Tectonic units of the Kaoko Belt (wz: Western zone; cz: Central zone; ez: Eastern zone; ki: Kamanjab Inlier; ec: Epupa Complex; st: Sesfontein thrust) and of the Damara Belt (nz: Northern zone; cz: Central zone; sz: Southern zone) after Miller (1983). A black square delimits the position of Fig. 4.2. Cratons indicated in inset: A: Amazon; C: Congo; K: Kalahari; RP: Rio de la Plata; SF: São Francisco; WA: West African. The Dom Feliciano Belt is located east of the Rio de la Plata Craton.

Because of lack of infrastructure and considerable topographic relief, the Kaoko Belt is best studied in NE–SW trending dry river valleys. Best exposed are the valleys of the Hoanib, Hoarusib and Gomatum rivers (Fig. 4.2). Recent geochronological investigations in the Hoanib River valley (Franz et al., 1999; Seth et al., 1998) have shown that there is Archaean basement in the Central zone (zircon ages of 2584–2645 Ma) as well as 1933–1985 Ma Palaeoproterozoic metagranitoids. The easternmost part of the Western zone has a single basement zircon age of 1507 Ma and a Pan- African monazite age of 554 Ma. In other parts of the Western zone, two groups of Pan-African ages of 656–645 Ma (zircon ages) and 552–580 Ma (zircon and monazite ages) have been found. A similar distribution of ages occurs in a river section farther north, the Gomatum–Hoarusib section (Fig. 4.2). An age of ~1980 Ma and imprecise ages between 2153 and 2384 Ma have been obtained by Kröner et al. (2004) for metagranitoids at the western margin of the Central zone. Kröner et al. (2004) have reported two groups of basement zircon ages of 1500–1530 Ma and 1650–1680 Ma, respectively, for orthogneisses and migmatites of the easternmost part of the Western zone and a Pan-African zircon ages between 730 and 550 Ma for granites in the Western zone.

4.4 The Puros Shear Zone

Field observation suggests that the Puros Shear Zone represents an important boundary between the structural and metamorphic units described above. Sillimanite- and cordierite-bearing low-pressure mineral assemblages dominate the eastern part of the Western zone west of the Puros Shear Zone, whereas a typical Barrovian succession of mineral assemblages is developed in meta-sediments eastward of the Puros Shear Zone (Gruner, 2000; Goscombe et al., 2003b). A hetero-geneous network of several metres wide ultramylonitic shear zones trending parallel to the main foliation today represents the Puros Shear Zone as a marked structure on the satellite images. This array of ultramylonites is developed within a ~10 to 15 km zone of steep, high- temperature metamorphic foliation along the contact between the Central and Western Kaoko zones, and this entire zone of subvertical fabric probably represents the high-temperature stage of the Puros Shear Zone activity.

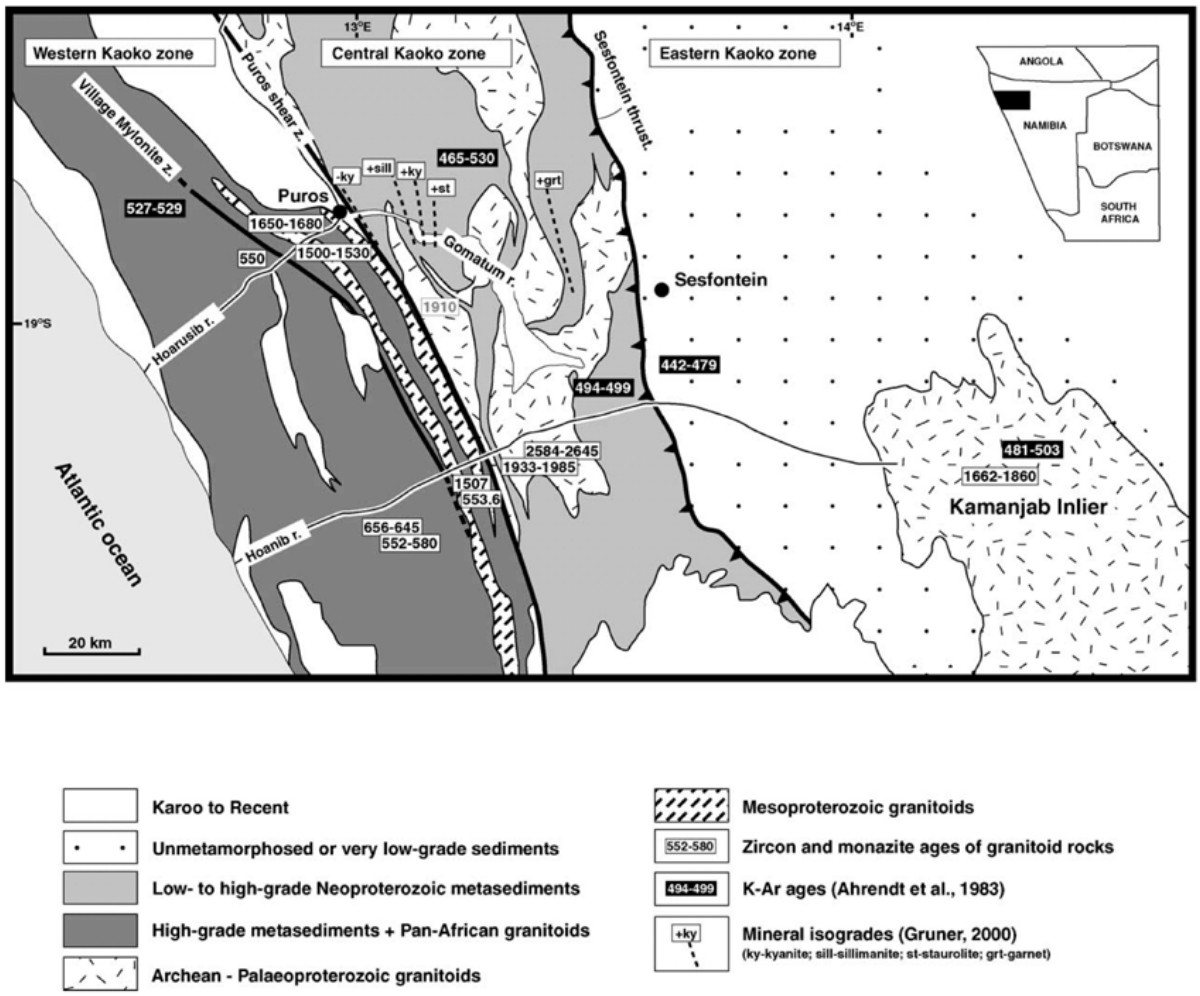

Fig. 4.2. Schematic geological map of the central part of the Kaoko Belt (see upper right inset for actual position of the figure). Tectonic zones of the belt are delimited after Miller (1983), references related to ages of granitoid rocks are listed in the text.

4.5 Basement–cover relationships and metamorphism in the Puros area

Detailed mapping and geochronological studies (Kröner et al., 2004) have shown, that the easternmost part of the Western Kaoko zone is built mostly of Mesoproterozoic basement migmatites and granitoid orthogneisses covered by migmatitized metasediments of unknown age (Figs. 4.2, 4.3). This segment of exhumed basement is bordered to the southwest by a major shear zone defined by Goscombe et al. (2003a) as the Village Mylonite Zone (Fig. 4.3). Farther to the southwest, only Pan-African granitoids were observed, and limited mapping has shown only metasedimentary country rocks. The Puros Shear Zone represents the northeastern limit of the Mesoproterozoic segment, and the Central zone exposed to the east is dominated by metasediments with exhumed Palaeoproterozoic granitoids in cores of kilometre-scale folds. The Mesoproterozoic segment exposed between the Puros and Village shear zones obviously represents a

zone of greater exhumation of a granitoid basement, the age of which cannot be compared to the Palaeoproterozoic ages recorded in the easterly Central Kaoko zone.

Gruner (2000) and Goscombe et al. (2003b) described metamorphism along the Gomatum–Hoarusib valley section. In the Central Kaoko zone, metamorphic conditions are characterized by a medium d*P*/d*T* (Barrovian type) metamorphic gradient with increasing grade towards the west (Fig. 4.2). For particular mineral zones metamorphic conditions were estimated by Gruner (2000) as follows: garnet zone—500±30 °C/9±1 kbar; staurolite zone—580 ±30 °C/7–8 kbar; kyanite zone—590±30 °C/6.5–8 kbar and kyanite–sillimanite–muscovite zone—650 ±20 °C/9±1.5 kbar. Goscombe et al. (2003b) provided *PT* data of 534±47 °C/9±1.1 kbar for the central part of the Central zone and 658±45 °C/8.5±1.6 kbar for the western part of the Central zone. In contrast, metamorphic conditions in the Western zone are characterized by a low d*P*/d*T* metamorphic gradient. Petrological studies have shown the presence of sillimanite–K- felspar and garnet–cordierite–sillimanite–K-felspar zones, and estimated metamorphic conditions corresponding to 690±40 °C/4.5±1 kbar and 750±30 °C/4–5.5 kbar, respectively (Gruner, 2000) or, alternatively, 843±64 °C/8.1±1.6 kbar and 811±58 °C/6.2±0.7 kbar, respectively (Goscombe et al., 2003b) are consistent with observed widespread melting. Garnet Sm–Nd geochronology has shown that the matrix assemblages in samples from both the Central and Western Kaoko zones have formed at ~576±15 Ma (Goscombe et al., 2003b). Our preliminary petrological investigations of the Central zone metasediments in the area north of the village of Puros have shown the presence of the kyanite–sillimanite–K- feldspar assemblage and thus confirm the presence of a medium d*P*/d*T* metamorphic gradient. The kyanite–sillimanite–muscovite zone gradually passes into the low-pressure sillimanite–K-feldspar zone, which seems to terminate at the Puros Shear Zone. Our investigation of metasediments of the Western zone revealed low-pressure metamorphic conditions dominated by a garnet–sillimanite–biotite–K-feldspar assemblage with rare occurrence of spinel-bearing metasediments.

4.6 Structural evolution west of the Puros Shear Zone

The eastern margin of the Western Kaoko zone (west of the Puros Shear Zone) is dominated by steep to subvertical metamorphic foliations. However, several domains close to the village of Puros (further termed as the D_1 domains; see Fig. 4.3) show only a moderately refolded, shallowly inclined metamorphic foliation, suggesting that the widespread subvertical fabric is the result of later stages of deformation.

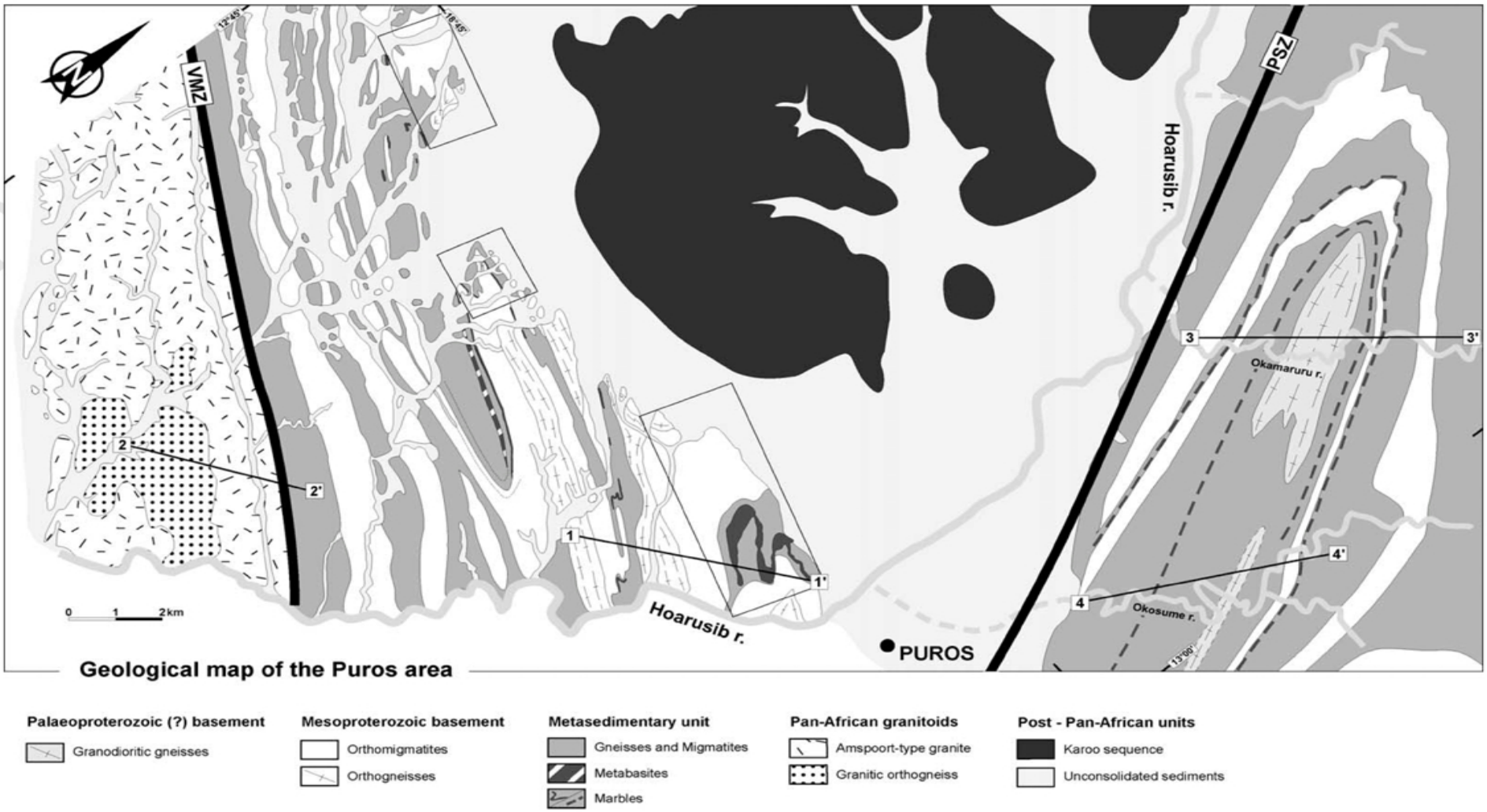

Fig.4.3. Geological map of the area studied. The map is the result of field mapping in the area SW of the village of Puros, two reconnaissance mapping profiles in the area NE of Puros, and of the interpretation of satellite images and aerial photographs of the area. Numbered solid black lines show the position of cross-sections presented in Figs. 5.4, 5.6, solid black rectangles delimit areas with well-preserved D_1 structures (D_1 domains—see text). Heavy solid black line labelled PSZ represents approximate position of the axial part of the Puros Shear Zone. The same line labelled VMZ represents approximate position of the axial part of the Village Mylonite Zone.

4.6.1 Deformation phase D_1

D_1 is characterized by the development of a shallow dipping migmatitic foliation S_1. S_1 is defined by compositional layering and preferred orientation of platy minerals in metasedimentary rocks and amphibolite, and by foliation-parallel oriented leucosomes and preferred orientation of biotite in granitoid migmatites. In the orthogneisses the S_1 foliation is characterized by the development of quartz and feldspar ribbons. Because of later refolding, the dip orientation of S_1 varies between SSW and NNE (Fig. 4.4a). L_1 is an aggregate or grain lineation and plunges mostly to the WNW at shallow to moderate angles (Fig. 4.4a). In localities with strongly folded S_1, it is not clear whether the lineation observed on the fold limbs represents folded L_1 or newly developed L_2 lineation. Isoclinal F_1 folds are rare and were refolded by later phases of deformation. Kinematic indicators are rare and do not provide unambiguous sense of movement during D_1. Observations in the D_1 domains show thrusting of the basement migmatites and orthogneisses over their sedimentary cover, but the amount of displacement is difficult to estimate.

4.6.2 Deformation phase D_2

All domains with well-preserved D_1 structures were heterogeneously affected by D_2, which resulted in refolding of the S_1 foliation (Fig. 4.5a) and rare development of an S_2 fabric. Open to close F_2 folds are common and have subvertical axial planes and fold axes plunging moderately to the NW, parallel to the L_1 or newly developed L_2 lineation. Domains with preserved D_1 structures are sharply bounded by a penetrative subvertical S_2 foliation, which is dominant in the entire eastern part of the Western zone, including the Puros Shear Zone itself. Associated L_2 lineations plunge at shallow angles to the NW, parallel to the lineation developed on the S_1 foliation planes. Numerous close to isoclinal F_2 folds preserved in the S_2 foliation (Fig. 4.5b) support the idea of a D_2 origin for the subvertical foliation in this area. Numerous kinematic indicators such as σ-objects, asymmetric boudinage and shear bands suggest a sinistral sense of shear during D_2. Rarely, high-temperature dextral shear bands have been observed in orthogneisses. We interpret these structures as passively rotated D_1 shear bands.

The S_2 foliation is of the same character as S_1. The development of a subvertical S_2 foliation coincided with the formation of foliation-parallel leucosomes in all lithologies. Granitoid migmatites have stromatitic character, and leucosomes form long bands locally connected by melt-filled shear bands. Similar structures are developed in the orthogneisses, but the extent of melting is lower. Strongly anatectic metasediments usually show lower amounts of biotite, whereas the de-

gree of partial melting is low in biotite-rich metasediments. Medium- to very coarse-grained veins of decimetre to metre width are developed in both metasedimentary and meta-igneous units. Rarely, extrusion of melt into the hinge zones of F_2 folds has been observed, forming aligned zones of melt pockets highlighting the S_2 axial planes (Fig. 4.5d). These observations suggest that thermal conditions of the transition between D_1 and D_2 coincide with widespread migmatitization observed W of the Puros Shear Zone.

4.6.3 Structural position of ~550 Ma Pan-African intrusions

Apart from widespread migmatitization, Pan- African high-temperature metamorphism in the study area resulted in the intrusion of several granitoid bodies. The most prominent is the intrusion of the porphyritic Amspoort monzogranite dated at ~550 Ma (sample BK19 in Seth et al., 1998 and samples NA 00/14 and 118/2 in Kröner et al., 2004). This monzogranite forms a NW–SE elongated sheet-like body (Fig. 4.3) suggesting emplacement into the S_2 fabric. However, porphyritic granitoids invaded both the flat-lying S_1 and vertical S_2 fabrics. This suggests that magmatic activity coincided with the progressive development of S_2. Limited ascent of melt pockets from migmatitized basement during D_2 suggests that migmatitization and the intrusion of large granitoid bodies were contemporaneous processes. This interpretation is supported by the fact that the age of a leucocratic melt filling neck zones of D_2 boudins is the same as the age of the Amspoort-type intrusion (Kröner et al., 2004).

4.6.4 D_3 fabric and the Village Mylonite Zone

The granitoid gneisses immediately southwest of the Amspoort-type intrusion (Figs. 4.3, 4.4b) show two crosscutting fabrics. A subvertical and partly migmatitic planar fabric is overprinted by a moderately dipping, non-migmatitic foliation (Fig. 4.4b). The strain intensity of the non-migmatitic foliation gradually increases towards the contact with the underlying deformed Amspoort-type granitoid body. Because of its orientation and migmatitic nature, relics of a subvertical foliation are interpreted to be S_2. The crosscutting fabric, labelled S_3, developed during amphibolite- facies conditions as documented by ductile deformation of feldspars.

Towards the NE, a gradual transition of the D_3 fabric into a subvertical orientation has been observed, and the NE edge of the Amspoort-type intrusion together with adjacent metasediments contain a subvertical solid-state mylonitic S_3 fabric (Fig. 4.5i), parallel to the S_2 fabric of the adjacent migmatites. This zone of intense solid-state deformation is also visible on the satellite image and has been defined by Goscombe et al. (2003a) as the Village Mylonite Zone

(Figs. 4.3, 4.4b). The S_3 fabric of the Village Mylonite Zone developed under low-temperature (greenschist- facies) conditions, which is documented by the brittle behaviour of feldspars accompanied by ductile deformation of quartz. Numerous discrete shear zones of brittle–ductile deformation have been observed parallel to the subvertical D_2 fabric. In this case, the distinction between S_2 and S_3 is not based on fabric orientation but on the temperature of deformation. An L_3 aggregate lineation is associated with S_3. In contrast to L_2, L_3 is horizontal or inclined only few degrees towards WNW or SSE (Fig. 4.4b). Rotated K- feldspar porphyroclasts in the granite (Fig. 4.5h), as well as σ- and δ-objects in mylonitic orthogneisses consistently show a sinistral sense of shear. F3 folds and kink- band folds with fold axes plunging moderately to the SE were observed in metasediments in the core of the Village Mylonite Zone (Fig. 4.5c).

4.7 Structural evolution east of the Puros Shear Zone

The deformation fabric along the western margin of the Central Kaoko zone (east of the Puros Shear Zone) is characterized by large-scale antiforms mostly composed of metasediments and cored by Palaeopro-terozoic granitoids (Figs. 4.3, 4.6). The southwestern limb of a kilometer-scale antiform immediately adjacent to the Puros Shear Zone shows numerous metre to decime-tre-scale tight to isoclinal folds. Their axial planes are parallel to the northwest-dipping foliation, suggesting D_2 refolding of an earlier D_1 fabric (Figs. 4.5e, 4.6). An L_2 lineation in this area has the same orientation as that observed W of the Puros Shear Zone, e.g. shallowly plunging to the NW, and kinematic indicators such as asymmetric σ-objects show a sinistral sense of movement. Close to isoclinal folds were not observed in the northeastern limb of the antiform. Instead, open to close recumbent folds were seen to refold a steep foliation (Figs. 4.5f, 4.6). Their axial planes show similar orientations as the foliation on the south- western limb of the antiform, and fold axes are parallel to the L_2 lineation. The granitoid gneiss in the core of the antiform shows numerous kinematic indicators (shear bands and isoclinal folds, Fig. 4.5g) with opposite sense of shear to indicators in the southwestern limb. The most plausible explanation of this feature is a D_1 origin for these indicators in the (probably flat-lying) S_1 foliation and their passive rotation during D_2.

We interpret the fabric of the antiform as a result of D_2 deformation superimposed on an early shallowly dipping D_1 fabric. The southwestern limb of the antiform represents an early D_1 fabric, which was rotated and shortened during D_2 as indicated by numerous tight to isoclinal F_2 folds. In contrast, lack of such folds in the northeastern limb suggests passive rotation of the S_1 foliation with minor folding during D_2. The development of open, recumbent folds is late and

probably attributed to the increasing role of overburden after relaxation of the D_2 deformation in this part of the study area.

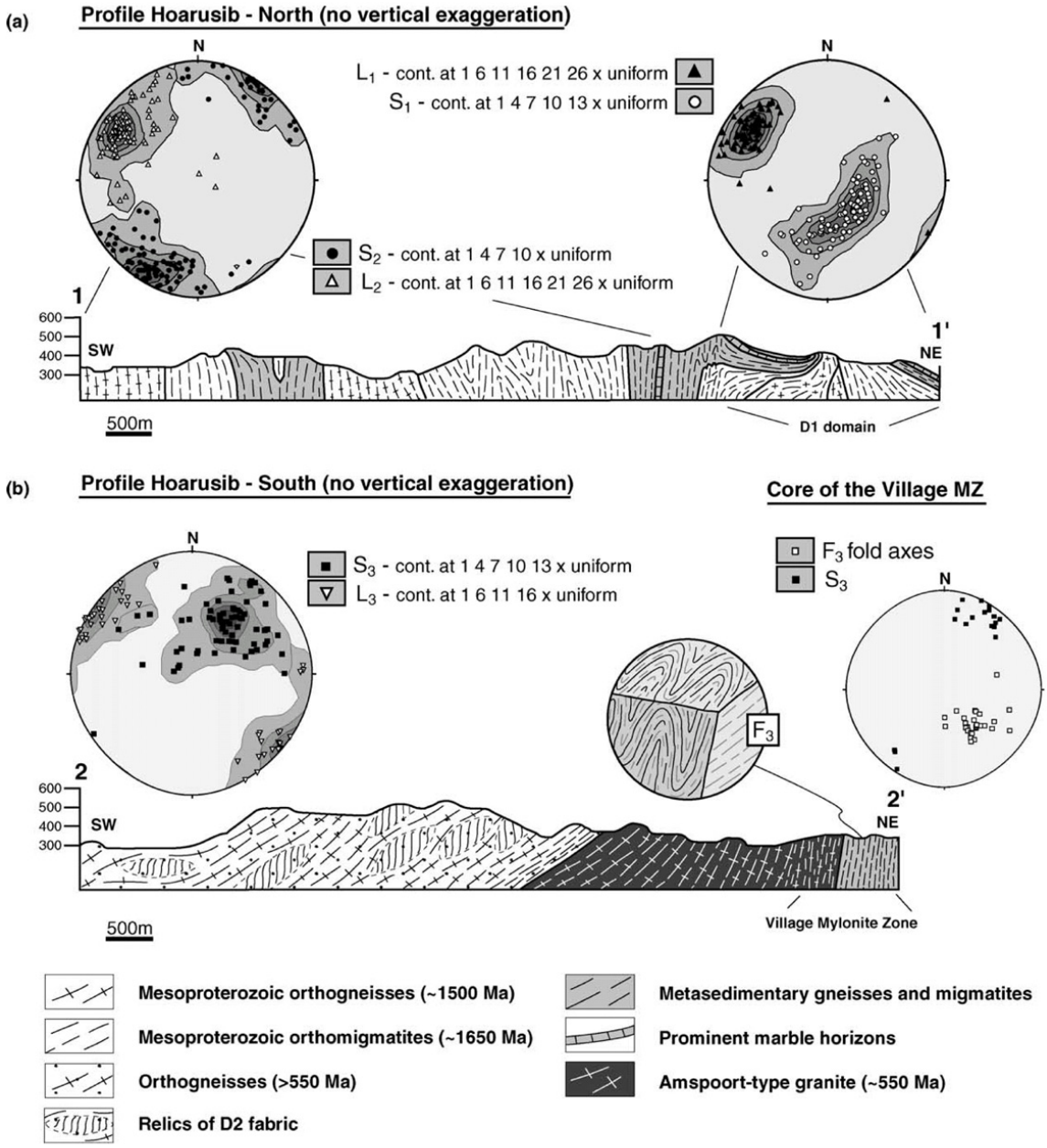

Fig. 4.4. Geological cross-sections over the Western Kaoko zone in the Puros area (see Fig. 4.3 for position of cross-sections). (a) The cross-section over the northeastern part of the Western Kaoko zone showing the relationship between the D_1 and D_2 deformations. The presence of folded D_1 domains (NE part of the cross-section) suggests early flat-lying D_1 metamorphic fabric. To the SW, S_1 fabric becomes intensively folded and later completely overprinted by subvertical S_2 foliation. (b) The cross-section over the southwestern part of the studied area shows relics of subvertical S_2 fabric in the pre-550 Ma granitoids, and its reworking by D_3 deformation. In the 550 Ma old Amspoort-type granite, only one solid-state fabric (S_3) is developed. Progressive steepening of the S_3 fabric and stress concentration along the NE edge of the Amspoort-type granite during D_3 is responsible for the development of the Village Mylonite Zone.

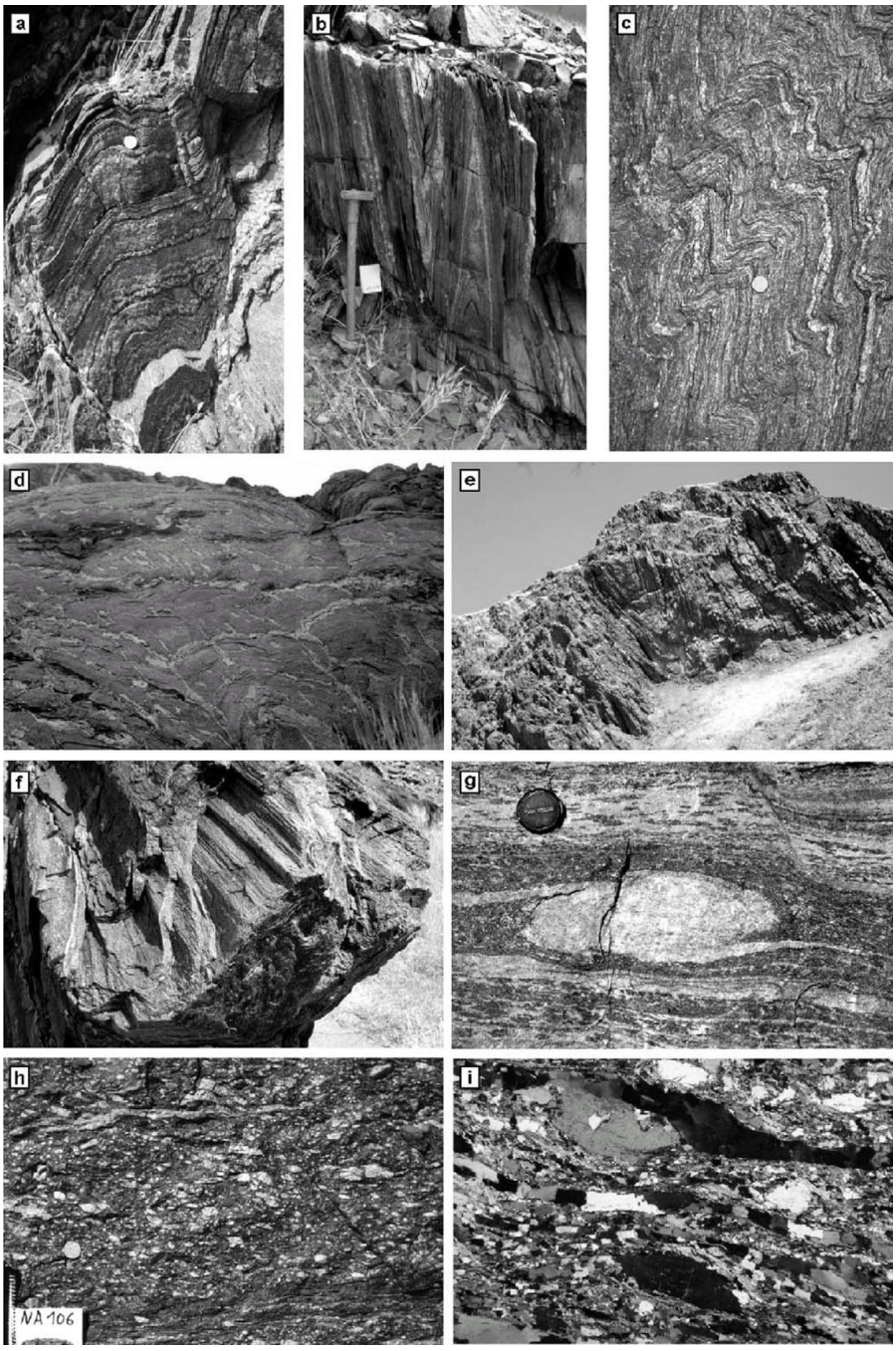

Fig. 4.5. (a) Relic migmatitic S_1 foliation in orthomigmatites of the Western zone folded by F_2 folds. (b) Isoclinal F_2 folds in amphibolites of the Western zone, surrounded by subvertical S_2 foliation. (c) F_2 kink-band folds associated with the deformation on the Village Mylonite Zone. (d) Migmatitic S_1 foliation folded during D_2. Flat migmatitic S_1 fabric and alignment of melt pockets in steep axial zones of the F_2 folds suggest, that the D_{1-2} transition occurred at high-temperature conditions. (e) Large F_2 fold in orthomigmatites of the Western zone at the contact with the Central zone. (f) Recumbent folds in metasediments of the eastern limb of a large-scale antiform at the western margin of the Central zone. (g) Isoclinal fold in granodioritic migmatites of the core of a large-scale antiform at the western margin of the Central zone. The foliation is subvertical and the fold suggests dextral sense of movement. (h) Deformed porphyric Amspoort-type granite in the core of the Village Mylonite Zone. The foliation is vertical and aligned K-feldspar pophyroclasts show sinistral sense of movement. (i) Photomicrograph of deformed porphyric Amspoort-type granite. Relics of K-feldspar porphyroclasts and ribbons of recrystallized quartz and feldspars document solid-state deformation of this granitoid body.

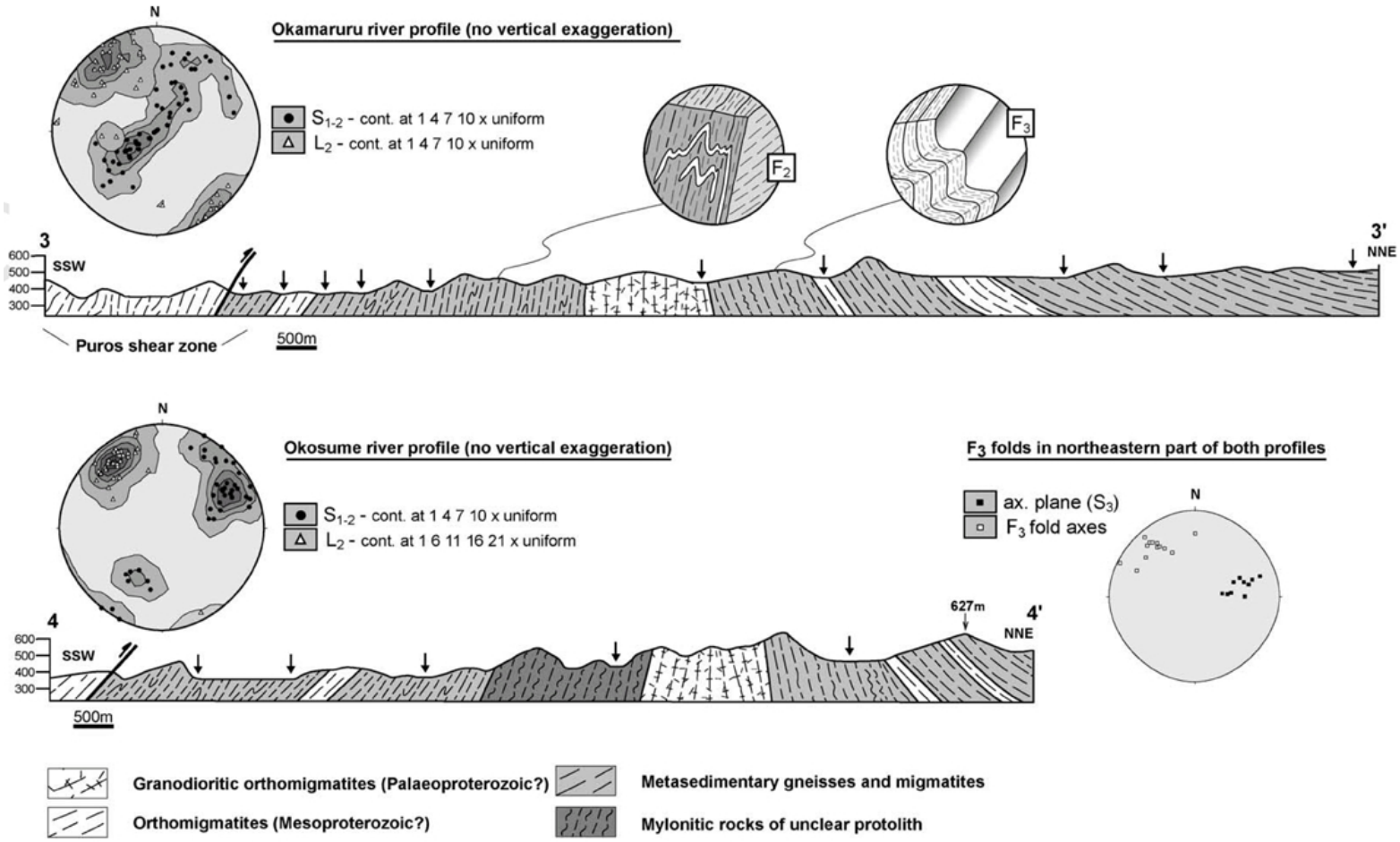

Fig. 4.6. Geological cross-sections over the westernmost part of the Central Kaoko zone in the Puros area (see Fig. 5.3 for position of cross-sections; the arrows show actual position of the Okamaruru and Okosume rivers). The fabric is characterized by a large-scale antiform built of metasediments with exhumed granitoid basement in its core. SW limb shows numerous closed to isoclinal F2 folds suggesting its strong shortening during D_2. In contrast, lack of these folds in the NE limb suggests only passive rotation of the S1 foliation during D_2 event. Gentle refolding of the steep fabric by recumbent kink-band folds suggests deformation activity during late D_2 to D_3.

4.8 Discussion

4.8.1 D_1 deformation and associated metamorphic conditions

The presence of D_1 domains in the area southwest of the Puros Shear Zone is strong evidence that the development of the subvertical S_2 fabric is a secondary feature affecting already existing metamorphic fabric. The question arises, whether the D_1 and D_2 fabrics have developed contemporaneously during transpressive deformation or if there is an evidence for two successive stages of their development. The theory of deformation partitioning involving thrusting and strike-slip deformation during transpression (Teyssier et al., 1995) assumes the development of a transcurrent shear zone accommodating the simple-shear component, whereas the deformation in the adjacent regions is contemporaneously accommodated by pure shear. In our case, the pure shear-dominated regions outside the Puros Shear Zone clearly show folded high-temperature foliation. We argue that any pure shear deformation under such a ductile conditions would result in the development of steep fabric slightly oblique to the major shear zone, whereas more distal, low-temperature parts might develop discrete zones of thrusting. We do indeed see this process, but it is superimposed on already present metamorphic foliation. Moreover, in the case of contemporaneous development of flat-lying foliation and subvertical transcurrent shear zones, the reverse case should be developed in which ductile, flat-lying fabric transects existing vertical foliation of the transcurrent shear zones. This case has never been observed. There is no indication of any high-temperature event between the emplacement of basement orthogneiss protolith (~1500 Ma) and the Neoproterozoic (~575–550 Ma) deformation and magmatism in the basement rocks of the study area (Goscombe et al., 2003b; Kröner et al., 2004), which would allow interpreting the observed D_1 fabric as pre-Neoproterozoic. In our interpretation, the parallelism of L_1 and L_2 lineations and ubiquitous presence of relics of pre- D_2 metamorphic foliation suggests that the D_1 and D_2 fabrics are part of a single progressive deformation that was separated in two distinct HT–MT deformation phases. Some authors consider such a two-phase evolution as a common tectonic process on convergent boundaries (McClellan et al., 2000).

The flat-lying S_1 foliation and WNW plunging L_1 lineation in the D_1 domains suggest that D_1 deformation was associated with east–southeast- directed thrusting, oblique with respect to the western flank of the Central Kaoko zone. Local D_1 thrusting of basement migmatites over their metasedimentary cover observed in the D_1 domains, as well as the development of the inverted metamorphism in the studied area (Gruner, 2000; Goscombe et al., 2003b) support this interpretation. Gruner (2000) and Goscombe et al. (2003b) estimated peak metamorphic pressures of ~9 kbar at ~650 °C for the westernmost (kyanite–sillimanite) zone of the Central Kaoko zone.

Metamorphic conditions in the eastern part of the Western Kaoko zone (sillimanite–K- feldspar zone) were estimated at ~690 °C at ~4.5 kbar (Gruner, 2000), or even 750–900 °C at 7–10 kbar (Goscombe et al., 2003b) which are consistent with observed melting during D_1–D_2. The presence of a garnet–sillimanite–biotite–K-feldspar assemblage in the folded S_1 foliation confirms that high-temperature/low-pressure conditions existed at peak conditions during D_1. Evidence for an earlier medium- or high-pressure history of the Western Kaoko zone has been provided by Goscombe et al. (2003b) who described inclusions of kyanite from garnets in the low-pressure assemblages. The low-pressure re-equilibration of the westernmost part of the Central Kaoko zone suggests the onset of equilibration of metamorphic conditions between the high-temperature Western zone and the medium-temperature Central zone, probably during transition between D_1 and D_2. In any case, high-temperature metamorphism and migmatitization during D_1 in the Western Kaoko zone and medium-pressure/medium-temperature metamorphic conditions in the western part of the Central Kaoko zone (Gruner, 2000; Goscombe et al., 2003b) suggest, that D_1 thrusting resulted in the development of a tectonically induced inverted metamorphic gradient in the central Kaoko Belt.

4.8.2 D_2 and the development of the Puros Shear Zone

Refolding of S_1 in the D_1 domains and subsequent development of a steep to sub-vertical S_2 foliation is associated with the development of a shallowly plunging L_2 lineation (Figs. 4.4a, 4.6). These data suggest that all rock types along the contact between the Western and Central Kaoko zones underwent strong deformation associated with NNE–SSW oriented shortening and WNW–ESE stretching. We interpret the post-D_1 evolution in the Puros area as follows: The contrasting thermal state between the colliding Western and Central Kaoko zones, as well as a high degree of obliquity during thrusting, led to concentration of deformation in the rheologically weaker, migmatitic unit of theWestern Kaoko zone after maximum thickening of the downgoing Central Kaoko zone had been achieved. Stress concentration along the contact between the hot migmatitic Western Kaoko zone and colder Central Kaoko zone led to the development of a large-scale transcurrent sinistral shear zone—the Puros Shear Zone. The high intensity of deformation along this shear zone is demonstrated by an almost complete reworking of the D_1 fabric to the southwest, and by strong shortening and deformation of the southwestern limb of the kilometer-scale antiform at the southwestern margin of the Central Kaoko zone (Figs. 4.4a, 4.6).

Extensive migmatitization reached a peak during the transition from D_1 to D_2. Emplacement of porphyritic granitoids into both the S_1 and S_2 fabrics coincided with this transition. The

Amspoort-type granite intruded mostly into the S_2 subvertical fabric, which is supported by field observation and by marked elongation of this granitoid body parallel to the D_2 fabric of the Western Kaoko zone. Similar ages for the Amspoort-type granite and leucocratic melt in migmatites (Kröner et al., 2004) is strong evidence that granite emplacement coincided with peak metamorphic conditions in surrounding lithologies.

4.8.3 D_3 and the evolution of the Village Mylonite Zone

Solid-state deformation of the Pan-African Amspoort-type granite (Fig. 4.5i), as well as medium- to low-temperature deformation of surrounding metasediments and basement granitoids suggests that the D_3 phase played an important role during decreasing temperatures. The Village Mylonite Zone represents a zone of concentrated D_3 deformation along the northeastern edge of the Amspoort-type intrusion and the adjacent metasediments. Regarding the localization of deformation, the development of the Village Mylonite Zone is strongly coupled with the earlier evolution of the D_2 fabric. Biotite-rich Amspoort-type granite (elongated parallel with the Puros Shear Zone) acted as a rheologically weak zone for strain localization during cooling of the entire unit. High-temperature D_2 deformation was more or less homogeneously distributed over the entire eastern margin of the Western Kaoko zone. However, cooling of the entire unit enhanced localization of deformation and resulted in the development of the Village Mylonite Zone. We assume that, after cooling of the unit (e.g., during the D_3), the Village Mylonite Zone took over the role of the Puros Shear Zone and accommodated most of the D_3 strain.

4.8.4 Tectonic evolution of the Puros area

In previous studies, the structure of the central Kaoko Belt has been interpreted as a result of transpressive deformation with strain partitioning into transcurrent and overthrusting components (Dürr and Dingeldey, 1996; Dürr et al., 1995; Goscombe et al., 2003a). In this view, both the subvertical high- temperature fabric along the Puros Shear Zone and the more shallow, medium-temperature fabric of the Central Kaoko zone developed at the same time. The observations of the above authors lead them to conclude that the structure of the central Kaoko Belt represents a half pop-up structure generated during transpression (Dürr and Dingeldey, 1996; Dürr et al., 1995; Goscombe et al., 2003a). However, our data document two separate HT–MT deformation phases responsible for the formation of the present-day structural pattern of the Central and Western zones, accompanied by localized brittle–ductile LT deformation.

In our interpretation, the structures associated with D_1 deformation indicate oblique thrusting as a mechanism responsible for crustal thickening of the Central Kaoko zone (Fig. 4.7a). There are several examples from high- to low-grade terrains, which document the early development of a thrust-related fabric and its subsequent reworking by localized large-scale transcurrent shear zones (e.g. Vassallo and Wilson, 2002; Carosi and Palmeri, 2002; Little et al., 2002; McClellan et al., 2000). Especially in the middle and lower crust, a significant period of underthrusting probably plays an important role in the development of a metamorphic fabric during oblique collision of crustal segments with initially different rheological profiles (Thompson et al., 2001), and the change in tectonic regime towards the development of localized (at any scale) transcurrent shear zones seems to be the result of increased resistance of the down-going plate due to buoyancy forces. In the case of the central Kaoko Belt, thickening is documented by Barrovian-type medium-pressure metamorphism in metasediments of the Central zone. Estimated peak pressure metamorphic conditions of ~9 kbar at ~650 °C (Gruner, 2000; Goscombe et al., 2003b) suggest that the western part of the Central zone must have been buried to depths of ~35 km. A metamorphic gradient with decreasing conditions towards the east indicates preservation of a palaeogradient developed during oblique underthrusting of the Central Kaoko zone below the Western Kaoko zone.

A collisional scenario requires at least the same depth of burial for the downgoing Central zone and overriding Western zone prior to its exhumation by thrusting. Kyanite inclusions in garnets from the LP assemblage of the Western zone (Goscombe et al., 2003b) suggest an earlier MP–HP history for this unit, but lack of a corresponding mineral assemblage does not allow any PT estimates. Metasediments in the D_1 domains only show sillimanite-bearing low-pressure assemblages in the matrix, and meta-igneous lithologies show the formation of foliation-parallel leucosomes. The obvious contrast between low-pressure assemblages developed during D_1 oblique thrusting in the overriding unit and preservation of medium-pressure assemblages in the underlying metasediments suggest that the overriding unit (i.e., the Western Kaoko zone) was subjected to a higher geothermal gradient than the underlying Central Kaoko zone. Elevated thermal conditions in this unit as well as influx of fluids released from progressively metamorphosed underlying metasediments of the Central zone probably led to complete transformation of potential early high- to medium-pressure assemblages and enhanced early migmatitization in the D_1 domains.

The development of a subvertical fabric along the contact between the Central and Western Kaoko zones represents a separate phase of deformation overprinting an early flat-lying fabric (Fig. 4.7b). Oblique thrusting ceased when metasediments of the western margin of the Central zone were buried to depths of 30–40 km, as inferred from recorded peak pressures. At this stage

the overriding Western unit was already partially molten and thus weaker than the underlying medium-temperature unit. The resulting rheological contrast and increasing buoyancy in the downgoing crustal segment inhibited further underthrusting of the Central zone under the Western zone, and the regime of D_1 oblique southeastward thrusting changed into D_2 sinistral transcurrent movement. Since the beginning of D_2, most deformation was of strike-slip character and concentrated in the weak Western zone, as documented by the almost complete transformation of the early D_1 fabric. In the Central Kaoko zone, the intensity of the D_2 overprint decreases rapidly with increasing distance from the Western zone, and approximately 20 km from the contact with the Western zone, the early metamorphic fabric was only refolded by large-scale folds suggesting pure shear-dominated deformation. The combination of strike-slip deformation along the contact of the Western and Central zone and pure shear deformation in more distal parts is consistent with a sinistral transpressional regime (Sanderson and Marchini, 1984; Tikoff and Teyssier, 1994). Intense deformation along the contact with the Western zone gave rise to the Puros Shear Zone. The replacement of kyanite by sillimanite at the western margin of the Central zone can be seen as a direct consequence of D_2 deformation imposed on the medium-pressure metasediments, and the extent of an intense D_2 overprint can thus be approximated by the width of the first sillimanite zone (Fig. 4.2).

4.8.5 The influence of D_2 and D_3 on the thermal evolution of the Western Kaoko zone

L_2 stretching lineations developed on subvertical S_2 planes are consistently plunging at shallow angles to the northwest (Fig. 4.4a) and their orientation suggests that there is a consistent component of exhumation of the Western Kaoko zone during D_2 sinistral transpression. The angle between the strike of the Puros Shear Zone and the L_1 lineation preserved in the D_1 domains approximates the initial obliquity of convergence between the Western and Central Kaoko zones, reaching values <25° in the Puros area. As the lineation shows almost identical orientation during D_1– D_3, we may assume that the angle of convergence did not change substantially in time. Thompson et al. (1997) have shown that in transpressive zones, an angle of convergence <30° leads to a substantial increase in temperature due to a low exhumation rate. In regions with a hot initial geotherm such a tectonic environment may result in a long period of high-temperature metamorphism associated with extensive melting. This is in good agreement with the high degree of melting in rocks of the eastern part of the Western Kaoko zone observed during the D_2 deformation.

Thompson et al. (1997) have shown that the angle of convergence <30° will result in a long time span between high-temperature and low-temperature events. In the case of the Kaoko Belt, identical conclusions can be deduced from geochronological data. Ahrendt et al. (1983) published K–Ar cooling ages for muscovite and biotite from the Central and Western Kaoko zone. In the area strongly affected by D_2– D_3 deformation, ages of 527–530 (±11) Ma suggest a ~20–25 Ma time span between high-grade metamorphism and melting (ca. 550 Ma—see above) and cooling of this part of the belt. Such time interval is consistent with that modelled by Thompson et al. (1997) for collisional zones with an angle of convergence of 30°. An identical orientation of D_2 and D_3 structures suggests that sinistral transpression was the controlling tectonic mechanism since high-temperature metamorphic conditions in the Western Kaoko zone have been attained. K–Ar cooling ages in the vicinity of the Sesfontein thrust fall in an interval between 442 and 479 Ma (Ahrendt et al., 1983). Such young ages may suggest that the latest deformation was transferred to the marginal parts of the orogen after cooling of the Western and Central zones and produced the low-angle Sesfontein thrust (Goscombe et al., 2003a).

4.8.6 Tectonic setting of the Kaoko Belt

It is problematic to infer any large-scale model of tectonic setting of the Kaoko Belt just from the geological information, since most of the original Kaoko Belt is missing due to opening of the Atlantic ocean.

As stated by Dürr and Dingeldey (1996), the lack of ophiolites or subduction-related high-pressure rocks casts doubt on the idea of subduction-related collision in the Kaoko Belt. The lack of eclogites in the Kaoko Belt may, however, be the result of long-lasting high- temperature metamorphism completely overprinting any earlier high-pressure assemblage. An important information for the interpretation of the geologic history of the Kaoko Belt is the onset of rift-related felsic volcanism along the thinned southern margin of the Congo Craton, which was dated by Hoffman et al. (1996) at ~756 Ma. However, this age may only apply to the Damara Belt, and it remains uncertain whether or not the onset of rifting at the southwestern margin of the Congo Craton occurred at the same time. Da Silva et al. (1999) and Hartmann et al. (2002) reported zircon ages of 762±8 and ~780 Ma for granitoids in the Dom Feliciano Belt (South American counterpart of the Kaoko Belt), which are similar to those of Hoffman et al. (1996).

Calc-alcaline batoliths in the Dom Feliciano Belt were dated at 620–590 Ma and interpreted as the deep part of a continental arc (Basei et al., 2000), whereas other authors relate magmatic rocks of this age to the syn-collisional peak of regional metamorphism (Babinski et al., 1997; da Silva et al., 1999; Hartmann et al., 2000). Two ages corresponding to early high-grade meta-

morphism at 656±8Ma and 645±3.5 Ma were obtained from the Western Kaoko zone by Seth et al. (1998) and by Franz et al. (1999), respectively. Franz et al. (1999) suggested that these ages may still be related to the rifting period and granulite-facies metamorphism in the lower crust. The above data suggest, that there is a time-span of about 140–170 million years between the onset of rifting and magmatic arc formation. All the younger ages of ~580–550 Ma obtained by Seth et al. (1998), Franz et al. (1999) and Kröner et al. (2004) may then correspond to collisional processes in the Kaoko Belt.

Very little is known about the tectonic position of pre-580 Ma magmatism in the coastal part of the Western Kaoko zone and about the tectonic evolution of the coastal part of the Kaoko Belt in general. Our field study shows that the boundary between the Western and Central Kaoko zones is a modified zone of underthrusting of the southwestern margin of the Congo Craton below a unit with a completely different geothermal gradient, and this suggests that the contact between these two units represents a major tectonic boundary controlling the tectonic evolution of the Pan-African Kaoko Belt.

4.9 Conclusions

Our study has shown that, prior to the development of the large-scale transcurrent Puros Shear Zone, a period of oblique underthrusting led to the development of an inverted metamorphic gradient in the central part of the Kaoko Belt. An early period of high-temperature sinistral transpression was responsible for almost complete reworking of an earlier, underthrusting-related fabric in the eastern part of the Western Kaoko zone and at the westernmost margin of the Central Kaoko zone. In the Western Kaoko zone, continuous sinistral transcurrent movements are documented by the development of the low-temperature Village Mylonite Zone, which is accompanied by a heterogeneous array of small-scale, low-temperature shear zones in migmatites of the eastern part of the Western Kaoko zone. Consistent kinematics and orientation of the stretching lineation in the high-temperature migmatites along the Puros Shear Zone and in low-temperature mylonites of the Village Mylonite Zone suggest that the Village Mylonite Zone took over the role of the Puros Shear Zone during cooling of the central part of the Kaoko Belt. In our interpretation, the Puros Shear Zone represents a modified major Pan-African thrust zone developed along strongly reworked western margin of the Congo Craton.

(a) **D1 - oblique thrusting**

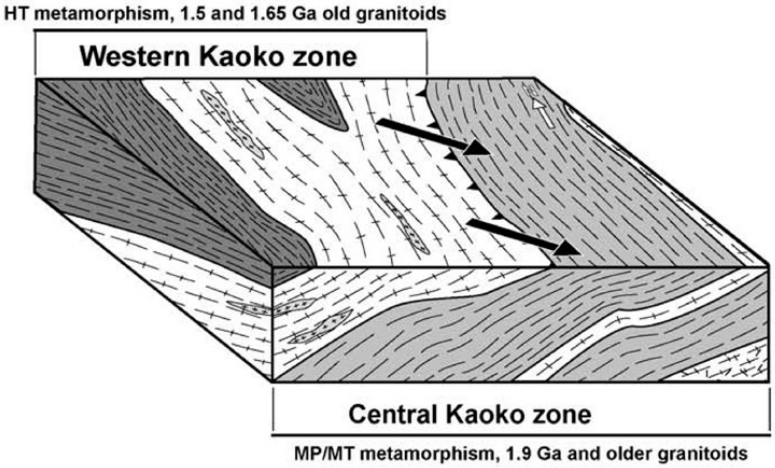

(b) **D2 - sinistral transpression**

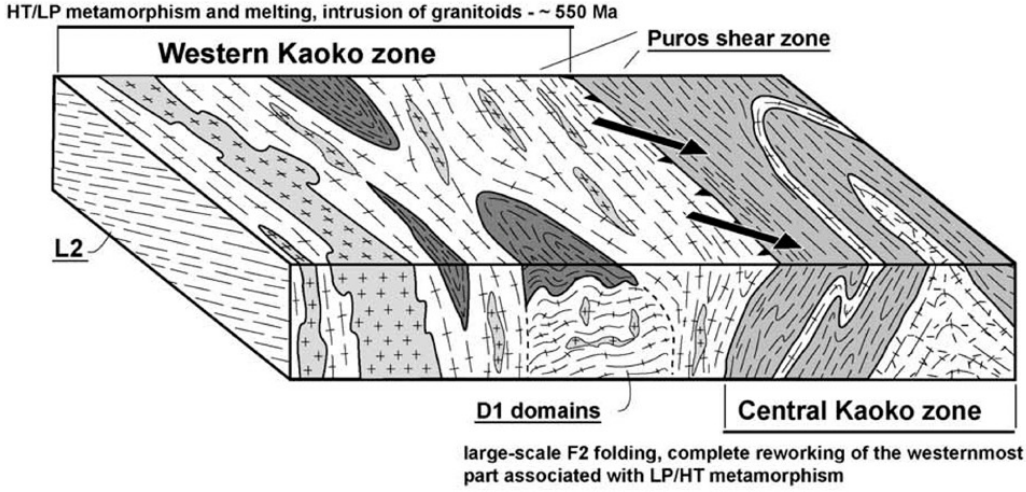

(c) **D3 - sinistral strike-slip**

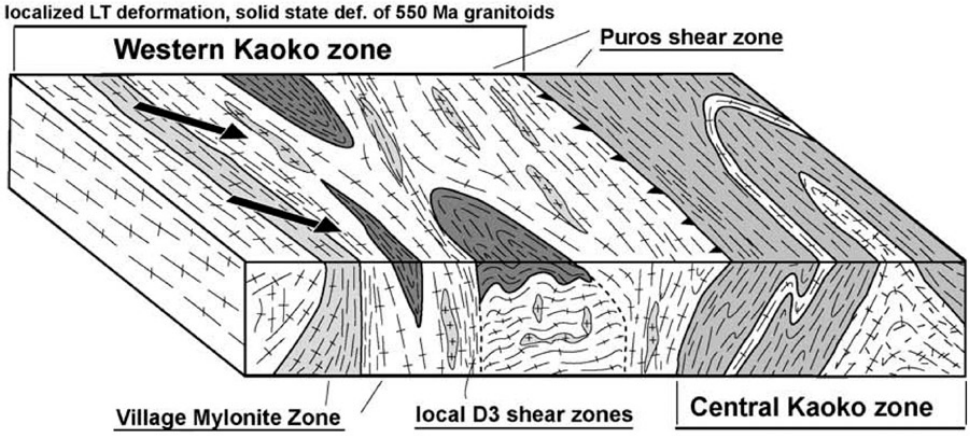

Fig. 4.7. Block diagrams showing three major deformation events responsible for the present-day geology of the central Kaoko Belt. (a) The development of flat-lying D_1 fabric suggests an early period of oblique thrusting. During this event, basement rocks of the Western Kaoko zone (upper plate) already show the development of foliation-parallel leucosomes. Northwestward underthrusting is responsible for the development of inverted metamorphic gradient in metasediments of the Central Kaoko zone (western margin of the Congo Craton). (b) After maximum possible thickening of the Central zone has been attained, oblique thrusting changes into sinistral transpression. This is justified by WSW–ENE shortening associated with strong folding of all lithologies and accompanied by strong NNW–SSE stretching. At this stage the Puros Shear Zone develops along the contact of the Central and Western zones. Enhanced partial melting and intrusion of dykes and magmatic bodies into subvertical D_2 fabric suggest that this change in deformation regime occurs at peak-temperature conditions. (c) D_3 is associated with decreasing temperature conditions and concentrates into narrow shear zones of brittle-ductile character. The low-temperature Village Mylonite Zone is the result of concentration of deformation at the northeastern edge of the Amspoort-type intrusion.

4.10 References

Ahrendt, H., Behr, H.-J., Clauer, N., Hunziker, J.C., Porada and H.,Weber, K. (1983). The northern branch: depositional development and timing of the structural and metamorphic evolution within the framework of the Damara orogen. In: Martin, H., Eder, F.W. (Eds.), Intracontinental Fold Belts. Springer-Verlag, Berlin, pp. 723–743.

Babinski, M., Chemale, F., van Schmus, W.R., Hartmann, L.A. and da Silva, L.C. (1997). U–Pb and Sm–Nd geochronology of the Neoproterozoic granitic-gneissic Dom Feliciano Belt, Southern Brazil. *Journal of South American Earth Science*, **10**, 263–274.

Basei, M.A.S., Siga Jr., O., Masquelin, H., Harara, O.M., Reis Neto, J.M. and Preciozzi, P. (2000). The Dom Feliciano Belt of Brazil and Uruguay and its foreland domain, the Rio de la Plata Craton, framework, tectonic evolution and correlation with similar provinces of southwest Africa. In: Cordani, U.G., Milani, E.J., Thomaz Filho, A., Campos, D.A. (Eds.), *Tectonic Evolution of South America*, **31**, pp. 311–334, IGC Rio de Janeiro.

Bozkurt, E. (2001). Neotectonics of Turkey—a synthesis. Geodin. Acta. 14, 3–30. Burger, A.J., Coerze, F.J., 1971. Radiometric age measurements on rocks from southern Africa to the end of 1971. *Bulletin Geological Survey Of South Africa*, **58**, 46.

Burger, A.J., Clifford, T.N. and Miller, R.McG. (1976). Zircon U–Pb ages of the Fransfontein granitic suite, northern South West Africa. *Precambrian Research*, 3, 403–431.

Carosi, R. and Palmeri, R. (2002). Orogen-parallel tectonic transport in the Variscan belt of northeastern Sardinia (Italy): implications for the exhumation of medium-pressure metamorphic rocks. *Geological Magazine*, **139**, 497–511.

Dingeldey, D.P., Dürr, S.B., Charlesworth, E.G., Franz, L., Okrusch, M. and Stanistreet, I.G. (1994). A geotraverse through the northern coastal branch of the Damara orogen west of Sesfontein, Namibia. *Journal of African Earth Science*, **19**, 315–329.

Dürr, S.B. and Dingeldey, D.P. (1996). The Kaoko belt (Namibia): part of a late Neoproterozoic continental-scale strike-slip system. *Geology*, **24 (6)**, 503–506.

Dürr, S.B., Dingeldey, D.P., Okrusch, M. and Franz, L. (1995). Transpression in the Panafrican Kaoko belt of northern Namibia: structural and petrological implications. *Zeitblatt Geologischer Paläontologie*, **1 (3/4)**, 495–505.

Egydio-Silva, M., Vauchez, A., Bascou, J. and Hippertt, J. (2002). High- temperature deformation in the Neoproterozoic transpressional Ribeira belt, southeast Brazil. *Tectonophysics*, **352**, 203–224.

Frantz, J.C. and Botelho, N.F. (2000). Neoproterozoic granitic magmatism and evolution of the eastern Dom Feliciano Belt in southernmost Brazil: a tectonic model. *Gondwana Research*, **3**, 7–19.

Franz, L., Romer, R.L. and Dingeldey, D.P. (1999). Diachronous Pan- African granulite-facies metamorphism (650 and 550 Ma) in the Kaoko belt, NW Namibia. *European Journal of Mineralogy*, **11**, 167–180.

Goscombe, B., Hand, M. and Gray, D. (2003a). Structure of the Kaoko Belt, Namibia: progressive evolution of a classic transpressional orogen. *Journal of Structural Geology*, **25**, 1049–1081.

Goscombe, B., Hand, M., Gray, D. and Mawby, J. (2003b). The metamorphic architecture of a transpressional orogen: the Kaoko Belt, Namibia. *Journal of Petrology*, **44**, 679–711.

Gruner, B. (2000). Metamorphoseentwicklung im Kaokogürtel, NW- Namibia: Phasen-petrologische und geothermobarometrische Untersuchungen panafrikanischer Meta-pelite. *Unpublished PhD Dissertation*, *University of Würzburg*, Germany.

Guj, P. (1970). The Damara Mobile Belt in the South-western Kaokoveld, South West Africa. Bull. *Precambrian Research Unit, University of Cape Town, South Africa, Bulletin,* **10**, 168pp.

Hartmann, L.A., Leite, J.A.D., Da Silva, L.C., Remus, M.V.D., McNaughton, N.J., Groves, D.I., Fletcher, I.R., Santos, J.O.S. and Vasconcellos, M.A.Z. (2000). Advances in SHRIMP geochronology and their impact on understanding the tectonic and metallogenic evolution of southern Brazil. *Australian Journal of Earth Sciences*, **47**, 829– 844.

Hartmann, L.A., Santos, J.O.S., Bossi, J., Campal, N., Schipilov, A. and McNaughton, N.J. (2002). Zircon and titanite U-Pb SHRIMP geochronology of Neoproterozoic felsic magmatism on the eastern border of the Rio de la Plata Craton, Uruguay. *Journal of South American Earth Science*, **15**, 229–236.

Hoffman, P.F., Hawkins, D.P., Isachen, C.E. and Bowring, S.A. (1996). Precise U–Pb zircon ages for early Damaran magmatism in the Summas Mountains and Welwitschia Inlier, northern Damara belt, Namibia. *Communications of the Geological Survey of Namibia*, **11**, 47–52.

Hole, J.A., Beaudoin, B.C. and Klemperer, S.L. (2000). Vertical extent of the newborn San Andreas fault at the Mendocino triple junction. *Geology*, **28**, 1111–1114.

Kröner, S., Konopásek, J., Kröner, A., Poller, U., Wingate, M.W.D., Passchier, C.W. and Hofmann, K.-H., (2004). U–Pb and Pb–Pb zircon ages for metamorphic rocks in the Kaoko belt of NW Namibia: a Palaeo- to Mesoproterozoic basement reworked during the Pan-African orogeny. S*outh African Journal of Geology*, **107**, 455-476.

Lamarche, G. and Lebrun, J.F. (2000). Transition from strike-slip faulting to oblique subduction: active tectonics at the Puysegur Margin, South New Zealand. *Tectonophysics*, **316 (1/2)**, 67–89.

Lebrun, J.F., Lamarche, G., Collot, J.Y. and Delteil, J. (2000). Abrupt strike-slip fault to subduction transition: the Alpine Fault- Puysegur Trench connection, New Zealand. *Tectonics*, **19**, 688–706.

Little, T.A., Holcombe, R.J. and Ilg, B.R. (2002). Kinematics of oblique collision and ramping inferred from microstructures and strain in middle crustal rocks, central Southern Alps, New Zealand. *Journal of Structural Geology*, **24**, 219–239.

Matte, P., Tapponnier, P., Arnaud, N., Bourjot, L., Avouac, J.P., Vidal, P., Qing, L., Pan, Y.S. and Yi,W. (1996). Tectonics of Western Tibet, between the Tarim and the Indus. *Earth and Planetary Science Letters*, **142**, 311–330.

McClellan, W.C., Tikoff, B. and Manduca, C.A. (2000). Two-phase evolution of accretionary margins: examples from the North American Cordillera. *Tectonophysics*, **326 (1/2)**, 37–55.

McCrory, P.A. (2000). Upper plate contraction north of the migrating Mendocino triple junction, northern California: implications for partitioning of strain. *Tectonics*, **19**, 1144–1160.

Miller, R.Mc.G. (1983). The Pan-African Damara Orogen of South West Africa/ Namibia. In: Miller, R.Mc.G. (Ed.), The Damara Orogen. *Geological Society of South Africa Special Publication*, **11**, 431–515.

Porada, H. (1989). Pan-African rifting and orogenesis in southern to equatorial Africa and eastern Brazil. *Precambrian Research*, **44**, 103–136.

Ring, U., Kröner, A., Buchwaldt, R., Toulkeridis, T. and Layer, P.W. (2002). Shear-zone patterns and eclogite-facies metamorphism in the Mozambique belt of northern Malawi, east-central Africa: implications for the assembly of Gondwana. *Precambrian Research*, **116**, 19–56.

Sanderson, D. and Marchini, W. (1984). Transpression. *Journal of Structural Geology*, **6**, 449–458.

Scheuber, E. and Gonzalez, G. (1999). Tectonics of the Jurassic- Early Cretaceous magmatic arc of the north Chilean Coastal Cordillera (22 degrees-26 degrees S): a story of crustal deformation along a convergent plate boundary. *Tectonics*, **18**, 895– 910.

Seth, B., Kröner, A., Mezger, K., Nemchin, A.A., Pidgeon, R.T. and Okrusch, M. (1998). Archaean to Neoproterozoic magmatic events in the Kaoko belt of NW Namibia and their geodynamic significance. *Precambrian Research*, **92**, 341–363.

da Silva, L.C., Hartmann, L.A., McNaughton, N.J. and Fletcher, I.R. (1999). SHRIMP U–Pb dating of Neoproterozoic granitic magmatism and collision in the Pelotas Batolith, southernmost Brazil. Intern. *International Geological Review*, **41**, 531–551.

Stanistreet, I.G. and Charlesworth, E.G. (2001). Damaran basement- cored fold nappes incorporating pre-collisional basins, Kaoko Belt, Namibia, and controls on Mesozoic super-continent break- up. *South African Journal of Geology*, **104**, 1–12.

Tegtmeyer, A. and Kröner, A. (1985). U–Pb zircon ages for granitoid gneisses in northern Namibia and their significance for Proterozoic crustal evolution of south-western Africa. *Precambrian Research*, **28**, 311–326.

Teyssier, C., Tikoff, B. and Markely, M. (1995). Oblique plate motion and continental tectonics. *Geology*, **23 (5)**, 447–450.

Thompson, A.B., Schulmann, K. and Ježek, J. (1997). Thermal evolution and exhumation in in obliquely convergent (transpressive) orogens. *Tectonophysics*, **280**, 171–184.

Thompson, A.B., Schulmann, K., Jezek, J. and Tolar, V. (2001). Thermally softened continental extensional zones (arcs and rifts) as precursors to thickened orogenic belts. *Tectonophysics*, **332**, 115–141.

Tikoff, B. and Teyssier, C. (1994). Strain modelling of displacement- field partitioning in transpressional orogens. *Journal of Structural Geology*, **16**, 1575–1588.

Vassallo, J.J. and Wilson, C.J.L. (2002). Palaeoproterozoic regional-scale noncoaxial deformation: an example from eastern Eyre Peninsula, South Australia. *Journal of Structural Geology*, **24**, 1–24.

Chapter 5

Delineation of crustal provinces in the Pan-African Kaoko Belt (Namibia): constraints from U-Pb and Pb-Pb zircon ages and Nd isotopes

(submitted to Gondwana Research)

Delineation of crustal provinces in the Pan-African Kaoko Belt (Namibia): constraints from U-Pb and Pb-Pb zircon ages and Nd isotopes

S. Kröner[1], A. Kröner[1], S. Jung[2]

[1]*Institut für Geowissenschaften, Universität Mainz, 55099 Mainz, Germany*

[2]*Fachbereich Geowissenschaften, Philipps Universität Marburg, 35032 Marburg, Germany*

5.1 Abstract

Closure of the Adamastor Ocean between the South American and African cratons in Neoproterozoic times resulted in the structurally complex Kaoko-Dom Feliciano Belt system exposed in northwestern Namibia and eastern Brazil. New zircon U-Pb ages for the Kaoko Belt confirm intrusion of granitic rocks at ~650 and 580-550 Ma. Previous authors erroneously interpreted this duality of ages as a result of a poly-metamorphic Pan-African history, whereas we favour the idea of an exotic terrane having been brought into contact with the western margin of the Congo Craton during a high-grade metamorphic event at ~580-550 Ma.

Neodymium mean crustal residence ages suggest subdivision of the belt into four parts. Close to the Atlantic Ocean, crustal residence ages <1.7 Ga with moderately negative $\varepsilon_{Nd(t)}$ characterize Neoproterozoic granitoids (Province I). A wide range of initial Sr isotopic values ($^{87}Sr/^{86}Sr_t$ = 0.7075 to 0.7225) suggests heterogeneous crustal sources for these granitoids. To the east of these rocks, Mesoproterozoic (1516-1448 Ma) and late Palaeoproterozoic (1776-1701 Ma) rocks with Nd model ages of 1.8-2.2 Ga occur in the central part of the belt and are probably related to the Eburnian orogenic cycle (Province II). The $\varepsilon_{Nd(t)}$ values of these granitoids are around zero and suggest a predominantly juvenile source. Late Archaean rocks with Nd model ages of 2.7 to 2.8 Ga constitute Province III in the central part of the belt and are distinct from two early Proterozoic samples taken near the Puros Shear Zone which show even older T_{DM} model ages of ~3.3 Ga (Province IV).

Key words: geochronology, Nd-Sr isotopes, Pan-African granitoids, Adamastor Ocean, metapelites

5.2 Introduction

There are several approaches to resolve the geodynamic history of an orogen. Structural analysis is a useful tool to obtain information on the kinematic evolution of an orogen, but one main problem is that only reconstructions of relative successions can be made, and no absolute timing of different tectonic processes can be deduced. Additionally, in deeply eroded belts the exposed rocks were commonly subjected to tectonic processes during high temperatures in the lower crust and, therefore, the early or pre-orogenic history may be obliterated or even annihilated, and only the last tectono-metamorphic event is preserved.

Using various isotopic systems on different minerals or whole-rock samples of granitoid and/or sedimentary origin is a powerful tool to obtain additional information about the formation of an orogen. Accessory minerals such as zircon and monazite are often resistant against resetting at high temperatures and may preserve partial records of older magmatic and/or metamorphic events (e.g., Gulson and Krogh, 1973; Kröner et al., 1994; Mezger and Krogstad, 1997; Copeland et al., 1988; Parrish, 1990; Zhu et al., 1997). Here, conventional U-Pb analyses of single zircon or monazite may unravel different thermal events. In-situ analyses using the high resolution ionprobe or laser ablation ICP-MS techniques may detect such events more precisely, and only the spot size and U-Pb-Th contents are limiting these techniques. Furthermore, major rock-forming minerals, such as garnet, may preserve a memory of their temperature and pressure history during mineral growth and, in some cases, retain information on earlier high-grade metamorphism (e.g. Mezger et al., 1989; Burton and O'Nions, 1991; Kelly et al., 1997; Argles et al., 1999).

Plutonic rocks of granitoid composition play an important role in understanding the evolution of an orogen because granitoids are the main component of the continental crust. They are formed and modified by distinct petrogenetic processes, and careful interpretation of their primary isotopic systematics, if preserved, can be used as a tracer for their origin and source characteristics. Therefore, Sm-Nd whole-rock analyses of granitoid rocks may provide important clues as to orogenic processes. Neodymium mean crustal residence (model) ages of crustal rocks reflect the age when a sample had the same isotope composition as its source, and thus corresponds to the time when the plutonic rock was separated from its source (DePaolo, 1981; Goldstein et al., 1984; Nelson and DePaolo, 1984; Michard et al., 1985; Liew and McCulloch, 1985). Therefore, Sm-Nd isotopic systematics have received considerable attention because the continental crust and the depleted mantle evolve differently due to their different Sm-Nd isotopic composition (Arndt and Goldstein, 1987). Additionally, Rare Earth Elements (REE) such as Sm and Nd are less mobile during high-grade metamorphism, hydrothermal alteration and chemical weathering than the alkali metals (e.g. Rb) or the alkaline earth metals (e.g. Sr). Nevertheless, in

many cases the Nd model ages do not correspond to a specific crust-formation event but reflect mixing of materials derived from the mantle and the continental crust at different times (Arndt and Goldstein, 1987). In this case, Nd model ages indicate an average retention period for Nd in the mantle, and O'Nions et al. (1983) introduced the term "crustal residence age" to characterize this process.

The geodynamic evolution of the Pan-African Kaoko Belt in NW Namibia has received considerable attention in recent years (e.g. Dürr et al. 1996; Gruner 2000; Seth et al. 1998, 2002; Kröner et al., 2004; Konopásek et al., 2005; Goscombe et al., 2003a,b and 2005), but the composition of many high-grade metamorphic rocks and the origin of granitoids in the core of the orogen are still poorly known. We present new U-Pb and Pb-Pb zircon and Sm-Nd, Rb-Sr and REE data for high-grade gneisses and granitoids in order to place further constraints on deep crustal processes that generated this belt.

5.3 Geological setting: The Kaoko - Dom Feliciano Belt system

The Kaoko Belt of NW Namibia evolved on the margin of the Congo Craton and belongs to a network of Neoproterozoic orogenic belts (Fig. 5.1a). Closure of the Adamastor Ocean (Hartnady et al., 1985), involving collision of the Kalahari and Congo Cratons in Africa and the Rio de la Plata Craton in South America, resulted in the structurally complex Kaoko-Dom Feliciano-Ribeira Belt system (Figs. 5.1a, b). The term 'Pan-African-Brasiliano Cycle' has been introduced by Porada (1979) to describe the successive opening and closure of the proto-South Atlantic.

Coward (1983) interpreted the Kaoko Belt (KB) as the northern continuation of the Damara Belt and, according to Miller (1983), the KB can be subdivided into three tectono-metamorphic domains, namely the Eastern Kaoko Zone (EKZ), Central Kaoko Zone (CKZ) and Western Kaoko Zone (WKZ) These are separated by the Sesfontein Thrust in the east and the Puros Shear Zone (PSZ) in the central part of the belt (Fig. 5.1b). The Sesfontein Thrust marks the contact of the Kaoko Belt with the Congo Craton, whereas the tectonic significance of the crustal-scale PSZ is still unknown although recent studies try to elucidate its tectonic role (Goscombe et al. 2005; Konopásek et al., 2005). In the CKZ Archaean and Mesoproterozoic basement rocks may represent reworked fragments of the adjacent Congo Craton (Seth et al. 1998). To the west of the PSZ another important shear zone, the Village Mylonite Zone (VMZ), has been described by Goscombe et al. (2003b), Kröner et al. (2004) and Konopásek et al. (2005). Based on conventional U-Pb, SHRIMP and Pb-Pb zircon dating of granitic gneisses, Kröner et al. (2004) have identified a Neoproterozoic terrane west of the VMZ, whereas older Meso- to Palaeoproterozoic rocks are exposed east of the VMZ (Fig. 5.2).

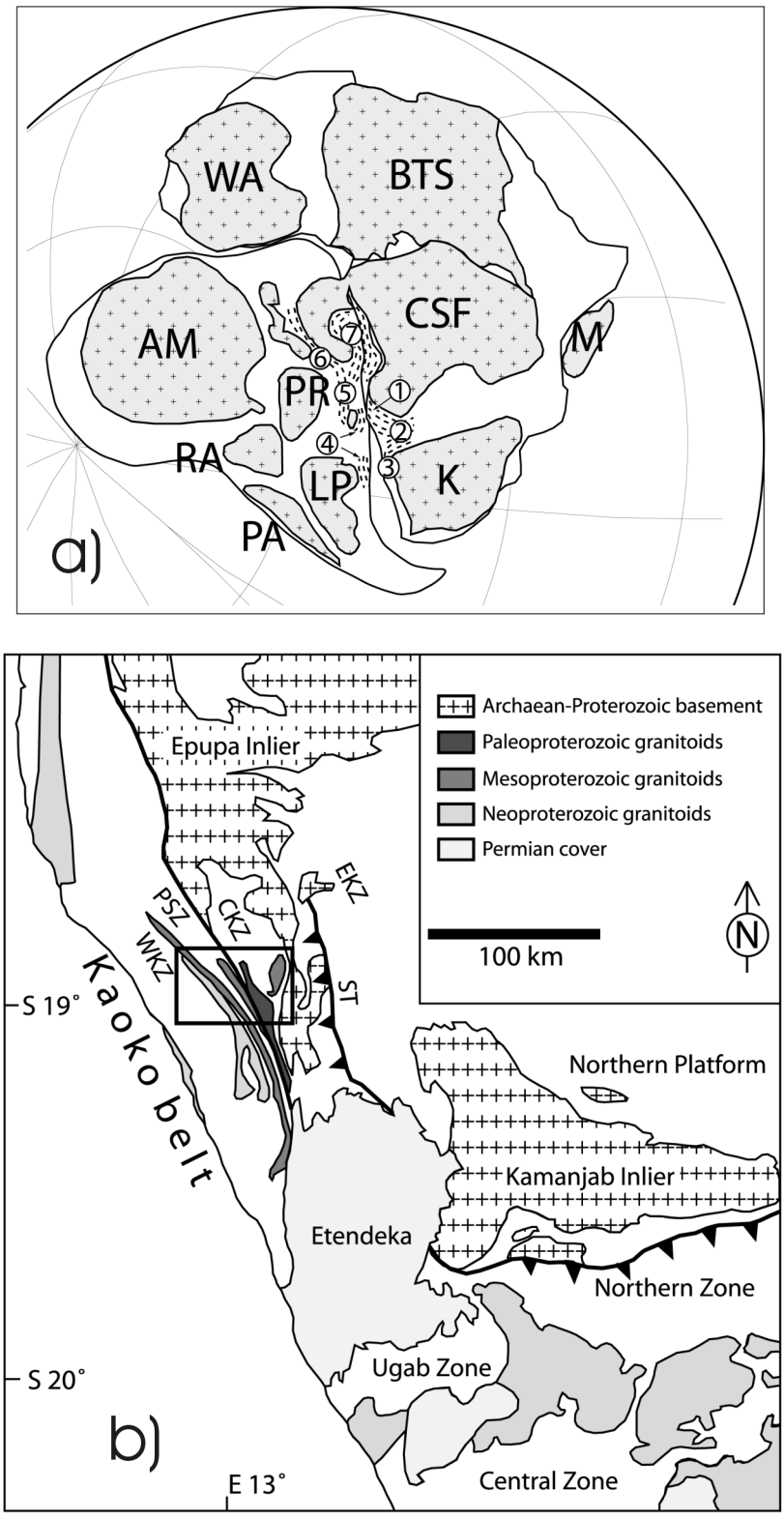

Fig. 5.1. (a) Modified reconstruction of the African and South American cratons at ~600 Ma after Cordani et al. (2003) and Trompette (1997). AM, Amazonia; BTS, Borborema–Trans-Sahara; CSF, Congo – São Francisco; K, Kalahari; LP, Rio de la Plata; PA, Pampia; PR, Paraná; RA, Rio Apa; WA, West Africa. Pan-African-Brasiliano belts: 1-Kaoko, 2-Damara, 3-Gariep, 4-Dom Feliciano, 5-Ribeira, 6-Brasília, 7-Araçuaí. (b) Schematic location map of the Kaoko and Damara belts modified after Miller (1983) and Goscombe et al. (2003a,b); the study area is marked by a box (Fig. 5.2). ST-Sesfontein Thrust, PSZ-Puros shear zone, EKZ-Eastern Kaoko Zone, CKZ-Central Kaoko Zone, WKZ-Western Kaoko Zone.

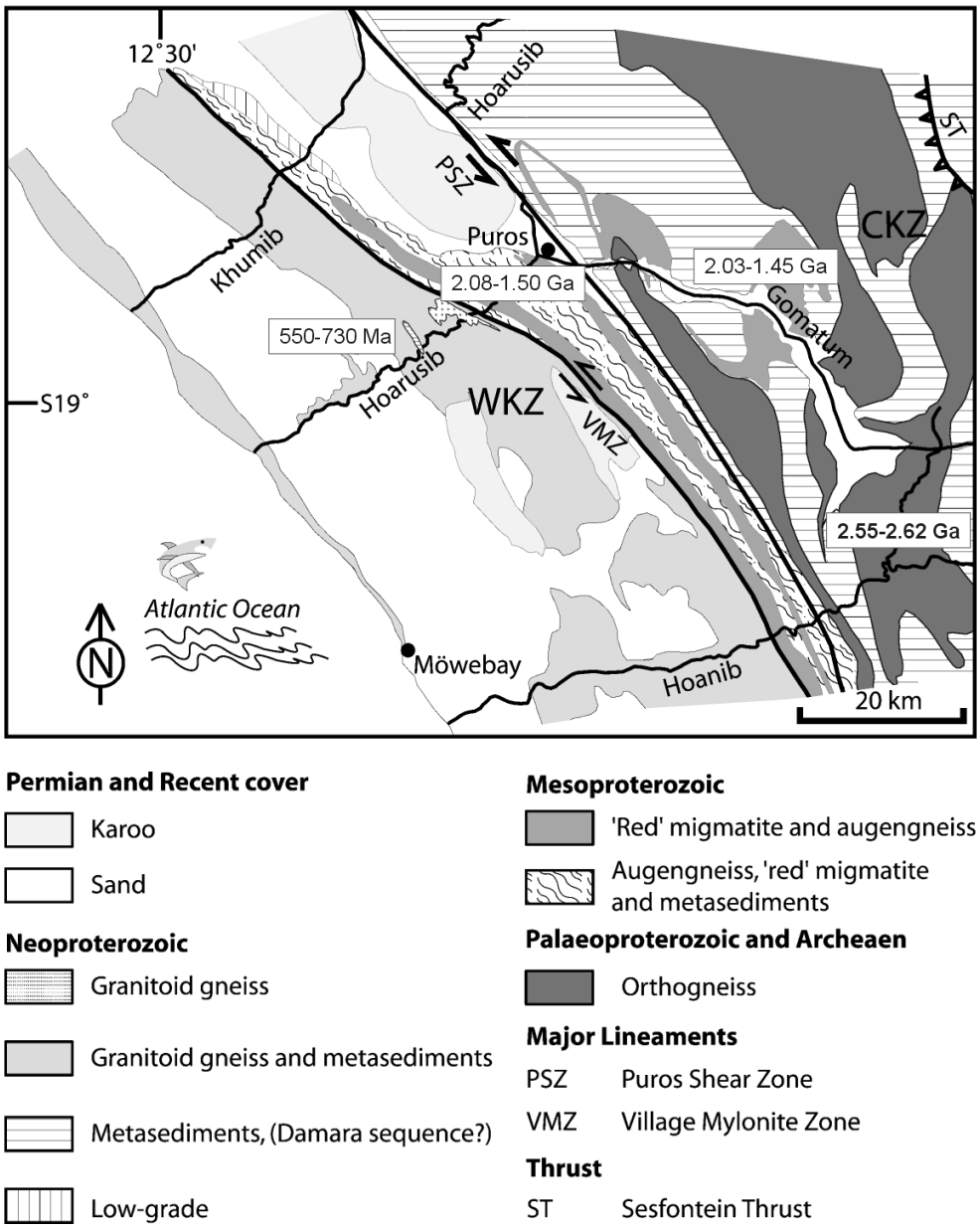

Fig. 5.2. Summary of dated samples showing Neoproterozoic terrane to the west (Kröner et al., 2004).

A first study of the structural and metamorphic evolution in the southern KB was undertaken by Guj (1970) who described prograde Barrovian-type metamorphism in the CKZ, using critical mineral assemblages in metapelitic rocks. More detailed work by later authors supported this observation (Miller, 1979; Dingeldey et al. 1994; Dürr et al. 1996; Gruner 2000; Goscombe et al. 2003a, 2005). Miller (1979) recognized the important tectono-metamorphic role of the PSZ and suggested that this lineament marks a boundary between two different metamorphic domains. Granulites of sedimentary and magmatic origin occur in the WKZ (Figs. 5.2, 5.4), and P-T estimates are in the range of 690-840 °C and 4-8 kbar (Gruner, 2000; Goscombe et al., 2003a). Whether these granulites belong to one single metamorphic event at ~580-550 Ma and were

generated during collision of the Rio de la Plata with the Congo Craton, or experienced a more complex polyphase metamorphic evolution is still a matter of debate (Franz et al. 1999; Goscombe et al., 2005; Kröner et al., submitted).

Systematic U-Pb zircon and whole-rock isotopic analyses of granitoid rocks (Sm-Nd, Rb-Sr and $\delta^{18}O$) have been performed by Seth et al. (1998, 2002), and additional zircon ages were reported by Kröner et al. (2004). Four different age provinces have been distinguished within the KB by combining the results of these authors, including an Archaean, a Palaeoproterozoic, a Palaeo- to Mesoproterozoic and a Neoproterozoic terrane (Fig. 5.2; Kröner et al., 2004). Based on Sm-Nd, Rb-Sr and O isotopes, Seth et al. (2002) suggested a juvenile source for the Archaean rocks, whereas the Palaeoproterozoic rocks probably incorporated recycled material of the Archaean domain. Mixing of at least two different sources and assimilation of older material was assumed for the generation of the Pan-African rocks (Seth et al., 2002).

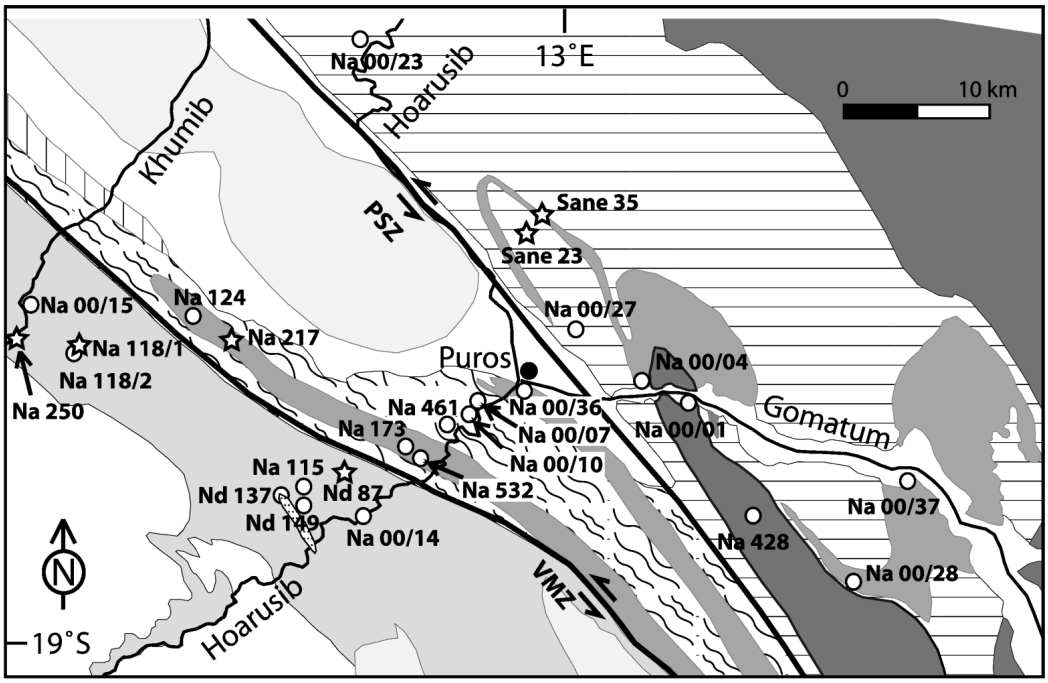

Fig. 5.3. Schematic and simplified geological map showing major rock units of the study area and sample localities. Base map modified after Guj (1970) and Goscombe et al. (2003b). Circles (Kröner et al., 2004) and stars (this work) indicate dated samples.

5.4 Sample preparation and analytical techniques

Fresh rock samples weighing about 5-6 kg each were crushed, and whole-rock powders were prepared by standard procedures using a jaw crusher, steel roller mill and agate mortar. Major element oxides and trace elements were determined by XRF on fused glass discs at the University of Mainz, and the data are presented in Table 5.1. REE were analysed by inductively coupled plasma mass spectrometry (ICP-MS) at the Max-Planck-Institute for Chemistry in Mainz after

calibration by adding two independent internal standards (In, Re) of known concentration. Zircon was concentrated using a magnetic separator and heavy liquids. Representative zircon grains with variable morphology, colour, and size were handpicked for age dating. For conventional U-Pb dating, single zircons were analysed using the HF-vapour transfer technique, developed by Krogh (1978) and Parrish (1987) and modified by Wendt and Todt (1991). The evaporation technique, developed by Kober (1986, 1987), involves repeated evaporation and deposition of Pb from chemically untreated single zircon grains or small grain fractions. The analytical procedures are detailed in Kröner et al. (2004).

For whole-rock isotopic analyses sample digestion using HF-HNO_3 was performed in vials inside Krogh-style Teflon bombs at 200 °C for several days. After dissolution the samples were dried and redissolved in 2.5N HCl. Strontium and REE were separated from the matrix by employing standard cation exchange columns with a DOWEX AG 50 W-X 12 resin and using 2.5 N HCl (Sr) and 6N HCl for the REE. Neodymium was separated from the other REE by using HDEHP-coated teflon columns and 0.12 N HCl for Nd and 0.3 N HCl for Sm. Strontium, Sm and Nd isotope analyses were carried out at the Max-Planck-Institute for Chemistry on a Finnigan MAT 261 multicollector mass spectrometer operated in static mode. Samarium and Nd were run on Re double and Sr on W single filaments. Nd isotopes were normalized to $^{146}Nd/^{144}Nd$: 0.7219. The total procedural blank for Nd was <40 pg and is negligible. Repeated measurement of the La Jolla Nd standard gave $^{143}Nd/^{144}Nd$: 0.511868±20 (n=12), whereas an $^{87}Sr/^{86}Sr$ ratio of 0.710238±27 was obtained for NBS 987. All $^{143}Nd/^{144}Nd$ ratios were normalized to $^{146}Nd/^{144}Nd$= 0.7219. Uncertainties in $^{143}Nd/^{144}Nd$ are reported for the last two digits. Typical analytical errors in the $^{147}Sm/^{144}Nd$ ratios are equal or better than 0.1 %.

5.5 U-Pb and Pb-Pb zircon geochronology on granitoids in the Hoarusib and Gomatum Valleys

Five orthogneiss samples were dated by conventional U-Pb geochronology (Table 5.3a), and one additional sample was dated using the Pb-Pb evaporation method (Table 5.3b)

Sample Nd 87 was collected in the Hoarusib valley west of the VMZ (Fig. 5.3, Table 5.2). The zircons are brownish and long-prismatic with slightly rounded terminations. Eight grains were analysed and yielded discordant ages, and the data define a regression line (MSWD = 1.8) with an upper concordia intercept age of 626±30 Ma (Fig. 5.5c). This age is interpreted to approximate the time of intrusion, whereas the lower intercept of 35±10 Ma probably resulted from recent Pb loss and has no geological meaning.

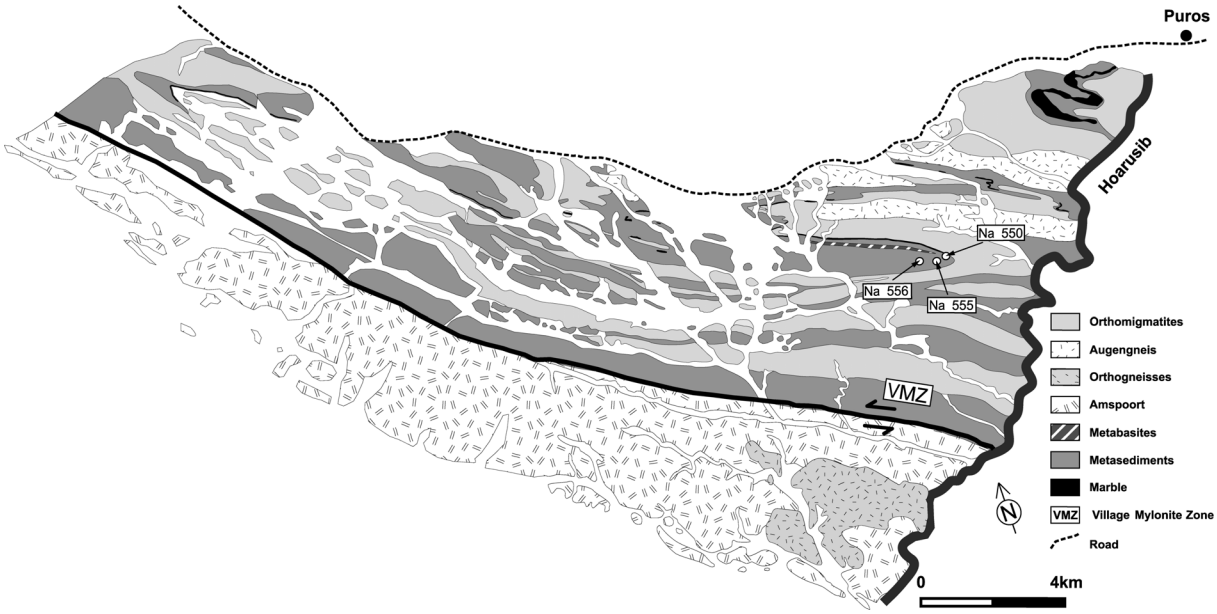

Fig. 5.4. Geological map showing major rock units and sample localities of metapelites in the eastern part of the WKZ. Base map modified after Konopasék et al. (2005).

Granite sample Na 118/1 was collected in the Khumib valley (Fig. 5.3) where this rock is in contact with the porphyritic 'Amspoort type' granite-gneiss (Na 118/2, Kröner et al., 2004). Evaporation of three yellow-brown, long-prismatic zircons yielded a mean $^{207}Pb/^{206}Pb$ age of 554±2 Ma (Fig. 5.5a). This is interpreted as a minimum age, since zircon frequently retains at least a partial record of different thermal events (Kröner et al., 1994; Mezger and Krogstad, 1997). Since the Kaoko Belt experienced no strong post-550 Ma metamorphic overprint, we interpret the Pb-Pb age to approximate the time of granite emplacement.

Farther to the west, in the Khumib valley, a greyish granite-gneiss is represented by sample Na 250. Seven long-prismatic, brownish zircons with slightly rounded terminations were analysed conventionally, and although the analyses are variably discordant they can be fitted to a well-defined regression line (MSWD = 1.6). The upper concordia intercept age of 663±5 Ma is interpreted as approximating the time of intrusion, whereas the lower intercept of 2±1 Ma is attributed to recent Pb loss (Fig. 5.5c).

A red migmatite (Na 217) was sampled between the Hoarusib and the Khumib valleys (Fig. 5.3; Kröner et al., 2004). Conventional analysis of four single zircons (yellowish-brown, long-prismatic, slightly rounded terminations) again produced discordant results with considerable scatter (MSWD = 75) and yielded imprecise upper and lower concordia intercept ages of 1714±51 and 185±85 Ma respectively (Fig. 5.5d). The upper intercept provides a minimum estimate for the emplacement of the precursor granite, whereas the lower intercept probably resulted from Pb loss at variable times and has no geological significance. Kröner et al. (2004) dated a red migmatite farther to the north at 1701±37 Ma, which is identical to the above age.

Zircons from two granitic gneiss samples collected in Gomatum Valley (Fig. 5.3) were analysed conventionally. Sane 35 was collected within the same tectonic unit as previously dated granitic gneisses (Na 00/04 and Na 00/37 in Kröner et al., 2004). The zircons are light brown, long-prismatic and have slightly rounded terminations. Regression calculation through four discordant analyses (MSWD = 2.1) yielded an upper intercept at 1742±10 Ma and a lower intercept at 290±26 Ma (Fig. 5.5e). Previous SHRIMP analyses of Na 00/04 and Na 00/37 yielded upper concordia intercept ages of 1750±23 and 1776±19 Ma respectively (Kröner et al., 2004). These previous results agree well with the above new data.

A tonalitic gneiss (Sane 23) was collected in an anticlinal structure close to sample Sane 35 (Fig. 5.3). Field observations as well as geochemical data (see Chapter 5.6) suggests that this sample is from the same granite body as the previously analysed sample Na 00/01 (Kröner et al., 2004). Four long-prismatic, yellow-brownish zircon grains yielded discordant results, with considerable scatter which can be fitted to a discordia line (MSWD = 57) with an imprecise upper intercept age of 2417±57 and a lower intercept at 889±180 Ma (Fig. 5.5f). Whereas the upper intercept is interpreted as the minimum age of emplacement for the precursor granite, the lower intercept does not seem to be due to a major thermal event and may be fortuitous. Nonetheless, lower Concordia intercept ages of ~850 Ma was also obtained on previously analysed zircon fractions from different samples (Kröner et al, 2004). However, these are difficult to interpret since no thermal event of this age is so far known from the Kaoko Belt. It is possible that the discordance patterns are either due to variable Pb loss at unspecified times, or are due to a mixture of various age components (old core, young rim), or both, and in this case the lower intercept has uncertain geological significance.

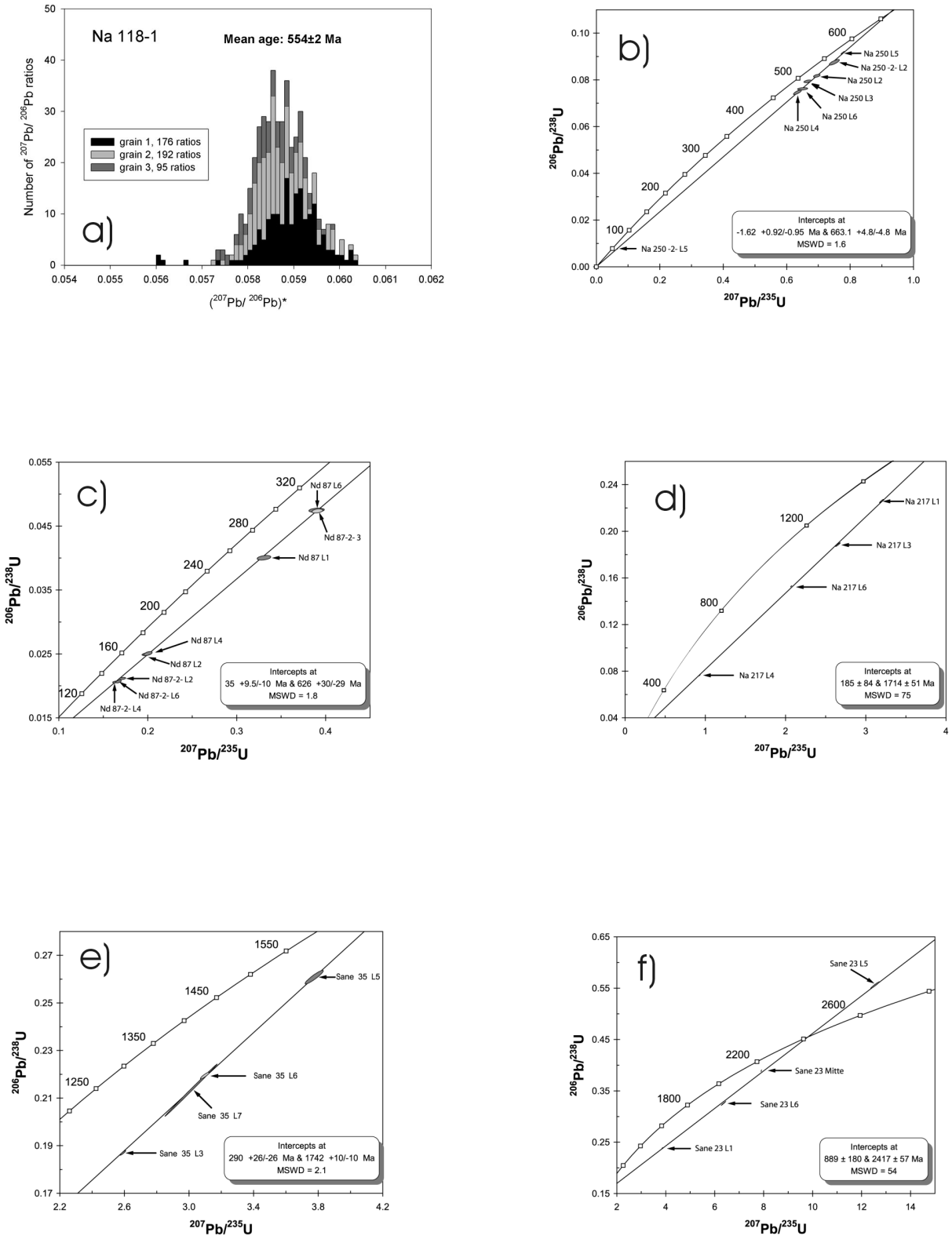

Fig. 5.5. (a) Histogram showing distribution of radiogenic lead isotope ratios derived from evaporation of single zircons from granitoid gneiss sample Na 118/1. (b-f) Concordia diagrams showing analytical data and ages for dated granitoid gneisses. Error ellipses are 2σ.

5.6 Geochemistry

5.6.1 Major, trace and Rare Earth elements

Apart from the samples discussed above, previously dated samples (Kröner et al., 2004) were analysed for major and trace elements including Rare Earth elements, and the results are presented in Table 5.1. In the intrusive rocks, the SiO_2 contents range from 61% to 77%. Only samples Na 532 and Na 00/10 have intermediate compositions (61.2% and 61.8% SiO_2), whereas all others are felsic in composition. According to O'Connor (1965) most rocks are classified as granite, some as granodiorite, and only the two oldest samples (Na 00/01 and Sane 23) are tonalites (Table 5.1 and Fig. 5.6a). The Aluminium Saturation Index (ASI: molar $Al_2O_3/[CaO+Na_2O+K_2O]$ or molar A/CNK; Shand, 1943) ranges from 0.86 to 1.22. In a molar A/NK versus ASI plot after Maniar and Piccoli (1989), samples Na 00/01, Sane 23, Na 00/10, Na 00/37 and Na 532 are metaluminous, whereas the others are peraluminous (Fig. 5.6b). The metasedimentary rocks plot in the field of peraluminous rocks.

Previous studies have shown that the Kaoko Belt experienced several granitoid intrusion events (Seth et al., 1998; Kröner et al., 2004). Some of these granitoids were subsequently metamorphosed under high-grade conditions (in the WKZ) and are locally situated directly in contact with each other, whereas elsewhere they are separated by major or minor shear zones (Goscombe et al., 2003a,b and 2005; Kröner et al, 2004). Major and trace element analyses can be used to establish whether there is a genetic link between the different granitic gneisses, or not. Harker diagrams were used to characterize the different age groups. There is a large variation in TiO_2, Al_2O_3, FeO (total), MgO, CaO and P_2O_5 amongst all age groups. Generally, the TiO_2, Al_2O_3, FeO (total), MgO, CaO and P_2O_5 contents are negatively correlated with the SiO_2 content in all age groups (Figs. 5.7a-f). A negative correlation of major elements is normally interpreted to result from fractionation processes. Furthermore, the major element contents in some age groups (e.g, ~1.5 Ga, ~2.0 Ga and ~2.4 Ga) is significantly different for the same degree of differentiation (same SiO_2 content). K_2O/Na_2O values are positively correlated with SiO_2 for almost all age groups, and only the early Pan-African granitoids (730-626 Ma) show no significant correlation and scatter between 0.8 and 1.6. In contrast, the late Archaean granitoids are negatively correlated with SiO_2.

The trace elements Zn and V decrease with increasing SiO_2, except for the metasediments, where Zn is positively correlated with SiO_2. For Co the older Pan-African granitoids (730-626 Ma) together with the late Palaeoproterozoic rocks (1776-1701 Ma) show no significant

correlation, whereas Co decreases with increasing SiO_2 in the other age groups. The Sr/Ba ratios are <1 and decrease with increasing SiO_2.

A powerful tool to identify mineral fractionation or accumulation processes is the analysis of trace and Rare Earth Elements. In a chondrite-normalized multi-element diagram, samples Na 00/01 and Sane 23 show similar trace element patterns with negative Nb anomalies (Figs. 5.8a-f). Samples of the other age groups show a similar pattern with relative depletion in Ba, Nb, Sr, P and Ti.

All samples show REE-enriched compositions with Ce_N/Yb_N ratios ranging between 9.0 and 52.4 for the Neoproterozoic rocks. The Ce_N/Yb_N ratios for most of the Meso- and Palaeoproterozoic rocks range from 6.5 to 13.2. Only migmatite sample Na 124 and the early Palaeoproterozoic tonalite have higher Ce_N/Yb_N ratios (38.0 and 46.8, Table 5.1). Samples Nd 149 and Na 00/01 exhibit the highest Ce_N/Yb_N ratios (52.4 and 46.8). One early Palaeoproterozoic and one Neoproterozoic sample (Na 00/01 and Na 250) are characterized by positive Eu-anomalies (Eu/Eu*>1), whereas all other samples have negative Eu-anomalies (Eu/Eu*<1, Fig. 5.7i, Figs. 5.9a-d).

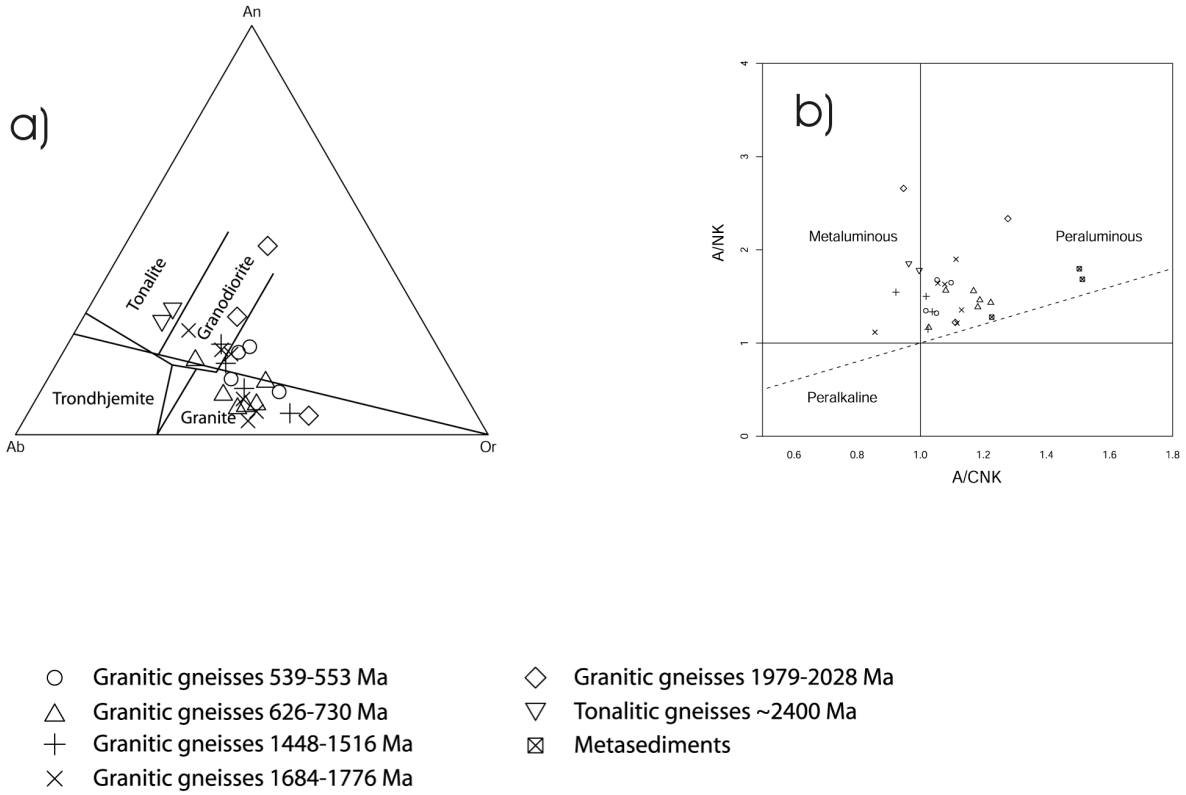

Fig. 5.6. (a) Normative Ab-An-Or triangular plot after O'Connor (1965) showing composition of analysed samples. (b) Molar A/NK vs. ASI plot after Maniar and Piccoli (1989).

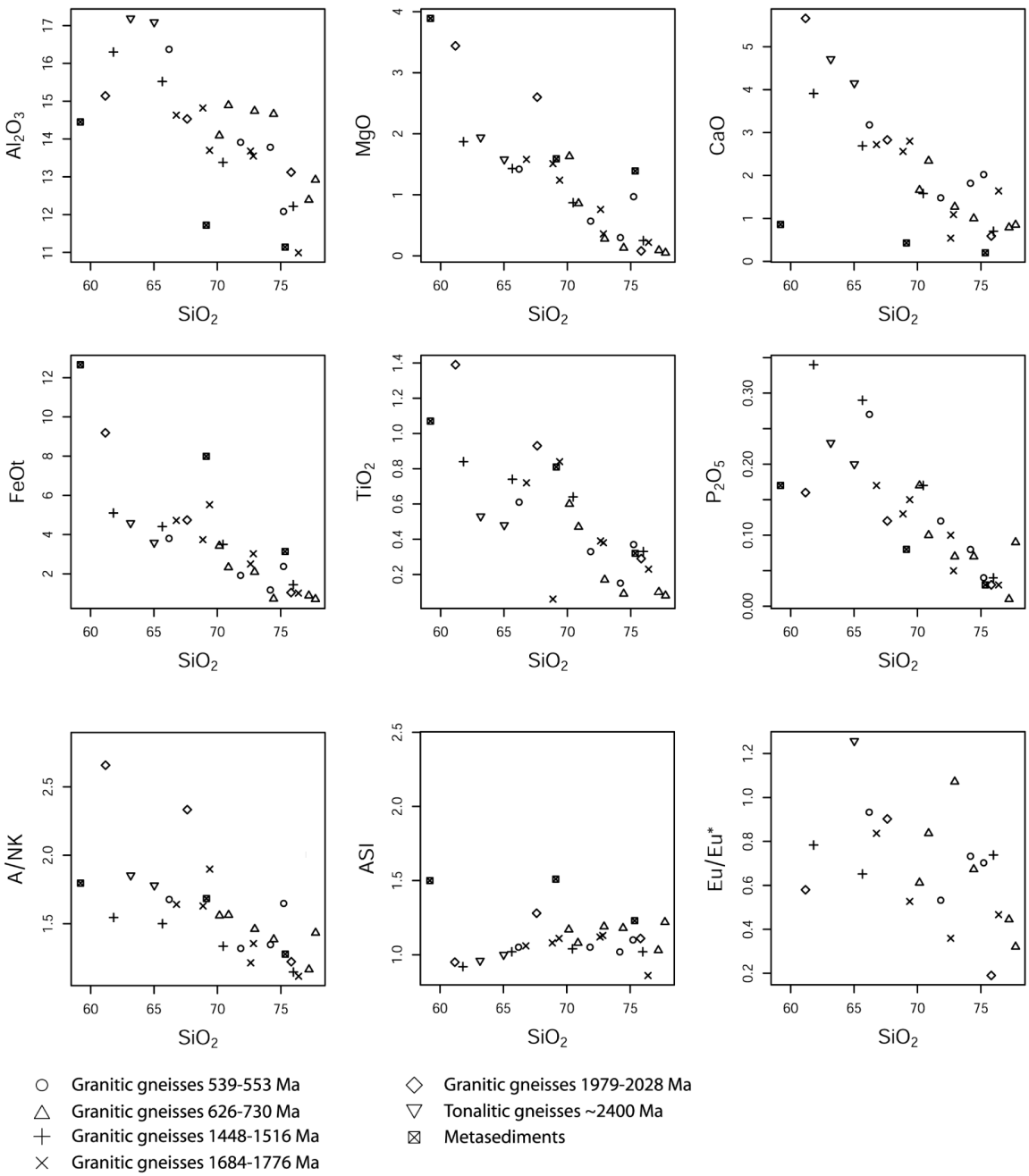

Fig. 5.7. Harker diagrams of SiO_2 vs. (a) Al_2O_3, (b) MgO, (c) CaO, (d) FeO^t, (e) TiO_2 and (f) P_2O_5. g) SiO_2 vs. molar A/NK and h) SiO_2 vs. molar A/CNK (ASI). i) SiO_2 vs. Eu/Eu*

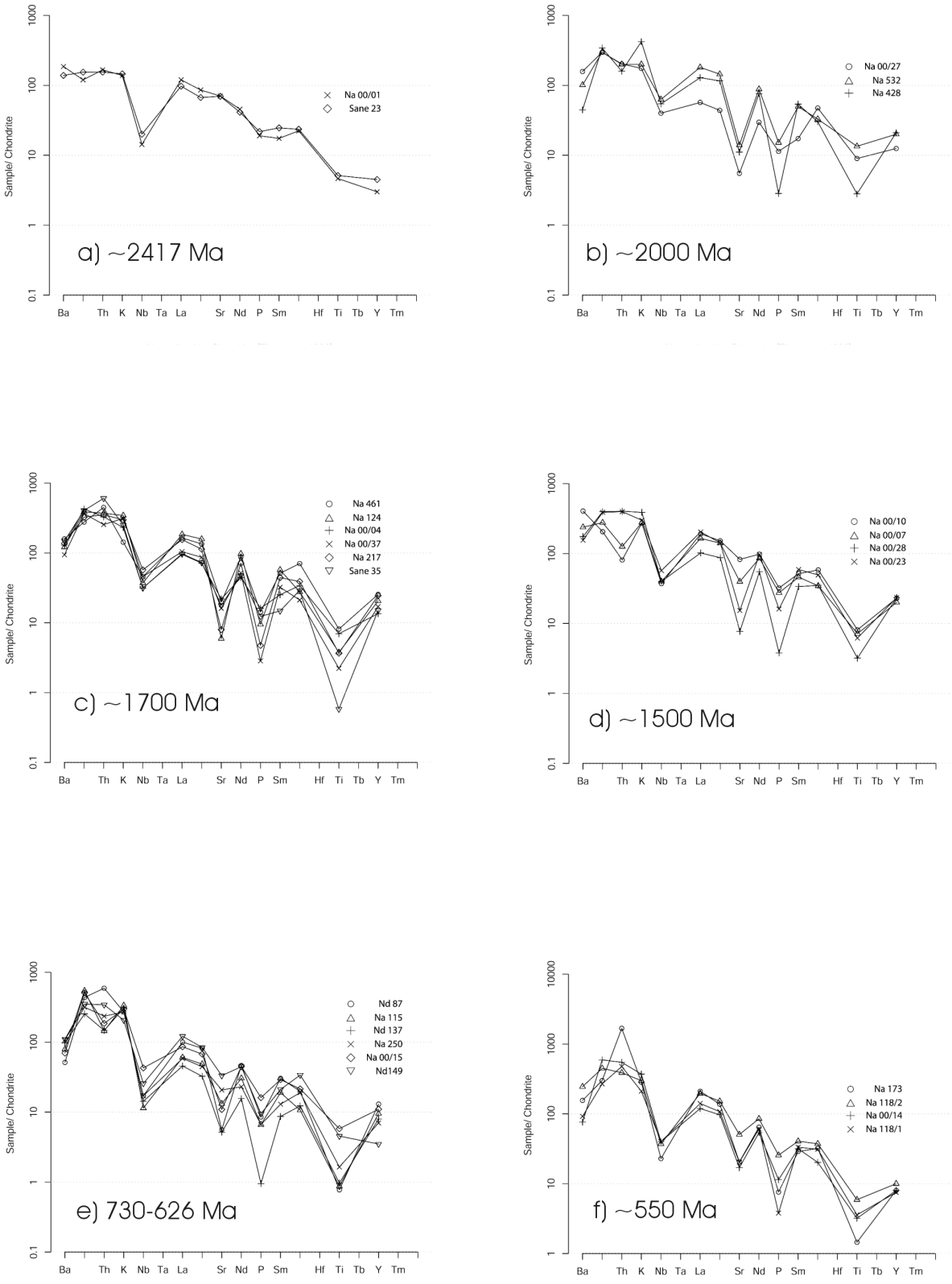

Figs. 5.8a-f. Chondrite-normalised multi-element variation diagram for granitoids of the Kaoko Belt. Normalising values from Thompson (1982).

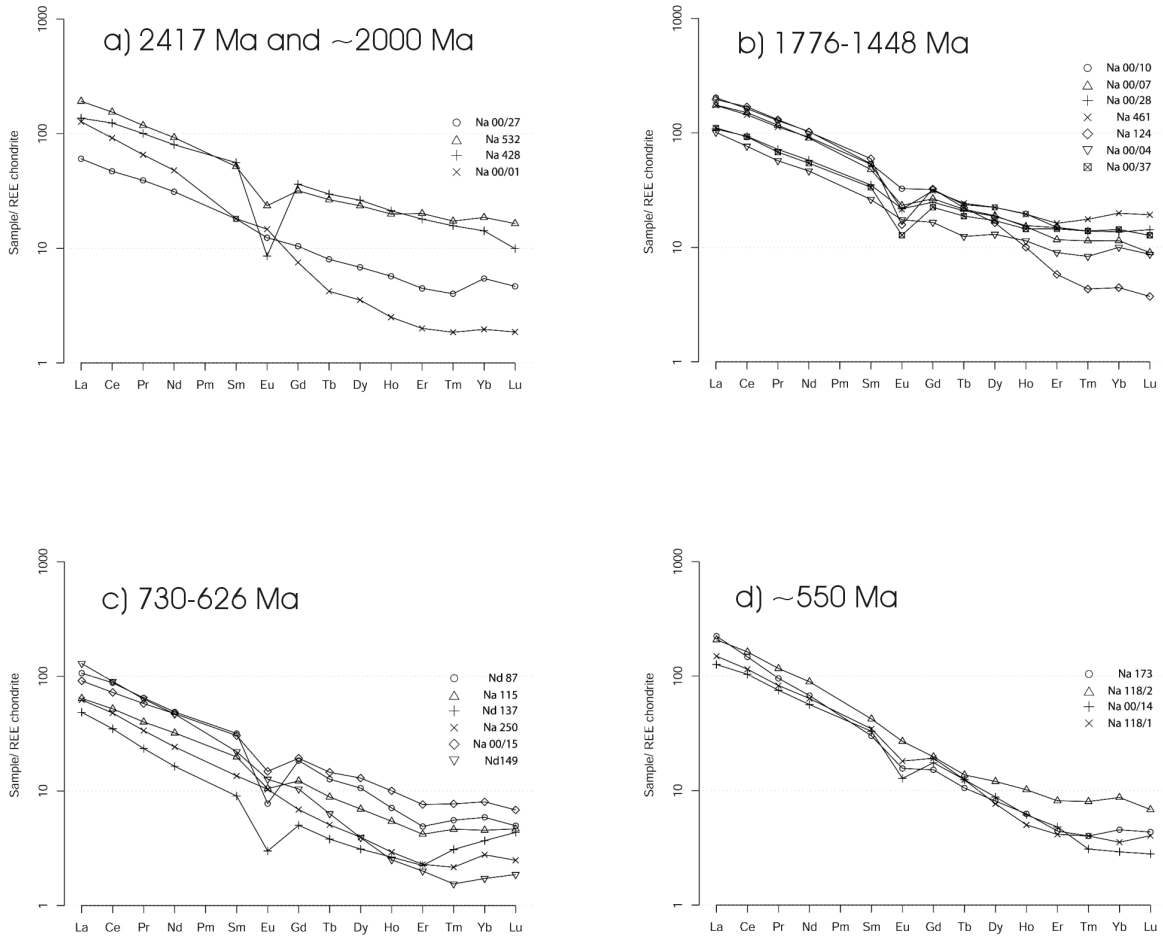

Figs. 5.9a-d. Chondrite-normalised rare earth element (REE) plot for granitoids of the Kaoko Belt. Normalising values from Boynton (1984).

5.6.2 Nd and Sr isotopes

Neodymium and Strontium isotopic analyses can be used to estimate the amount of juvenile or old crustal component of the source. Moreover, numerous studies have shown that Nd isotopic mapping can be used to identify distinct crustal provinces (e.g., Bennett and DePaolo, 1987; Milisenda, 1994; Dickin, 1998). Nd and Sr isotopic data are presented in Table 5.4a and b. The $^{147}Sm/^{144}Nd$ ratios vary between 0.087 and 0.138, whereas most samples plot around ~0.11 which is a typical value for the continental crust (Liew and Hofmann 1988; Milisenda et al. 1994). All samples are plotted in a ε_{Nd} versus time [Ma] diagram to illustrate the Nd isotopic evolution (Fig. 5.10b).

The oldest analysed rocks are Na 00/01 and Sane 23, and both are supposed to belong to the same tectonic unit. They have $\varepsilon_{Nd(t)}$ values of -8.1 and -7.1, respectively. These *early*

Palaeoproterozoic rocks (~2400 Ma) yielded T_{DM} ages of ~3.3 Ga. The $\varepsilon_{Nd(t)}$ values for the *middle Palaeoproterozoic rocks (2028-1979 Ma)* are -3.5 and -4.0, and the corresponding mean crustal residence ages are 2.7 and 2.8 Ga. In the late *Palaeoproterozoic rocks (1776-1701 Ma)*, the $\varepsilon_{Nd(t)}$ vary between +1.8 and -0.3, and the T_{DM} ages are between 2.0 and 2.2 Ga. The *Mesoproterozoic gneisses (1516-1448 Ma)* have slightly lower $\varepsilon_{Nd(t)}$ of -0.9 to -3.3, and the T_{DM} ages are between 1.8 and 1.9 Ga (Table 5.4a; Fig. 5.10a). The $\varepsilon Nd_{(t)}$ values of the *Pan-African (730-626 and 554-540 Ma)* granitoids tend to be slightly lower for the younger granitoids (-3.4 to -6.4) than for the older samples (-2.2 to -4.1). Only sample Nd 137 (661±21 Ma) shows a relatively high $\varepsilon_{Nd(t)}$ of +3.2). The youngest sample (Na 1273, 539±6 Ma) represents a leucocratic melt portion of a migmatite and has a very low $\varepsilon_{Nd(t)}$ of -10.8.

The Nd mean crustal residence ages are presented in a histogram (Fig. 5.10a) and show that, apart from sample Nd 137 (T_{DM}=1.0 Ga), the model ages for the Pan-African igneous rocks cluster around 1.6 Ga. A mean T_{DM} of ~2.0 Ga was calculated for three metasedimentary rocks. Most, if not all, of the granitoids reached amphibolite- to granulite-facies metamorphic conditions, and Sr and Rb were likely re-mobilised during the Pan-African event. Hence, only the $^{87}Sr/^{86}Sr$ values for the Pan-African gneisses were determined and are presented in a ε_{Nd} versus $^{87}Sr/^{86}Sr$ diagram. The $^{87}Sr/^{86}Sr_0$ range from 0.7119 to 0.7606 with initial $^{87}Sr/^{86}Sr$ values ranging from 0.7075 to 0.7225 (Fig. 5.11).

5.7 Discussion and Conclusions

5.7.1 Implications of the zircon and Nd model ages for the evolution of the Kaoko Belt

Our conventional U-Pb zircon ages for granitoid gneisses in Gomatum Valley (this work and Kröner et al., 2004) indicate late Palaeoproterozoic emplacement for these rocks (Sane 35, Na 00/04, Na 00/34) which were thrust over older basement of ~2400 Ma (Na 00/01, Sane 23) during the Pan-African orogeny (Konopásek et al., 2005). Additionally, the previously proposed subdivision of the Kaoko Belt in the Puros area into Neo-, Meso- and Palaeoproterozoic terranes (Kröner et al., 2004) is confirmed by the new zircon data. Illustrating all available zircon ages in a simplified geological map (Figs. 5.2, 5.13, and Kröner et al., 2004), it becomes apparent that several phases of igneous activity occurred during the Pan-African event. Most zircon crystallisation ages are interpreted as intrusion ages and are ~650 Ma and 580-550 Ma (Seth et al., 1998; Franz et al., 1999; Kröner et al., 2004; this work). This duality in age distribution was interpreted as evidence for a polymetamorphic history of the Kaoko Belt (Seth et al., 1998; Franz

et al., 1999), although intrusion ages of granitoid rocks do not necessarily imply that these rocks intruded during high-grade metamorphism. On the other hand, monazite in these rocks is likely to be a product of regional metamorphism, and so far only one sample yielded a monazite age of ca. 650 Ma (Franz et al. 1999).

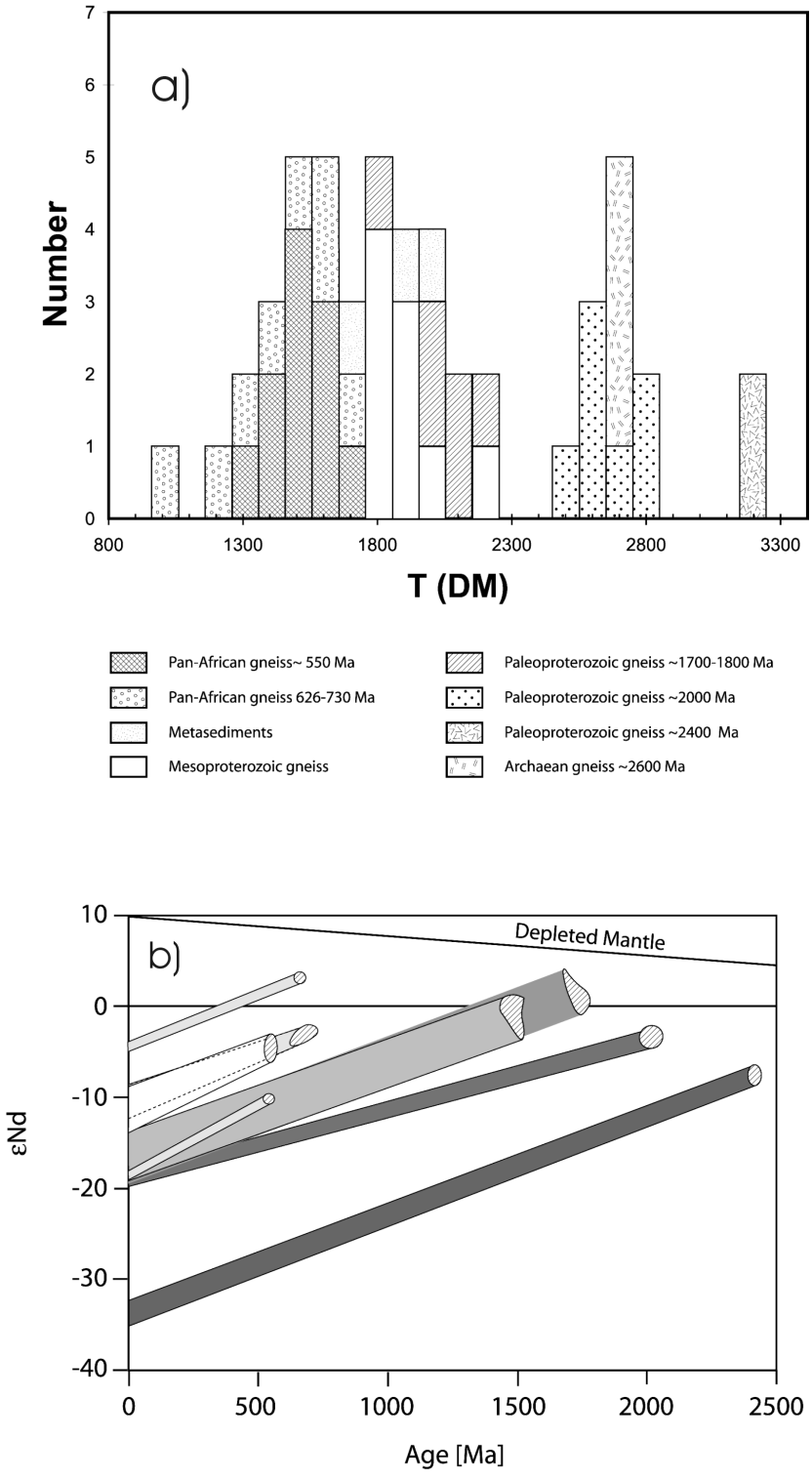

Fig. 5.10. (a) Histogram showing distribution of Nd model ages for the Kaoko Belt (this work and Seth et al., 2002). (b) Nd evolution diagram showing $\varepsilon_{Nd(t)}$ values for granitoid rocks of the Kaoko Belt. The isotopic evolution line for the depleted mantle is from Goldstein et al. (1984).

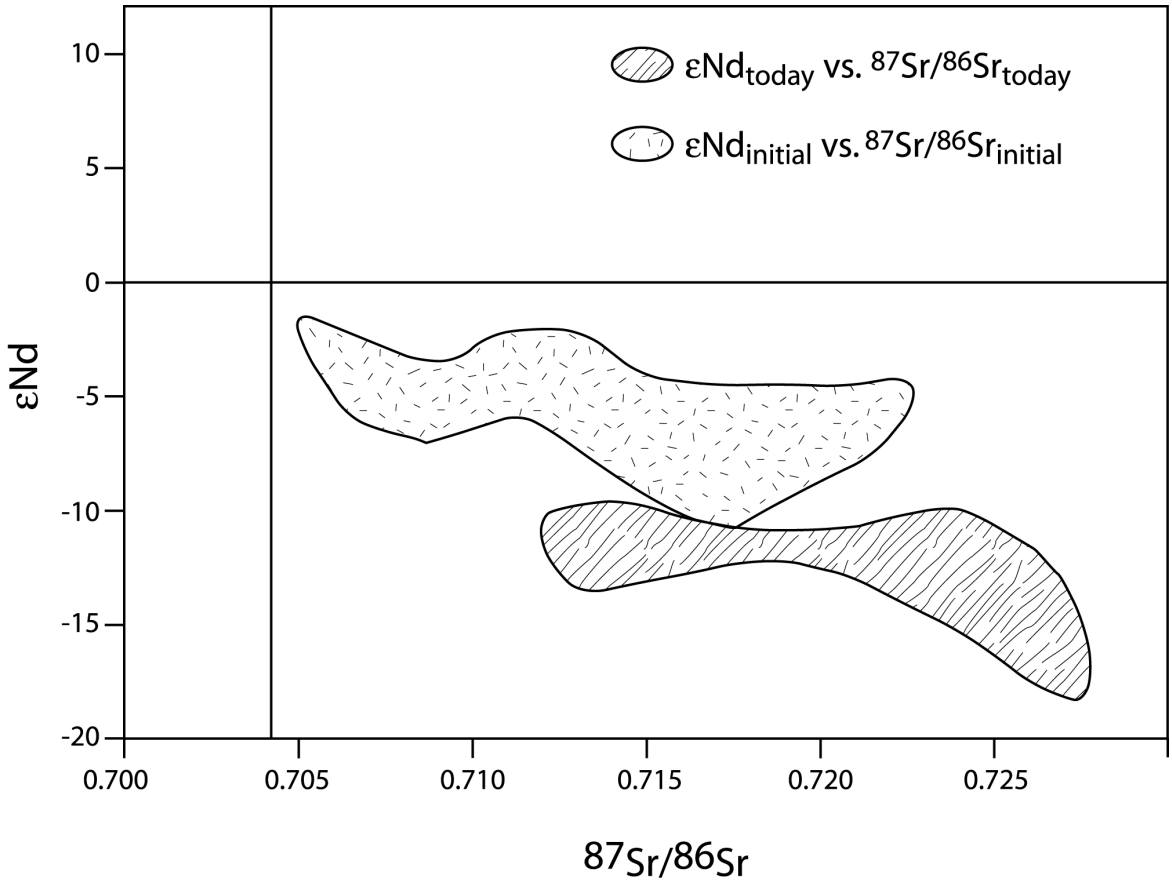

Fig. 5.11. ε_{Nd} vs. $^{87}Sr/^{86}Sr$ diagram showing Pan-African rocks from the Kaoko Belt (this work and Seth et al, 2002).

Alternatively, we suggest that the igneous rocks with older Pan-African ages represent fragments or a fragment of an exotic terrane of unknown origin (South America? Ribeira-Dom Feliciano Belt?), that was incorporated into the lower crustal lithologies of the Kaoko Belt during accretion and collision at ~580-550 Ma. Diachronous regional metamorphism in the Kaoko Belt is incompatible with previous tectonic models. A granulite-facies event at ~650 Ma would be contemporaneous with the inferred depositional ages of Damaran sediments between 750-600 Ma although the significance of these ages is still a matter of debate (Miller, 1983; Hoffmann 1994; Prave, 1996; Stanistreet et al., 2001). One possible geodynamic model would be an extensional tectonic setting, which seems to be incompatible with assumed crustal shortening at that time (Miller, 1983; Prave, 1996; Franz et al., 1999). An alternative but unlikely geological scenario would be deep crustal convergence and shallow crustal extension (Sandiford and Powell, 1986) which, for instance, has been inferred for the Saxonian granulites in the mid-European Variscan belt (e.g. Zulauf et al., 1998; DEKORP, 1999; Arnold et al. 2001). Consequently, we favour the idea of an exotic terrane that was brought into tectonic contact with the autochthonous part of the belt during convergence and high-grade metamorphism at ~580-550 Ma.

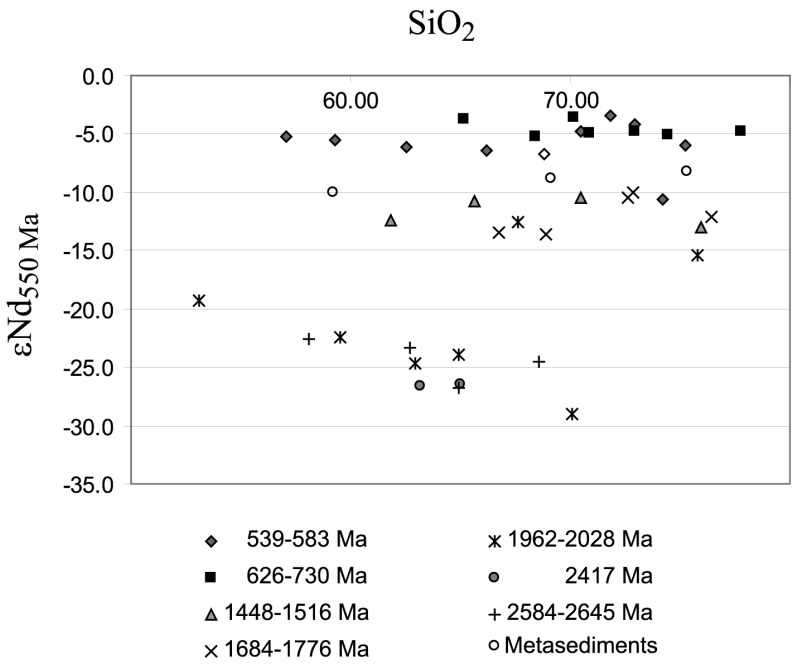

Fig. 5.12. ε_{Nd} vs.SiO_2 showing granitic gneisses from this work and Seth et al. (2002)

5.7.2 Generation of granitoid gneisses in the Kaoko Belt

Implications for petrogenetic processes that led to the generation of granitoid bodies in the Kaoko Belt are based on geochemical and isotopic studies. As pointed out above, the six age groups defined by the dated granitoid gneisses have different trace and REE patterns that, by implication, are suggestive of different sources.

5.7.2.1 Major and trace elements

A general feature of trace element patterns for crustal rocks is the relative depletion in Nb, Sr, P and Ti. These primary negative anomalies may be slightly increased by either assimilation (A) or fractional crystallisation processes (FC) of minerals that have a large distribution coefficient for these elements. In the case of AFC processes a increase in SiO_2 with decreasing ε_{Nd}, should be observed, pointing in the direction of a possible contaminant (e.g. metasedimentary or meta-igneous rocks of various ages). This feature was not observed, and the ε_{Nd} value seems to be independent from SiO_2 content (Fig. 5.12). Instead, the concentration of major elements decrease with increasing SiO_2 content within the age groups (Figs. 5.7a-f), which may be indicative of igneous processes linked to fractional crystallisation. In this case, the negative Sr anomaly characterizes removal of plagioclase, whereas the negative Nb and Ti anomalies may be due to amphibole and/or phlogopite and rutile and/or sphene removal. Alternatively, the trace element patterns reflect the presence of these minerals in the residuum during partial melting.

Granitic rocks are often subdivided into I-, S-, M-, C-, and A-types, but the most popular discrimination is between I- and S-type granitoids (Chappell and White, 1974). Chappell and White (1984) referred derivation of I-type granitoids to deeper crustal levels ('infracrustal') than S-type granitoids ('supracrustal'), but this discrimination seems to be only suitable for granitoids generated from simple sources. However, granitoid rocks are rarely derived from a single source but, instead, are often mixtures of mantle-derived mafic melts (e.g., underplated gabbros) and crustal melts that may have incorporated metasedimentary components. Our isotopic analyses suggest mixing of heterogeneous sources, which argues against a straight forward application the above classification, at least in the high-grade Kaoko Belt.

The positive Eu anomalies of tonalitic gneiss sample Na 00/01 and granitic gneiss sample Na 250 are indicative of plagioclase accumulation. This is corroborated by high abundances of Ba (1283 ppm) and Sr (830 ppm) in sample Na 00/01. The preservation of negative Eu anomalies in all other granitoids may be interpreted as the result of plagioclase fractionation during fractional crystallization processes or plagioclase being retained in the residual source during melting. Except for the early Palaeoproterozoic rocks, the geochemical analyses suggest that fractionation of plagioclase, amphibole and probably sphene/rutile played an important role in the generation of these granitoids.

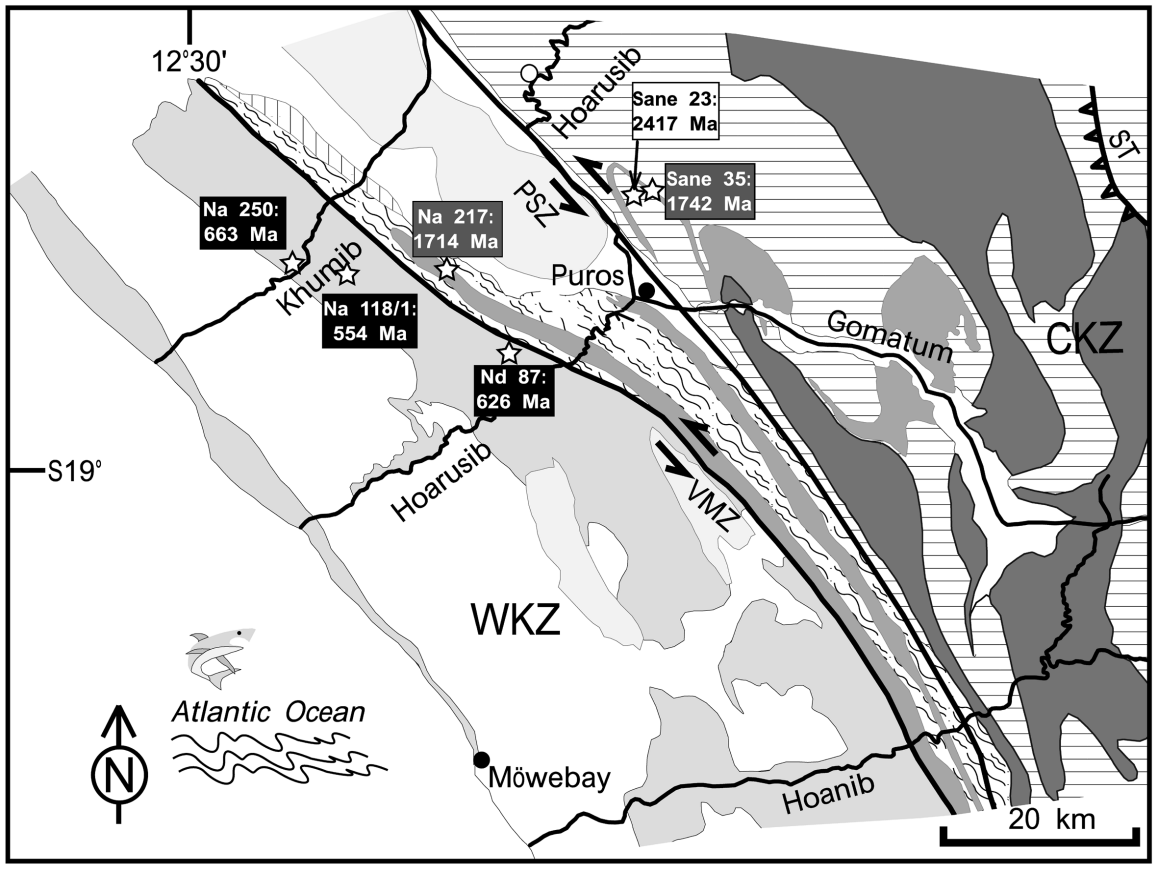

Fig. 5.13. Zircon ages shown on the geological base map of the Kaoko Belt.

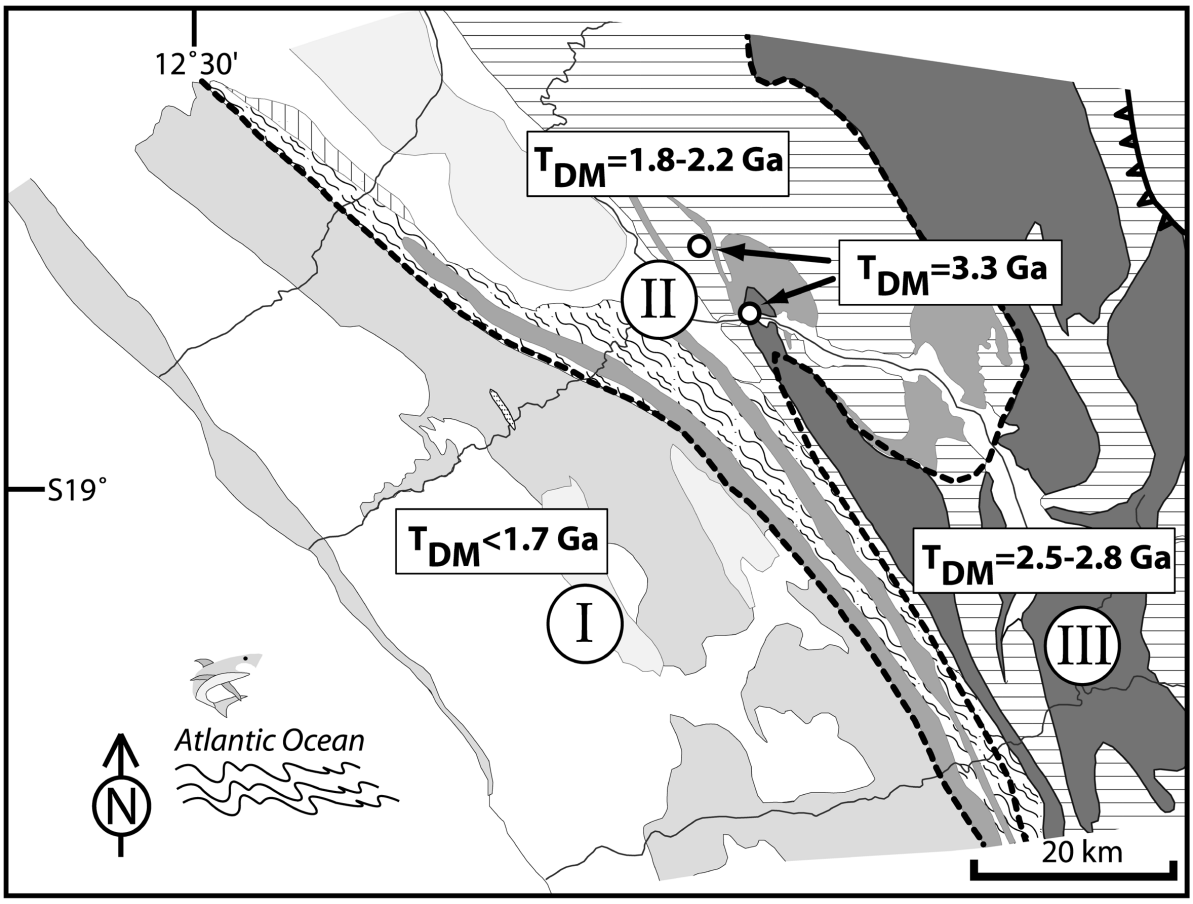

Fig. 5.14. Subdivision of the Kaoko Belt crust into 4 parts, referred to as Provinces I-IV.

5.7.2.2 Nd and Sr isotopes

Numerous isotopic studies have demonstrated that Nd isotopic patterns can be used for characterisation and delineation of crustal segments or terranes (e.g., DePaolo, 1983, 1984; Bennett and DePaolo, 1987). As shown in Fig. 5.14, our analysed samples allow a subdivision of the Kaoko Belt crust into four parts, referred to as Provinces I to IV. Province I is characterised by model ages <1.7 Ga and is restricted to Pan-African granitoids in the west. The boundary with Province II is the VMZ (Village Mylonite Zone, Fig. 5.2) were T_{DM} ages of 1.8 to 2.2 Ga occur. These granitoids are probably related to the Eburnian (Transamazonian) orogenic cycle. Late Archaean and middle Palaeoproterozoic rocks with model ages of 2.5 to 2.8 Ga constitute Province III and are isotopically distinct from two early Proterozoic samples taken from the Hoarusib area near the PSZ (Puros Shear Zone, Figs. 5.3, 5.14) which display even older T_{DM} ages of ~3.3 Ga (Province IV). A delineation of Province IV is not possible because of limited data and, therefore, only the sample localities are indicated. These provinces are also illustrated in the crystallisation age vs. model age and $\varepsilon_{Nd(0)}$ versus $f_{Sm/Nd}$ (or $^{147}Sm/^{144}Nd$) diagrams of Figs. 5.15a and 5.15b. Most $f_{Sm/Nd}$ values are 40-50 % lower than those of chondritic meteorites, which is typical for crustal rocks (Fig. 5.15c, Ben Othman et al., 1984).

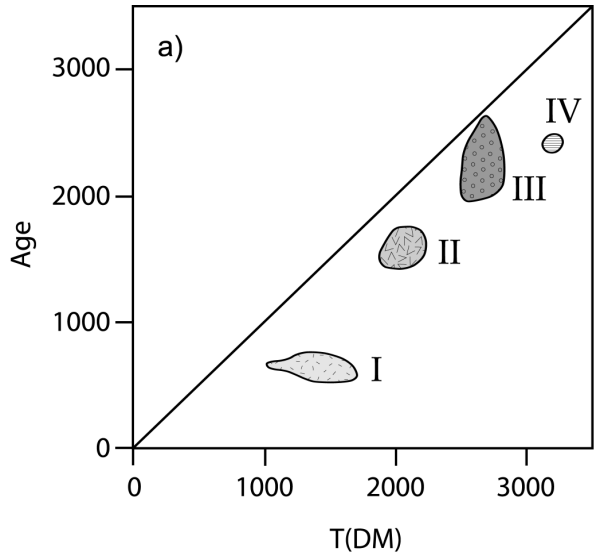

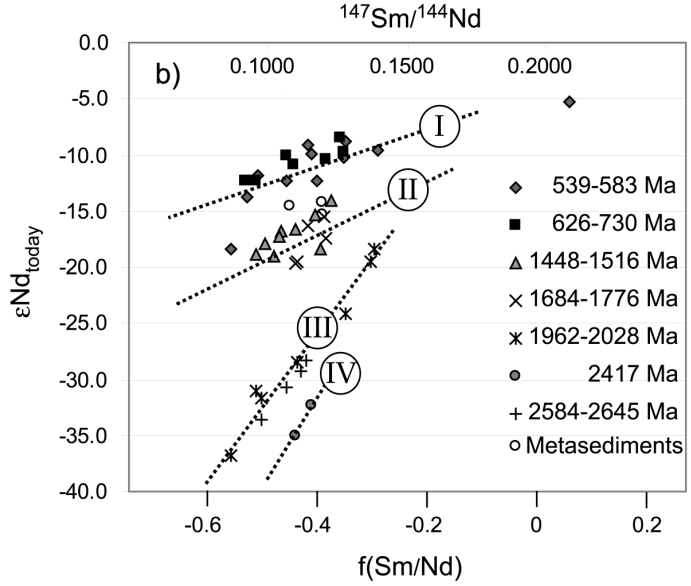

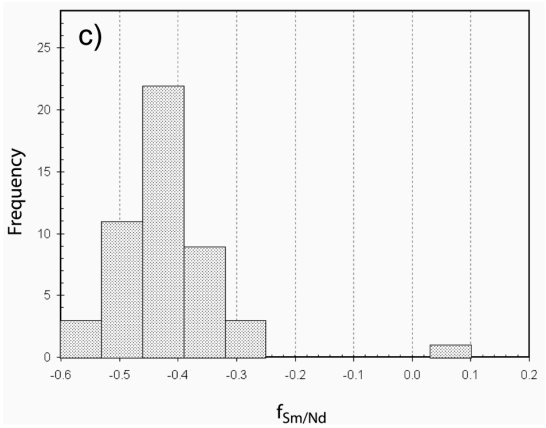

Fig. 5.15. (a) Crystallisation age vs. model age. (b) $\varepsilon_{Nd(0)}$ vs. $f_{Sm/Nd}$. Regression lines indicate the four different provinces. c) $f_{Sm/Nd}$ values vs. frequency. Data from this work and Seth et al. (2002).

Furthermore, Nd isotopic analyses can be used for distinguishing between old, reworked crust and juvenile crust and is consequently fundamental for understanding crustal evolution and genesis. The $Nd_{(t)}$ values of the late Palaeo- and Mesoproterozoic granitoids are around zero and suggest a predominantly juvenile source. Even migmatite samples Na 124 and 217 have positive $Nd_{(t)}$ of +1.4 and +1.8, and only sample Na 00/28 reveals a pronounced crustal component ($\varepsilon_{Nd(t)}$ = -3.3). We therefore conclude that samples Na 124 and 217 are igneous migmatites of which the precursor rocks were derived from melts that contain a significant juvenile component. It is thus unlikely that these migmatites originated from anatexis of the surrounding pre-Neoproterozoic rocks. In contrast, the middle and early Palaeoproterozoic rocks have significantly lower $Nd_{(t)}$ values of –3.8 to –8.1, suggesting derivation from magmas that contained a substantial component of reworked old crustal material. In the Mesoproterozoic granitoids, Archaean crust of predominantly juvenile origin (Seth et al., 1998 and 2002) was reworked during the Proterozoic. The Pan-African granitoids yielded moderately negative $\varepsilon_{Nd(t)}$ values, suggesting derivation from crustal protoliths not much older than the granitoids themselves. However, the wide range in initial Sr isotopic ratios ($^{87}Sr/^{86}Sr_{(t)}$ = 0.7075-0.7225) suggests heterogeneous crustal sources for the Neoproterozoic granitoids (Fig. 5.11).

5.7.2.3 Palaeogeographic implications

The Kaoko Belt developed on the southwestern margin of the Congo Craton and the corresponding orogen in Brazil and Uruguay, the Dom Feliciano Belt, at the eastern margin of the Rio de la Plata Craton (Fig. 5.1a). The Adamastor Ocean separated these two cratons in Neoproterozoic times (Hartnady et al., 1985), but the width of this ocean is still a matter of considerable debate (Hartnady et al., 1985; Hartnady, 1991; Stanistreet et al., 1991; Dürr and Dingeldey 1996). There is no obvious field evidence for the involvement of oceanic lithosphere in the formation of the Dom Feliciano-Kaoko orogen since blueschists, eclogites, ophiolites and igneous rocks with typical subduction signatures are lacking. The geochemical data of all Neoproterozoic granitoids in the two belts suggest formation in a continental collision environment, and peralkaline and/or alkaline granitoids (e.g. syenites) that usually indicate the beginning of a Wilson cycle (Barbarin, 1999), are absent.

Blueschists and 'cold' eclogites are typical rocks signifying rapid subduction and exhumation. Thompson et al. (1997) proposed that such rocks occur in frontal continental collision environment, i.e. collision with a high pure/simple shear ratio. With increasing obliquity of collision the Thompson et al. (1977) model predicts slower descent and uplift rates, resulting in

Barrovian-type and granulite-facies ('hot eclogite') rocks. Oblique collision in the Kaoko Belt of about 70-80° has been inferred by several authors (Dürr and Dingeldey, 1996; Goscombe et al. 2003; 2005; Konopásek et al., 2005), and the observed rocks are consistent with the model of Thompson et al. (1997). Furthermore, the Pan-African (Brasiliano) granitoids on both sides of the Atlantic have moderately negative $\varepsilon_{Nd(t)}$ values and T_{DM} model ages between 1.2 and 1.7 Ga (Babinski et al, 1997; Cordani and Sato, 1999; Seth et al., 2002; this work).

5.8 References

Argles, T.W., Prince, C.I., Foster, G.L. and Vance, D. (1999). New garnets for old? Cautionary tales from young mountain belts. *Earth and Planetary Science Letters*, **172**, 301–309.

Arndt, N.T. and Goldstein, S.L. (1987). Use and abuse of crust-formation ages. *Geology*, **15**, 893-895.

Arnold, J., Jacoby, W.R., Schmeling, H. and Schott, B. (2001). Continental collision and the dynamic and thermal evolution of the variscan orogenic crustal root – numerical models. *Journal of Geodynamics*, **31**, 273-291.

Babinski, M., Chemale, F., vanSchmus, W.R., Hartmann, L.A. and DaSilva, L.C. (1997). U-Pb and Sm-Nd geochronology of the Neoproterozoic granitic-gneissic Dom Feliciano belt, Southern Brazil. *Journal Of South American Earth Sciences*, **10** (3-4), 263-274.

Barbarin, B. (1999). A review of the relationships between granitoid types, their origins and their geodynamic environments. *Lithos*, **46**, 605–626.

Bennett, V.C. and DePaolo, D.J. (1987). Proterozoic crustal history of the western United States as determined by neodymium isotopic mapping. *Geological Society of America Bullentin*, **99**, 674-685.

Ben Othman, P., Polve, M. and Allegre, C.J. (1984). Nd-Sr isotopic composition of granulites and constraints on the evolution of the lower continental crust. *Nature*, **307**, 510-515.

Boynton, W.V. (1984). Geochemistry of the rare earth elements: meteorite studies. In: Henderson P. (ed.), Rare earth element geochemistry. Elsevier, pp. 63-114.

Burton, K.W. and O'Nions, R.K. (1991). High-resolution garnet chronometry and the rates of metamorphic processes. *Earth and Planetary Science Letters*, **107**; 3-4, 649-671.

Chappell, B.W. and White, A.J.R. (1974). Two contrasting granite types. *Pacific Geology*, **8**, 173-174.

Chappell, B.W. and White, A.J.R. (1984). I- and S-type granites in the Lachlan Fold Belt, southeastern Australia. *In*: Keqin X. and Guangchi T. eds. *Geology of Granites and Their Metallogenic Relations*, pp. 87–101. Science Press, Beijing.

Cordani, U.G. and Sato, K. (1999). Crustal evolution of the South American Platform, based on Nd isotopic systematics on granitoid rocks. *Episodes*, **22**, 167– 173.

Cordani, U. G., D'Agrella-Filho, M. S., Brito-Neves, B. B. and Trindade, R. I. F (2003). Tearing up Rodinia: the Neoproterozoic palaeogeography of South American cratonic fragments. *Terra Nova*, **15** (5), 350-359.

Copeland, P., Parrish, R.R. and Harrison, T.M. (1988). Identification of inherited radiogenic Pb in monazite and implications for U–Pb systematics. *Nature*, **333**, 760– 763.

Coward, M.P. (1983). The tectonic history of the Damara Belt. In: Miller, R.Mc.G. (Ed.), The Damara Orogen. *Geological Society of South Africa Special Publication*, **11**, 431–515.

DEKORP and Orogenic Processes Working Groups (1999). Structure of the Saxonian Granulites: Geological and geophysical constraints of the exhumation of high-pressure/high-temperature rocks in the mid-European Variscan belt. *Tectonics*, **18**, 756-773.

DePaolo, D.J. (1981). Neodymium isotopes in the Colorado Front range and crust –mantle evolution in the Proterozoic. *Nature*, **291**, 193-196.

DePaolo, D.J. (1983). The mean life of continents: Estimates of continental recycling rates from Nd and Hf isotopic data and implications for mantle structure. *Geophysical Research Letter*, **10**, 705-708.

De la Roche, H., Leterrier, J., Grande, C.P. and Marchal, M. (1980). A classification of volcanic and plutonic rocks using R1-R2 diagrams and element analyses – its relation and nomenclature. *Chemical Geology*, **29**, 183-210.

Dickin, A.P. (1998). Nd isotope mapping of a cryptic continental suture, Greenville Province of Ontario. *Precambrian Research*, **91**, 433-444.

Dingeldey, D.P., Dürr, S.B., Charlesworth, E.G., Franz, L., Okrusch, M. and Stanistreet, I.G. (1994). A geotraverse through the northern coastal branch of the Damaran Orogen west of Sesfontein, Namibia. Namibia. *Journal of African Earth Science*, **19**, 315–329.

Dürr, S.B. and Dingeldey, D.P. (1996). The Kaoko belt (Namibia): part of a late Neoproterozoic continental-scale strike-slip system. *Geology*, **24**, 503–506.

Faure, G., 1986. Principles of isotope geology. *John Wiley and Sons*, New York, U.S.A., 589pp.

Franz, L., Romer, R.L. and Dingeldey, D.P. (1999). Diachronous Pan-African granulite-facies metamorphism (650 Ma and 550 Ma) in the Kaoko belt, NW Namibia. *European Journal of Mineralogy*, **11**, 167-180.

Goldstein, S.L., O'Nions, R.K. and Hamilton, P.J. (1984). A Sm-Nd isotopic study of atmospheric dusts and particulates from major river systems. *Earth and Planetary Sciences Letters*, **70**, 221-236.

Goscombe, B., Hand, M., Gray, D. and Mawby, J. (2003a). The metamorphic architecture of a transpressional orogen: the Kaoko belt, Namibia. *Journal of Petrology*, **44**, 679-711.

Goscombe, B., Hand, M. and Gray, D. (2003b). Structure of the Kaoko belt, Namibia: progressive evolution of a classic transpressional orogen. *Journal of Structural Geology*, **25**, 1049–1081.

Goscombe, B., Gray, D and Hand, M. (2005). Extrusional Tectonics in the Core of a Transpressional Orogen; the Kaoko Belt, Namibia. *Journal of Petrology*, Advance Access published.

Gruner, B. (2000). Metamorphoseentwicklung im Kaokogürtel, NW-Namibia: Phasen-petrologische und geothermobarometrische Untersuchungen panafrikanischer Metapelite. *Unpublished PhD thesis*, *University of Würzburg*, Germany, 248pp.

Guj, P. (1970). The Damara mobile belt in the south-western Kaokoveld, South West Africa. *Precambrian Research Unit*, *University of Cape Town*, *South Africa*, *Bulletin*, **10**, 168pp.

Gulson, B. L. and Krogh, T.T. (1973). Old lead components in the young Bergell Massif, south-east Swiss Alps. *Contributions to Mineralogy and Petrology*, **40**, 239-252.

Hartnady, C., Joubert, P. and Stowe, C. (1985). Proterozoic crustal evolution in southwestern Africa. *Episodes*, **8 (4)**, 236-244.

Hartnady, C. (1991). About turn for supercontinents. *Nature*, **352**, 476-478.

Hoffman, P.F. (1991). Did the breakout of Laurentia turn Gondwanaland inside-out? *Science*, **252**, 1409-1412.

Jacobson, S.B. and Wasserburg, G.J. (1980). Sm–Nd isotope evolution of chondrites. *Earth and Planetary Science Letters*, **50**,139–155.

Kelley, S.P., Bartlett, J.M., Harris, N.W.B. (1997). Pre-metamorphic Ar–Ar ages from biotite inclusions in garnet. *Geochimica et Cosmochimica Acta*, **61**, 3873–3878.

Kober, B. (1986). Whole-grain evaporation for $^{207}Pb/^{206}Pb$ investigation on single zircons using a double-filament thermal ion source. *Contributions to Mineralogy and Petrology*, **93**, 482-490.

Kober, B. (1987). Single-zircon evaporation combined with Pb^{+} emitter-bedding for $^{207}Pb/^{206}Pb$-age investigation using thermal ion mass spectrometry, and implications to zirconchronology. *Contributions to Mineralogy and Petrology*, **96**, 63-71.

Konopásek, J., Kröner, S., Kitt, S.L., Passchier, C.W. and Kröner, A. (2005). Oblique collision and evolution of large-scale transcurrent shear zones in the Kaoko belt, NW Namibia. *Precambrian Research*, **136**, 139-157.

Krogh, T.E., 1978. Vapour transfer for the dissolution of zircons in a multi-sample capsule, at high pressure. *In:* R.E. Zartman (Editor), 4th International Conference of Geochronology, Cosmochronology, Isotope Geology, *U.S. Geological Survey Open-File Report*, **78-701**, 233-234.

Kröner, A., Jaeckel, P. and Williams, I.S. (1994). Pb-loss patterns in zircons from a high-grade metamorphic terrain as revealed by different dating methods; U-Pb and Pb-Pb ages of igneous and metamorphic zircons from northern Sri Lanka. *Precambrian Research*, **66**, 151-181.

Kröner, S., Konopásek, J., Kröner, A., Poller, U., Wingate, M.W.D., Passchier, C.W. and Hofmann, K.-H. (2004). U-Pb and Pb-Pb zircon ages for metamorphic rocks in the Kaoko Belt of NW Namibia: A Palaeo- to Mesoproterozoic basement reworked during the Pan-African orogeny. *South African Journal of Geology*, **107(3)**, 455-476.

Kröner, S., Jung, S., Kröner, A. (submitted). An unusual old Sm-Nd garnet-whole rock age from the granulite-facies Western Kaoko Zone (Namibia): Evidence for a Neoproterozoic cryptic high-grade polymetamorphic event? *Lithos*.

Liew, T.C. and McCulloch, M.T. (1985). Genesis of granitoid batholiths of Peninsular Malaysia and implications for models of crustal evolution; evidence from a Nd-Sr isotopic and U-Pb zircon study. *Geochimica et Cosmochimica Acta.*, **49** (2), 587-600.

Liew, T.C. and Hofmann, A.W (1988). Precambrian crustal components, plutonic associations, plate environment of the Hercynian Fold Belt of central Europe: Indications from a Nd and Sr isotopic study. *Contributions to Mineralogy and Petrology*, **98**, 129-138.

Ludwig, K.R. (1999). ISOPLOT/Ex version 2.01, a geochronological toolkit for Microsoft Excel. *Berkeley Geochronology Center*, *Special Publication*, **1a**, 47.

Maniar, P.D. and Piccoli, P.M. (1989). Tectonic discrimination of granitoids. *Bulletin of the American Geological Society*, **101**, 635 – 643.

McCulloch, M.T. and Wasserburg, G.J. (1978). Sm-Nd and Rb-Sr chronology of continental crust formation. *Science*, **200**, 1002.

Mezger K., Hanson G. N. and Bohlen S. R. (1989). U-Pb systematics of garnet: Dating the growth of garnet in the Late Archaean Pikwitonei granulite domain at Cauchon and Natawahunan lakes, Manitoba, Canada. *Contributions to Mineralogy and Petrology*, **101**, 136–148.

Mezger, K. and Krogstad, E.J. (1997). Interpretation of discordant U-Pb zircon ages: an evaluation. *Journal of Metamorphic Geology*, **15**, 127-140.

Michard, A., Gurriet, P., Soudant, M. and Albarède, F. (1985). Nd isotopes in French Phanerozoic shales: external vs. internal aspects of crustal evolution. *Geochimica et Cosmochimica Acta*, **49**, 601-610.

Milisenda, C.C., Liew, T.C., Hofmann, A.W. and Köhler, H. (1994). Nd isotopic mapping of the Sri Lanka basement: update and additional constraints from Sr isotopes. *Precambrian Research*, **66**, 95-110.

Miller, R.McG. (1979). The Okahandja Lineament, a fundamental tectonic boundary in the Damara Orogen of South West Africa/Namibia. *Transactions of the Geological Society of South Africa,* **82,** 349-361.

Miller, R.Mc.G. (1983). The Pan-African Damara Orogen of South West Africa/Namibia. In: Miller, R.Mc.G. (Ed.), The Damara Orogen. *Geological Society of South Africa Special Publication*, **11**, 431–515.

Nelson, B.K. and DePaolo, D.J (1984). 1,700-Myr greenstone volcanic successions in southwestern North America and isotopic evolution of Proterozoic mantle. *Nature*, **312**, 143–146.

O'Nions, R.K., Hamilton, P.J. and Hooker, P.J. (1983). A Nd isotope investigation of sediments related to crustal development in the British Isles. *Earth and Planetary Sciences Letters*, **63**, 229-240.

O'Connor, J.T. (1965). A classification for quartz-rich igneous rocks based on feldspar ratios. *US Geological Survey Professional Paper*, **B525**, 79-84.

Parrish, R.R. (1987). An improved microcapsule for zircon dissolution in U-Pb geochronology. *Isotope Geoscience*, **66**, 99-102.

Parrish, R.R. (1990). U-Pb dating of monazite and its application to geological problems. *Canadian Journal of Earth Sciences*, **27**, 1431-1450.

Porada, H. (1979). The Damara-Ribeira orogen of the Pan-African-Brasiliano cycle in Namibia (South West Africa) and Brazil as interpreted in terms of continental collision. *Tectonophysics*, **57**, 237-265.

Porada, H. (1989). Pan-African rifting and orogenesis in southern to equatorial Africa and Eastern Brazil. *Precambrian Research*, **44**, 103–136.

Prave, A.R. (1996). Tale of three cratons: Tectonostratigraphic anatomy of the Damara orogen in northwestern Namibia and the assembly of Gondwana. *Geology*, **28**, 1115-1118.

Sandiford, M. and Powell, R. (1986). Deep crustal metamorphism during continental extension: modern and ancient examples. *Earth and Planetary Sciences Letters*, **79 (1-2)**, 151-158.

Seth, B., Jung, S. and Hoernes, S. (2002). Isotope constraints on the origin of the Pan-African granitoid rocks in the Kaoko belt, NW Namibia. *South African Journal of Geology*, **105**, 179-192.

Seth, B., Kröner, A., Mezger, K., Nemchin, A.A., Pidgeon, R.T. and Okrusch, M. (1998). Archaean to Neoproterozoic magmatic events in the Kaoko belt of NW Namibia and their geodynamic significance. *Precambrian Research*, **92**, 341–363.

Shand, S. J. (1943). The Eruptive Rocks, 2nd edition. New York: John Wiley, 444 pp.

Stanistreet, I.G., Kukla, P.A., and Henry, G. (1991). Sedimentary basinal responses to a Late PrecambrianWilson Cycle: the Damara Orogen and Nama Foreland. Namibia. *Journal of African Earth Science*, **13**, 141–156.

Taylor, S.R. and McLennan, S.M. (1985). The continental crust: its composition and evolution. Blackwell, Oxford.

Thompson, R.N. (1982). British Tertiary volcanic province. *Scottish Journal of Geology*, **18**, 49-107.

Thompson, A.B., Schulmann, K., Jezek, J. (1997). Thermal evolution and exhumation in obliquely convergent (transpressive) orogens. *Tectonophysics*, **280**, 171–184.

Wendt, J.I. and Todt, W. (1991). A vapour digestion method for dating single zircons by direct measurement of U and Pb without chemical separation. *Terra Abstracts*, **3**, 507-508.

Zhu, X. K., O'Nions, R. K., Belshaw, N.S. and Gibb, A.J. (1997). Significance of in situ SIMS chronometry of zoned monazite from the Lewisian granulites, northwest Scotland. *Chemical Geology*, **135**, 35-53.

Zulauf, G., Bues, C., Dörr, W., Fiala, J., Kotkova, J., Scheuvens, D. and Veijnar, Z. (1998). Extrusion tectonics due to thermal softening of a thickened crustal root: The Bohemian Massif in Lower Carboniferous times. *Terra Nostra*, *Alfred Wegner Stiftung*, **98**, 177-180.

5.9 Appendix

Table 5.1. Major [wt%], trace [ppm] and rare earth [ppm] element composition of granitic (G), granodioritic (GD) and tonalitic (T) gneisses from the Kaoko belt (NW Namibia). *LOI* Lost on ignition; *ASI* aluminium saturation index; Eu/Eu* europium anomaly; n.d. not determined; d.l. < detection limit.

Sample	Na 173	Na 118/2	Na 00/14	Na 118/1	Nd 87	Na 115	Nd 137	Na 250	Na 00/15	Nd 149	Na 00/23	Na 00/10	Na 00/07
Age [Ma]	539	549	550	553	626	655	661	663	694	730	1448	1502	1513
	G	G	G	G	G	G	G	G	G	GD	G	GD	G
SiO2	74.18	66.2	71.83	75.22	77.74	74.44	77.22	72.94	70.16	70.88	70.45	61.81	65.66
Al2O3	13.78	16.37	13.91	12.08	12.92	14.66	12.39	14.74	14.09	14.89	13.38	16.3	15.52
Fe2O3	1.31	4.23	2.13	2.64	0.79	0.81	0.99	2.33	3.81	2.59	3.89	5.67	4.9
MnO	0.02	0.07	0.03	0.04	0.01	0.02	0.04	0.02	0.06	0.04	0.08	0.06	0.05
MgO	0.3	1.42	0.57	0.97	0.05	0.13	0.09	0.28	1.63	0.86	0.87	1.87	1.43
CaO	1.82	3.18	1.48	2.02	0.85	1	0.79	1.27	1.66	2.34	1.58	3.91	2.69
Na2O	3.51	3.09	2.88	2.45	2.9	3.24	3.54	3.56	2.65	3.82	3.24	3.82	3.65
K2O	4.12	4.32	5.36	3.05	3.92	4.85	4.44	3.91	4.32	2.99	4.33	3.94	4.01
TiO2	0.15	0.61	0.33	0.37	0.08	0.09	0.1	0.17	0.6	0.47	0.64	0.84	0.74
P2O5	0.08	0.27	0.12	0.04	0.09	0.07	0.01	0.07	0.17	0.1	0.17	0.34	0.29
LOI	0.317	0.58	0.55	0.76	0.46	0.538	0.24	0.509	0.36	0.59	0.5	0.77	0.64
Total	99.59	100.34	99.19	99.64	99.81	99.85	99.85	99.80	99.51	99.57	99.13	99.33	99.58
An	8.51	14.01	6.56	9.76	3.63	4.50	3.85	5.84	7.13	10.96	6.73	15.81	11.45
Ab	29.70	26.15	24.37	20.73	24.54	27.42	29.95	30.12	22.42	32.32	27.42	32.32	30.89
Or	24.35	25.53	31.67	18.02	23.16	28.66	26.24	23.10	25.53	17.67	25.59	23.28	23.70
ASI	1.02	1.05	1.05	1.10	1.22	1.18	1.03	1.19	1.17	1.08	1.04	0.92	1.02
Sc	2	7	6	8	1	2	3	3	7	5	12	14	11
V	5	75	29	51	6	10	10	13	77	50	37	87	69
Cr	6	30	14	49	3	8	43	7	48	33	14	21	13
Co	106	9	37	4	0	0	2	54	59	5	38	61	55
Ni	4	10	5	14	3	1	4	2	21	12	8	14	7
Cu	2	13	d.l.	4	3	3	5	3	16	3	8	9	10
Zn	10	62	36	39	20	23	15	35	69	52	75	74	85
Ga	15	19	16	13	13	15	10	16	18	17	17	21	19
Rb	105	157	207	94	153	191	89	111	178	123	136	72	97
Sr	241	597	200	240	66	156	61	245	129	393	181	974	469
Y	16	20	16	15	26	19	16	14	22	7	47	46	40
Zr	219	255	138	213	136	73	84	130	147	232	338	399	236
Nb	8	13	14	14	6	4	5	6	15	9	20	13	14
Ba	1075	1692	525	634	355	547	679	748	483	761	1071	2795	1644
Pb	30	28	34.4	25	27	32	18	25	27.4	25	28.6	17.5	16.8
Th	70.4	16.3	23	20	24.9	6.1	6.2	9.9	7.8	14.4	16.7	3.4	5.3
U	4.6	1.8	1.4	1.8	3.2	1.3	0.4	1.6	1.6	2	3.9	0.6	1.4
La	69.32	64.43	39.18	46.33	33.03	19.92	15.06	19.28	28.33	40.08	67	63	54.28
Ce	119.04	131.51	83.87	92.88	71.04	42.05	28.17	38.7	58.53	72.99	123	131.84	121.69
Pr	11.67	14.24	9.19	10.1	7.91	4.88	2.86	4.1	7.06	7.73	15	15.64	14.25
Nd	40.62	53.62	33.88	38.24	29.34	19.26	9.83	14.53	28.36	28.12	61	61.75	54.13
Sm	5.86	8.24	6.43	6.75	6.19	3.86	1.76	2.64	5.93	4.29	12	10.48	9.34
Eu	1.15	1.98	0.94	1.33	0.57	0.77	0.22	0.76	1.09	0.93	n.d.	2.39	1.71
Gd	3.93	5.11	4.54	4.97	4.77	3.17	1.3	1.78	5	2.69	n.d.	8.3	6.89
Tb	0.5	0.65	0.59	0.59	0.6	0.42	0.18	0.24	0.69	0.3	n.d.	1.12	1.02
Dy	2.61	3.87	2.83	2.47	3.41	2.24	1	1.27	4.17	1.26	n.d.	7.2	6.09
Ho	0.45	0.73	0.44	0.36	0.51	0.39	0.19	0.21	0.72	0.18	n.d.	1.41	1.09
Er	0.93	1.71	1.01	0.87	1.03	0.88	0.47	0.48	1.6	0.42	n.d.	3.14	2.45
Tm	0.13	0.26	0.1	0.13	0.18	0.15	0.1	0.07	0.25	0.05	n.d.	0.45	0.37
Yb	0.95	1.82	0.61	0.74	1.23	0.95	0.77	0.58	1.68	0.36	n.d.	3	2.39
Lu	0.14	0.22	0.09	0.13	0.16	0.15	0.14	0.08	0.22	0.06	n.d.	0.41	0.29
Hf	4.55	4.03	2.69	1.78	3.22	1.58	1.58	2.54	2.11	3.28	n.d.	1.49	0.38
Eu/Eu*	0.73	0.93	0.53	0.7	0.32	0.67	0.44	1.07	0.61	0.84	n.d.	0.78	0.65
CeN/YbN	32.41	18.69	35.56	32.47	14.94	11.45	9.46	17.26	9.01	52.44	n.d.	11.37	13.17
CeN/SmN	4.9	3.85	3.15	3.32	2.77	2.63	3.86	3.54	2.38	4.11	n.d.	3.04	3.14
EuN/YbN	3.44	3.09	4.38	5.11	1.32	2.3	0.81	3.73	1.84	7.35	n.d.	2.27	2.03
Sum REE	257.3	288.39	183.7	205.89	159.97	99.09	62.05	84.72	143.63	159.46	n.d.	310.13	275.99

(Table 5.1 continued)

Sample	Na 00/28	Na 461	Na 124	Na 217	Sane 35	Na 00/04	Na 00/37	Na 00/27	Na 532	Na 428	Na 00/01	Sane 23
Age [Ma]	1516	1684	1701	1715	1742	1752	1776	1979	2008	2028	2400	2417
	G	GD	G	G	G	GD	G	GD	GD	G	T	T
SiO2	75.99	69.39	72.62	72.84	68.86	66.77	76.4	67.62	61.17	75.82	65.02	63.16
Al2O3	12.22	13.7	13.68	13.55	14.82	14.63	10.99	14.53	15.14	13.12	17.09	17.19
Fe2O3	1.61	6.14	2.78	3.36	4.16	5.25	1.13	5.27	10.21	1.16	3.99	5.1
MnO	0.03	0.07	0.02	0.02	0.07	0.09	0.05	0.22	0.18	0.02	0.05	0.07
MgO	0.25	1.24	0.76	0.36	1.51	1.58	0.22	2.6	3.44	0.08	1.58	1.94
CaO	0.7	2.8	0.54	1.09	2.56	2.72	1.64	2.83	5.66	0.59	4.15	4.71
Na2O	2.78	3.03	3.58	3.25	3.14	3.22	3.02	2.12	1.56	2.52	4.52	4.25
K2O	5.62	2.06	4.97	4.3	3.63	3.34	4.51	2.53	2.89	6.09	2	2.11
TiO2	0.33	0.84	0.39	0.38	0.06	0.72	0.23	0.93	1.39	0.29	0.48	0.53
P2O5	0.04	0.15	0.1	0.05	0.13	0.17	0.03	0.12	0.16	0.03	0.2	0.23
LOI	0.44	0.369	0.35	0.184	0.555	0.89	1.32	0.879	0.839	0.042	0.64	0.47
Total	100.01	99.789	99.79	99.38	99.50	99.38	99.54	99.65	102.64	99.76	99.72	99.76
An	3.21	12.91	2.03	5.08	11.85	12.38	3.19	13.26	25.88	2.73	19.28	21.60
Ab	23.52	25.64	30.29	27.50	26.57	27.25	25.55	17.94	13.20	21.32	38.25	35.96
Or	33.21	12.17	29.37	25.41	21.45	19.74	26.65	14.95	17.08	35.99	11.82	12.47
ASI	1.02	1.11	1.12	1.13	1.08	1.06	0.86	1.28	0.95	1.11	1.00	0.96
Sc	4	16	6	8	14	13	2	20	30	2	4	9
V	18	47	22	15	64	79	10	145	189	8	68	74
Cr	6	23	9	24	27	24	d.l.	149	93	2	26	40
Co	38	31	32	4	11	54	36	20	43	0	53	8
Ni	5	7	5	7	11	13	2	37	29	0	8	9
Cu	7	0	5	1	11	d.l.	d.l.	4	16	1	d.l.	22
Zn	30	36	14	15	57	66	27	23	125	15	50	68
Ga	14	17	16	17	17	17	13	17	21	12	19	20
Rb	139	97	136	114	142	149	128	104	104	120	42	54
Sr	91	233	70	94	209	258	190	65	165	131	830	822
Y	47	51	41	49	30	27	34	25	40	42	6	9
Zr	240	482	189	266	199	233	145	324	225	206	153	161
Nb	14	16	13	20	11	11	16	14	22	19	5	7
Ba	1207	1098	838	944	1028	894	650	1091	698	308	1283	957
Pb	25.4	7	10	8	18	16.9	18	3	22	18	9.3	15
Th	16.9	18.8	15.5	14.8	25.4	13.8	10.7	8.5	8.4	6.7	7	6.5
U	1.7	1.6	5.9	2.8	2.8	d.l.	1.4	1	0.4	0.9	d.l.	1.4
La	33.55	53.98	60.73	51	32	31.38	34.29	18.73	59.56	42.38	39.47	32
Ce	75.5	116.41	136.63	98	63	61.81	74.86	38.01	124.9	100.19	74.21	58
Pr	8.76	13.75	15.92	10	6	6.97	8.29	4.78	14.42	12.25	8	4
Nd	34.59	55.07	61.25	45	30	27.89	32.61	18.73	55.61	48.12	28.76	26
Sm	6.84	10.37	11.62	9	3	5.11	6.54	3.52	10.09	10.92	3.54	5
Eu	1.6	1.58	1.16	n.d.	n.d.	1.28	0.94	0.91	1.73	0.63	1.08	n.d.
Gd	6.42	8.11	8.39	n.d.	n.d.	4.28	5.8	2.7	8.24	9.4	1.95	n.d.
Tb	0.99	1.15	1.05	n.d.	n.d.	0.59	0.89	0.38	1.26	1.41	0.2	n.d.
Dy	6.02	7.2	5.28	n.d.	n.d.	4.19	5.52	2.2	7.57	8.47	1.14	n.d.
Ho	1.11	1.4	0.72	n.d.	n.d.	0.82	1.04	0.41	1.43	1.53	0.18	n.d.
Er	3.13	3.41	1.22	n.d.	n.d.	1.89	3.05	0.94	4.23	3.78	0.42	n.d.
Tm	0.45	0.57	0.14	n.d.	n.d.	0.27	0.45	0.13	0.56	0.51	0.06	n.d.
Yb	2.85	4.16	0.93	n.d.	n.d.	2.09	2.99	1.14	3.89	2.97	0.41	n.d.
Lu	0.46	0.62	0.12	n.d.	n.d.	0.28	0.41	0.15	0.53	0.32	0.06	n.d.
Hf	2.13	7.26	3.46	n.d.	n.d.	1.31	0.93	1.91	1.07	1.6	0.33	n.d.
Eu/Eu*	0.74	0.53	0.36	n.d.	n.d.	0.84	0.47	0.9	0.58	0.19	1.26	n.d.
CeN/YbN	6.85	7.24	38	n.d.	n.d.	7.65	6.48	8.62	8.31	8.73	46.82	n.d.
CeN/SmN	2.66	2.71	2.84	n.d.	n.d.	2.92	2.76	2.61	2.99	2.21	5.06	n.d.
EuN/YbN	1.6	1.08	3.55	n.d.	n.d.	1.74	0.89	2.27	1.26	0.6	7.49	n.d.
Sum REE	182.27	277.78	305.16	n.d.	n.d.	148.85	177.68	92.73	294.02	242.88	159.48	n.d.

Table 5.2. Summary of obtained ages, dating method and sample locations

	Sample	E	S	Method	Age in [Ma]
Palaeo-Proterozoic	Sane 23	12.9626	18.6653	U-Pb	2417±57
	Na 00/01	13.0738	18.7904	U-Pb	~2400
	Na 428	13.1102	18.8962	U-Pb	2028±15
	Na 532	12.8764	18.8515	U-Pb	2008±18
	Na 00/27	12.9850	18.7260	U-Pb	1979±38
	Na 00/37	13.2338	18.8504	SHRIMP	1776±2
	Na 00/04	12.9852	18.7248	SHRIMP	1752±3
	Sane 35	12.9739	18.6476	U-Pb	1742±10
	Na 217	12.7778	18.7788	U-Pb	1714±54
	Na 124	12.7170	18.7340	U-Pb	1701±37
	Na 461	12.8993	18.8207	U-Pb	1684±8
Meso-Proterozoic	Na 00/28	13.1848	18.9356	U-Pb	1516±54
	Na 00/07	12.9158	18.8043	Pb-Pb	1513±1
	Na 00/10	12.9161	18.8093	U-Pb,Pb-Pb	1502±3
	Na 00/23	12.8586	18.4869	U-Pb	1448±31
Neo-Proterozoic	Nd149	12.7762	18.8884	U-Pb	730±15
	Na 00/15	12.6066	18.7202	SHRIMP	694±9
	Nd137	12.7644	18.8825	U-Pb	661±21
	Na 115	12.7857	18.8721	U-Pb	655±39
	Na 250	12.5924	18.7507	U-Pb	663±5
	Nd 87	12.7829	18.8512	U-Pb	626±30
	Na 00/14	12.8256	18.8909	Pb-Pb	550±1
	Na 118/1	12.6668	18.7555	Pb-Pb	554±2
	Na 118/2	12.6666	18.7552	Pb-Pb	549±4
	Na 173	12.8645	18.8413	U-Pb	539±6

Table 5.3a. Pb and U analytical data for conventional zircon analysis in granitic gneisses in Kaokoland, Namibia.

			isotopic ratios				Age [Ma], 2σ error		
	Utot	^{206}Pb	^{207}Pb*	^{206}Pb*	^{206}Pb*		^{206}Pb*	^{207}Pb*	^{206}Pb*
	Pb*	^{204}Pb	^{235}U	^{238}U	^{207}Pb*	Cor.	^{235}U	^{238}U	^{207}Pb*
ND 87 L1	21.80	257	0.3305± 63	0.0400±3	0.0599± 9	0.383	253± 2	290± 5	600±34
ND 87 L2	29.61	215	0.1977± 38	0.0250± 2	0.0573±10	0.326	159± 1	183± 3	503±37
ND 87 L4	36.15	235	0.2000± 40	0.0251± 3	0.0577± 9	0.516	160± 2	185± 3	520±35
ND 87 L6	18.93	257	0.3895± 71	0.0474± 3	0.0595±11	0.252	299± 2	334± 5	587±40
ND 87 -2- L2	41.98	191	0.1710± 30	0.0213± 1	0.0583± 9	0.337	136± 1	160± 3	542±34
ND 87 -2- L3	18.96	196	0.3904± 51	0.0473± 3	0.0598± 8	0.369	298± 2	335± 4	597±29
ND 87 -2- L4	44.11	207	0.1631± 24	0.0207± 1	0.0571± 7	0.394	132± 1	153± 2	496±28
ND 87 -2- L6	42.82	214	0.1669± 27	0.0208± 2	0.0582± 7	0.528	133± 1	157± 2	536±28
Na 250 L2	10.76	172	0.6944± 84	0.0816± 6	0.0617± 7	0.508	506± 3	535± 5	665±24
Na 250 L3	9.74	542	0.6655± 95	0.0792± 5	0.0609± 6	0.509	492± 3	518± 6	636±22
Na 250 L4	11.42	488	0.6337± 04	0.0746± 8	0.0616± 5	0.780	464± 5	498± 6	661±17
Na 250 L5	9.35	1500	0.7771± 48	0.0914± 4	0.0617± 1	0.926	564± 3	584± 3	663± 4
Na 250 L6	11.82	585	0.6500± 127	0.0760± 4	0.0620±10	0.285	472± 2	508± 8	674±34
Na 250 -2- L2	9.74	308	0.7502± 130	0.0873±10	0.0623± 5	0.807	540± 6	568± 8	684±18
Na 250 -2- L5	11.43	675	0.0668± 4	0.0078± 1	0.0622± 1	0.762	50± 1	66± 1	679± 5
Na 217 L1	3.71	6510	3.1959± 208	0.2256±11	0.1028± 2	0.936	1311± 6	1456± 5	1675± 3
Na 217 L3	4.42	2849	2.6509± 252	0.1884±13	0.1021± 2	0.944	1112± 7	1315± 7	1662± 4
Na 217 L6	5.54	11583	2.0706± 70	0.1528± 4	0.0983± 1	0.980	916± 2	1139± 2	1592± 1
Na 217 L4	11.56	5342	0.9309± 65	0.0767± 4	0.0880± 1	0.980	477± 3	668± 3	1382± 2
Sane 23 Mitte	2.06	2080	7.9122± 53	0.3891±16	0.1475± 4	0.851	2119± 7	2221± 6	2317± 4
Sane 23 L1	3.62	1756	3.8600± 300	0.2385±13	0.1174± 3	0.896	1379± 7	1605± 6	1918± 5
Sane 23 L5	1.42	3295	12.5661±1508	0.5550±54	0.1642± 4	0.974	2846±22	2648±211	2500± 4
Sane 23 L6	2.51	4033	6.3654± 704	0.3256±33	0.1418± 2	0.991	1817±16	2028± 10	2249± 2
Sane 35 L3	4.35	2476	2.5908± 151	0.1871± 8	0.1004± 2	0.917	1106± 4	1298± 4	1632± 3
Sane 35 L5	3.18	6281	3.7753± 464	0.2606±23	0.1051± 4	0.930	1493±12	1588± 10	1716± 6
Sane 35 L6	3.67	2411	3.0989± 232	0.2194±12	0.1024± 2	0.912	1279± 6	1432± 6	1668± 4
Sane 35 L7	3.81	4448	3.0126±1320	0.2133±90	0.1024± 2	0.999	1247±47	1411± 33	1668± 4

Table 5.3b. Isotopic data from single grain zircon evaporation.

Sample no.	Zircon colour and morphology	Grain no.	Mass scansa)	Mean 207 Pb/ 206 Pb ratio and 2-σ m error b)	^{207}Pb/ ^{206}Pb age and 2-σ m error
Na 118/1	brownish, long-prismatic		176	0.058810±103	560±6
			192	0.058598±079	553±4
			95	0.058428±114	546±6
mean of 3		1-3	436	**0.058643±057**	**554±2**

a) Number of ^{207} Pb / ^{207} Pb ratios evaluated for age assesssment
b) Observed mean ratio corrected for nonradiogenic Pb where necessary. Errors based on uncertainties in counting statistics.

Table 5.4a. Sm-Nd isotope data of granitic and metasedimentary rocks from the Kaoko Belt. Zircon ages from Kröner et al. (2004) and this work.

Sample	Age	Nd [ppm]	Sm [ppm]	Sm/Nd	($^{143}Nd/^{144}Nd)_{meas.}$	+/-	($^{143}Nd/^{144}Nd)_{initial}$	$^{147}Sm/^{144}Nd$	εNd_{today}	$\varepsilon Nd_{initial}$	T (DM)
NA 173	539	40.6	5.9	0.14	0.511697	5	0.511390	0.0869	-18.4	-10.8	1675
Na 00 12	~550	30.5	6.5	0.21	0.512191	9	0.511730	0.1278	-8.7	-3.9	1603
NA 00-14	550	33.9	6.4	0.19	0.512167	12	0.511756	0.1142	-9.2	-3.4	1430
NA 118-1	553	38.2	6.8	0.18	0.512008	9	0.511623	0.1063	-12.3	-5.9	1545
NA 118-2	549	53.6	8.2	0.15	0.511934	8	0.511601	0.0925	-13.7	-6.4	1465
ND 87	626	29.3	6.2	0.21	0.512141	10	0.511620	0.1269	-9.7	-4.1	1670
NA 115	655	19.3	3.9	0.20	0.512103	13	0.511586	0.1205	-10.4	-4.1	1621
ND 137	661	9.8	1.8	0.18	0.512416	11	0.511950	0.1075	-4.3	3.2	1006
NA-250	663	14.5	2.7	0.18	0.512079	18	0.511604	0.1093	-10.9	-3.5	1488
NA 00-15	694	28.4	5.9	0.21	0.512202	8	0.511629	0.1259	-8.5	-2.2	1553
ND 149	730	28.1	4.3	0.15	0.512006	9	0.511566	0.0919	-12.3	-2.5	1372
Na 00 23	1448	70.6	12.8	0.18	0.511788	9	0.510745	0.1096	-16.6	-0.4	1896
Na 00 05	~1500	30.3	5.2	0.17	0.511776	7	0.510745	0.1046	-16.8	0.9	1829
Na 00 36A	~1500	45.8	8.9	0.19	0.511854	10	0.510702	0.1169	-15.3	0.1	1932
Na 00 36B	~1500	88.4	14.1	0.16	0.511671	10	0.510726	0.0958	-18.9	0.5	1829
Na 00 36D	~1500	38.1	7.8	0.20	0.511918	10	0.510706	0.1230	-14.0	0.1	1954
Na 00 36E	~1500	73.3	11.9	0.16	0.511718	6	0.510743	0.0989	-17.9	0.9	1815
NA 00-10	1502	61.8	10.5	0.17	0.511660	8	0.510652	0.1021	-19.1	-0.9	1941
NA 00-07	1513	54.1	9.3	0.17	0.511752	10	0.510719	0.1039	-17.3	0.7	1849
NA 00-28	1516	34.6	6.8	0.20	0.511695	7	0.510508	0.1191	-18.4	-3.3	2216
NA 124	1701	61.3	11.6	0.19	0.511804	10	0.510527	0.1141	-16.3	1.8	1954
Na 217	1715	45.0	9.0	0.20	0.511845	13	0.510491	0.1200	-15.5	1.4	2007
Sane 35	1742	30.0	5.0	0.17	0.511631	13	0.510371	0.1100	-19.6	-0.3	2120
NA 00-04	1752	27.9	5.1	0.18	0.511636	10	0.510365	0.1103	-19.5	-0.1	2119
NA 00-37	1776	32.6	6.5	0.20	0.511743	8	0.510332	0.1207	-17.5	-0.1	2179
NA 00-27	1979	18.7	3.5	0.19	0.511697	9	0.509895	0.1383	-18.4	-3.5	2736
NA 428	2028	48.1	10.9	0.23	0.511634	10	0.509810	0.1366	-19.6	-4.0	2796
NA 00-01	2417	28.8	3.5	0.12	0.510844	10	0.509091	0.1100	-35.0	-8.1	3207
Sane 23	2417	26.0	5.0	0.19	0.510984	8	0.509140	0.1158	-32.3	-7.1	3181
Metasediments											
Na 550		68.5	13.6	0.20	0.511908	11		0.1197	-14.2		1904
Na 555		45.6	8.1	0.18	0.511893	9		0.1078	-14.5		1722
Na 556		68.5	13.6	0.20	0.511848	11		0.1197	-15.4		1995

Table 5.4b. Rb-Sr isotope data of granitic rocks from the Kaoko Belt.

Sample	Age	Sr [ppm]	Rb [ppm]	($^{87}Sr/^{86}Sr)_{meas.}$	$^{87}Rb/^{86}Sr$	($^{87}Sr/^{86}Sr)_{550Ma}$
NA 173	539	241	105	0.727410	1.2596	0.717534
NA 00-14	550	200	207	0.731854	2.9923	0.708392
NA 118-1	553	240	94	0.720312	1.1324	0.711434
NA 118-2	549	597	157	0.713157	0.7603	0.707196
ND 87	626	69	116	0.760608	4.8605	0.722499
NA 115	655	156	191	0.742721	3.5398	0.714967
ND 137	661	61	89	0.752595	4.2182	0.719522
NA-250	663	245	111	0.719812	1.3099	0.709542
NA 00-15	694	129	178	0.744611	3.9893	0.713332
ND 149	730	393	123	0.717447	0.9049	0.710352

Chapter 6

An unusual old Sm-Nd garnet-whole rock age from the granulite-facies Western Kaoko Zone (Namibia): Evidence for a Neoproterozoic cryptic high-grade polymetamorphic event?

(submitted to Lithos)

An unusual old Sm-Nd garnet-whole rock age from the granulite-facies Western Kaoko Zone (Namibia): Evidence for a Neoproterozoic cryptic high-grade polymetamorphic event?

S. Kröner[1], S. Jung[2], A. Kröner[1]

[1]*Institut für Geowissenschaften, Universität Mainz, 55099 Mainz, Germany*

[2]*Fachbereich Geowissenschaften, Philipps Universität Marburg, 35032 Marburg, Germany*

6.1 Abstract

Continental collision of the Kalahari and Congo Cratons in Africa and the Rio de la Plata Craton in South America resulted in a structurally complex Neoproterozoic orogenic belt system, the Kaoko-Dom Feliciano-Ribeira belt. It is uncertain whether these three cratons collided more or less simultaneously during one orogenic event at ~580-550 Ma or whether the belt owes its structural and metamorphic features to several so far poorly constrained events. The Kaoko Belt of NW Namibia, representing the belt system between the southern Congo Craton and the Rio de la Plata Craton, is an ideal object to study these complexities. Within this belt, high-grade meta-igneous and metasedimentary rocks of the sillimanite-K-feldspar zone contain large garnet porphyroblasts that grew during peak metamorphic granulite-facies conditions. Minimum P-T conditions of peak metamorphism were 731±10 °C at 6.7±1.2 kbar, substantially lower than those previously reported.

A well-defined Sm-Nd garnet-whole rock errorchron obtained on a single meta-igneous rock yielded an unexpectedly old age of 692±13 Ma, which is interpreted as an inherited metamorphic age reflecting an early Pan-African granulite-facies event. We show that the dated garnets survived a younger high-grade metamorphism that occurred between ca. 570 and 520 Ma and maintained their old Sm-Nd isotopic systematics, implying that the closure temperature for garnet in this sample was higher than 730 °C. The metamorphic peak of the younger event was dated on monazite at 567±5 Ma by the Electron Probe Microanalyser (EPMA). These results imply fast heating and cooling rates at different times during the Pan-African orogeny that prevented isotopic homogenisation at the sample scale. Moreover, it is suggestive that trace element diffusion is considerably shorter than major element diffusion. From a regional viewpoint, it is possible that these specific meta-igneous granulites may be unrelated to the early Pan-African metamorphic evolution of the Kaoko Belt and may represent a so far unrecognised terrane.

Key words: Sm-Nd garnet age, EPMA dating, P-T thermo-barometry, granulite-facies, Neoproterozoic terrane, Kaoko Belt.

6.2 Introduction

The conventional approach to date high-grade metamorphism is to analyse U-Th rich accessory minerals (monazite, allanite, titanite, zircon) and link the obtained ages to petrographic, structural and thermobarometric results. Assigning ages to a given P-T path remains a challenge because it is uncertain whether the accessory minerals grew or equilibrated at the same P-T conditions as recorded in the observed mineral equilibria. Attention has also focused on the dating of major rock-forming minerals such as garnet and staurolite (e.g., Mezger et al., 1989; Burton and O'Nions, 1991; Vance and O'Nions, 1990; Lanzirotti and Hanson, 1993, 1995), which recorded variable aspects of their pressure and temperature history during their growth. However, several studies (Zhou and Henson, 1995, Henson and Zhou, 1995; DeWolf et al., 1996) have shown that tiny (<5μm) REE-rich inclusions of accessory minerals (e.g. monazite, allanite) may severely disturb the original parent-daughter isotopic systematics of rock-forming minerals. However, some advances in the development of step-wise leaching techniques have been made to resolve the contributions from the lattice of the host mineral and those from microscopic inclusions (e.g., Frei and Kamber, 1995; Zhou and Henson, 1995).

Garnet is generally the major mineral used for the reconstruction of P-T paths because it is involved in a number of reactions useful for thermobarometry (e.g., Essene, 1989), and the ability to date the growth of garnet is a powerful tool to assign precise ages to a given P-T path. However, in order to date peak metamorphic conditions, the closure temperature of a given isotopic system must be equal to, or higher than, the temperature that prevailed during regional metamorphism. Application of the U-Pb system in garnet to date granulite-facies rocks has been successful due to the inferred high (>800 °C) closure temperature for U-Pb in this mineral (Mezger et al., 1989). Additionally, Sm-Nd dating of garnet has also been used to constrain ages of prograde metamorphism (Burton and O'Nions, 1991; Vance and O'Nions, 1992; Henson and Zhou, 1995), but a straightforward application of this dating technique has been hampered by uncertainties on the closure temperature for this isotopic system in garnet. Due to the relatively high temperatures and/or long times required for re-equilibration of chronologically useful trace and major elements in garnet via diffusion (e.g., Elphick et al., 1985), garnet not only records the time and physical conditions during growth but commonly retains a record of these conditions after subsequent thermal events.

Comparing dating of other minerals with high blocking temperatures (U-Pb on zircon or monazite) with Sm-Nd on garnet, the latter is often used as a powerful geochronological tool for the interpretation of high-grade metamorphic terrains (e.g., Jung and Mezger, 2003a), but is probably the isotopic system with the largest uncertainty concerning the closing temperature. Early investigations by Humphries and Cliff (1982) suggested that the blocking temperature (T_C) in an almandine-pyrope garnet is ca. 725±30 °C for a cooling rate of 5 °C/Ma. On the other

hand, these authors calculated a T_C for an $Alm_{1.6}Py_{0.9}Gross_{0.5}$ garnet of less than a few mm in diameter for a slowly cooled terrain at ~600 °C. Patchett and Ruiz (1987) estimated T_C for garnets of unknown composition to be in the same range of 600-700 °C for a cooling rate of 3.5 °C/Ma. Other studies indicated similar closure temperatures of about 600±30 °C (Burton et al., 1995; Humphries and Cliff, 1982; Mezger et al., 1992; Patchett and Ruiz, 1987), implying that the system only records the cooling history of high-grade metamorphic terrains. Higher closure temperatures of 800-850 °C have been calculated by Jagoutz (1988) and Cohen et al. (1988), suggesting that the Sm-Nd isotopic systematics may be preserved at or near peak metamorphic conditions, depending on rock type. In a revision of results for samples studied by Cohen et al. (1988), Burton et al. (1995) showed that the T_C for garnets is in the range of 640-825 °C for grain sizes between 1 and 9 mm and for a cooling rate of 3.7° C/Ma.

Intermediate values around 700-750 °C as a reasonable estimate for the closure temperature of Sm-Nd in granulite-facies garnets have been suggested by Zhou and Henson (1995) and Henson and Zhou (1995), although their samples seem to have been affected by both regional and contact metamorphism.

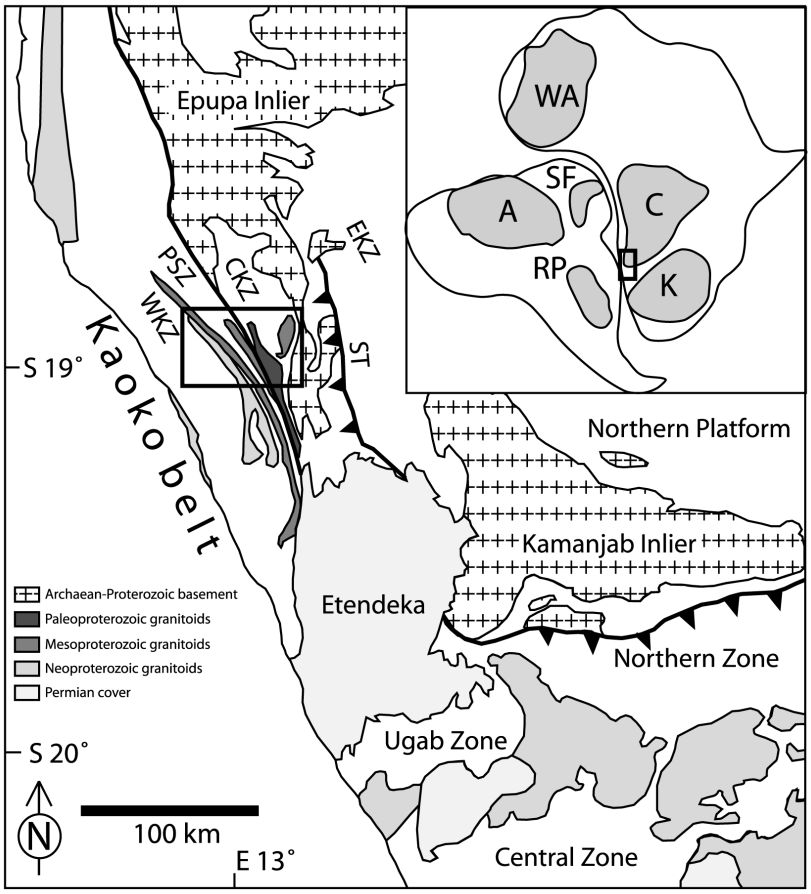

Fig. 6.1. Schematic location map of the Kaoko and Damara belts modified after Miller (1983) and Goscombe et al. (2003a,b); the investigated area is marked by a box (Fig. 6.2). Cratons indicated in inset: A: Amazon; C: Congo; K: Kalahari; RP: Rio de la Plata; SF: São Francisco; WA: West African. The Dom Feliciano Belt lies east of the Rio de la Plata Craton. ST-Sesfontein Thrust, PSZ-Puros shear zone, EKZ-Eastern Kaoko Zone, CKZ-Central Kaoko Zone, WKZ-Western Kaoko Zone.

In summary, T_C in garnet varies depending on several parameters, particularly cooling rate, grain size and the presence of fluids. Usually, common accessory minerals used for isotopic dating such as zircon and monazite do not vary strongly in grain size (typical range is 50-500 μm), whereas the grain size of garnet can be very variable (μm to several cm). Additionally, some other important parameters are (i) the variable chemical composition of garnet (e.g. Humphries and Cliff 1982); (ii) the different diffusion rate for major elements (Grauert et al. 1974); and (iii) the mineral adjacent to garnet into which Nd diffuses (Burton et al. 1995).

The Kaoko Belt in NW Namibia belongs to a Neoproterozoic belt system whose geodynamic evolution is still poorly constrained. It is still an open question whether this mountain belt experienced a simple, single-phase metamorphic evolution or a more complex polyphase history. Estimates for the age of the main high-grade metamorphic event in the western Kaoko belt were presented by Goscombe et al. (2003a) on the basis of Sm-Nd garnet whole-rock ages that range from 592±21 to 567±14 Ma. These ages appear to be older than the peak of metamorphism in the central Damara Orogen which occurred at 520±10 Ma (Jung, 2000). However, many Sm-Nd garnet whole-rock ages from the western Kaoko belt are significantly younger (Jung, unpubl. results) than those presented by Goscombe et al (2003a) and range from 564±5 to 522±6 Ma, more compatible with those obtained from the central Damara orogen.

We present a seven-point Sm-Nd garnet-whole rock errorchron from a well-studied gneiss sample from the western part of the Kaoko belt in the Hoarusib area. A combination of petrographic observations, thermobarometric calculations and geochronological data, together with a discussion of the ages so far available, allows us to place constraints on the time of peak metamorphism in this segment of the belt. As stated previously, high-grade metamorphic garnets may often show a significant amount of tiny (μ-sized) REE-rich inclusions (e.g., Henson and Zhou, 1995; Jung and Mezger, 2001). Elimination of such inclusions by handpicking is beyond the reach of most physical purification processes, and we have therefore used an improved leaching technique. We show that some of the analysed garnet fractions contained μ-sized LREE-enriched inclusions, but the inclusion-bearing garnet fractions plot on, or very close to, the errorchron defined by the leached garnet separates. Taken together the results have important implications for the equilibration of small inclusions in the host mineral and for the closure temperature of Sm-Nd in garnet at water-undersaturated high-grade metamorphic conditions.

6.3 Analytical techniques

6.3.1 Garnet

Garnet was analysed on a JEOL Superprobe (WDS system) at the University of Mainz. Operating conditions were 15 kV and 12 nA, with a peak counting time of 20 s. The ZAF correction procedure was applied to the data; errors in the major oxides are estimated to be about 1-2 % relative. Element mapping was carried out using an accelerating voltage of 20 kV and a beam current of 20 nA.

The leaching procedure follows Zhou and Henson (1995) with some modifications. After crushing and sieving the samples, garnet was concentrated by magnetic separation, heavy liquids and handpicking that produced high purity mineral separates. However, initial isotopic analyses yielded high Nd concentrations and low Sm/Nd ratios, indicating the presence of undetected minerals with low Sm/Nd ratios, most probably monazite. The handpicked garnet separates were again sieved to obtain two different grain fractions (<170μm and >170μm). After separation, ca. 1 g of both garnet fractions was ground in an agate ball mill for ca. 60 min to reduce the grain size to <5μm. This procedure exposed most of the μm-sized monazite crystals. The garnet powder was subsequently leached with 6 N HCl and a mixture of 2:1 6 N HNO_3/6 N HCl in a 10 ml Savilex screw-top beaker on a hot plate for one hour at 180 °C. This leaching procedure resulted in a loss of weight of approximately 30-50 %. After each leaching step the sample was centrifuged, and the leaching solution was decanted. Subsequently, the residue was washed three times with ultra pure water. The sample was spiked with a mixed $^{149}Sm/^{150}Nd$ tracer and was subsequently treated with doubly distilled 7 N HNO_3 that oxidized the garnet. Sample digestion using HF- HNO_3 was performed in vials inside Krogh-style Teflon bombs at 200 °C for several days. After complete dissolution the samples were dried down and redissolved in 2.5N HCl.

REE were separated from the matrix by using standard cation exchange columns with a DOWEX AG 50 W-X 12 resin using 6N HCl for the REE. Neodymium and Sm were separated from the other REE by using HDEHP coated teflon columns and 0.12 N HCl for Nd and 0.3 N HCl for Sm. Sm and Nd isotopic analyses were carried out at the Max-Planck-Institut für Chemie at Mainz using thermal ionisation mass spectrometry with a Finnigan MAT 261 multicollector mass spectrometer operating in the static mode. Sm and Nd were run on Re double filaments. Neodymium isotopes were normalized to $^{146}Nd/^{144}Nd$: 0.7219. The total procedural blank for Nd was <40 pg and is considered to be negligible. Repeated measurements of the La Jolla Nd standard gave $^{143}Nd/^{144}Nd$: 0.511868 ± 0.000020 (2σ; n=12). Uncertainties in the $^{143}Nd/^{144}Nd$ are reported at the last two digits. Typical analytical errors in the $^{147}Sm/^{144}Nd$ ratios are equal or better than 0.1%.

6.3.2 Monazite

Monazite was analysed in-situ in 60 μm-thick thin sections on a JEOL microprobe at the University of Mainz. Operation conditions were 15 kV and 100 nA with a spot size of 5 μm. To avoid Pb contamination, thin sections require lead-free polishing because Pb can be deposited on grain boundaries (Scherrer et al. 2000). Thus, quartz disks have been used for polishing. Due to high luminescence (high Th content) in backscatter electron images (BSE images) monazite can be easily detected and EDS then verified the identification. Analysed lines were Pb*Mß*, U*Mß* and Th*Mα*. Counting times on Pb were 400 sec, 120 sec for U and 70 sec for Th. During acquisition time standard monazite grains (Finger et al. 1998, 2003) were analysed to control measurement conditions and reliability of the method (Table 6.1). The recommended age is 341±2 Ma (Friedl, 1997) - confirmed by the Electron Probe Microanalyser (Finger et al. 2003) - and could be reproduced at 337.1±4.6 Ma (2σ, MSWD = 0.6, probability = 0.82).

6.4 Previous work

6.4.1 Tectonic evolution of the Kaoko Belt and adjacent Damara orogen

The NNW-trending Kaoko Belt and the perpendicular ENE-trending Damara Belt are part of the Neoproterozoic mobile belt system of western Gondwana, which is generally interpreted to have resulted from continental collision between the Congo Craton, the Kalahari Craton (both in present Africa) and the Rio de la Plata Craton (present South America; Fig. 6.1). The Kaoko Belt is subdivided into an Eastern, Central and Western Kaoko Zone, based on tectono-stratigraphic observations by Miller (1983). These tectonic units are separated by two major discontinuities exhibiting different metamorphic and structural histories (Figs. 6.2, 6.3, Miller, 1979; Miller, 1983; Gruner, 2000; Goscombe et al., 2003a). The ~400 km long crustal-scale Puros Shear Zone (PSZ) separates the Western Kaoko Zone (WKZ) from the Central Kaoko Zone (CKZ). The westerly dipping Sesfontein Thrust (ST) marks the contact where the Kaoko Belt is thrust onto the Congo Craton. The tectonic evolution of the belt is characterized by three phases of deformation that developed under ductile (D1 and D2) and ductile to brittle (D3) conditions (Goscombe et al., 2003a, b; Konopásek et al., 2005). Metasedimentary migmatites and intrusive rocks occur in the WKZ, and Konopásek et al. (2005) suggested that migmatization occurred during the transition from D1 (ESE thrusting) to D2 (NNE-SSW shortening).

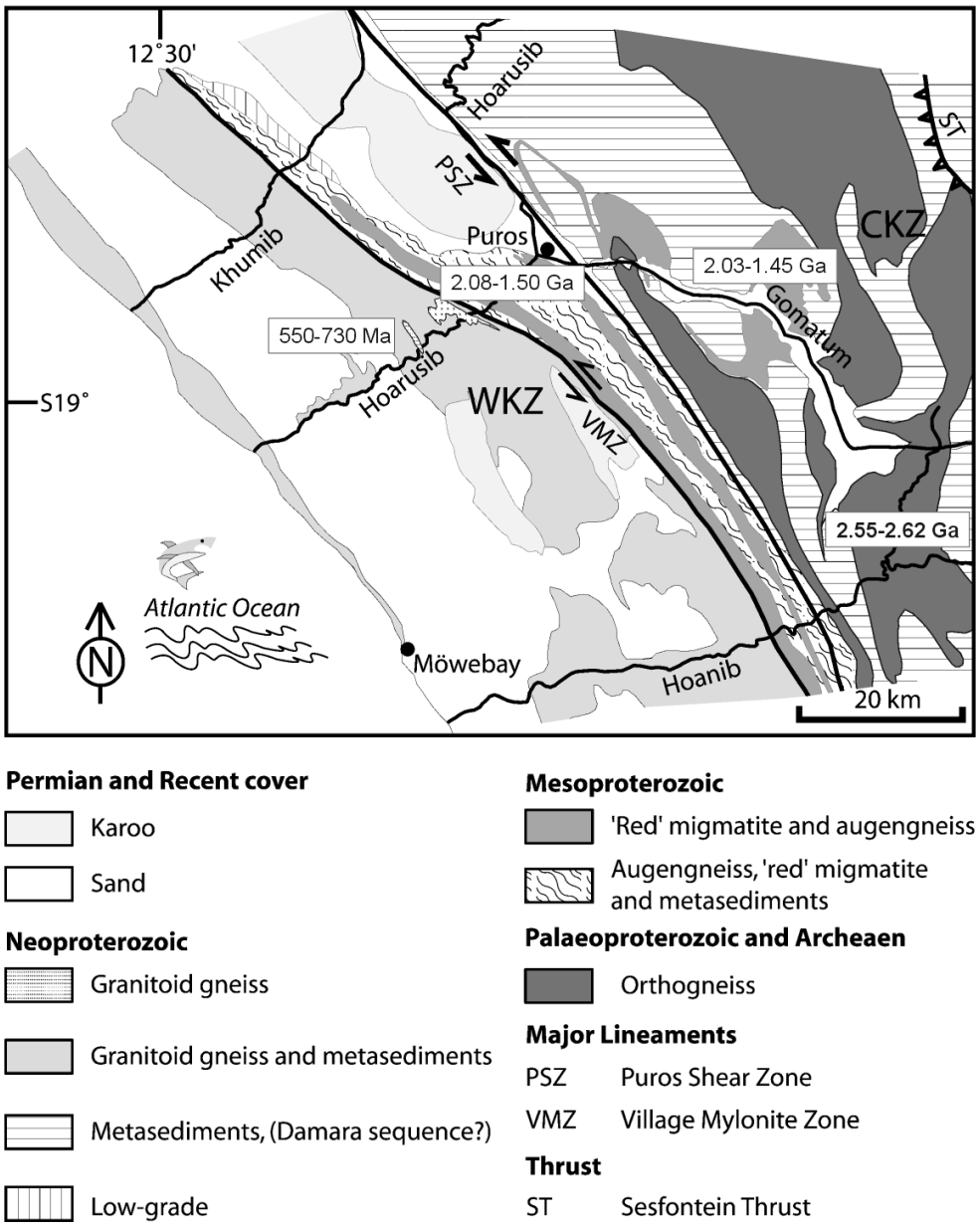

Fig. 6.2 Schematic and simplified geological map showing major rock units of the study area. Base map modified after Guj (1970) and Goscombe et al. (2003).

Pre-Pan-African basement orthogneisses yielded late Archaean (2.62-2.55 Ga) and Palaeo- to Mesoproterozoic (2.03-1.45 Ga) U-Pb and Pb-Pb zircon ages in the CKZ and WKZ (Seth et al. 1998; Franz et al. 1999; Kröner et al., 2004). Kröner et al. (2004) have also shown that the WKZ is marked by an important mylonitic shear zone, the Village Mylonite Zone (VMZ) exposing a Pan-African terrane to the west and a Meso- to Palaeoproterozoic terrane to the east (Fig. 6.2).
The counterpart of the Kaoko Belt in South America is the Dom Feliciano Belt in southeastern Brazil (Porada, 1989; Basei et al, 2000). Kröner et al. (2004) summarized the main similarities and differences in the evolution of these two belts. From this it would appear that both orogenic

belts only underwent a common tectonic history during the latest Neoproterozoic and earliest Palaeozoic.

Coward (1983) interpreted the Kaoko Belt as the 'northern arm' of the Damara Belt. The Damara Belt has been subdivided into three tectono-stratigraphic units: a Northern, Central and Southern Zone (Miller, 1983; Porada, 1989). In this belt, peak metamorphism reached 700-750 °C/~5 kbar between ~540 Ma and 504 Ma in the central part as indicated by numerous U-Pb monazite and Sm-Nd garnet-whole rock ages obtained from migmatites, metapelites and granites (Jung, 2000; Jung and Mezger, 2001; Jung and Mezger, 2003a).

The Gariep Belt is seen as the southern continuation of the Kaoko Belt, separated by the Damara orogen (e.g., Frimmel et al. 1996a). The initial phase of rifting in this belt (741±6 Ma, Pb-Pb zircon ages; Frimmel et al. 1996b) was coeval with incipient rifting along the northern margin of the Damara Belt (756±2 Ma; Hoffman et al., 1996) and the peak of regional metamorphism was dated at 545±2 Ma on amphibolite dykes by means of the $^{40}Ar/^{39}Ar$ method (Reid et al., 1991).

6.4.2 Metamorphic and temporal constraints on the evolution of the Kaoko Belt

Guj (1970) first described the metamorphism in the Kaoko Belt and demonstrated a prograde Barrovian-type metamorphic evolution from the Sesfontein Thrust in the CKZ to the WKZ, using critical mineral assemblages. He recognized seven different metamorphic zones starting from the Sesfontein Thrust with greenschist-facies rocks (chlorite-sericite phyllite) up to amphibolite-facies rocks (sillimanite zone) west of the Puros Shear Zone (PSZ) between the Hoarusib and Hoanib Rivers. West of the PSZ, Guj (1970) estimated temperatures at around 670-700 °C for at least 2 kbar for the assemblage sil±grt+bt+kfs±ms+pl+qtz (mineral abbreviations after Spear, 1993). Re-investigations of the area confirmed the Barrovian-type metamorphism in the CKZ and, additionally, cordierite was detected in the WKZ (Fig. 6.3; Miller, 1979; Dingeldey et al. 1994; Dürr et al. 1996; Gruner 2000; Goscombe et al. 2003a). Miller (1979) suggested that the PSZ marks an important boundary between two different metamorphic domains. He speculated about a high-pressure-low-temperature domain in the CKZ due to the occurrence of kyanite and staurolite, but several authors confirmed a medium-pressure/medium-temperature metamorphic environment (e.g., Dingeldey et al. 1994; Dürr et al. 1996; Gruner 2000).

In the westernmost part of the CKZ, close to the PSZ in the kyanite-sillimanite-muscovite-zone, ~650 °C and ~9 kbar were calculated by Gruner et al. (2000) and Goscombe et al. (2003a) for the peak of regional metamorphism. In the WKZ, peak P-T estimates vary between 690±40 °C/4.5±1 kbar and 843±64 °C/8.1±1.6 kbar in the sillimanite-K-feldspar-zone, and between 750±30 °C/4-5.5 kbar and 811±58 °C/6.2±0.6 kbar in the garnet-cordierite-sillimanite-K-feld-

spar zone (Gruner 2000, Goscombe et al. 2003a). The variation between these distinct temperature and pressure estimates in the sillimanite-K-feldspar-zone obtained by these authors is probably due to different assumptions about the prevailing water activity a_{H_2O} during metamorphism.

Seth et al. (1998) and Franz et al. (1999) speculated about a diachronous Pan-African metamorphism at 656-645 Ma and 560-550 Ma, based on distinct U-Pb zircon and monazite ages obtained on different gneisses in the WKZ. However, both authors failed to give a clear-cut description of the textures and internal structures of zircon and monazite, together with a precise discussion of the ages and, therefore, we consider it equally possible that the older U-Pb ages represent primary crystallization ages of the igneous precursors. Therefore, the idea of distinct Pan-African metamorphic episodes is still speculative. On the other hand, Goscombe et al. (2003a) presented Sm-Nd garnet-whole rock ages obtained on metamorphic garnets from metapelitic rocks west of the VMZ and within the garnet-cordierite-sillimanite-K-feldspar zone that range from 595±13 to 573±8 Ma and these age determinations seem to be more reliable than previous age determinations.

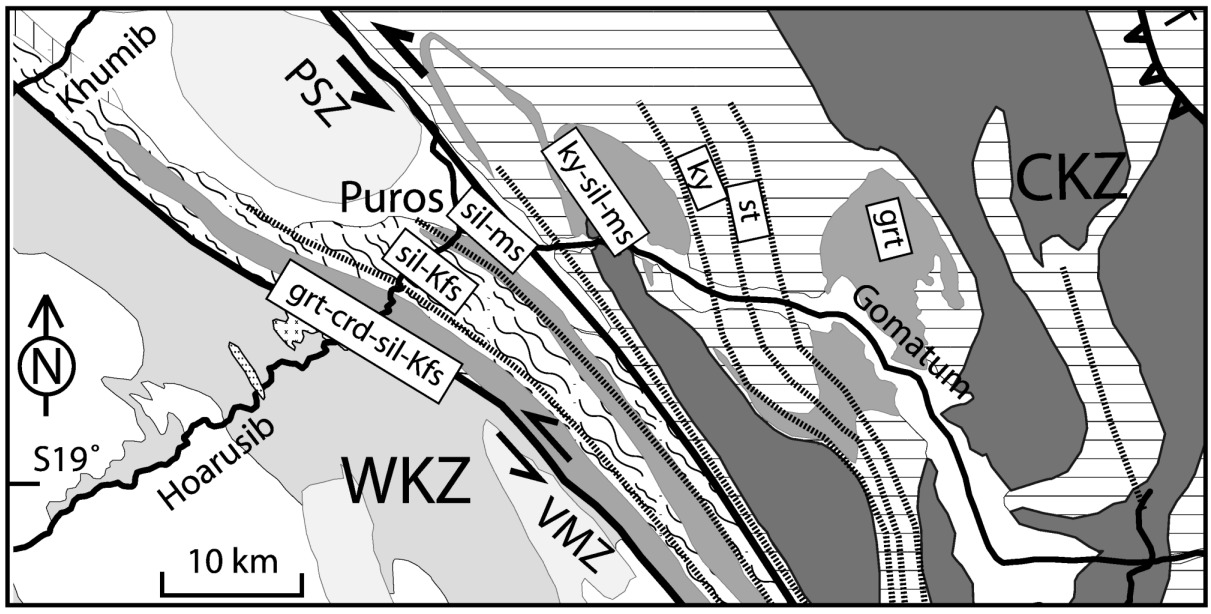

Fig. 6.3. Metamorphic isograds from Guj (1970) and Gruner (2000) in the Hoarusib and Gomatum valleys.

6.5 Data presentation

6.5.1 Petrography

The area investigated is located west of Puros village in the WKZ. Three metapelite (Na 550, Na 555 and Na 556) and two meta-igneous samples (Na 551 and Na 553) were collected in the sil-kfs-zone within a synclinal structure (Fig. 6.4). The tectonic style of this segment is strongly influenced by the two bordering mylonitic shear zones, namely the PSZ and the VMZ. The

structural history of this part of the Kaoko Belt was described in detail by Konopásek et al (2005) and by Kröner et al. (2004). Major and trace elements were determined by XRF and are presented in Table 6.2. Three samples – Na 550, Na 551 and Na 553 – were used for P-T calculations and are characterized as follows.

In general, all samples contain garnet, quartz, K-feldspar and plagioclase. Garnet is pretectonic (Fig. 6.5a) and is almost entirely composed of the almandine and pyrope component. Plagioclase is oligoclase as is typical for amphibolite-facies conditions (Spear, 1993). Decomposition features of albite in orthoclase (string- to mesoperthite) have been observed in K-feldspar containing up to 37 mol-% albite (Fig. 6.5b) which may be indicative for exsolution at high temperatures (e.g., Masberg et al., 1992). Lepidoblastic biotite as well as fibrolitic to prismatic sillimanite defines the foliation. Primary muscovite is absent in all samples.

Sample Na 550 contains a quartz-K-feldspar-biotite-garnet-plagioclase assemblage with a seriate-interlobate matrix (Moore, 1970) and a grain size of ~0.1-2 mm. The matrix is composed of quartz, K-feldspar, biotite and plagioclase. Quartz forms anhedral grains. Garnet consists almost entirely of the almandine and pyrope component (X_{Fe}=0.84; X_{Mg}=0.13) and forms porphyroblasts less than 10 mm in diameter and contains inclusions of biotite and quartz. K-feldspar forms porphyroblasts less than 4 mm, in size, is slightly brownish under plane-polarized light (PPL), and contains up to 37 mol-% of the albite component. Compared to sample Na 551 and Na 553, this sample contains more biotite (~5%) and plagioclase (~3%, $an_{13}ab_{85}$). Biotite is lepidoblastic and has a X_{Fe} between 0.53 and 0.69 (X_{Fe}= molar Fe/[Fe/Mg]).

Sample Na 551 has the same mineral assemblage as Na 550, but additionally it contains sillimanite, rutile and ilmenite. The matrix is seriate-interlobate but with a finer grain size than sample Na 550 and Na 553 (≤1 mm), and composed of quartz, K-feldspar, biotite and plagioclase. For garnet (≤6 mm), plagioclase (≤2 mm, $an_{14}ab_{82}$) and K-feldspar (≤2 mm, ab_{37}) porphyroblastic textures have been observed. Inclusions of quartz in garnet (X_{Fe}=0.80; X_{Mg}=0.12) are common. Only few biotite grains (~1%, X_{Fe}=0.61-0.74) occur.

The assemblage quartz, garnet, K-feldspar, biotite, sillimanite and plagioclase is diagnostic for sample Na 553. The matrix consists of quartz, K-feldspar, biotite, plagioclase and is inequigranular-interlobate (Moore 1970), with grain sizes ranging from ~0.1 to 1mm. Garnet (≤5mm) and K-feldspar (≤3mm) exhibit porphyroblastic textures. K-Feldspar is very clear under PPL and contains up to 37 mol-% of the albite component. Inclusions of quartz, sillimanite and biotite occur in some garnets (X_{Fe}=0.70; X_{Mg}=0.28). Plagioclase has an anorthite content of about 12 mol%. Sillimanite is prismatic suggesting high temperatures during formation (Larson and Sharp, 2001; Fig. 6.5a). There is only few biotite in this sample and the grain size of biotite is less than 0.5mm. In contrast to sample Na 550 and Na 551, biotite is greenish under PPL with X_{Fe}=0.30-

0.45. The low X_{Fe} and the greenish colour indicate that retrograde conditions overprinted the original biotite.

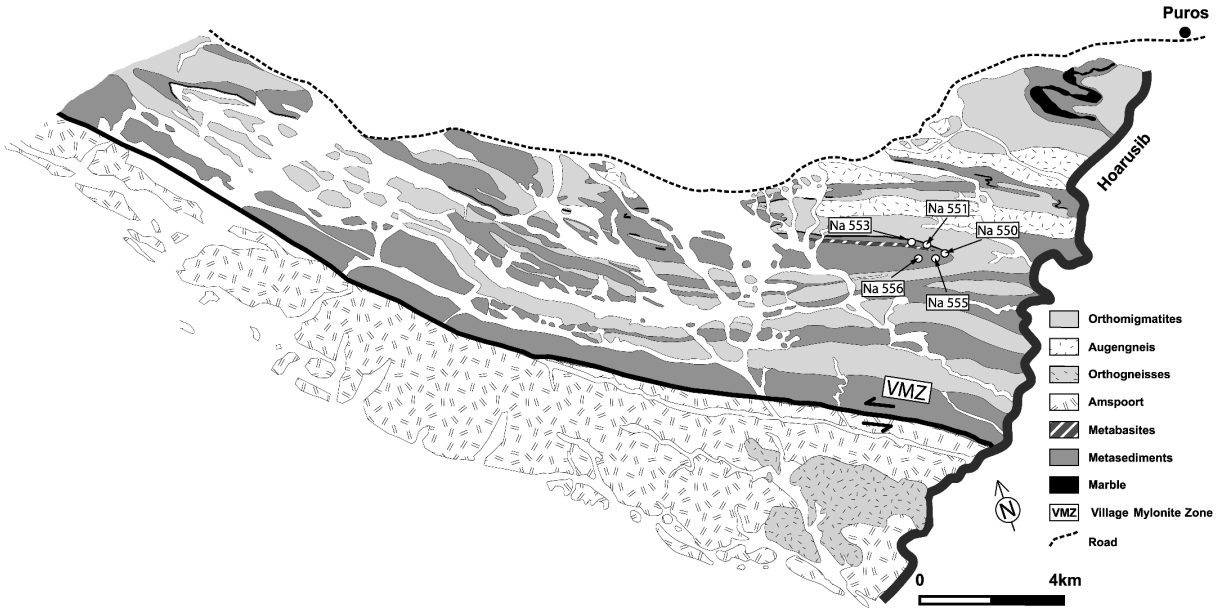

Fig. 6.4. Geological map showing major rock units and sample localities in the eastern part of the WKZ. Map modified after Konopásek et al. (2005).

6.5.2 Sm-Nd isotopic systematics of garnet

Nd concentrations range from 0.45 to 3.00 ppm, whereas Sm concentrations vary between 1.04 and 1.94 ppm. Sm-Nd garnet analyses of the larger grain fractions show higher Sm and Nd, lower $^{143}Nd/^{144}Nd$ and lower $^{147}Sm/^{143}Nd$ than the smaller grain fractions (Table 6.3). Moreover, the strongly leached garnet fractions have lower Nd concentrations but higher Sm concentrations than the less or unleached fractions. However, Nd and Sm abundances are similar within duplicate analyses. The data points are reasonably well aligned in a correlation diagram, and the Sm-Nd age calculated for a garnet-whole rock seven-point errorchron (MSWD = 6.0) in metapelite Na 553 yielded an age of 692±13 Ma (Fig. 6.6). All measurements were performed within one day (except one garnet fraction) to be sure that analytical conditions did not change during data acquisition. The garnet fraction measured three months earlier, which was not considered for age calculation, does not plot exactly on the errorchron, but confirms the above age or is even slightly older.

6.5.3 Petrographic, mineralogical and geochemical characteristics of metapelitic and meta-igneous rocks within the sillimanite-K-feldspar zone

West of the PSZ, granitoid migmatites are interlayered with pelitic rocks. The absence of primary muscovite indicates that the muscovite-breakdown reaction has occurred, implying $a_{H_2O}<1.0$ (Spear, 1993). This metamorphic zone is characterized by the appearance of K-feldspar with sillimanite which is the result of the KASH reaction

$ms+qtz \leftrightarrow kfs+Al_2SiO_5+H_2O$ [1]

(Spear, 1993) and/or by a second major reaction that produced sillimanite in Barrovian facies rocks;

$ms_{ss}+ab_{ss}+qtz \leftrightarrow kfs_{ss}+sil+H_2O$ [2]

('second sillimanite isograd', CKNASH; Spear, 1993).

Biotite is present in metapelites, and to the west, close to the Village Mylonite Zone, the KFMASH reaction $bt+sil+qtz \leftrightarrow crd+kfs+H_2O$ can be observed. Within the sil-kfs zone, garnet, biotite, plagioclase, quartz and accessory minerals (e.g. rutile, zircon and monazite) may be present, besides sillimanite and K-feldspar, in metapelitic rocks.

In samples Na 551 and Na 553, only little biotite was observed, and K-feldspar and garnet occurs besides quartz and sillimanite (Fig. 6.5c). These features can be interpreted to result from a biotite-consuming reaction

$bt+sil+pl+qtz \leftrightarrow grt+kfs+H_2O$ [3] or

$bt+sil+pl+qtz \leftrightarrow grt+kfs+melt$ [4] (Spear, 1993; Spear and Kohn, 1996).

If a small amount of H_2O was present, another possible reaction would be

$bt+sil+pl+qtz+H_2O \leftrightarrow grt+kfs+melt$ [5]

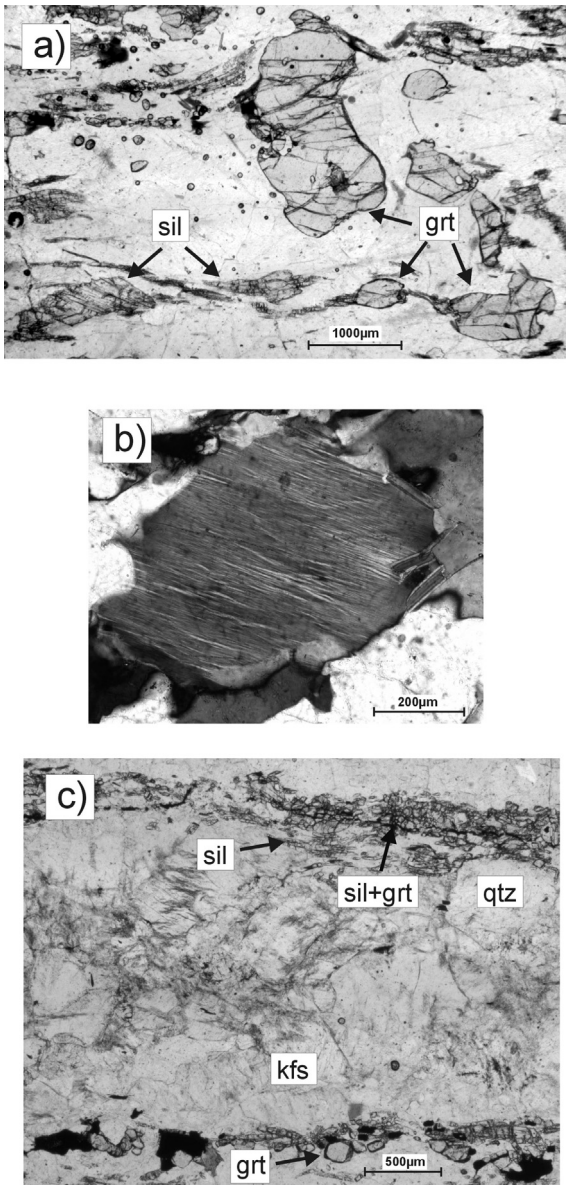

Figs. 6.5 a-c. Thin sections from Na 553 rocks in the sil-kfs zone. a) Porphyroblastic garnet and prismatic sillimanite. b) Unmixing textures of albite in ortho-clase. c) Feldspar and garnet besides quartz and sillimanite. These textural features may be the result of the biotite consuming reaction bt+sil+pl+qtz =grt+kfs+melt.

The Aluminium Saturation Index (ASI: molar $Al_2O_3/[CaO+Na_2O+K_2O]$ or molar A/CNK) ranges from 1.2 to 2.4 (Shand, 1943) and in a molar A/NK versus ASI diagram, all samples plot in the field of peraluminous rocks (Maniar and Piccoli 1989; see Table 6.2., Fig. 6.7). Garnet porphyroblasts were observed in all samples, and the size varies between 0.1 and 10 mm. Garnet is unzoned and shows flat X_{Fe}, $X_{Mg,}$ X_{Ca} and X_{Mn} elemental profiles (Figs. 6.8a-c) which are explained by progressive homogenisation attributed to intra-crystalline diffusion processes during high-grade metamorphism (e.g. Woodsworth, 1977; Yardley 1977; Anderson and Olimpio, 1977). These major element characteristics of garnet in the sil-kfs zone were also observed by Gruner (2000). Prograde zoning of garnet has been documented in all other metamorphic areas east of the PSZ (Gruner, 2000; Goscombe et al., 2003a). The change in garnet zoning across the Kaoko Belt from dominantly growth zoning (in the east) to diffusion zoning (in the west) was also recognized by Gruner (2000). This feature has often been noticed within orogenic belts with increasing metamorphic grade (e.g. Tracy et al., 1976; Woodsworth, 1977; Yardley 1977; Anderson and Olimpio, 1977, Carlson and Schwarze, 1997) and may be used as 'change in zoning pattern' isograd maps across mountain belts (Yardley, 1977). Nevertheless, major element maps and profiles show only the behaviour of major elements, whereas Rare Earth Elements (i.e., Sm and Nd) probably behave differently (Prince et al., 2000; Magloughlin and Koenig, 2002). However, little work on trace element and REE zoning in garnet has so far been undertaken (e.g., Spear and Kohn, 1999; Prince et al., 2000; Koenig et al., 2001; Magloughlin and Koenig, 2002).

6.5.4 An evaluation of pressure-temperature variation in the western Kaoko Belt

Prograde metamorphism of high-grade metamorphic rocks is usually characterized by dehydration reactions with increasing temperature and generally culminates in partial melting at higher temperatures.

From petrographic observations we suggest that partial melting in rocks of appropriate composition occurred in the study area. The muscovite-out reaction (reaction [2], Fig. 6.9a) produced sillimanite and indicates temperatures above 650 °C (IP1 in NaKFMASH, Fig. 6.9b; Spear et al. 1999). In metapelitic rocks, the decomposition of biotite and sillimanite and the appearance of garnet, cordierite, or orthopyroxene together with petrographic evidence for partial melting may be interpreted to mark the transition from amphibolite- to granulite-facies conditions. In the present study, it is suggested, that a biotite-consuming reaction [3] occurred although cordierite and orthopyroxene was not found in thin sections due to the Fe-Mg poor but Al-rich composition of the host rocks. However, cordierite appears farther west in rocks of more suitable bulk composition. The absence of cordierite indicates that the samples investigated in this study were too Al-poor to crystallize cordierite besides sillimanite or had an unsuitable

Fe/Mg ratio. The absence of orthopyroxene suggests that the temperature did not exceed 865 °C at 8.5 kbar (IP4 in NaKFMASH; Spear et al. 1999).

Peak metamorphic conditions were calculated at 710-736 °C and 5.6-7.7 kbar (Table 6.3; Fig. 6.9c) using the THERMOCALC v3.21 program (Powell and Holland, 2001) with an internally consistent dataset, assuming the water activity a_{H_2O}=0.5 which can be inferred to be typical for granulite-facies rocks. Activities of mineral endmembers have been calculated with the AX-program (Holland, 2001). These results are further confirmed by three different fluid-independent GASP geothermometers (Table 6.3). For sample Na 553, the temperature obtained by the GASP thermometer indicates re-equilibration at lower P-T conditions (578±7 °C; 3.4±1.1kbar) due to a retrograde overprint of biotite (see above). The average calculated peak temperature is in agreement with previous work by Gruner (2000) who calculated 690±40 °C, but is significantly lower than the calculated temperature of 843±64 °C determined by Goscombe et al. (2003a). Gruner (2000) calculated a thermal gradient of about 50 °C/km, indicating a Buchan-type metamorphism, whereas the Goscombe et al. (2003a) data suggest a regional metamorphic gradient more typical for orogenic thickened continental crust. The calculated retrograde P-T conditions of 578±7 °C at 3.4±1.1kbar are in agreement with the inferred retrograde conditions of 583±85 °C at 4.4±1.2kbar calculated by Goscombe et al. (2003a). Peak metamorphic conditions were exemplified in a petrographic grid with isopleths of molar Fe/(Fe+Mg) for garnet (Fig. 6.9b; Spear et al, 1999).

6.5.5 Sm-Nd garnet systematics

Previous studies from the central Damara orogen have shown that garnets from high-grade areas with homogeneous major element patterns and temperatures in excess of 700 °C yielded distinct Sm-Nd garnet whole-rock ages (Jung and Mezger, 2001, 2003a). These ages are similar or even higher than corresponding U-Pb monazite ages for the same sample. Therefore, in view of the higher T_C for U-Pb in monazite (> 850 °C) than for Sm-Nd in garnet, the Sm-Nd garnet-whole rock ages were interpreted as prograde mineral ages that date the time of high-grade metamorphism and garnet growth. These conclusions were subsequently supported by U-Pb garnet ages (Jung and Mezger, 2003b). The calculated peak temperature obtained on garnet-biotite pairs is in the range of ca. 710-740 °C, and garnets show no major element zoning (Figs. 6.8a-c). Therefore, the Sm-Nd garnet-whole rock age obtained in this study is also interpreted to approximately date the peak of regional metamorphism in the study area.

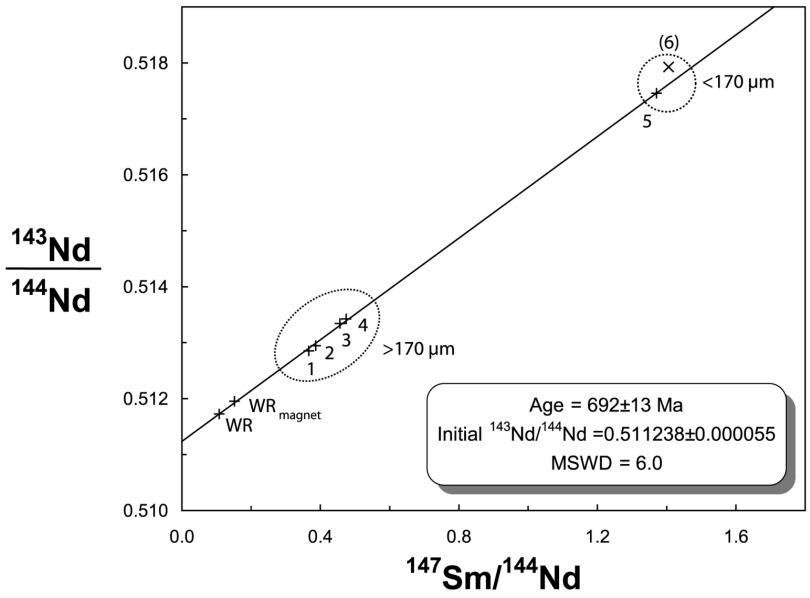

Fig. 6.6. $^{143}Nd/^{144}Nd$ vs. $^{147}Sm/^{144}Nd$ diagram of the different garnet fraction together with the whole rock of the analysed metapelite from the sil-kfs zone in the WKZ. Note: Point 6 has not been used for age calculation (see text).

Mineral separates of garnet with grain sizes <170 µm and >170 µm, consisting of unleached and leached fractions, together with the whole-rock composition have been used to construct a seven-point errorchron. The anomalously old age obtained for the garnet fractions may be caused by artificial effects associated with the leaching technique, or may be the result of undetected inclusions of various but older ages, or may be caused by partial resetting of an originally older garnet generation during Pan-African high-grade metamorphism.

Several authors have demonstrated that chemical leaching generates no fictitious Sm-Nd ages (e.g. Henson and Zhou, 1995; De Wolf et al. 1996; Jung and Mezger, 2001; Jung and Mezger, 2003a) because LREE-rich accessory minerals such as monazite, allanite and apatite are removed by chemical leaching of the garnet fractions without fractionating elements with similar chemical properties (i.e., LREE), and therefore do not disturb the Sm-Nd systematics.

Unradiogenic $^{143}Nd/^{144}Nd$ ratios, coupled with low $^{147}Sm/^{143}Nd$ but high Nd abundances could be an indication for contamination with LREE-rich inclusions that have $^{143}Nd/^{144}Nd$ ratios close to the whole-rock composition (Jung and Mezger, 2001). It has been demonstrated that µ-sized inclusions of monazite may dominate the Sm-Nd budget of garnet of the respective parent-daughter isotopes (e.g., Mezger et al., 1989; Lanzirotti and Hanson, 1995; DeWolf et al., 1996; Koenig and Magloughlin, 2000; Jung and Mezger, 2001). We confirm that in our study high Nd concentrations are coupled with low $^{143}Nd/^{144}Nd$ values and low $^{147}Sm/^{143}Nd$ ratios, therefore supporting the above idea (Fig. 6.10). The extent to which these LREE-rich inclusions perturb the calculated Sm-Nd garnet-whole rock age depends on the degree of isotopic re-equilibration of the inclusions during garnet growth.

Supposing no isotopic re-equilibration and the inclusions to be older than the garnet growth, this would lower the apparent Sm-Nd garnet-whole rock age (Prince et al., 2000). Nonetheless, it has been shown that it is impossible to obtain an isochron relationship between a whole-rock and several garnet fractions that have inclusions with variable Sm/Nd ratios (e.g. Prince et al., 2000). The most prominent effect of LREE-enriched inclusions in garnet is to significantly lower the Sm/Nd ratio, thereby increasing the relative error on the age determination. In this case, the Sm-Nd ratio represents a mixing line between pure garnet and the inclusions, however, if the inclusions are separated from the whole-rock matrix at the time of garnet growth, then the Sm-Nd isotopic systematics may also have age significance.

Therefore, the good linear arrangement shown by the garnets analysed in this study implies that the ca. 700 Ma age is robust and geologically meaningful. However, since the garnet shows no major element zonation, this age may reflect closure of the Sm-Nd isotopic system following homogenisation. Finally, it is necessary to state that the safest approach to garnet dating is to analyse multiple mineral separates. In this case, contamination by LREE-enriched accessory phases is indicated by variable Sm/Nd ratios, similar to the case study presented here. In our case, all garnet analyses yielded reproducible ages that agree within error, indicating that the inclusions must have been isolated from the whole-rock at the same time the garnets grew.

Incorporation of LREE-enriched accessory phases in the garnet may yield ages that are apparently *younger* than the "true" garnet-whole rock age (Prince et al. 2000). A special case may be the introduction of zircon into garnet, which can elevate Sm and Nd concentrations but is also capable of fractionating these two elements and, therefore, may induce apparently *older* ages upon a garnet-whole rock age. However, low concentrations of Sm and Nd in zircon would require unrealistically large amounts of zircon inclusions, which have not been observed.

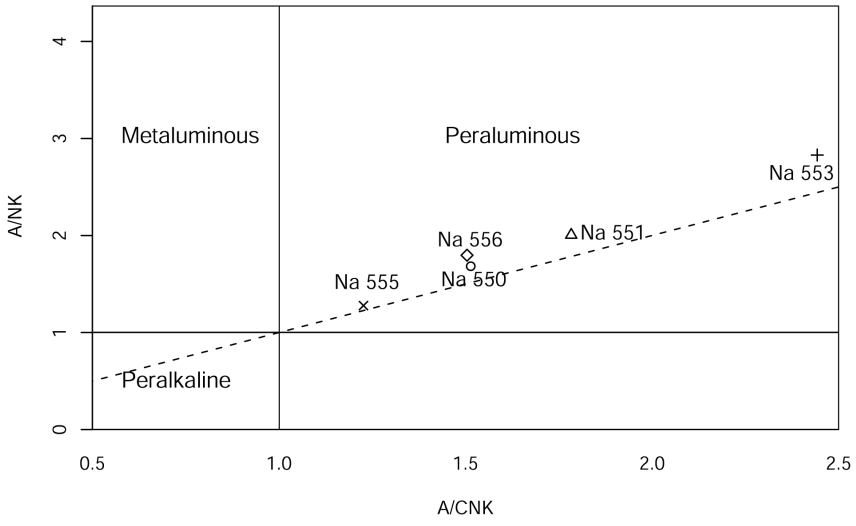

Fig. 6.7. Molar A/NK vs. A/CNK of the investigated samples after Maniar and Piccoli (1989) on the basis of Shand's index (1943).

Finally, it is possible that the anomalously old age of ca. 700 Ma is the result of partial resetting of an older (Proterozoic?) Sm-Nd garnet whole rock age during the granulite-facies event at around 550 Ma. This is theoretically possible because granulite-facies conditions at 550 Ma exceeded 800 °C (Goscombe et al., 2003), a temperature that is significantly higher than most reliable estimates of T_C for Sm-Nd in garnet. We consider the possibility of partial resetting as unlikely because (i) Proterozoic or Archaean garnet-whole rock ages have so far not been reported from the Kaoko Belt and (ii) in this case, the enclosed monazite must not only have the same (Proterozoic) age as the garnet, but it must also have at least partly re-equilibrated during the Pan African granulite-facies event at ca. 550 Ma. This speculative scenario implies that all inclusions within the garnet and the garnet itself must have equilibrated to the same extent in order to preserve the "errorchron" relationship presented in Fig. 6.6, an assumption which is highly unlikely. It is even more unlikely that multiple generations of older monazites also re-equilibrated to the same extent.

6.5.6 U-Th-Pb age dating of monazite in high-grade metamorphic rocks of the Hoarusib valley

Several studies have shown that inheritance does occur in monazite (Copeland et al. 1988; Parrish 1990; Zhu et al. 1997; Cherniak et al. 2004). Cherniak et al. (2004) suggested a blocking temperature in excess of 900 °C for a 10 μm sized monazite grain and a cooling rate of 10°C, much higher than temperatures reached in most regional metamorphic terranes. In order to constrain the age effect that inclusions of monazite may have on the Sm-Nd systematics of garnet, several monazite grains were analysed with the Electron Probe Microanalyser (EPMA). Several studies have shown that this method provides reliable ages (Suzuki et al. 1994; Montel et al. 1996; Braun et al. 1998; Finger et al. 1998; Cocherie and Albarède 2001) and, compared to other in-situ measurement like Laser Ablation ICP-MS, it is a fast and cheap alternative. The limitations of the chemical U-Th-Pb_{total} age are controlled by the detection limit and precision of the EPMA (Figs. 6.11a-c).

Between 1 and 12 analytical points per monazite grains were measured with the EPMA, and thus 277 points on 147 grains in four different metapelite samples (Fig. 6.4) have been obtained. All concentrations of Th, U and Pb are given in Table 6.1, together with the calculated individual spot-ages. The calculated Th*, U/Pb, Th/Pb and R are also presented. The expected error in the concentration of each element is directly correlated with the absolute amount of each element (Figs. 6.11a-c).

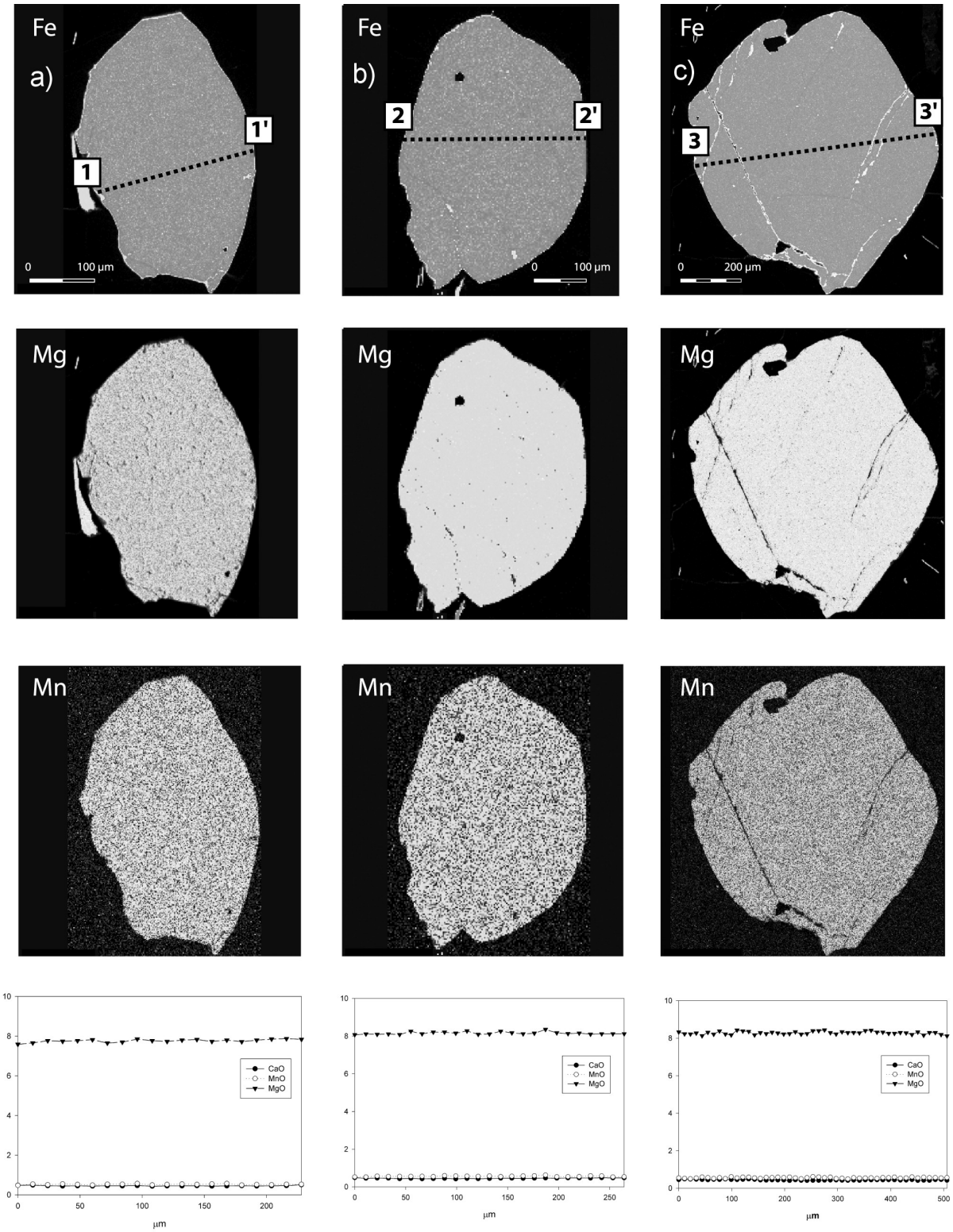

Figs. 6.8a-c. Chemical composition maps and elemental profiles (in wt%) of garnet from the sil-kfs zone in the WKZ showing homogeneous element distribution and flat elemental profiles.

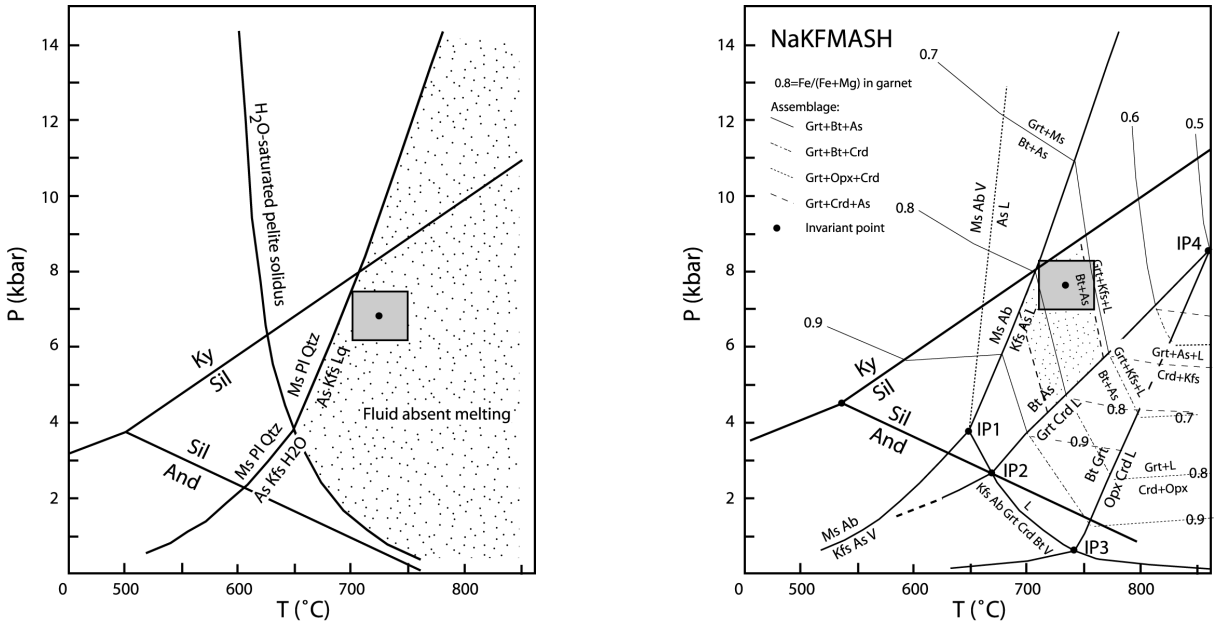

Fig. 6.9. (a) Selected melting reactions after Spear and Kohn (1996) for a metapelite containing subsolidus assemblage grt+bt+Al_2SiO_5+ms+pl+qtz. (b) Petrographic grid for the NaKFMASH system showing contours of X_{Fe} in garnet (molar Fe/[Fe+Mg]) in selected divariant assemblages after Spear et al. (1999). The dotted square indicates the calculated X_{Fe} in the analysed samples. The grey square in Figs. a and b gives the calculated peak conditions with THERMOCALC v3.21.

The results are presented using the Th/Pb versus U/Pb plot after Cocherie and Albarède (2001). Three age groups can be distinguished (Figs. 6.12a-c), and the youngest monazite grains have a mean U-Th-Pb age of 567±5 Ma (Fig. 6.12a). This age is interpreted to reflect the last Pan-African metamorphic overprint in this region and is in agreement with a U-Pb zircon age of 564±13 Ma for an anatectic granite some 60 km south of our study area (Seth et al., 1998) and with Sm-Nd garnet whole rock ages presented by Goscombe (2003a) from the WKZ that range from 595±13 to 573±8 Ma. Additionally, monazite also preserved older ages (Figs. 6.12b and 6.12c). Using the discrimination diagram after Cocherie and Albarède (2001), Mesoproterozoic ages of 1481±7 Ma and 1584±9 Ma can be recognized. A histogram and relative probability plot (Figs. 6.13a, b) illustrate that monazite grains in the different samples that experienced similar high-grade metamorphic conditions inherited distinct monazite populations. In sample Na 553, for example, monazite preserved only Mesoproterozoic ages, whereas in samples Na 555 and Na 556, monazite yielded only Pan-African ages. In contrast, sample Na 550 preserved both Meso-proterozoic and Pan-African monazite ages. This inheritance has also been observed in BSE images, where dark-coloured areas (low Th-content) are characterized by Pan-African ages (Figs. 6.14a-c). For this monazite population, it seems likely that the development of Pan-African monazite is due to recrystallisation of primary monazite of Mesoproterozoic age or reflects a new period of monazite growth during Pan-African high-grade metamorphism.

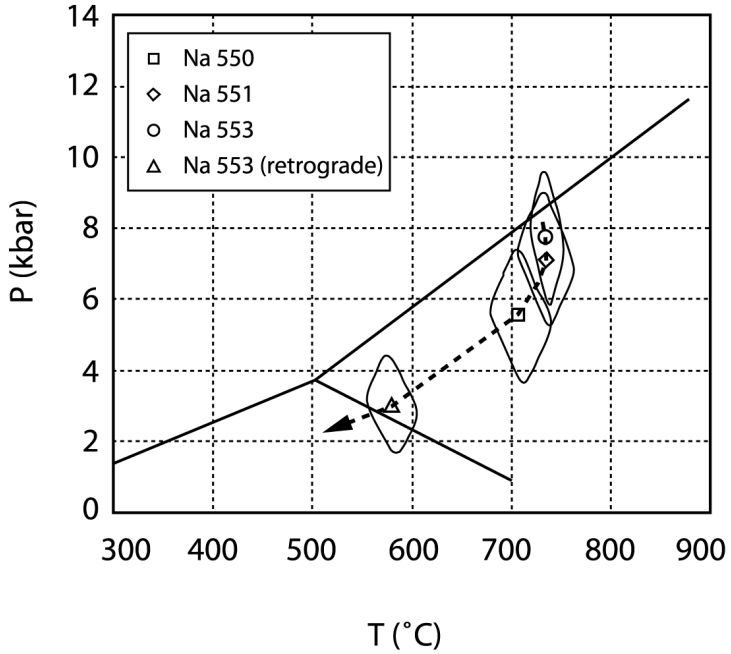

Fig. 6.9c) Calculated P-T conditions with THERMOCALC v3.21 for the investigated samples.

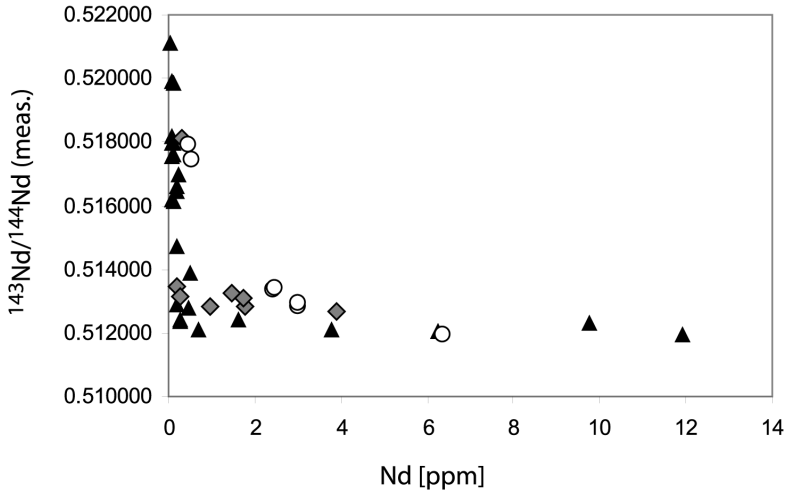

Fig. 6.10. $^{143}Nd/^{144}Nd$ vs. Nd [ppm] from the analysed garnets showing decreasing $^{143}Nd/^{144}Nd$ isotope ratios with increasing Nd concentration from this study (open circles) and the literature. Garnet data from Jung and Mezger (2003a, filled triangles) and Goscombe et al. (2003a, filled squares).

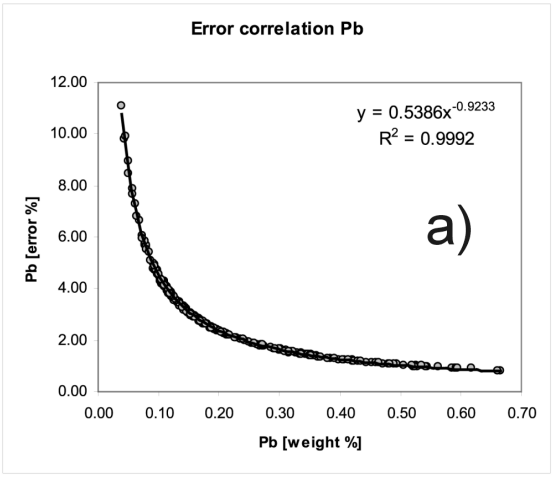

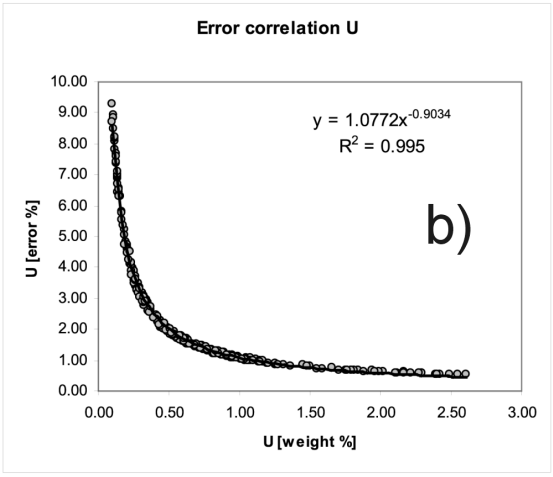

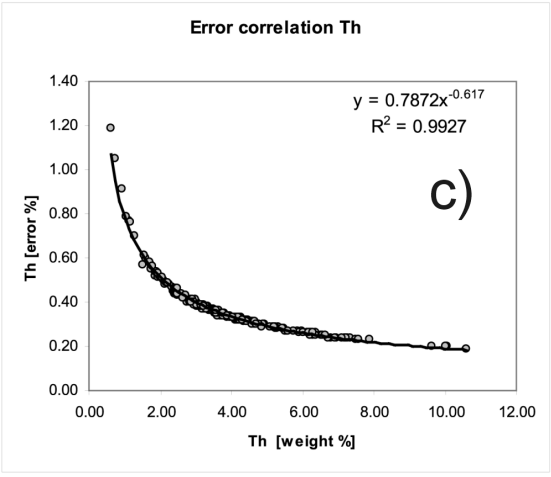

Figs. 6.11a-c. Standard deviation of Pb, U and Th vs. the amount of Pb, U and Th (in weight %) from 277 monazite analyses by EPMA. The expected error for each element is directly correlated with the absolute amount of each element.

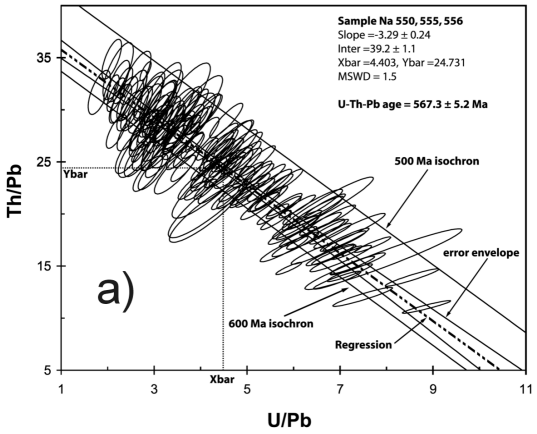

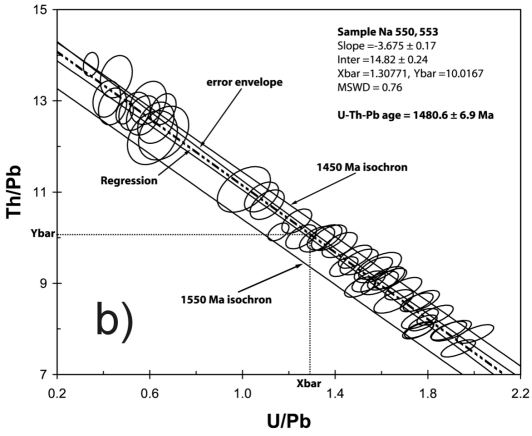

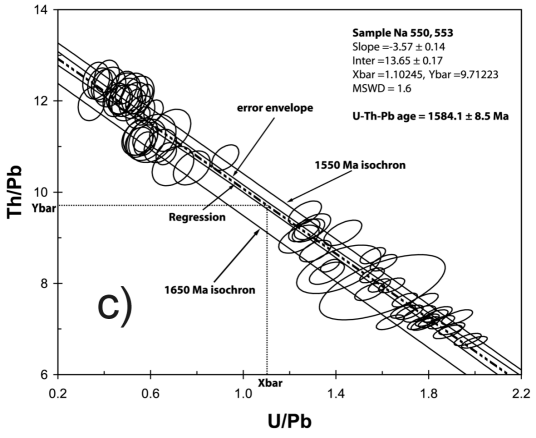

Figs. 6.12a-c. Th/Pb vs. U/Pb plot for monazite from metapelitic rocks in the Kaoko Belt after Cocherie and Albarède (2001). The best regression line (dotted line) has the same slope within the error on the calculated slope as the two theoretical isochrons at (a) 500 and 600 Ma, (b) 1450 and 1550 Ma and (c) 1550 and 1650 Ma. The Xbar and Ybar show the position of the weighted mean point. The error-envelope (fine line) corresponds to two symmetrical hyperbolas.

As stated previously, sample Na 553 which was used for Sm-Nd garnet-whole rock dating, contains only Mesoproterozoic monazite. Due to the observation that inheritance of older monazite in garnet can only cause *younger* Sm-Nd garnet whole-rock ages (Prince et al., 2000), inclusion of such monazite is not the cause for the well-constrained Sm-Nd whole rock garnet age of ca. 700 Ma. A simple mass balance calculation illustrates that for a monazite grain with dimensions of 100 μm*50 μm*50 μm, a rim age of ca. 600 Ma and an inherited core with 80 μm*30 μm*30 μm with an age of ca. 1500 Ma (i.e., sample Na 550-6, Fig. 6.14a), only 1/3 of the monazite contributes to the older age. If this applies to all monazite grains to the same extent, the corresponding "overall monazite age" is ca. 1200 Ma, again significantly older the Sm-Nd whole rock-garnet age obtained in this study.

6.6 Discussion and Conclusion

There have been speculations on the Pan-African polymetamorphic evolution of the Kaoko Belt, and these are based on distinct U-Pb zircon and monazite ages (Seth et al. 1998, Franz et al. 1999). An age of ~580-550 Ma (Seth et al., 1998) is interpreted to reflect the time of intrusion of the syntectonic precursor rocks of gneisses close to the inferred peak of high-grade metamorphism and seems consistent with a tectonic model of Coward (1983), who interpreted the Kaoko Belt as the northern extension of the Damara Belt. Metamorphic ages between ~540 and 504 Ma obtained in the high-grade central Damara orogen and in the Gariep Belt (545±2 Ma) are broadly consistent with this interpretation (Reid et al., 1991; Frimmel et al., 1996a; Jung, 2000; Jung and Mezger, 2001; Jung and Mezger, 2003a). On the other hand, an age of ~650 Ma, based on U-Pb monazite and zircon dating of a metapelitic gneiss from the WKZ close to the Atlantic Ocean (Franz et al. 1999) remains enigmatic. Moreover, reliable radiometric ages older than 560 Ma within the central Damara orogen are rare and are based on Rb-Sr whole-rock dating which is a questionable technique if applied to high-grade rocks.

Thermobarometric calculations on metapelites indicate average P-T conditions in the sillimanite-K-feldspar zone at 731±10 °C and 6.7±1.2 kbar. Our new Sm-Nd garnet age of ~690 Ma indicates that an older granulite-facies event may have occurred in the Kaoko Belt and outlasted the second high-grade event at ~580-550 Ma, which has been confirmed by EPMA dating on monazite grains. As described above, our seven-point errorchron is reasonably well constrained and is unlikely to be an artefact of leaching or some unconstrained effects caused by low Sm/Nd inclusions, resulting in isotopic disequilibrium between garnet, inclusion and whole-rock.

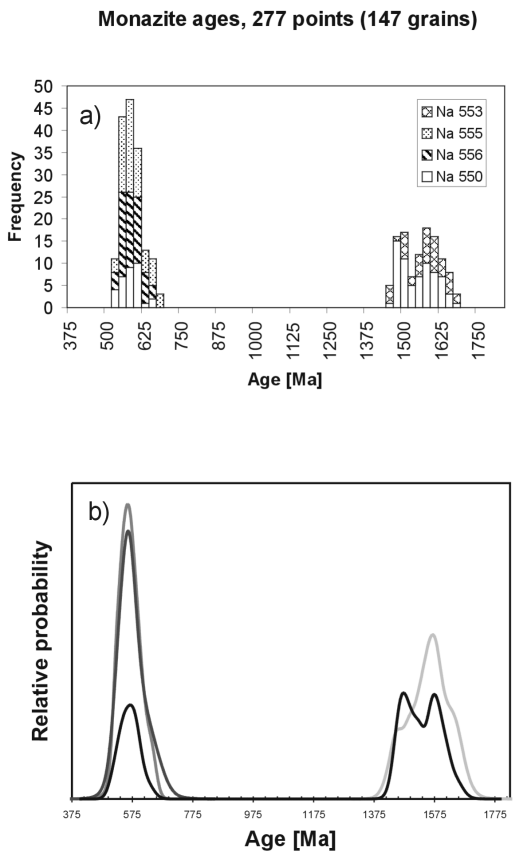

Fig. 6.13. (a) Histogram and (b) relative probability plot showing the U-Pb-Th age of the analysed monazites spots.

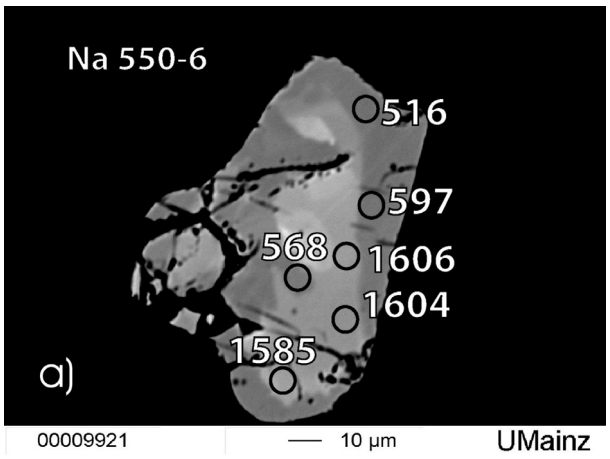

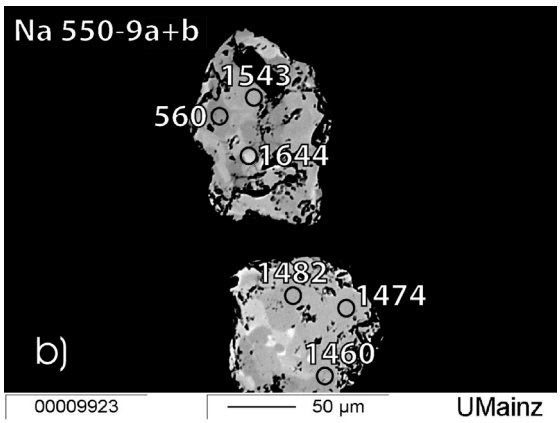

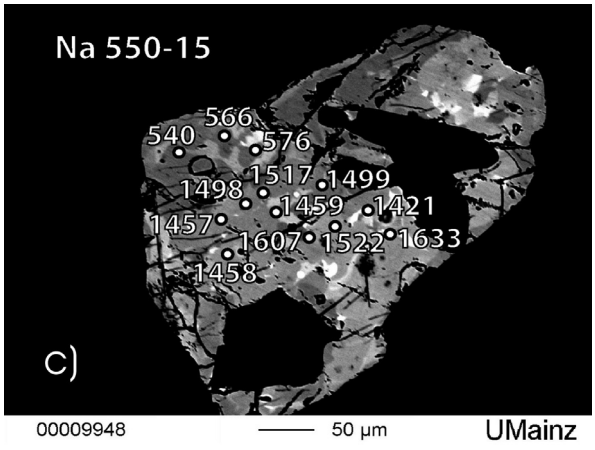

Figs. 6.14a-c. BSE images from three monazites grains from sample Na 550 showing Pan-African ages (dark areas, low Th content) and Neoproterozoic ages (bright areas, high Th content).

Franz et al. (1999) speculated on two possible scenarios for diachronous metamorphism in the Kaoko Belt, involving either extension-related metamorphism at ~650 Ma, or collision of an exotic terrane derived from the Ribeira Belt with the Congo Craton. These authors hypothesized that a granulite-facies event at ~650 Ma would have been contemporaneous with the deposition of Damaran sediments. They argued that this scenario would only be possible in an extension-related tectonic setting. So far, this tectonic setting is not supported by independent geochemical or structural data. The second possibility – derivation of a terrane from South America – is so far only supported by rare U-Pb zircon ages of 655±2 Ma and 595±12 Ma from the Ribeira belt of SE Brazil (Ebert et al., 1996). The 655 Ma age is derived from two concordant zircon fractions, but three zircon fractions show inheritance of older material (lower concordia intercept at 650-700 Ma; upper concordia intercept at 1900-2100 Ma). Ebert et al. (1996) interpreted the ~650 Ma age to be contemporaneous with ductile thrusting of basement rocks. Other authors identified the oldest Neoproterozoic metamorphic event in the Ribeira Belt to be in the range of 610-605 Ma (concordant titanite and discordant zircon analyses, Machado et al., 1996; Heilbron and Machado, 2003), which is substantially younger than our age of ~700 Ma.

Kröner et al. (2004), using conventional U-Pb and SHRIMP analyses on zircon, have shown that intrusion of granitoid melts at ~650 Ma and 580-550 Ma occurred in the WKB (e.g., Seth et al. 1998), but also at 730 Ma, 694 Ma and ~660 Ma. In fact, the zircon and monazite ages obtained by Seth et al. (1998) and Franz et al. (1999) may thus equally represent primary crystallization ages of the igneous precursors and may not reflect high-grade metamorphism. Our new results apparently argue against diachronous granulite-facies regional metamorphism within the belt. The Kaoko Belt is marked by several large crustal-scale discontinuities (e.g. Guj, 1970; Dingeldey et al. 1994; Goscombe et al, 2003b; Konopásek et al., 2005), and this favours the idea that our study area may be a part of an exotic terrane of unknown origin.

6.7 References

Anderson, D.E. and Olimpio, J.C. (1977). Progressive homogenization of metamorphic garnets, South Morar, Scotland: Evidence for volume diffusion. *Canadian Mineralogist*, **15**, 205-216.

Basei, M.A.S., Siga Jr., O., Masquelin, H., Harara, O.M., Reis Neto, J.M. and Preciozzi, P. (2000). The Dom Feliciano Belt of Brazil and Uruguay and its foreland domain, the Rio de la Plata Craton, framework, tectonic evolution and correlation with similar provinces of southwest Africa. In: U. G. Cordani, E. J. Milani, A Thomaz Filho and D A. Campos (Editors), *Tectonic Evolution of South America*, 31th International Geological Congress, Rio de Janeiro, Brazil, 311-334.

Braun, I., Montel, J.-M. and Nicollet, C. (1998). Electron microprobe dating of monazites from high-grade gneisses and pegmatites of the Kerala Khondalite Belt, southern India. Chemical *Geology*, **146**, 65-85.

Burton, K.W., Kohn, M.J., Cohen, A.S. and O'Nions, R.K. (1995). The relative diffusion of Pb, Nd, Sr and O in garnet. *Earth and Planetary Science Letters*, **133**, 199–211.

Burton, K.W. and O'Nions, R.K. (1991). High-resolution garnet chronometry and the rates of metamorphic processes. *Earth and Planetary Science Letters*, **107 (3-4)**, 649-671.

Carlson, W. and Schwarze, E. (1997). Petrological significance of prograde homogenization of growth zoning in garnet: an example from the Llano Uplift. *Journal of Metamorphic Geology*, **15**, 631-644.

Cherniak, D.J., Watson, E. B., Grove, M. and Harrison, T.M. (2004). Pb diffusion in monazite: A combined RBS/SIMS study. *Geochimica et Cosmochimica Acta*, **68**, 829-840.

Cocherie, A. and Albarède, F. (2001). An improved U-Th-Pb age evaluation for electron micro-probe dating of monazite. *Geochimica et Cosmochimica Acta*, 65 (24), 4509-4522.

Cohen, A.S., O'Nions, R.K., Siegenthaler, R., Griffin, W.L., 1988. Chronology of the pressure–temperature history recorded by a granulite terrain. *Contributions to Mineralogy and Petrology*, 98, 303–311.

Copeland, P., Parrish, R.R. and Harrison, T.M. (1988). Identification of inherited radiogenic Pb in monazite and implications for U–Pb systematics. *Nature*, **333**, 760– 763.

Coward, M.P. (1983). The tectonic history of the Damara Belt. In: Miller, R.Mc.G. (Ed.), The Damara Orogen. *Geological Society of South Africa Special Publication*, **11**, 431–515.

DeWolf, C.P., Zeissler, C.J., Halliday, A.N., Mezger, K., and Essene, E.J. (1996). The role of inclusions in U–Pb and Sm–Nd garnet geochronology: stepwise dissolution experiments and trace uranium mapping by fission track analysis. *Geochimica et Cosmochimica Acta*, **60**, 121– 134.

Dingeldey, D.P., Dürr, S.B., Charlesworth, E.G., Franz, L., Okrusch, M. and Stanistreet, I.G. (1994). A geotraverse through the northern coastal branch of the Damaran Orogen west of Sesfontein, Namibia. Namibia. *Journal of African Earth Science*, **19**, 315–329.

Dürr, S.B. and Dingeldey, D.P. (1996). The Kaoko belt (Namibia): part of a late Neoproterozoic continental-scale strike-slip system. *Geology*, **24**, 503–506.

Ebert, H.D., Chemale, Jr., G., Balinski, M., Artur, A.C. and van Schmus, W.R. (1996). Tectonic setting and U/Pb zircon dating of the plutonic Socorro Complex in the transpressive Rio Paraíba do Sul Shear Belt, SE Brazil. *Tectonics*, **15**, 688-699.

Elphick, S.C., Ganguly, J. and Loomis, L.P. (1985). Experimental determination of cation diffusivities in alumosilicate garnets: I. Experimental methods and diffusion data. *Contributions to Mineralogy and Petrology*, **90**, 36–44.

Essene, E.J. (1989). The current status of thermobarometry in metamorphic rocks. *Geological Society Special Publications*, **43**, 1-44.

Finger F., Broska I., Roberts M. P. and Schermaier A. (1998). Replacement of primary monazite by apatite-allanite-epidote coronas in amphibolite facies granite gneiss from the eastern Alps. *American Mineralogist*, **83**, 248–258.

Finger, F., Broska, I., Haunschmid, B., Hrasko, L., Kohút, M., Krenn, E. Petrík, I. Riegler, G. and Uher, P. (2003). Electron-microprobe dating of monazites from Western Carpathian basement granitoids: plutonic evidence for an important Permian rifting event subsequent to Variscan crustal anatexis. *International Journal Earth Sciences*, **92**, 86-98.

Franz, L., Romer, R.L. and Dingeldey, D.P. (1999). Diachronous Pan-African granulite-facies metamorphism (650 Ma and 550 Ma) in the Kaoko belt, NW Namibia. *European Journal of Mineralogy,* **11**, 167-180.

Frei, R. and Kamber, B.S. (1995). Single mineral Pb-Pb dating. *Earth and Planetary Science Letters*, **129 (1-4)**, 261-268.

Friedl, G. (1997). U/Pb-Datierungen an Zirkonen und Monaziten aus Gesteinen vom österreichischen Anteil der Bömischen Masse. *Unpublished PhD thesis, University of Salzburg.*

Frimmel, H.E., Hartnady, C.J.H. and Koller, F. (1996a). Geochemistry and tectonic setting of magmatic units in the Pan-African Gariep Belt, Namibia. *Chemical Geology*, **130**, 101-121.

Frimmel, H.E., Klötzli, U.S. and Siegfried, P.R. (1996b). New Pb–Pb single zircon age constraints on the timing of Neoproterozoic glaciation and continental break-up in Namibia. *The Journal of Geology*, **104**, 459–469.

Goscombe, B., Hand, M., Gray, D. and Mawby, J. (2003a). The metamorphic architecture of a transpressional orogen: the Kaoko belt, Namibia. *Journal of Petrology*, **44**, 679-711.

Goscombe, B., Hand and M. Gray, D. (2003b). Structure of the Kaoko belt, Namibia: progressive evolution of a classic transpressional orogen. Journal of Structural Geology, **25**, 1049–1081.

Grauert, B., Hänny, R. and Soptrajanova, G. (1974). Geochronology of a polymetamorphic and anatectic Gneiss Region: The Moldanubicum of the Area Lam-Deggendorf, Eastern Bavaria, Germany. *Contributions to Mineralogy and Petrology*, **45**, 37-63.

Gruner, B. (2000). Metamorphoseentwicklung im Kaokogürtel, NW-Namibia: Phasen-petrologische und geothermobarometrische Untersuchungen panafrikanischer Metapelite. *Unpublished PhD thesis*, *University of Würzburg*, Germany, 248pp.

Guj, P. (1970). The Damara mobile belt in the south-western Kaokoveld, South West Africa. Precambrian Research Unit, University of Cape Town, South Africa, Bulletin 10, 168pp.

Hensen, B.J. and Zhou, B. (1995). Retention of isotopic memory in garnets partially broken down during an overprinting granulite- facies metamorphism: implications for the Sm–Nd closure temperature. *Geology*, **23**, 225– 228.

Hoffman, P.F., Hawkins, D.P., Isachsen, C.E. and Bowring, S.A. (1996). Precise U–Pb zircon ages for early Damaran magmatism in the Summas Mountains and Welwitschia Inlier, northern Damara belt, Namibia. *Communications of the Geological Survey of Namibia*, **11**, 47–52.

Heilbron, M. and Machado, N. (2003). Timing of terrane accretion in the Neoproterozoic–Eopaleozoic Ribeira orogen (se Brazil). *Precambrian Research*, **125**, 87-112.

Holland, T. (2001). A program to calculate activities of mineral endmembers from chemical analyses. *Homepage of Tim Holland*, www.esc.cam.ac.uk/astaff/holland/

Humphries, F.J. and Cliff, R.A. (1982). Sm-Nd dating and cooling history of Scourian granulites, Sutherland. *Nature*, **295**, 515-517.

Jagoutz, E. (1988). Nd and Sr systematics in an eclogite xenolith from Tanzania: evidence for frozen mineral equilibria in continental lithosphere. *Geochimica et Cosmochimica Acta*, **52**, 1285–1293.

Jung, S. (2000). High-temperature, mid-pressure clockwise P-T paths and melting in the development of regional migmatites: The role of crustal thickening and repeated plutonism. *Geological Journal*, **35**, 345-359.

Jung, S. and Mezger, K. (2001). Geochronology in migmatites - a Sm-Nd, U-Pb and Rb-Sr study from the Proterozoic Damara belt (Namibia): implications for polyphase development of migmatites in high-grade terranes. *Journal of Metamorphic Geology*, **19**, 77-97.

Jung, S. and Mezger, K. (2003a). Petrology of basement-dominated terranes: I. Regional metamorphic T-t path from U-Pb monazite and Sm-Nd garnet geochronology (Central Damara orogen, Namibia). *Chemical Geology*, **198**, 223-247.

Jung, S. and Mezger, K. (2003b). U-Pb garnet chronometry in high-grade rocks – Case studies from the central Damara orogen (Namibia) and implications for the interpretation of Sm-Nd garnet ages and the role of high U-Th inclusions *Contributions to Mineralogy and Petrology*, **146**, 382-396.

Koenig, A.E., Magloughlin and J.F., Ridley, W.I. (2001). Quantitative trace element mapping using laser ablation ICP-MS. *Eos Transaction AGU*, **82 (47)**, Fall Meeting Supplementary, V51B-1006.

Koenig, A. E. and Magloughlin, J. F. (2000). Inclusions and chemical heterogeneities in garnet: problems, pitfalls, and potential for Sm-Nd geochronology. *Eos Transaction AGU*, **81 (48)**, Fall Meeting Supplementary, V62B-28.

Konopásek, J., Kröner, S., Kitt, S.L., Passchier, C.W., Kröner, A. (2005). Oblique collision and evolution of large-scale transcurrent shear zones in the Kaoko belt, NW Namibia. *Precambrian Research*, **136**, 139-157.

Kröner, S., Konopásek, J., Kröner, A., Poller, U., Wingate, M.W.D., Passchier, C.W. and Hofmann, K.-H. (2004). U-Pb and Pb-Pb zircon ages for metamorphic rocks in the Kaoko Belt of NW Namibia: A Palaeo- to Mesoproterozoic basement reworked during the Pan-African orogeny. *South African Journal of Geology*, **107**, 455-476.

Lanzirotti, A and Hanson, G.N. (1993). U-Pb dating of staurolite. Abstracts with Programs – *Geological Society of America*, **25 (6)**, page 35.

Lanzirotti, A and Hanson, G.N. (1995). U-Pb dating of major and accessory minerals formed during metamorphism and deformation of metapelites. *Geochimica et Cosmochimica Acta*, **59 (12)**, 2513-2526.

Larson, T. E. and Sharp, Z. D. (2001). Aluminium silicate polymorph transformations and the significance of fibrolite verses prismatic sillimanite. A study from the 'triple-point isobar', New Hampshire. Abstracts with Programs – *Geological Society of America*, **33 (6)**, page 18.

Machado, N., Valladares, C., Heilbron, M. and Valeriano, C. (1996). U-Pb geochronolohy of the central Ribeira belt (Brazil) and implications for the evolution of the Brazilian Orogeny. *Precambrian Research*, **79**, 347-361.

Magloughlin, J.F. and Koenig, A.E. (2002). REE systematics in metamorphic garnet: insights from LA-ICP-MS. Goldschmidt Conference, Davos, Switzerland. *Geochimica et Cosmochimica Acta*, **66 (15A)**, 474.

Maniar, P.D. and Piccoli, P.M. (1989). Tectonic discrimination of granitoids. *Bulletin of the American Geological Society*, **101**, 635 – 643.

Masberg, H.P., Hoffer, E. and Hoernes, S. (1992). Microfabrics indicating granulite-facies metamorphism in the low-pressure central Damara Orogen, Namibia. *Precambrian Research*, **55**, 243-257.

Mezger K., Hanson G. N. and Bohlen S. R. (1989). U-Pb systematics of garnet: Dating the growth of garnet in the Late Archaean Pikwitonei granulite domain at Cauchon and Natawahunan lakes, Manitoba, Canada. *Contributions to Mineralogy and Petrology*, **101**, 136–148.

Mezger, K. Essene, E.J. and Halliday, A.N. (1992). Closure temperature of the Sm-Nd system in metamorphic garnets. *Earth and Planetary Science Letters*, **113**, 397-409.

Miller, R.McG. (1979). The Okahandja Lineament, a fundamental tectonic boundary in the Damara Orogen of South West Africa/Namibia. Trans. *Geological Society of South Africa*, **82**, 349-361.

Miller, R.Mc.G. (1983). The Pan-African Damara Orogen of South West Africa/Namibia. In: Miller, R.Mc.G. (Ed.), The Damara Orogen. *Geological Society of South Africa Special Publication*, **11**, 431–515.

Montel, J-M., Foret, S., Veschambre, M., Nicollet, C. and Provost, A (1996). Electron microprobe dating of monazite. *Chemical Geology*, **131**, 37-53.

Moore, A.C. (1970). Descriptive terminology for the textures of rocks in granulite facies terrain. *Lithos*, **3**, 123-127.

Parrish, R.R. (1990). U-Pb dating of monazite and its application to geological problems. *Canadian Journal of Earth Sciences*, **27**, 1431-1450.

Patchett, P.J. and Ruiz, J. (1987). Nd isotopic ages of crust formation and metamorphism in the Precambrian of eastern and southern Mexico. *Contributions to Mineralogy and Petrology*, **96**, 523–528.

Porada, H. (1989). Pan-African rifting and orogenesis in southern to equatorial Africa and Eastern Brazil. *Precambrian Research*, **44**, 103–136.

Powell, R. and Holland, T. (2001). Course Notes for "THERMOCALC Workshop 2001: Calculating Metamorphic Phase Equilibria". *Homepage of Roger Powell*, ftp://www.esc.cam.ac.uk/pub/minp/thermocalc/

Prince, C.I., Kosler, J., Vance, D. and Günther, D. (2000). Comparison of laser ablation ICP-MS and isotope dilution REE analyses — implications for Sm–Nd garnet geochronology. *Chemical Geology*, **168**, 255–274.

Reid, D.L., Ransome, I.G.D., Onstott, T.C. and Adams, C.J. (1991). Time of emplacement and metamorphism of Late Precambrian mafic dykes associated with the Pan-African Gariep orogeny, Southern Africa: implications for the age of the Nama Group. *Journal of African Earth Science*, **13**, 531-541.

Scherrer, N. C., Engi, M., Gnos, E., Jakob, V. and Liechti, A. (2000). Monazite analysis, from sample preparation to microprobe age dating and REE quantification. *Schweizerische Mineralogische und Petrologische Mitteilungen*, **80**, 93-105.

Seth, B., Kröner, A., Mezger, K., Nemchin, A.A., Pidgeon, R.T. and Okrusch, M. (1998). Archaean to Neoproterozoic magmatic events in the Kaoko belt of NW Namibia and their geodynamic significance. *Precambrian Research*, **92**, 341–363.

Shand, S. J. (1943). The Eruptive Rocks, 2nd edition. New York: John Wiley, 444 pp.

Spear, F.S. (1993). Metamorphic phase equilibria and pressure-temperature-time paths. *Mineralogical Society of America*, Washington DC, 799pp.

Spear, F.S. and Kohn, J.M. (1996). Trace element zoning in garnet as a monitor of crustal melting. *Geology*, **24**, 1099-1102.

Spear, F.S., Kohn, J.M. and Cheney, J.T. (1999). P-T paths from anatectic pelites. *Contributions to Mineralogy and Petrology*, **134**, 17-32.

Suzuki, K., Adachi, M. and Kajizuka, I. (1994). Electron microprobe observations of Pb diffusion in metamorphosed detrital monazites. *Earth and Planetary Science Letters*, **128**, 391-405.

Tracy, R. J., Robinson, P. and Thompson, A. B. (1976). Garnet composition and zoning in the determination of temperature and pressure of metamorphism, central Massachusetts. *American Mineralogist*, **61**, 762-775.

Vance, D. and O'Nions, R.K. (1990). Isotopic chronometry of zoned garnets: growth kinetics and metamorphic histories. *Earth and Planetary Science Letters*, **97 (3-4)**, 227-240.

Vance, D. and O'Nions, R. K. (1992). Prograde and retrograde thermal histories from the Central Swiss Alps. *Earth and Planetary Science Letters*, **114**, 113-129.

Woodsworth, G. J. (1977). Homogenization of zoned garnets from pelitic schists. *Canadian Mineralogist*, **15**, 230-242.

Yardley, B. W. D. (1977). An empirical study of diffusion in garnet. *American Mineralogist*, **62**, 793-800.

Zhou, B. and Hensen, B.J. (1995). Inherited Sm/Nd isotope components preserved in monazite inclusions within garnets in leucogneiss from East Antarctica and implications for closure temperature studies. *Chemical Geology*, **121**, 317–326.

6.8 Appendix

Table 6.1. Analytical data for monazite grains from metapelitic and meta-igneous rocks[1]
Sample Na 550

Pkt	Age [Ma]	± [Ma]	Th*	Th	error absolut	U	error absolut	Pb	error absolut	U/Pb	error absolut	Th/Pb	error absolut	R
8	570	21	4.854	2.730	0.012	0.6411	0.0105	0.1240	0.0046	5.17	0.28	22.02	0.91	0.909
12	517	16	6.548	4.610	0.014	0.5876	0.0104	0.1516	0.0047	3.88	0.19	30.41	1.03	0.862
16	539	15	6.972	3.830	0.013	0.9506	0.0111	0.1684	0.0047	5.64	0.22	22.74	0.71	0.915
11p1	586	19	5.155	3.850	0.013	0.3933	0.0092	0.1357	0.0045	2.90	0.16	28.37	1.04	0.813
12p2	545	18	5.553	3.500	0.013	0.6210	0.0097	0.1356	0.0045	4.58	0.23	25.81	0.96	0.900
12p7	524	18	5.593	3.450	0.012	0.6492	0.0099	0.1312	0.0046	4.95	0.25	26.30	1.01	0.911
13p2	632	20	5.006	3.210	0.013	0.5394	0.0095	0.1420	0.0045	3.80	0.19	22.61	0.81	0.867
13p3	566	19	5.241	3.620	0.013	0.4894	0.0094	0.1330	0.0045	3.68	0.20	27.22	1.03	0.866
13p5	577	20	4.854	3.010	0.012	0.5564	0.0095	0.1256	0.0045	4.43	0.23	23.96	0.95	0.899
14p10	582	16	6.075	3.160	0.012	0.8790	0.0100	0.1583	0.0046	5.55	0.22	19.96	0.65	0.922
14p12	626	21	4.631	3.340	0.012	0.3878	0.0091	0.1303	0.0045	2.98	0.17	25.63	0.98	0.823
14p3	592	24	4.177	2.640	0.011	0.4631	0.0094	0.1110	0.0045	4.17	0.25	23.78	1.06	0.890
14p4	603	24	4.051	2.470	0.011	0.4760	0.0093	0.1096	0.0045	4.34	0.26	22.54	1.02	0.897
14p6	571	20	4.943	3.040	0.012	0.5745	0.0095	0.1265	0.0045	4.54	0.24	24.03	0.95	0.901
14p7	595	20	5.010	3.190	0.012	0.5484	0.0095	0.1338	0.0046	4.10	0.21	23.84	0.90	0.886
15p14	576	17	5.783	3.630	0.013	0.6497	0.0097	0.1495	0.0045	4.35	0.20	24.28	0.82	0.891
15p15	540	18	5.615	3.610	0.013	0.6066	0.0097	0.1358	0.0045	4.47	0.22	26.58	0.98	0.897
15p16	566	20	4.999	3.530	0.012	0.4437	0.0094	0.1269	0.0045	3.50	0.20	27.82	1.09	0.855
1p-1-2	594	18	5.726	4.160	0.014	0.4718	0.0102	0.1528	0.0047	3.09	0.16	27.23	0.92	0.811
3p1	558	20	4.941	3.170	0.012	0.5350	0.0097	0.1235	0.0045	4.33	0.24	25.67	1.03	0.891
4p4	537	16	6.290	3.560	0.012	0.8262	0.0101	0.1512	0.0046	5.46	0.23	23.54	0.80	0.922
5p1	578	17	5.953	4.190	0.013	0.5318	0.0094	0.1543	0.0046	3.45	0.16	27.15	0.89	0.853
5p-1-1	546	18	5.742	3.710	0.013	0.6146	0.0105	0.1405	0.0046	4.37	0.22	26.41	0.96	0.883
5p2	590	14	7.006	3.990	0.013	0.9090	0.0101	0.1855	0.0046	4.90	0.18	21.51	0.61	0.905
6p-1-1	534	19	5.457	3.540	0.013	0.5804	0.0104	0.1307	0.0046	4.44	0.24	27.08	1.06	0.887
6p-1-2	553	18	5.601	3.580	0.013	0.6108	0.0104	0.1389	0.0046	4.40	0.22	25.77	0.95	0.885
6p-1-3	508	17	5.905	3.890	0.013	0.6113	0.0105	0.1344	0.0046	4.55	0.23	28.94	1.10	0.892
6p-1-4	540	18	5.592	3.910	0.013	0.5089	0.0103	0.1355	0.0046	3.76	0.20	28.86	1.08	0.856
6p2	516	18	5.529	3.790	0.013	0.5271	0.0096	0.1278	0.0046	4.12	0.22	29.66	1.17	0.887
6p3	597	18	5.498	3.770	0.013	0.5204	0.0097	0.1474	0.0046	3.53	0.18	25.58	0.88	0.854
6p5	568	19	5.443	4.000	0.013	0.4357	0.0094	0.1387	0.0046	3.14	0.17	28.84	1.04	0.832
7p4	562	17	6.058	3.140	0.012	0.8815	0.0110	0.1524	0.0046	5.78	0.25	20.60	0.71	0.918
9ap5	560	16	6.132	3.320	0.012	0.8494	0.0101	0.1539	0.0046	5.52	0.23	21.57	0.72	0.921
2	1461	22	5.119	3.430	0.013	0.4711	0.0103	0.3430	0.0050	1.37	0.05	10.00	0.18	0.542
4	1481	23	4.946	3.350	0.012	0.4443	0.0102	0.3361	0.0050	1.32	0.05	9.97	0.19	0.529
12p1	1473	20	5.425	3.800	0.013	0.4526	0.0095	0.3667	0.0050	1.23	0.04	10.36	0.18	0.524
12p4	1467	23	4.630	2.950	0.012	0.4684	0.0096	0.3116	0.0049	1.50	0.05	9.47	0.19	0.588
12p5	1462	22	4.994	3.050	0.012	0.5423	0.0097	0.3348	0.0049	1.62	0.05	9.11	0.17	0.611
12p6	1480	23	4.823	2.950	0.012	0.5213	0.0096	0.3275	0.0049	1.59	0.05	9.01	0.17	0.606
12p9	1462	21	5.337	3.430	0.012	0.5319	0.0097	0.3579	0.0049	1.49	0.05	9.58	0.17	0.585
13p13	1501	19	5.793	3.020	0.012	0.7702	0.0099	0.3988	0.0050	1.93	0.05	7.57	0.12	0.667
13p6	1498	24	4.515	2.670	0.011	0.5128	0.0094	0.3104	0.0048	1.65	0.06	8.60	0.17	0.622
14p-1-1	1466	22	5.125	3.450	0.013	0.4670	0.0102	0.3448	0.0050	1.35	0.05	10.01	0.18	0.535
14p-1-2	1467	18	6.271	3.620	0.013	0.7389	0.0107	0.4218	0.0051	1.75	0.05	8.58	0.14	0.617
15p10	1517	20	5.522	3.430	0.012	0.5802	0.0097	0.3846	0.0050	1.51	0.04	8.92	0.15	0.587
15p11	1459	21	5.202	3.090	0.012	0.5893	0.0098	0.3479	0.0050	1.69	0.05	8.88	0.16	0.627
15p13	1499	21	5.177	3.570	0.012	0.4465	0.0095	0.3563	0.0049	1.25	0.04	10.02	0.17	0.529
15p3	1522	16	7.452	5.280	0.015	0.6022	0.0097	0.5214	0.0052	1.15	0.03	10.13	0.13	0.504

15p6	1458	20	5.402	3.110	0.012	0.6396	0.0098	0.3610	0.0049	1.77	0.05	8.61	0.15	0.643
15p8	1457	20	5.456	3.400	0.012	0.5737	0.0097	0.3644	0.0050	1.57	0.05	9.33	0.16	0.606
15p9	1498	18	6.132	3.950	0.013	0.6063	0.0098	0.4218	0.0050	1.44	0.04	9.36	0.14	0.573
1p-1-3	1493	20	5.618	3.480	0.013	0.5945	0.0104	0.3849	0.0050	1.54	0.05	9.04	0.15	0.577
1p4	1522	18	6.052	3.370	0.012	0.7436	0.0099	0.4229	0.0050	1.76	0.04	7.97	0.12	0.638
2p1	1452	28	3.825	2.380	0.011	0.4035	0.0095	0.2547	0.0048	1.58	0.07	9.34	0.22	0.607
2p10	1467	20	5.464	3.050	0.012	0.6728	0.0099	0.3674	0.0049	1.83	0.05	8.30	0.14	0.647
2p2	1475	22	4.979	2.680	0.011	0.6402	0.0099	0.3367	0.0049	1.90	0.06	7.96	0.15	0.658
2p8	1500	16	6.970	3.900	0.013	0.8530	0.0102	0.4796	0.0051	1.78	0.04	8.13	0.11	0.639
3p2	1449	19	5.729	3.000	0.012	0.7621	0.0101	0.3803	0.0050	2.00	0.05	7.89	0.13	0.675
3p5	1521	17	6.739	3.750	0.013	0.8287	0.0101	0.4704	0.0051	1.76	0.04	7.97	0.11	0.636
3p7	1479	20	5.595	3.020	0.012	0.7170	0.0100	0.3794	0.0050	1.89	0.05	7.96	0.14	0.657
4p7	1496	21	5.176	2.920	0.012	0.6270	0.0099	0.3551	0.0049	1.77	0.05	8.22	0.15	0.635
4p8	1457	19	5.856	3.560	0.012	0.6407	0.0099	0.3911	0.0050	1.64	0.05	9.10	0.15	0.613
9bp1	1482	25	4.427	3.230	0.012	0.3333	0.0093	0.3012	0.0048	1.11	0.05	10.72	0.21	0.488
9bp2	1474	25	4.422	3.260	0.012	0.3238	0.0093	0.2993	0.0048	1.08	0.05	10.89	0.22	0.477
9bp3	1460	22	4.916	3.240	0.012	0.4674	0.0095	0.3293	0.0049	1.42	0.05	9.84	0.18	0.570
10p1	1534	17	6.418	3.280	0.012	0.8689	0.0103	0.4520	0.0051	1.92	0.04	7.26	0.11	0.654
10p2	1549	17	6.772	3.670	0.013	0.8576	0.0102	0.4818	0.0052	1.78	0.04	7.62	0.11	0.635
10p3	1581	17	6.728	3.390	0.012	0.9198	0.0103	0.4887	0.0051	1.88	0.04	6.94	0.10	0.647
11p2	1654	19	6.023	3.280	0.012	0.7501	0.0099	0.4589	0.0051	1.63	0.04	7.15	0.11	0.611
13p10	1616	20	5.489	3.190	0.012	0.6311	0.0097	0.4083	0.0050	1.55	0.04	7.81	0.12	0.597
13p11	1559	26	4.164	2.760	0.011	0.3878	0.0092	0.2986	0.0048	1.30	0.05	9.24	0.19	0.543
13p12	1559	18	6.201	3.250	0.012	0.8149	0.0099	0.4439	0.0051	1.84	0.04	7.32	0.11	0.648
13p8	1526	25	4.292	2.740	0.011	0.4301	0.0093	0.3009	0.0049	1.43	0.05	9.11	0.18	0.583
13p9	1645	26	4.172	2.600	0.011	0.4303	0.0092	0.3162	0.0048	1.36	0.05	8.22	0.16	0.557
14p1	1585	20	5.541	2.960	0.012	0.7110	0.0098	0.4038	0.0050	1.76	0.05	7.33	0.12	0.634
14p2	1611	30	3.548	2.360	0.011	0.3263	0.0092	0.2631	0.0048	1.24	0.06	8.97	0.20	0.524
15p1	1633	20	5.719	4.670	0.014	0.2875	0.0092	0.4307	0.0050	0.67	0.03	10.84	0.16	0.334
15p4	1607	16	7.349	4.010	0.013	0.9176	0.0103	0.5432	0.0052	1.69	0.04	7.38	0.10	0.615
1p1	1528	17	6.861	4.070	0.013	0.7731	0.0100	0.4815	0.0052	1.61	0.04	8.45	0.12	0.610
1p10	1598	17	6.559	3.550	0.012	0.8276	0.0099	0.4819	0.0051	1.72	0.04	7.37	0.10	0.629
1p2	1581	23	4.846	3.230	0.012	0.4454	0.0094	0.3526	0.0049	1.26	0.04	9.16	0.16	0.532
1p3	1541	23	4.721	3.190	0.012	0.4236	0.0094	0.3344	0.0049	1.27	0.05	9.54	0.18	0.532
1p5	1611	23	4.706	3.040	0.012	0.4577	0.0092	0.3491	0.0049	1.31	0.04	8.71	0.16	0.549
1p6	1574	24	4.657	3.090	0.012	0.4322	0.0093	0.3373	0.0049	1.28	0.05	9.16	0.17	0.541
2p3	1587	15	8.099	4.250	0.014	1.0600	0.0105	0.5908	0.0053	1.79	0.03	7.19	0.09	0.634
2p5	1589	13	9.118	4.760	0.014	1.2000	0.0107	0.6659	0.0054	1.80	0.03	7.15	0.08	0.631
2p6	1578	16	7.298	4.040	0.013	0.8980	0.0102	0.5292	0.0052	1.70	0.04	7.63	0.10	0.618
2p7	1574	16	7.233	4.280	0.014	0.8143	0.0102	0.5234	0.0052	1.56	0.03	8.18	0.11	0.591
3p3	1621	14	8.847	5.540	0.015	0.9075	0.0103	0.6604	0.0054	1.37	0.03	8.39	0.09	0.558
3p4	1565	15	7.832	4.100	0.013	1.0300	0.0105	0.5631	0.0053	1.83	0.04	7.28	0.09	0.642
4p1	1566	15	7.557	3.680	0.013	1.0700	0.0106	0.5436	0.0052	1.97	0.04	6.77	0.09	0.654
4p10	1570	16	7.217	3.720	0.013	0.9647	0.0103	0.5204	0.0052	1.85	0.04	7.15	0.10	0.646
4p2	1562	14	8.168	3.930	0.013	1.1700	0.0108	0.5858	0.0053	2.00	0.04	6.71	0.08	0.659
4p6	1530	16	7.194	4.350	0.014	0.7879	0.0102	0.5054	0.0052	1.56	0.04	8.61	0.12	0.596
5p-1-2	1567	15	8.189	4.130	0.014	1.1200	0.0114	0.5894	0.0054	1.90	0.04	7.01	0.09	0.630
6p4	1606	16	7.334	3.860	0.013	0.9547	0.0103	0.5415	0.0052	1.76	0.04	7.13	0.09	0.626
6p6	1604	15	7.943	4.160	0.013	1.0400	0.0104	0.5857	0.0053	1.78	0.03	7.10	0.09	0.630
6p7	1585	15	8.140	4.720	0.014	0.9419	0.0103	0.5934	0.0053	1.59	0.03	7.95	0.10	0.604
7p1	1565	16	7.442	4.260	0.014	0.8782	0.0111	0.5354	0.0054	1.64	0.04	7.96	0.11	0.590
9ap1	1543	22	5.044	3.850	0.013	0.3302	0.0092	0.3579	0.0049	0.92	0.04	10.76	0.18	0.429
9ap4	1644	33	3.357	2.850	0.011	0.1388	0.0090	0.2547	0.0048	0.54	0.05	11.19	0.25	0.272

Sample Na 553

Pkt	Age [Ma]	± [Ma]	Th*	Th	error absolut	U	error absolut	Pb	error absolut	U/Pb	error absolut	Th/Pb	error absolut	R
28p2	1447	15	7.901	7.250	0.017	0.1817	0.0095	0.5253	0.0053	0.35	0.02	13.80	0.17	0.183
35p3	1436	22	5.267	4.450	0.014	0.2285	0.0094	0.3472	0.0050	0.66	0.04	12.82	0.22	0.324
38p1	1496	27	4.223	3.790	0.013	0.1204	0.0094	0.2906	0.0049	0.41	0.04	13.04	0.26	0.206
39p1	1444	31	3.561	3.060	0.012	0.1401	0.0094	0.2362	0.0048	0.59	0.05	12.96	0.31	0.284
42p1	1481	28	3.934	3.420	0.013	0.1431	0.0094	0.2678	0.0048	0.53	0.04	12.77	0.28	0.258
43p2	1498	17	7.186	6.310	0.016	0.2433	0.0097	0.4950	0.0052	0.49	0.02	12.75	0.17	0.251
49p3	1503	27	4.121	3.670	0.013	0.1253	0.0093	0.2850	0.0049	0.44	0.04	12.88	0.27	0.221
49p4	1436	29	3.865	3.450	0.012	0.1161	0.0094	0.2550	0.0048	0.46	0.05	13.53	0.31	0.224
49p6	1473	31	3.586	3.040	0.012	0.1520	0.0095	0.2428	0.0048	0.63	0.05	12.52	0.30	0.295
50p2	1477	29	3.776	3.250	0.012	0.1465	0.0094	0.2563	0.0048	0.57	0.05	12.68	0.29	0.273
52p1	1484	38	2.773	2.090	0.010	0.1901	0.0096	0.1890	0.0047	1.01	0.08	11.06	0.33	0.433
53p1	1510	43	2.456	2.080	0.010	0.1043	0.0093	0.1706	0.0046	0.61	0.07	12.19	0.39	0.283
53p2	1484	42	2.565	2.150	0.011	0.1154	0.0094	0.1749	0.0047	0.66	0.07	12.29	0.39	0.306
26	1587	28	4.127	3.630	0.013	0.1369	0.0094	0.3020	0.0050	0.45	0.04	12.02	0.24	0.226
23p2	1623	33	3.427	2.700	0.012	0.1994	0.0096	0.2564	0.0049	0.78	0.05	10.53	0.25	0.358
24p1	1624	31	3.637	3.000	0.012	0.1748	0.0094	0.2724	0.0049	0.64	0.05	11.01	0.24	0.309
24p2	1581	24	4.830	4.230	0.014	0.1653	0.0096	0.3519	0.0051	0.47	0.03	12.02	0.21	0.234
31p1	1646	22	5.450	4.580	0.014	0.2382	0.0096	0.4141	0.0051	0.58	0.03	11.06	0.17	0.284
34p2	1568	33	3.465	3.080	0.012	0.1061	0.0094	0.2503	0.0049	0.42	0.05	12.31	0.29	0.210
34p3	1634	39	2.857	2.400	0.011	0.1251	0.0092	0.2153	0.0048	0.58	0.06	11.15	0.30	0.282
34p4	1576	30	3.730	3.240	0.012	0.1352	0.0094	0.2709	0.0049	0.50	0.04	11.96	0.26	0.247
34p5	1566	32	3.569	3.110	0.012	0.1267	0.0094	0.2575	0.0049	0.49	0.05	12.08	0.28	0.244
34p6	1569	37	2.961	2.430	0.011	0.1465	0.0093	0.2140	0.0048	0.68	0.06	11.36	0.30	0.324
35p1	1636	35	3.225	2.730	0.011	0.1356	0.0094	0.2434	0.0048	0.56	0.05	11.22	0.27	0.268
35p2	1576	28	4.124	3.520	0.013	0.1664	0.0096	0.2994	0.0049	0.56	0.04	11.76	0.24	0.269
35p4	1559	20	6.064	5.220	0.015	0.2332	0.0096	0.4354	0.0052	0.54	0.03	11.99	0.18	0.269
35p6	1585	79	1.276	0.736	0.008	0.1488	0.0093	0.0930	0.0046	1.60	0.18	7.92	0.47	0.602
35p8	1652	39	2.817	2.270	0.011	0.1496	0.0094	0.2147	0.0047	0.70	0.06	10.57	0.28	0.323
36p5	1619	45	2.420	2.020	0.010	0.1098	0.0093	0.1807	0.0047	0.61	0.07	11.18	0.35	0.289
39p2	1577	26	4.415	3.970	0.013	0.1226	0.0094	0.3209	0.0049	0.38	0.04	12.37	0.23	0.192
39p3	1552	18	6.488	5.460	0.015	0.2842	0.0097	0.4638	0.0051	0.61	0.03	11.77	0.16	0.301
40p1	1544	31	3.634	3.150	0.012	0.1340	0.0094	0.2584	0.0048	0.52	0.05	12.19	0.28	0.252
41p2	1632	25	4.694	3.950	0.013	0.2038	0.0096	0.3534	0.0050	0.58	0.04	11.18	0.20	0.279
41p3	1548	25	4.519	4.040	0.013	0.1325	0.0094	0.3222	0.0049	0.41	0.04	12.54	0.23	0.206
43p1	1527	15	8.479	7.240	0.017	0.3434	0.0099	0.5957	0.0054	0.58	0.02	12.15	0.14	0.287
44p1	1560	34	3.352	2.930	0.012	0.1164	0.0096	0.2409	0.0049	0.48	0.05	12.16	0.30	0.234
47p1	1574	27	4.246	3.800	0.013	0.1230	0.0093	0.3081	0.0048	0.40	0.04	12.33	0.24	0.198
48p1	1615	58	1.797	1.110	0.009	0.1887	0.0095	0.1336	0.0046	1.41	0.12	8.31	0.35	0.549
48p3	1653	28	4.087	3.460	0.013	0.1715	0.0095	0.3119	0.0050	0.55	0.04	11.09	0.22	0.268
48p5	1581	15	8.490	7.220	0.017	0.3498	0.0100	0.6187	0.0055	0.57	0.02	11.67	0.13	0.288
49p1	1641	30	3.858	3.490	0.013	0.1009	0.0094	0.2924	0.0049	0.35	0.04	11.94	0.24	0.174
49p2	1576	29	3.795	3.430	0.013	0.1006	0.0088	0.2756	0.0049	0.37	0.04	12.45	0.27	0.194
49p5	1558	30	3.782	3.260	0.012	0.1441	0.0094	0.2714	0.0049	0.53	0.04	12.01	0.26	0.259
50p1	1546	26	4.342	3.800	0.013	0.1499	0.0095	0.3092	0.0049	0.48	0.04	12.29	0.24	0.237
51p2	1541	31	3.650	3.140	0.012	0.1410	0.0094	0.2589	0.0048	0.54	0.05	12.13	0.27	0.264

Sample Na 555

Pkt	Age [Ma]	± [Ma]	Th*	Th	error absolut	U	error absolut	Pb	error absolut	U/Pb	error absolut	Th/Pb	error absolut	R
2	570	22	4.721	3.320	0.013	0.4228	0.0101	0.1208	0.0046	3.50	0.22	27.48	1.15	0.844
4	583	25	4.037	3.000	0.012	0.3127	0.0098	0.1056	0.0046	2.96	0.22	28.41	1.35	0.809
7	585	23	4.560	3.580	0.013	0.2956	0.0100	0.1198	0.0047	2.47	0.18	29.88	1.27	0.753
9	543	27	3.764	3.090	0.012	0.2040	0.0096	0.0917	0.0046	2.22	0.22	33.70	1.81	0.724
11	535	20	5.040	3.640	0.013	0.4239	0.0102	0.1209	0.0047	3.51	0.22	30.11	1.27	0.845
14	597	24	4.192	3.150	0.012	0.3137	0.0099	0.1125	0.0046	2.79	0.20	28.00	1.25	0.788
19	577	24	4.239	3.300	0.013	0.2833	0.0098	0.1099	0.0046	2.58	0.20	30.03	1.36	0.766
21	538	20	5.229	3.600	0.013	0.4929	0.0102	0.1261	0.0047	3.91	0.23	28.55	1.16	0.868
25	539	30	3.344	2.500	0.011	0.2554	0.0098	0.0808	0.0045	3.16	0.30	30.94	1.88	0.824
29	574	25	4.156	3.320	0.013	0.2524	0.0098	0.1072	0.0046	2.35	0.19	30.97	1.45	0.740
30	559	22	4.537	3.290	0.013	0.3768	0.0100	0.1138	0.0046	3.31	0.22	28.91	1.27	0.832
33	609	24	4.196	3.140	0.012	0.3177	0.0100	0.1149	0.0046	2.77	0.20	27.33	1.21	0.783
10p1	568	26	3.817	2.660	0.011	0.3492	0.0099	0.0973	0.0046	3.59	0.27	27.34	1.40	0.853
10p2	590	24	4.334	3.640	0.013	0.2093	0.0098	0.1150	0.0047	1.82	0.16	31.65	1.40	0.653
10p-2-1	643	30	3.229	2.390	0.011	0.2519	0.0090	0.0934	0.0044	2.70	0.22	25.59	1.33	0.794
11p1	622	35	2.751	1.860	0.010	0.2678	0.0091	0.0769	0.0044	3.48	0.32	24.19	1.50	0.856
14p1	594	35	2.720	1.950	0.010	0.2320	0.0090	0.0726	0.0044	3.20	0.32	26.86	1.76	0.839
14p2	567	23	4.214	3.150	0.012	0.3214	0.0091	0.1072	0.0045	3.00	0.21	29.38	1.34	0.823
15p1	544	23	4.413	3.380	0.013	0.3124	0.0098	0.1077	0.0046	2.90	0.22	31.38	1.46	0.802
15p2	546	22	4.585	3.430	0.013	0.3492	0.0100	0.1122	0.0046	3.11	0.22	30.57	1.37	0.818
15p-2-2	612	26	3.745	2.890	0.012	0.2571	0.0090	0.1030	0.0044	2.50	0.19	28.06	1.32	0.774
15p3	557	43	2.299	1.610	0.010	0.2083	0.0097	0.0575	0.0045	3.62	0.45	28.00	2.37	0.858
17p1	573	15	6.711	5.520	0.015	0.3595	0.0092	0.1729	0.0045	2.08	0.11	31.93	0.93	0.711
17p-1-1	528	22	4.733	3.380	0.013	0.4098	0.0101	0.1121	0.0046	3.66	0.24	30.15	1.35	0.854
17p-1-2	561	21	4.747	3.350	0.013	0.4219	0.0101	0.1194	0.0046	3.53	0.22	28.06	1.19	0.846
17p-1-3	520	21	4.907	3.380	0.013	0.4628	0.0102	0.1144	0.0046	4.05	0.25	29.55	1.30	0.875
17p2	557	18	5.646	4.560	0.014	0.3282	0.0091	0.1411	0.0045	2.33	0.14	32.32	1.14	0.755
17p3	576	18	5.658	4.600	0.014	0.3193	0.0091	0.1464	0.0045	2.18	0.13	31.42	1.07	0.733
18p1	532	30	3.226	2.430	0.011	0.2411	0.0090	0.0770	0.0044	3.13	0.30	31.56	1.95	0.836
20p-1-1	560	13	8.385	3.420	0.013	1.5000	0.0120	0.2102	0.0048	7.14	0.22	16.27	0.43	0.931
26p1	555	20	4.878	3.980	0.013	0.2715	0.0090	0.1216	0.0045	2.23	0.16	32.73	1.31	0.740
26p-1-1	640	36	2.771	2.070	0.011	0.2105	0.0097	0.0798	0.0045	2.64	0.27	25.94	1.61	0.774
26p-1-2	554	26	3.865	2.340	0.011	0.4609	0.0101	0.0960	0.0046	4.80	0.33	24.38	1.28	0.904
26p4	579	22	4.516	3.060	0.012	0.4391	0.0090	0.1173	0.0044	3.74	0.22	26.09	1.09	0.875
26p6	584	22	4.600	3.690	0.013	0.2744	0.0090	0.1207	0.0045	2.27	0.16	30.57	1.24	0.746
27p1	632	22	4.552	3.610	0.012	0.2830	0.0089	0.1294	0.0045	2.19	0.14	27.90	1.06	0.736
28p1	534	18	5.917	4.940	0.015	0.2959	0.0099	0.1418	0.0047	2.09	0.14	34.84	1.26	0.702
28p2	523	21	4.874	3.100	0.012	0.5375	0.0103	0.1141	0.0046	4.71	0.28	27.17	1.21	0.900
31p1	545	23	4.454	3.330	0.013	0.3399	0.0100	0.1088	0.0046	3.12	0.22	30.61	1.42	0.821
31p2	559	25	4.020	2.980	0.012	0.3142	0.0099	0.1009	0.0046	3.11	0.24	29.53	1.47	0.820
32p1	543	23	4.379	3.270	0.012	0.3355	0.0099	0.1067	0.0046	3.14	0.23	30.65	1.43	0.821
32p2	565	19	5.334	4.200	0.014	0.3423	0.0100	0.1354	0.0047	2.53	0.16	31.02	1.18	0.761
32p3	549	23	4.570	3.500	0.013	0.3235	0.0100	0.1126	0.0047	2.87	0.21	31.08	1.40	0.798
34p2	618	30	3.309	2.420	0.011	0.2672	0.0096	0.0919	0.0046	2.91	0.25	26.33	1.43	0.809
3p1	535	25	3.917	3.110	0.012	0.2444	0.0091	0.0941	0.0044	2.60	0.22	33.05	1.68	0.781
3p-1-2	522	34	2.921	2.050	0.010	0.2639	0.0098	0.0683	0.0045	3.86	0.40	30.01	2.14	0.870
3p-1-3	601	53	1.857	1.150	0.009	0.2130	0.0097	0.0501	0.0045	4.25	0.57	22.95	2.23	0.888
3p7	561	26	3.723	2.940	0.011	0.2365	0.0089	0.0938	0.0044	2.52	0.21	31.34	1.61	0.780
3p8	658	54	1.735	1.030	0.008	0.2112	0.0089	0.0513	0.0043	4.12	0.52	20.08	1.85	0.890
4p1	535	58	1.636	0.612	0.007	0.3100	0.0091	0.0391	0.0043	7.93	1.11	15.65	1.92	0.961

4p3	564	23	4.190	3.020	0.011	0.3532	0.0091	0.1060	0.0044	3.33	0.23	28.49	1.30	0.847
4p4	650	31	3.169	2.400	0.011	0.2307	0.0090	0.0926	0.0044	2.49	0.22	25.92	1.35	0.772
4p5	561	26	3.760	2.970	0.012	0.2385	0.0090	0.0947	0.0044	2.52	0.21	31.36	1.59	0.778
6p1	551	24	4.287	2.890	0.012	0.4222	0.0101	0.1059	0.0046	3.99	0.27	27.29	1.30	0.872
6p2	598	25	3.977	2.880	0.012	0.3304	0.0098	0.1068	0.0046	3.09	0.22	26.97	1.27	0.819
6p3	597	25	3.988	3.000	0.012	0.2975	0.0098	0.1070	0.0046	2.78	0.21	28.04	1.32	0.791
6p4	563	26	3.914	2.870	0.012	0.3153	0.0098	0.0988	0.0046	3.19	0.25	29.05	1.47	0.828
7p1	666	28	3.487	2.490	0.011	0.2987	0.0091	0.1044	0.0044	2.86	0.21	23.85	1.12	0.811
7p2	627	24	4.027	2.850	0.012	0.3536	0.0091	0.1134	0.0044	3.12	0.20	25.13	1.09	0.831
7p4	632	61	1.561	0.936	0.009	0.1876	0.0089	0.0443	0.0043	4.23	0.61	21.14	2.26	0.897
7p5	536	25	3.903	2.440	0.011	0.4428	0.0093	0.0937	0.0044	4.73	0.32	26.04	1.34	0.909
8p-1-1	566	27	3.781	2.890	0.012	0.2689	0.0098	0.0960	0.0046	2.80	0.24	30.10	1.56	0.793
8p-1-2	568	21	4.772	3.690	0.013	0.3268	0.0099	0.1217	0.0046	2.69	0.18	30.32	1.26	0.780
8p2	537	29	3.319	2.120	0.010	0.3630	0.0093	0.0799	0.0044	4.54	0.37	26.53	1.59	0.904
8p3	526	40	2.420	1.750	0.010	0.2029	0.0090	0.0571	0.0044	3.55	0.43	30.65	2.52	0.863
9p1	656	27	3.575	2.530	0.011	0.3133	0.0090	0.1054	0.0044	2.97	0.21	24.00	1.11	0.820

Sample Na 556

	Age	±			error		error		error		error		error	
Pkt	[Ma]	[Ma]	Th*	Th	absolut	U	absolut	Pb	absolut	U/Pb	absolut	Th/Pb	absolut	R
7	583	16	6.351	3.630	0.013	0.8206	0.0107	0.1659	0.0047	4.95	0.20	21.88	0.70	0.900
14	606	25	3.925	1.280	0.009	0.7962	0.0107	0.1064	0.0046	7.48	0.42	12.03	0.60	0.941
17	549	18	5.765	3.330	0.013	0.7364	0.0108	0.1417	0.0047	5.20	0.25	23.50	0.86	0.907
21	531	18	5.668	1.870	0.010	1.1500	0.0115	0.1346	0.0046	8.54	0.38	13.89	0.55	0.948
22	564	22	4.537	1.740	0.010	0.8446	0.0110	0.1145	0.0046	7.38	0.39	15.20	0.69	0.942
28	564	18	5.709	3.260	0.012	0.7396	0.0107	0.1442	0.0047	5.13	0.24	22.61	0.82	0.906
31	565	19	5.401	2.930	0.012	0.7463	0.0107	0.1366	0.0046	5.46	0.26	21.45	0.82	0.914
36	527	13	7.997	3.210	0.012	1.4500	0.0120	0.1884	0.0047	7.70	0.26	17.04	0.49	0.938
39	564	16	6.413	4.010	0.013	0.7257	0.0106	0.1622	0.0047	4.47	0.19	24.72	0.79	0.886
40	589	17	6.125	3.600	0.013	0.7609	0.0107	0.1618	0.0047	4.70	0.20	22.25	0.72	0.891
41	529	17	6.208	3.390	0.013	0.8534	0.0111	0.1471	0.0047	5.80	0.26	23.05	0.82	0.919
10p1	547	17	6.128	3.110	0.012	0.9127	0.0104	0.1502	0.0046	6.08	0.26	20.71	0.72	0.930
10p2	548	18	5.547	2.590	0.011	0.8941	0.0104	0.1360	0.0045	6.57	0.30	19.04	0.72	0.937
10p3	574	26	3.769	1.520	0.009	0.6787	0.0100	0.0968	0.0046	7.01	0.44	15.70	0.83	0.948
11p1	580	13	7.901	5.870	0.016	0.6127	0.0099	0.2057	0.0047	2.98	0.12	28.54	0.73	0.812
11p2	641	13	8.342	6.210	0.016	0.6400	0.0102	0.2404	0.0048	2.66	0.10	25.83	0.59	0.776
11p3	595	14	7.614	4.910	0.015	0.8145	0.0101	0.2032	0.0047	4.01	0.14	24.16	0.63	0.875
12p1	543	15	6.847	3.980	0.014	0.8673	0.0104	0.1664	0.0047	5.21	0.21	23.92	0.75	0.912
12p-1-1	551	17	5.896	2.630	0.011	0.9874	0.0111	0.1454	0.0047	6.79	0.29	18.09	0.66	0.935
12p-1-2	579	21	4.754	1.980	0.010	0.8367	0.0109	0.1233	0.0046	6.79	0.34	16.06	0.68	0.936
12p-1-3	609	21	4.681	1.740	0.010	0.8849	0.0110	0.1276	0.0046	6.93	0.33	13.64	0.57	0.934
12p-1-4	571	18	5.659	2.180	0.011	1.0500	0.0111	0.1445	0.0046	7.27	0.31	15.09	0.56	0.939
12p-1-5	566	26	3.830	1.750	0.010	0.6280	0.0105	0.0970	0.0046	6.47	0.41	18.04	0.95	0.935
12p-1-6	595	21	4.686	2.020	0.010	0.8033	0.0108	0.1248	0.0046	6.44	0.32	16.19	0.68	0.930
12p2	537	19	5.243	3.200	0.012	0.6183	0.0100	0.1261	0.0046	4.90	0.26	25.38	1.03	0.911
13p1	528	18	5.567	3.300	0.013	0.6866	0.0100	0.1317	0.0046	5.21	0.26	25.06	0.97	0.917
14p1	518	37	2.656	1.290	0.009	0.4139	0.0096	0.0615	0.0045	6.73	0.65	20.98	1.68	0.949
14p2	544	14	7.247	3.280	0.012	1.2000	0.0109	0.1763	0.0047	6.81	0.24	18.60	0.57	0.937
15p1	570	18	5.742	3.130	0.012	0.7884	0.0102	0.1467	0.0046	5.37	0.24	21.34	0.75	0.916
15p-1-1	523	17	6.117	2.970	0.012	0.9536	0.0111	0.1431	0.0047	6.66	0.29	20.75	0.76	0.935
15p-1-2	557	17	6.184	3.220	0.012	0.8955	0.0110	0.1543	0.0047	5.80	0.25	20.87	0.71	0.919
16p1	576	19	5.219	2.160	0.011	0.9229	0.0104	0.1345	0.0046	6.86	0.31	16.06	0.63	0.940
17p1	583	21	4.831	2.620	0.012	0.6666	0.0101	0.1263	0.0047	5.28	0.27	20.74	0.86	0.918
17p2	648	14	7.297	3.130	0.012	1.2500	0.0108	0.2121	0.0047	5.89	0.18	14.76	0.39	0.919

18p1	554	16	6.200	1.700	0.010	1.3600	0.0112	0.1536	0.0047	8.85	0.34	11.07	0.40	0.948
18p2	622	26	3.867	1.790	0.010	0.6243	0.0100	0.1078	0.0046	5.79	0.34	16.60	0.80	0.928
18p3	576	20	4.971	2.390	0.011	0.7788	0.0102	0.1282	0.0046	6.07	0.30	18.64	0.76	0.932
18p4	547	17	5.873	2.500	0.011	1.0200	0.0106	0.1438	0.0047	7.09	0.30	17.39	0.64	0.943
19p1	584	19	5.225	1.960	0.010	0.9843	0.0105	0.1366	0.0046	7.21	0.32	14.35	0.56	0.941
19p2	582	25	3.969	1.910	0.010	0.6210	0.0099	0.1035	0.0046	6.00	0.36	18.45	0.91	0.933
1p1	522	14	7.467	5.320	0.015	0.6505	0.0101	0.1748	0.0047	3.72	0.16	30.43	0.91	0.862
1p-1-1	534	14	7.480	5.170	0.015	0.6993	0.0106	0.1790	0.0047	3.91	0.16	28.88	0.85	0.861
1p-1-2	569	10	10.626	7.890	0.018	0.8260	0.0107	0.2715	0.0049	3.04	0.09	29.06	0.59	0.804
1p2	612	18	5.544	3.710	0.013	0.5519	0.0098	0.1523	0.0046	3.62	0.18	24.36	0.83	0.858
20p1	578	15	6.788	4.790	0.014	0.6028	0.0098	0.1762	0.0047	3.42	0.15	27.19	0.81	0.850
21p1	619	16	6.761	4.200	0.014	0.7701	0.0102	0.1879	0.0048	4.10	0.16	22.35	0.64	0.879
22p1	546	20	5.146	2.200	0.011	0.8911	0.0104	0.1256	0.0046	7.09	0.34	17.52	0.73	0.945
2p1	633	15	7.045	4.450	0.014	0.7793	0.0101	0.2003	0.0047	3.89	0.16	22.22	0.59	0.796
33p1	534	25	3.928	1.940	0.010	0.6017	0.0105	0.0939	0.0046	6.41	0.42	20.66	1.11	0.936
33p2	547	22	4.673	2.600	0.011	0.6270	0.0105	0.1144	0.0046	5.48	0.31	22.73	1.02	0.918
34p1	559	13	8.013	5.260	0.015	0.8316	0.0108	0.2008	0.0048	4.14	0.15	26.20	0.70	0.870
34p2	541	15	6.849	4.210	0.014	0.7983	0.0108	0.1661	0.0047	4.81	0.20	25.35	0.80	0.895
34p3	519	8	13.548	10.62	0.020	0.8874	0.0110	0.3153	0.0050	2.81	0.08	33.68	0.60	0.781
3p1	600	19	5.457	3.180	0.012	0.6858	0.0099	0.1468	0.0046	4.67	0.21	21.66	0.77	0.901
4p1	553	16	6.202	3.650	0.013	0.7713	0.0102	0.1537	0.0046	5.02	0.22	23.75	0.80	0.909
4p2	610	18	5.816	3.420	0.013	0.7210	0.0100	0.1592	0.0046	4.53	0.20	21.48	0.71	0.896
5p1	587	16	6.489	3.310	0.013	0.9584	0.0104	0.1706	0.0047	5.62	0.22	19.40	0.61	0.921
5p2	601	24	4.219	1.940	0.010	0.6863	0.0100	0.1137	0.0046	6.04	0.33	17.06	0.78	0.932
5p3	531	28	3.557	1.550	0.009	0.6076	0.0098	0.0844	0.0046	7.20	0.50	18.36	1.10	0.952
5p4	587	18	5.553	2.600	0.011	0.8901	0.0104	0.1461	0.0046	6.09	0.26	17.80	0.64	0.929
6p1	571	24	4.224	2.050	0.010	0.6563	0.0100	0.1081	0.0046	6.07	0.35	18.96	0.90	0.934
7p1	562	12	9.062	6.140	0.016	0.8826	0.0103	0.2284	0.0048	3.86	0.13	26.88	0.63	0.866
8p1	552	13	7.775	4.780	0.014	0.9052	0.0104	0.1924	0.0047	4.70	0.17	24.84	0.69	0.899
9p1	531	19	5.266	2.450	0.011	0.8526	0.0103	0.1250	0.0046	6.82	0.33	19.60	0.81	0.943
9p2	538	24	4.226	2.050	0.010	0.6584	0.0100	0.1017	0.0046	6.47	0.39	20.16	1.01	0.941

Standard F-5

	Age	±			error		error		error		error		error	
F5	[Ma]	[Ma]	Th*	Th	absolut	U	absolut	Pb	absolut	U/Pb	absolut	Th/Pb	absolut	R
4.1	340	8	9.070	7.110	0.017	1.9600	0.0120	0.2045	0.0047	22.66	0.28	34.29	0.89	0.962
4.5	330	8	8.960	6.970	0.017	1.9900	0.0125	0.1974	0.0047	10.08	0.30	35.31	0.92	0.961
4.6	339	8	8.860	6.900	0.017	1.9600	0.0120	0.2007	0.0047	18.66	0.29	30.29	0.89	0.963
4.7	339	8	8.160	6.280	0.016	1.8800	0.0118	0.1873	0.0047	19.66	0.31	31.29	0.92	0.964
4.8	347	10	6.830	5.240	0.015	1.5900	0.0114	0.1610	0.0047	20.66	0.36	32.29	1.03	0.965
4.9	337	10	6.740	5.190	0.015	1.5500	0.0113	0.1536	0.0046	21.66	0.38	33.29	1.12	0.968
6.1	323	9	8.000	6.190	0.016	1.8100	0.0118	0.1738	0.0048	0.53	0.35	12.77	1.07	0.969
6.2	348	9	7.000	5.250	0.015	1.7500	0.0116	0.1696	0.0046	0.49	0.35	12.75	0.93	0.967
6.3	340	8	8.370	6.580	0.016	1.7900	0.0116	0.1878	0.0047	0.44	0.30	12.88	0.96	0.963
6.4	342	8	8.690	6.930	0.017	1.7600	0.0116	0.1931	0.0047	0.46	0.28	13.53	0.96	0.961
6.5	327	9	8.350	6.640	0.017	1.7100	0.0116	0.1775	0.0047	0.63	0.32	12.52	1.08	0.964
7.1	336	12	5.710	4.400	0.014	1.3100	0.0110	0.1298	0.0046	0.57	0.44	12.68	1.31	0.969
7.2	344	12	5.700	4.430	0.014	1.2700	0.0110	0.1311	0.0047	1.01	0.43	11.06	1.31	0.967
7.3	326	13	5.400	4.190	0.013	1.2100	0.0109	0.1180	0.0046	0.61	0.49	12.19	1.49	0.971
7.4	345	12	5.560	4.310	0.014	1.2500	0.0110	0.1286	0.0046	0.66	0.43	12.29	1.30	0.967
7.6	326	12	5.940	4.670	0.014	1.2700	0.0109	0.1276	0.0046	2.66	0.44	14.29	1.43	0.969

[1)] Note: Th*,Th, U and Pb data are presented as weight %; all errors are at a 2-σ level.

Table 6.2. Major [wt%], trace [ppm] and rare earth [ppm] element composition of metapelitic rocks. from the Kaoko belt (NW Namibia). LOI Lost on ignition; ASI aluminium saturation index; d.l. < detection limit.

Sample	Na 550	Na 551	Na 553	Na 555	Na 556
SiO2	69.13	76.65	76.92	75.35	59.2
Al_2O_3	11.72	12.61	11.71	11.14	14.45
Fe_2O_3	8.88	4.12	5.51	3.49	14.07
MnO	0.05	0.17	0.07	0.04	0.11
MgO	1.59	0.36	1.44	1.39	3.89
CaO	0.43	0.43	0.36	0.2	0.86
Na_2O	1.75	1.5	1.2	1.99	3.06
K_2O	3.77	3.53	2	5.03	2.78
TiO_2	0.81	0.15	0.09	0.32	1.07
P_2O_5	0.08	0.04	0.04	0.03	0.17
LOI	0.38	0.53	0.37	0.55	0.5
Total	98.59	100.09	99.71	99.53	100.16
ASI	1.5	1.8	2.4	1.2	1.5
An	1.6	1.9	1.5	0.8	3.2
Ab	14.8	12.7	10.2	16.8	25.9
Or	22.3	20.9	11.8	29.7	16.4
Sc	10	5	6	10	22
V	39	8	11	6	167
Cr	15	13	9	17	63
Co	16	3	7	3	19
Ni	9	4	5	4	31
Cu	35	237	4	5	23
Zn	29	132	15	48	16
Ga	19	16	15	16	20
Rb	108	95	23	120	101
Sr	45	62	64	40	43
Y	68	40	139	53	46
Zr	405	166	210	417	166
Nb	25	10	4	27	18
Ba	999	643	1547	1553	630
Pb	6	30	7	14	4
Th	15.9	8.2	8.8	13.4	8.4
U	3.6	1.1	d.l.	3.9	0.8
La	39	28	34	44	21
Ce	84	51	57	93	45
Pr	7	2	5	8	3
Nd	36	19	22	43	17
Sm	6	4	4	5	3

Table 6.3. P-T estimates for metapelites in the WKZ.

	T (°C)		
	Na 550	Na 551	Na 553
Thermocalc 3.21	710±24	735±22	736±12
FS78 a)	719±80	755±69	575±41
HS82 b)	727±80	764±69	580±41
T76 c)	705±57	731±49	597±31
		P (kbar)	
Thermocalc 3.21	5.57±0.61	7.13±0.64	7.73±0.35
B92 d)	5.69±0.51	7.31±0.43	3.4±1.1

a) Ferry & Spear 1978

b) Hodges & Spear 1982

c) Thompson 1976

d) Bhattacharya et al. 1992

Table 6.4. Sm-Nd garnet and whole rock data for metapelitic rocks.

	147/144	error (a)	143/144	error (a)	Sm (ppm)	Nd (ppm)
553WR	0.1078	1	0.511725	6	8.13	45.58
553WR* (b)	0.1515	2	0.511953	27	6.38	25.46
1	0.3665	4	0.512855	24	1.81	2.99
2	0.3864	4	0.512945	22	1.92	3.00
3	0.4563	5	0.513343	6	1.85	2.45
4	0.4745	5	0.513425	33	1.94	2.47
5	1.3706	14	0.517457	16	1.19	0.53
6	1.4055	14	0.517926	8	1.04	0.45

(a) errors refer to the last 1-2 digits

(b) mineral separate after magnetic separator before handpicking and leaching